TAILORED-DESIGN OF RADIATION MODIFIED IMPRINTED POLYMER ADSORBENT FOR SELECTIVE REMOVAL OF TARGETED ION

NOR AZILLAH FATIMAH BINTI OTHMAN

A thesis submitted in partial fulfilment of the requirement for the award of the degree of Doctor of Philosophy in Science and Technology

Faculty of Science and Technology

Gunma University

2020

ABSTRACT

Adsorption has been proven as an effective process for the separation of metal ions, especially at relatively low concentration. However, conventional chelating polymer adsorbents suffer limitation of selectivity. Ion-imprinted polymer has been receiving great attention due to its selective recognition of targeted ion in solution via cavity imparted into the polymers. This research aims to develop a grafted ion-imprinted polymer (IIP) adsorbent for the selective recognition of thorium ion in acidic aqueous system. A new concept of surface imprinting in the synthesis of IIP is proposed by using radiation induced graft polymerization and crosslinking techniques. The concept is based on the usage of polyolefin non-woven fiber (PE/PP-NWF) that consists of polypropylene (PP) core and polyethylene (PE) sheath as the polymer substrate and the creation of an imprinted layer grafted onto the surface of the substrate via two different approach, namely '*ex-situ*' and '*in-situ*' template impregnation.

In the '*ex-situ*' approach, an amine-based monomer, 2-(Dimethylamino)ethyl methacrylate (DMAEMA) was covalently bonded onto the PE/PP-NWF through graft polymerization (denoted as P-DMAEMA) and followed by template, thorium complexation through adsorption. Afterwards, the P-DMAEMA was crosslinked with divinylbenzene (DVB) to form the cavity of IIP and finally the template was removed. The physicochemical properties of the synthesized polymer adsorbents were characterized. The effect of operational parameters was investigated in batch adsorption experiment. The experimental data were correlated with several isotherm and kinetic models for the determination of the adsorption potential. It was found that P-DMAEMA showed favourable adsorption towards uranium (U(VI)) compared to thorium (Th(IV)). After crosslinking process, the IIP showed a reverse selectivity pattern with the highest selectivity coefficient ratio of Th(IV) over U(VI) was 3.1. However, based on the overall results, the selectivity ratio is still not satisfactory.

Thus, another attempt has been made to investigate the '*in-situ*' approach in the synthesis of IIP by replacing amine with phosphoric functional group to improve the

selectivity of the adsorbent. In this approach, firstly the complexation of Th(IV) with the polymerizable monomer, 2-hydroxyethyl methacrylate phosphoric acid (2-HMPA) was prepared. Next, Th(IV) was trapped by creating a three-dimensional crosslinked network surrounding the complex and simultaneously it was grafted onto PE/PP-NWF with the aid of DVB. Lastly, the template ion was eluted, leaving a cavity of the template. The stability of 2-HMPA emulsion containing Th (IV) template and the optimum absorbed radiation dose required was investigated. The mechanism of imprint molecules interaction was evaluated, and it was found that the carbonyl and phosphate group are predominant to construct the metal ion-monomer complex. The IIP achieved maximum distribution coefficient of 3.3 g/L and selectivity coefficient ratio of Th(IV) over U(VI) was 9.5 within 90 minutes of contact time at pH 3.5. The adsorption kinetics of IIP followed the second-order kinetic model for both Th(IV) and U(VI) adsorption and the IIP can maintain 78% regeneration efficiency after four cycles. The findings of this study will help in designing adsorbents for future application in radioactive wastewater research.

Aim: To develop grafted ion-imprinted polymer (IIP) adsorbent for the selective recognition of Thorium (Th) ion in an acidic aqueous system

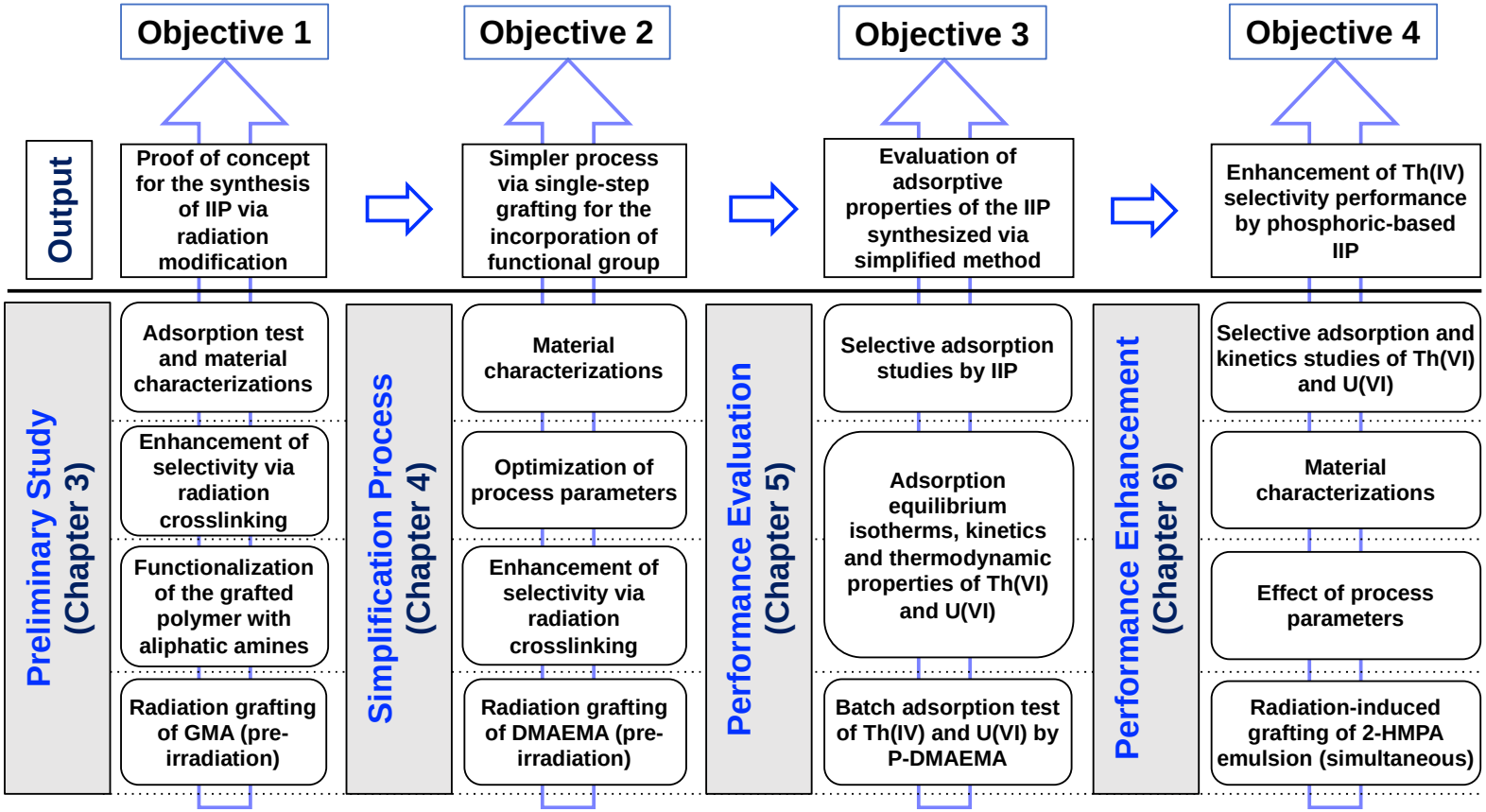

TABLE OF CONTENTS

LIST OF TABLES

LIST OF FIGURES

LIST OF ABBREVIATION

2-HMPA	2-hydroxyethyl methacrylate phosphoric acid
Ce	Cerium
Cu	Copper
DSC	Differential scanning calorimetry
DVB	Divinylbenzene
EGDMA	Ethylene glycol dimethacrylate
FT-IR	Fourier transform infrared spectroscopy
Gd	Gadolinium
ICP-MS	Inductively couple plasma- Mass spectrometry
IIP	Ion-imprinted polymer
La	Lanthanum
MF	Molecular formula
MW	Molecular weight
Nd	Neodymium
NIP	Non- imprinted polymer
NWF	Non-woven fiber
Pb	Lead
REE	Rare earth element
RSM	Response surface methodology
SEM	Scanning electron microscopy
TGA	Thermogravimetric analysis
Th	Thorium
TWEEN20	Polyoxyethylenesorbitan monolaurate
U	Uranium
XAFS	X-ray absorption fine structure
XPS	X-ray photoelectron spectroscopy
XRD	X-ray diffraction

LIST OF SYMBOLS

C_e	Concentration of analyte in the solution at equilibrium (mg/L)
C_f	Final concentration of analyte in the solution (mg/L)
C_i	Initial concentration of analyte in the solution (mg/L)
k_1	Rate constant for pseudo first order sorption (1/min)
k_2	Rate constant for pseudo first order sorption (mg/min)
k_d	Distribution coefficient
K_F	Freundlich adsorption constants
K_L	Langmuir adsorption constants related to adsorption energy
q_{cal}	Calculated adsorption capacity at equilibrium (mg/g)
q_e	Adsorption capacity at equilibrium (mg/g)
q_{exp}	Experimental adsorption capacity (mg/g)
q_t	Adsorption capacity at *t* time (mg/g)
R^2	Correlation coefficients
W_f	Final weight (g)
W_i	Initial weight (g)
°C	degree celcius
Δ	delta
ΔG^0	Gibb's free energy (kJ/mol)
ΔH^0	Enthalpy change (kJ/mol)
ΔH_f	Heat of fusion (J/g)
K	Selectivity coefficient
K'	Relative selectivity coefficient
R	Gas constant (8.314 J/mol K)
T	Temperature (K)
t	Time (min)
V	Volume of the solution (L)

α	alpha
β	beta
γ	gamma
θ	theta
λ	lambda
µ	micro

LIST OF APPENDICES

APPENDIX **TITLE** **PAGE**

CHAPTER 1

INTRODUCTION

1.1 Introduction

Over the past few decades, many researchers have reviewed the feasibility of functional polymeric materials for mining wastewater treatment [1-3]. Polymeric adsorbent, either from a synthetic polymer or natural resources has been well documented in several excellent reviews [4-6]. Incorporation of chelating ligands or anchoring sites with functional groups containing donor atoms like nitrogen, oxygen, or phosphorus by graft polymerization of monomer enables the metal ions to bound to the polymer ligand. In such circumstances, this study aims to propose a radiation modified polymer adsorbent to be further investigated for its potential to selectively remove targeted ions from wastewater. The adsorbents were modified as imprinted polymers, where it was synthesized, characterized and examined as a selective adsorbent for the elimination of thorium cations from aqueous solutions in a binary metal system. The functionalized polymeric adsorbents would be feasibly applied as ameliorants and remediation agents for aqueous systems polluted by heavy metals and radioelements, notably from mining wastewaters.

Adsorbents used in adsorption processes of pollutants should meet several important requirements such as; the adsorbents should have good adsorption capacity and it should have high tolerance with a wide range of wastewater parameters. Therefore, according to the above-mentioned desired properties; a synthetic polymer, polypropylene coated polyethylene non-woven fiber (PE/PP-NWF) has been chosen as the most suitable polymer substrate to be modified by introducing different functional groups for selective removal of targeted ion. The concept of imprinting proposed in this study is based on the creation of an imprinted polymer layer grafted onto the surface of the base polymer, PE/PP-NWF. Two approaches were implemented during the process of the imprinted

polymer layer creation. The first approach was an '*ex-situ'* approach, whereby the functional monomer covalently bonded onto the polymer substrate through graft polymerization and followed by attachment of template to the functional group via adsorption process. Subsequently, co-polymerization with crosslinker was carried out to form a cavity of the template. The second approach was an *'in-situ'* approach, whereby firstly, a complexation is carried out between a specific ligand with the ion template, and then the complexation is grafted onto the substrate. Both approaches were designed in a way that resembles the unique fitting of a key to its corresponding lock of imprinted polymer. Subsequent removal of the template leaves binding sites cavities complementary in shape, size and functional groups orientation in the polymer network which are able to rebind with the template in both high affinity and selectivity.

Selective removal enables separation of only the targeted metal ion from a multi-elements solution. Selective removal of metal ions could simplify the purification process thereafter without any other interference ions. Therefore, the reuse of recovered metals becomes very much viable in any required sectors. Although the main objective of metal removal from waste is to meet required regulations, the recovery and reuse of it could offer some economic benefits [7]. Numerous studies had been conducted on selective removal of metal ions using multiple techniques. Liu *et al.* [8] had developed two types of inorganic chelating fibers which imposed high selectivity for mercury and cesium. The fibers were prepared by low-cost glass fiber substrate coated with organosilsesquioxane pre-polymer which followed by subsequent crosslinking process. The fibers are extremely efficient in removing low concentrations of mercury and cesium ions from water even in the presence of high concentrations of sodium or potassium ions as interference. On the other hand, Gu and co-workers [9] had prepared triethylenetetramine-grafted polyacrylamide/vermiculite (g-PAM/OVerm) adsorbent. The g-PAM/OVerm was synthesized via in situ polymerization of acrylamide and subsequent graft polymerization of triethylenetetramine onto the surfaces of PAM/OVerm via Mannich reaction. The g-PAM/OVerm exhibited higher selectivity for lead in comparison with zinc, cadmium and copper ions with adsorption capacity of 219.4 mg/g. Meanwhile, in this study, the radiation modified PE/PP non-woven adsorbent polymer were proposed to be investigated for its potential to selectively remove thorium from mining wastewater.

1.2 Problem Statement

Malaysia has among the largest reserve of world class mineral potentials such as gold, tin, iron, bauxite, limestone, granite, industrial minerals, clay minerals, coal and even heavy minerals, according to the statistical records from the Ministry of Natural Resources and Environment Malaysia and the Department of Minerals and Geoscience, Malaysia [10, 11]. However, the mining industry is in particular accounts for major environmental threats, where it contributes by huge amounts of wastes containing heavy metals and, in some cases, radioactive elements. Tin mining is one of the oldest industries in Malaysia that have started since the 1820s. The tin mining had created numerous environmental problems such as a threat to natural reserves due to damage to natural drainage, pollution, and destruction of natural habitats. The tin-tailing in the ex-mining area has become one of the most important heavy minerals reserves in Malaysia. Tin-tailing or widely known as '*amang*' in Malaysia is the remaining mineral after tin oxide has been extracted from tin ores minerals. Heavy minerals such as ilmenite ($FeOTiO_2$), monazite ($(Ce, La, Nd, Gd, Th)PO_4$), xenotime (YPO_4) and zircon ($ZrSiO_4$) can be recovered from *amang* [12]. Among these, monazite and xenotime are particularly worrying since monazite and xenotime consist of numerous radionuclides such as Th and U. Discharges from abandoned tin mining get their way into the nearby lake and river through remobilization of surface deposition by rainwater. Investigation by Hamzah, Z. *et al.* [13] reported that after more than 40 years, the lake nearby abandoned tin mining site in Kampung Gajah, Malaysia still consists of high concentration of uranium and thorium, with the mean metal concentrations for U-238 and Th-232 were found to be 30.6 ppm and 85.7 ppm respectively. These radioelements need to be removed before further waste treatment, in accordance to the Malaysian Environmental Quality Act, 1974. (Act 127) [14].

Research on separation technologies are advancing over the years, in which many are either in use or are in various stages of development. Current technologies for separation of thorium from solution include liquid/solid-phase extraction, electrodeposition, and chromatography. Among these, liquid-liquid or commonly known as solvent extraction is a widely used method for metal separation in the industry [15]. Although solvent extraction seems to be an efficient and simple method for metal separation, but it also has some disadvantages such as the requirement of costly amount

of organic solvents as well as the possibility of generation of toxic organic waste. Solvent extraction is also time consuming, especially when a multiple extraction is required. Furthermore, solvent extraction is inefficient at low metal concentration. There are several techniques known for solvent extraction, namely acid digestion and alkaline fusion. Malaysian Nuclear Agency has been pioneering the alkaline fusion process to separate uranium and thorium. Kones J. *et al.* [16] performed alkaline fusion solvent extraction and they successfully recovered 69% thorium and 84% uranium from xenotime, while monazite showed lower recovery percentage, which is 62% for thorium and 41% for uranium. However, as seen from the results, they cannot fully separate the radioelements from the solution and considerable amount of thorium and uranium still left in the effluents. Thorium and uranium from dilute solutions can be pre-concentrated using adsorbent prior to extraction, which may result in optimizing the efficiency in subsequent purification steps for the production of nuclear-grade material. Thus, in recent years, many efforts have been devoted to obtaining selective separation techniques for the residual radioelements collected from this process.

Solid-phase extraction is considered as an emerging advanced technique to overcome limitation of liquid-phase solvent extraction. The separation of metal ions using selective adsorbent, particularly ion-imprinted polymer (IIP) has been receiving great attention because of their good stability, reusability and high selectivity [15, 17, 18] towards the targeted ion. An IIP has special coordination, which is capable of recognizing ions and can achieve effective recognition of targeted ionic in solution due to a memory effect imparted into the polymers [19]. Therefore IIPs have attracted increasing interest as a unique technique to synthesize highly selective adsorbents for a solid phase extraction [19, 20].

Conventional ion-imprinted polymers are prepared by copolymerization of functional monomer and crosslinker in the presence of a molecular template altogether. This method has several shortcomings. It suffers low rebinding capability due to limited access to the binding sites, which caused by the highly rigid crosslinked structure. In addition, the poor accessibility will be resulted to slow mass transfer that eventually will affect the binding kinetics. Therefore, surface imprinting method was investigated in order to resolve these problems. Generally, the surface imprinted polymers are prepared by generating binding cavities onto or near the surface of the imprinted polymers [17, 21].

The advantages of surface imprinted polymers are in its ability to form a uniform distribution of produced adsorbent, low consumption of template and materials, high thermal stability, easily control of reaction parameters while having high selectivity towards targeted ion [22-24]. This research purposed a new concept of imprinting in the synthesis of the ion-imprinted polymer (IIP), by taking into consideration the general theoretical concept of the surface imprinting. The new concept of imprinting introduced in this study is based on the usage of polypropylene coated polyethylene non-woven fiber (PE/PP-NWF) as the base polymer and the creation of an imprinted polymer layer grafted onto the surface of the base polymer via '*ex-situ*' and '*in-situ*' template impregnation approach. Thus far, no study was found in the literature that focused on utilization of grafted adsorbent as ion-imprinted polymer. The imprinted polymer prepared using radiation provides effective and simple method to introduce the functional group and to "imprint" the template onto surface of polymers. In addition, any types of polymer such as fibers, fabrics, films, particle and other materials can be prepared using this method, with no chemical initiator left in the substrate of the imprinted polymers [25]. As the creation of the imprinted polymer layer can be well controlled, the obtained layer is expected to have a homogenous distribution. Furthermore, the shape and properties of the substrate can be conserved.

1.3 Research Objectives

This research aim is to develop a grafted ion-imprinted polymer (IIP) adsorbent for the selective recognition of targeted ion in an acidic condition. To fulfil this, four detail objectives can be written as below;

i. To evaluate a technique of radiation grafting with subsequent crosslinking to produce ion-imprinted amine-based adsorbent.

ii. To simplify the process of radiation grafting and crosslinking techniques toward enhancing the selectivity of thorium.

iii. To evaluate the performance of the ion-imprinted adsorbent for adsorption of thorium in various ion solution.

iv. To improve the selectivity of the adsorbent by replacing amine with a phosphoric functional group.

1.4 Research Framework and Scopes

The research framework is presented in Figure 1.1.

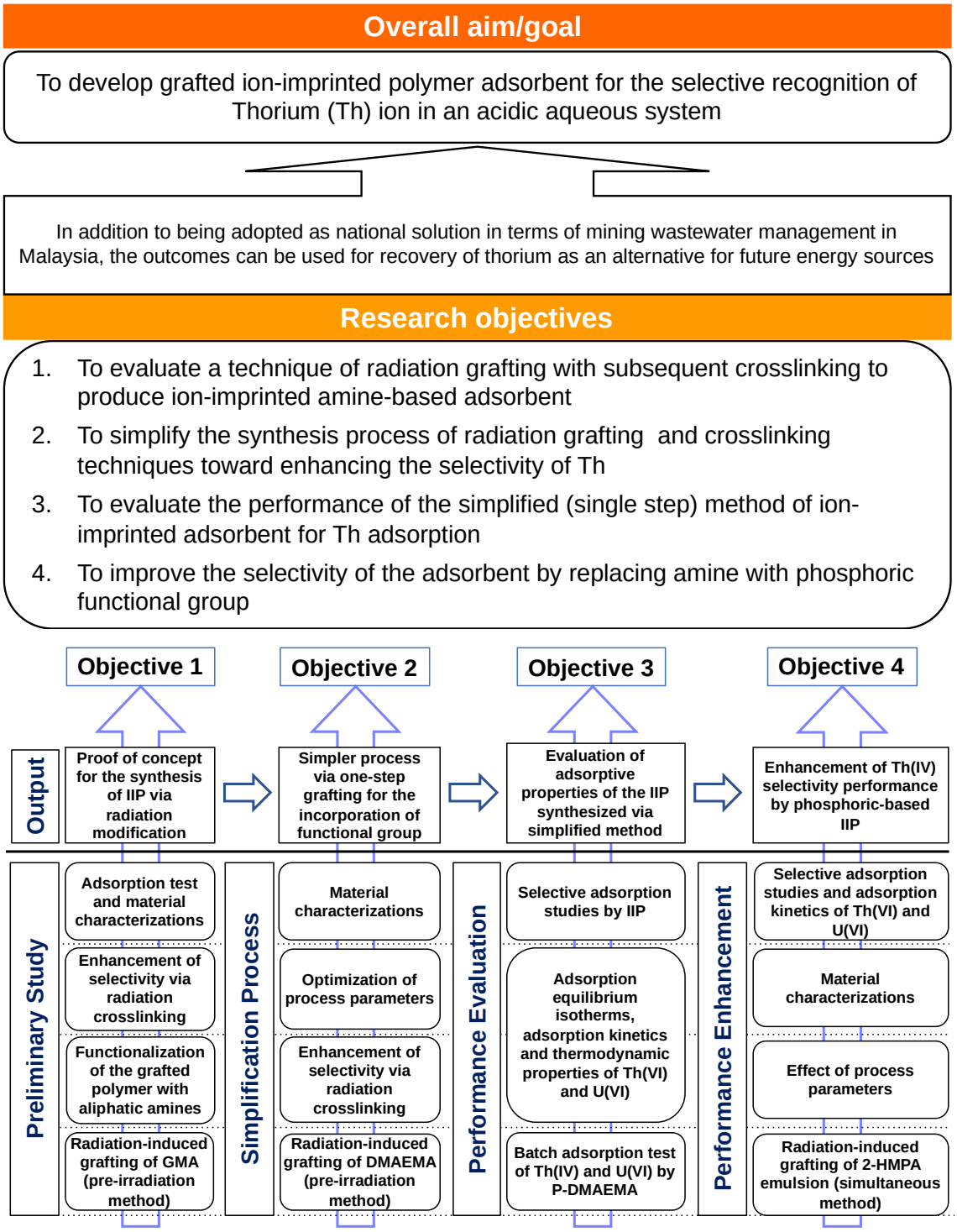

Figure 1.1. Flowchart of the research framework

A preliminary investigation was started by using glycidyl methacrylate (GMA) - grafted amine-based adsorbent for copper uptake. This type of adsorbent has been widely used for metal adsorbent, especially for copper, thus high adsorption capacity can be anticipated. The purpose of this action was to eliminate the uncertainty risk during the preparation of IIP, and also to ensure a better understanding of the mechanism and behaviour of the prepared polymer. The radiation grafting of poly-GMA onto PE/PP-NWF and followed by subsequent functionalization of the grafted PE/PP-NWF was demonstrated. The prepared adsorbents were adsorbed with copper as the ion template and were radiation crosslinked to establish the binding sites cavities complementary to the template. The physicochemical properties of the adsorbents were characterized. The adsorption selectivity of the adsorbents towards copper in the binary system (copper and lead as co-existing metal species in the solution) were evaluated. The scope of work can be outlined as follows;

(i) Preparation of adsorbent precursor by radiation grafting of GMA onto PE/PP-NWF and subsequently, the poly(GMA) grafted PE/PP-NWF were chemically functionalized using different aliphatic amines under different reaction parameters. The functionalization parameters that were investigated included;

- Amine composition varied at 50:50 wt%, 60:40 wt% and 70:30 wt%.
- The Dg (%) of the grafted adsorbent was in the range of 100 to 250%.
- Reaction temperature was varied between 60 to 80 ºC.
- Reaction time took place from 15 minutes to 2 hours.

(ii) Determination of the physicochemical properties of the prepared polymer adsorbents using various characterization techniques including;

- Physical characterization: Morphological studies were done using FE-SEM, and structure of the polymer was evaluated using XAFS.
- Chemical characterization: Chemical composition was investigated using FTIR and additionally using XPS to investigate the binding states.

(iii) The performance of prepared adsorbents towards Cu(II) and its selectivity in Cu(II) and Pb(II) binary metal species. The reaction parameters that were investigated included the effect of different aliphatic amines at different contact time in the range from 15 to 480 minutes.

Based on these preliminary findings, amine-based adsorbents were synthesized using single-step radiation grafting to simplify the multi-step modification process. Parametric studies on radiation grafting of amine methacrylate, 2-(Dimethylamino)ethyl methacrylate (DMAEMA) was conducted and evaluated to investigate the adsorbing phenomena in more detail. Subsequently, the IIP was prepared with the presence of thorium ion as template. P-DMAEMA was subjected to further modification via radiation crosslink to synthesize the ion-imprinted polymer (IIP) and characterization of the IIP in terms of polymer properties was conducted. The scope of work can be outlined as follows;

(i) Preparation of adsorbent precursor by radiation grafting of DMAEMA onto PE/PP-NWF to synthesis amine-based adsorbent under various grafting parameters including;

- Absorbed radiation dose was studied in the range of 30 to 100 kGy.
- Concentration of monomers ranging from 3 to 10 wt% of the weight fraction
- The reaction time was varied between 1 and 5 hours. The grafting rate was evaluated from the results.
- Reaction temperature was varied in the range of 30 to 60 ºC. From the results, activation energy was calculated.

(ii) Preparation of radiation crosslinked DMAEMA-grafted adsorbent as ion-imprinted polymer. The parameters that were investigated included;

- Crosslinker concentration, which varied in the range of 10 wt% to 20 wt%.
- Absorbed radiation dose, which varied in the range of 30 to 120 kGy.
- Template, Th(IV) concentration which varied in the range of 25 to 100 ppm.

- Dg (%) of the adsorbent precursor, which was varied in the range of 10 to 100%.
- Reaction temperature, which varied at three different temperatures, 60, 70 and 80 ^{o}C.

(iii) Determination of the physicochemical properties of the newly prepared polymer adsorbents using various characterization techniques including;

- Physical characterization: Morphological studies were done using FE-SEM, and structural properties were evaluated using XRD.
- Thermal properties and stability were tested using TGA.
- Chemical characterization: Chemical composition was investigated using FTIR and additionally using XPS to investigate the binding states.

The adsorption performance of P-DMAEMA was assessed in batch mode experiments. The study was conducted for both thorium and uranium in single system (only single metal species of thorium in the solution) to understand the adsorption behaviours and metal preferences of the polymer. The sorption capacity was evaluated with respect to several operating parameters. The data were evaluated using isotherm models and kinetic studies were carried out to understand the adsorption process of the adsorbent. Subsequently, the changes of adsorption behaviours and performance were further investigated using IIP by applying the adsorbent in a binary system (thorium and uranium as co-existing metal species in the solution) to determine the selectivity. The scope of work can be outlined as follows;

(i) The performances of prepared adsorbents towards Th(IV) and U(VI) in single metal species were tested under the same conditions. The reaction parameters that were investigated included;

- pH was set in the range of 1 to 3.5.
- Dg (%) of the adsorbent precursor was chosen in the range of 20 to 120%.

- Initial Th(IV) and U(VI) concentration was varied in the range from 25 to 300 mg/L.
- Reaction temperature was varied at three different temperatures, 30, 40 and 50 ºC.
- Reaction time, which was varied up to 240 minutes.

(ii) Determination and comparison of Th(IV) and U(VI) adsorption mechanism of P-DMAEMA adsorbent. The studies included;

- Adsorption equilibrium isotherms using Langmuir and Freundlich models.
- Investigation of the kinetics of Th(IV) and U(VI) adsorption using two kinetic models: pseudo-first order and pseudo-second order
- Evaluation of adsorption thermodynamic and determination of Gibb's free energy change, enthalpy change and entropy change.

1.5 Structure of Thesis

This thesis contains seven (7) chapters. Chapter 1 introduces the research background, problem statement, research objectives and scopes. Research flow, along with the scopes of the study, are detailed out. Chapter 2 presents the critical review on the adsorbent, including pollutants, particularly in mining wastewater, thorium resource, adsorbent and adsorption of pollutants and several fundamental investigations regarding its limitations, technological options and prospects. Chapter 3 details out the preliminary investigation using GMA-grafted amine-based adsorbent as ion-imprinted polymer for copper uptake. Chapter 4 simplifies the multi-step modification process and presents the results and discussion and describes the effects of various grafting parameters on the synthesis of amine-based ion-imprinted adsorbent and instrumental characterization of the adsorbent precursor. Chapter 5 contains the results and discussion, which represents the performance of the newly prepared adsorbent with respect to adsorption capacity, equilibrium isotherms, kinetics and thermodynamics of thorium and uranium. Chapter 6 concludes the synthesis of phosphorus-based adsorbent as ion-imprinted polymer and its selective removal of thorium. The essential conclusions, and recommendations for the future directions of development are summarized in Chapter 7.

CHAPTER 2

LITERATURE REVIEW

2.1 Introduction

This chapter explores the dominant themes of the research: pollutants in water systems, particularly in mining wastewaters and its removal technologies, adsorbent for removal of pollutants, the mechanism of the adsorption process, and the potential of the adsorbent to be tailor-made to selectively remove the corresponding pollutants. It also examines the pertinent literature on the development of imprinted polymer for the selective adsorption and other relevant areas necessary for understanding the work in this thesis.

2.2 Mining Wastewater

The environmental problems arising from mining activities has been a critical concern because it can deteriorate water quality and quantity, which will pose a negative impact on human community and natural ecosystem. Mining activities constitute dangers such as risk of pit floods, potential of unregulated discharges and environmental pollution through a number of mechanisms, including physical disruption of the soil, mine tailings dumping, dust emissions of heavy metals into the air, and the production of large amounts of heavy metal acid drainage [26]. One of the most shocking environmental disaster in Malaysia's mining history, the Mamut copper mine in the Eastern Malaysian state of Sabah had caused disastrous water contamination via acid mineral drainage. Prior to suspension of its operation, the copper mine had generated about 250 metric tons of overburden and waste rocks and over 100 metric tons of tailings. Ali B.N.M. *et al.* critically evaluated the degree of contamination, particularly heavy metal pollution of the Mamut River polluted from the abandoned Mamut copper mine [27]. They found out that after 15 years of its closure, some heavy metals such as copper, nickel, and lead still exceeded the limit established in quality guidelines. On the other hand, by-products from

mineral mining has also become a major concern due to the large amount of radioactive waste produced. For example, monazite and xenotime are the by-product from the alluvial tin mining industry. A large amount of uranium and thorium was found in undissolved solid during the post-leaching stage [28].

Malaysia is stated to have about 30 metric tons which is equivalent to 0.03% of global world reserve of rare earth minerals [29]. Even though there are a few drawbacks of mineral mining, Malaysia is currently looking into opportunities in utilizing rare earths for its economic growth due to the increasing global demand for rare earth. Therefore, as Malaysia is moving towards establishing rare earth based industries, in line with the Government of Malaysia's initiative to explore strategic new resources [30], more dynamic research is in need to ensure the safety of the technologies while disseminating Malaysia's own potential wealth in rare earth resources. The production of the radioactive waste along the process has caused controversy, especially on the previous events of Asian Rare Earth (ARE) [31] and Lynas Advanced Materials Processing (LAMP) [32] processing plants in Malaysia. LAMP generates 32,000 tons per year of waste water residues containing thorium with concentration of 1655 ppm [33, 34]. Because of its chemical toxicity and radioactivity which poses a significant health threat to living organisms, the removal of thorium from natural environment is needed to comply with the radioactive limitation of waste residues [15, 35]. Apart from the difficulties to store the waste, the disposal also is very costly and there is a great concern to the possibility of leaching out to the nature. On the other hand, there is also a demand to recover thorium from waste residues to meet increasing interest of thorium usage as future energy source and other application in various industries [36]. Therefore, it is necessary to develop a new material for the remediation of the contaminated water and to support the back-end of rare earth processing by recovering selective materials from marginal resources such as low-grade minerals or low concentration effluents.

The type and quantity of pollutants present in the wastewater system depends heavily on the nature of the industry involved. For example, by-product from the alluvial tin mining industry produced lanthanides (such as Ce, La, Y, Nd) and actinides (such as Th, U) traces in the wastewater [28]. The major risks posed by these pollutants are the serious impact to soil and water due to their toxicity and their inability to degrade chemically or biologically in the environment. These pollutants also have the tendency to

accumulate in the food chain, thus prolonged exposure to it may cause several health issues such as damage to the central nervous system, cardiovascular and gastrointestinal systems, degenerative diseases and may increase the risk of cancers [37].

2.3 Thorium Resource

Thorium is one of the naturally occurring rare radioactive material (NORM) which is predominantly found in rare earth minerals. Tin-tailing or widely known as '*amang*' in Malaysia is the remaining mineral after tin oxide has been extracted from tin ores minerals. Heavy minerals such as ilmenite ($FeOTiO_2$), monazite ((Ce, La, Nd, Gd, Th)PO_4), xenotime (YPO_4) and zircon ($ZrSiO_4$) can be recovered from *amang* [12]. In Malaysia, monazite and xenotime are largely produced and exploited for their rare earth elements (REE). Monazite is a crucial ore for uranium, neodymium, lanthanum and cerium which is found in pacer deposits abundantly [38]. On the other hand, xenotime belongs to rare earth phosphate, generally known as yttrium phosphate containing 67% of REE, mostly of heavier elements [39]. The contents of monazite and xenotime are tabulated in Table 2.1 and Table 2.2 respectively.

Monazite and xenotime are in particular concern since monazite and xenotime consist of high concentration of thorium, which requires a regulatory control as tabulated in Table 2.3. Aside from thorium resource from monazite and other tin-tailing by-product minerals, thorium also can be found from granitic rocks and their respective residual soil deposits in Malaysia. As depicted in Figure 2.1, thorium is widely distributed in Peninsular of Malaysia, with the highest concentration of 180 – 300 ppm concentrated at each sampling point. The study done by Sanusi *et al.* found volcanic extrusive, intermediate granitic intrusive and granitic rock are the main geological probabilities for thorium deposits [40].

Table 2.1. The rare earth composition of Malaysia's monazite. Measurements were determined using EDXRF

	MF	Elements		MF	Elements
1	Al_2O_3	Aluminum oxide (1.3%)	15	PbO	Lead(II) oxide (0.1%)
2	SiO_2	Silicon dioxide (2.1%)	16	SnO_2	Tin(IV) oxide (0.3%)
3	P_2O_5	Phosphorus pentaxide (12.9%)	17	ThO_2	Thorium oxide (7.1%)
4	Cl	Chlorine (308 ppm)	18	UO_2	Uranium oxide (0.2%)
5	K_2O	Potassium oxide (471 ppm)	19	CeO_2	Cerium oxide (38.4%)
6	CaO	Calcium Oxide (0.4%)	20	Nd_2O_3	Neodymium(III) oxide (10.0%)
7	TiO_2	Titanium dioxide (0.6%)	21	Sm_2O_3	Samarium(III) oxide (2.1%)
8	F	Flouride (1.3%)	22	Tb_4O_7	Tetraterbium heptoxide (0.4%)
9	SO_3	Sulfur trioxide (0.2%)	23	Dy_2O_3	Dysprosium(III) oxide (4.4%)
10	Fe_2O_3	Ferric oxide (0.8%)	24	Ta_2O_5	Tantalum Pentoxide (0.2%)
11	ZnO	Zinc oxide (451 ppm)	25	Er_2O_3	Erbium(III) oxide (3.9%)
12	As_2O_3	Arsenic trioxide (387 ppm)	26	Yb_2O_3	Ytterbium(III) oxide (724 ppm)
13	Y_2O_3	Yttrium oxide (2.1%)	27	HfO_2	Hafnium(IV) oxide (<0.01%)
14	ZrO_2	Zirconium oxide (0.9%)	28	WO_3	Tungsten trioxide (0.4%)

Table 2.2. The rare earth composition of Malaysia's xenotime. Measurements were determined using EDXRF

	MF	Elements		MF	Elements
1	Al_2O_3	Aluminum oxide (2.8%)	16	La_2O_3	Lanthanum oxide (0.6%)
2	SiO_2	Silicon dioxide (3.4%)	17	ThO_2	Thorium oxide (0.9%)
3	P_2O_5	Phosphorus pentaxide (19.7%)	18	UO_2	Uranium oxide (1.3%)
4	Cl	Chlorine (0.06%)	19	CeO_2	Cerium oxide (1.2%)
5	K_2O	Potassium oxide (0.2%)	20	Nd_2O_3	Neodymium(III) oxide (0.8%)
6	CaO	Calcium Oxide (0.3%)	21	Sm_2O_3	Samarium(III) oxide (0.6%)
7	TiO_2	Titanium dioxide (14.5%)	22	Tb_4O_7	Tetraterbium heptoxide (0.4%)
8	Cr_2O_3	Chromium(III) oxide (2.3%)	23	Dy_2O_3	Dysprosium(III) oxide (4.4%)
9	MnO	Manganese(II) oxide (0.7%)	24	Ho_2O_3	Holmium Oxide (<0.01%)
10	Fe_2O_3	Ferric oxide (2.4%)	25	Er_2O_3	Erbium(III) oxide (3.9%)
11	ZnO	Zinc oxide (0.06%)	26	Yb_2O_3	Ytterbium(III) oxide (4.5%)
12	Rb_2O_3	Rubidium oxide (<0.01%)	27	HfO_2	Hafnium(IV) oxide (<0.01%)
13	Y_2O_3	Yttrium oxide (43%)	28	SO_3	Sulfur trioxide (0.6%)
14	ZrO_2	Zirconium oxide (1.2%)	29	WO_3	Tungsten trioxide (<0.01%)
15	Nb_2O_5	Niobium pentoxide (<0.01%)	30	Gd_2O_3	Gadolinium(III) oxide (1.8%)

Table 2.3. Thorium composition in various rare earth ores

Minerals	**Thorium concentration (ppm)**	**References**
Monazite	2,525 – 54,100	[41-43]
Xenotime	916 – 6,200	[43, 44]
Ilmenite	34.9 – 800	[40, 43]
Zircon	309 − 3,090	[43, 45]

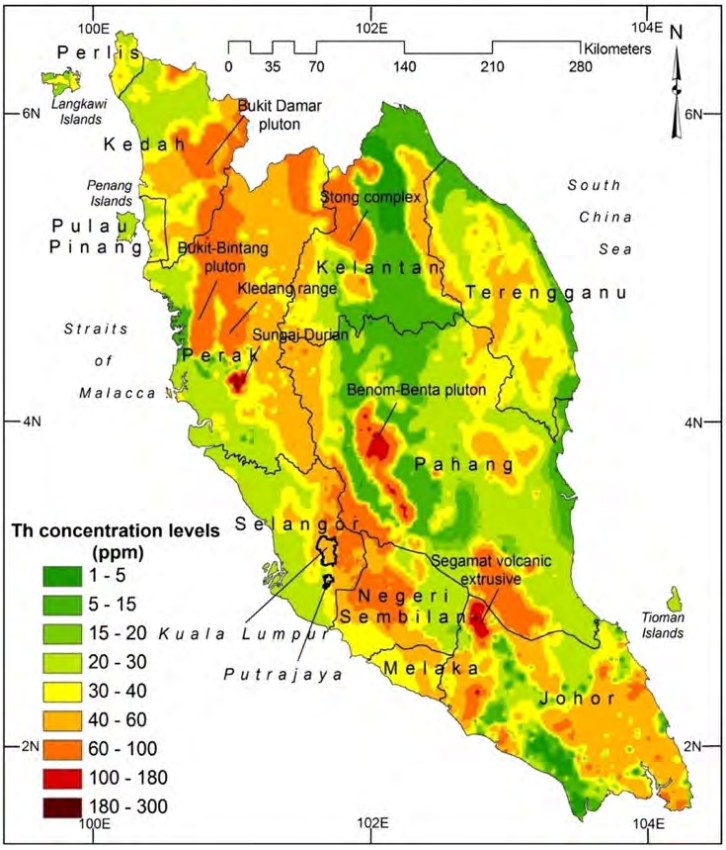

Figure 2.1. Distribution map of thorium in Peninsular Malaysia [40]

All these metals have numerous industrial uses and also considered as valuable metals. Leading REE processing plants were rapidly developed around the world as it has conquered the worldwide economy at large. Although REE processing is promising as economical assets but the types of residues generated still consists of traces of thorium and uranium abundantly. New technology for separation or recovery of thorium from the residues is very much viable to be utilized in multiple ways, especially as an alternative for future energy.

2.4 Mining Wastewater Treatment

Malaysia is blessed with abundant of water with approximately 98% of water supply is obtained from fresh water systems mainly composed of rivers, reservoirs and lakes [46]. The main sources of fresh water are rivers and stream, the supply of which comes from accumulated rainfall on hillsides, where water flows downhill into the river catchment. Being located in a tropical region, Malaysia receives a total of 990 billion m^3 of annual rainfall, 147 billion m^3 of which becomes surface runoff [47]. Meanwhile, the

groundwater resource is estimated safe yield of 64 billion m^3. Therefore, in that sense, Malaysia experienced no physical water scarcity. However, spatial and temporal distribution of rainfall is not uniform, which resulted to more storage and optimization of rainfall is required. Although water is abundant, but its resources are confronted with several issues. Population growth, expansion of urbanisation, industrial, and agriculture activities, have led to rapid increase in water demands and exerting pressure more on water resources. Previous studies of water resources concluded that unregulated human activities threaten water quality and quantity, thus making some resources unfit for consumption [48-50]. The source of pollution resulted from mining activities, namely heavy metals, toxic metals and radioelements pollution has been a critical concern and impacts negatively on the sustainability of water resources in Malaysia. Therefore, in due consideration of their toxicity and regulatory aspect, the mining wastewater need to be treated first before it is allowed to be discharged to the environment. However, as the composition of the waste varies from where they were mined and the process undertaken to generate the waste, there is no one single standard procedure for the treatment of the mining wastewater. Some of currently available treatment methods are as follow;

(i) Solvent extraction:

This process involves an organic solvent to extract the metals and an aqueous solution containing the metals; by which, the metals passes through into the appropriate organic phase. Furthermore, the extracted metals in the organic phase are re-extracted and stripped into stripping aqueous solution contacted with the organic solvent [51]. Thereafter, once the metals have been removed, the organic solvent is recycled for further use. Solvent extraction method for separation of metal ions provides the benefits of strong kinetics, high capacity and selectivity. However, a significant disadvantage is the limited aqueous solubility. Not only does it add to the cost of the system by losing reagents organics through evaporation and entrainment, the toxic organic solvent also harmful to the water system if not handled properly. Furthermore, due to the large amounts of extractants required, this process is not suitable for diluted or low concentration of metal ion solution. Therefore, solvent extraction may not be an effective method to be used in this study.

(ii) Electrolysis:

Electrolysis separates an aqueous flow into two distinguish phase, enriched and depleted flow under the influence of an electrical field. In the industrial field, electrolysis is used in the treatment of acid mine drainage [52] and the extraction of metal ions [53, 54]. Due to the expensive cost, it is uncommon to use electrolysis method in effluent treatment. However, in some cases where the concentrate is of high value, it may be appropriate to use electrolysis in certain circumstances.

(iii) Ion exchange:

The use of ion exchange resins in heavy metal ion adsorption has been increasing in recent years and is considered as one of the most effective technique for wastewater treatment. The resins contain functional groups that is responsible for complexation with metal ions. The process is commonly applied for water remediation of metal finishing industry [55], radioactive contaminants from nuclear industry effluent [56], and for recovering precious metals [57]. During the process, ion exchange resin is contacted with the contaminated solution. Once the resin is loaded with metal ions, it will undergo stripping process with an appropriate elute. A group of researchers from Brazil [58] used commercial cationic ion exchange resin, S-100 for the separation of neodymium from effluents generated from chemical treatment of Brazilian monazite sand. However, one of the critical problems with ion exchange is due to low metal ion selectivity for treatment of aqueous waste containing metal ion mixtures. Therefore, instead of direct wastewater feed, they used low cerium carbonates as the feed material which require additional separation step. In comparison to solvent extraction method, the slow kinetics of ion exchange resin is the downside of this method, although it may be improved by increasing the resin physical properties such as porosity. While heavy metal ions can be effectively removed from wastewater by ion exchange in many situations, the usage of ion exchange resin is not so effective for mining wastewater. In addition, the cost of most ion exchange resin is too high for single-use application. Therefore, the resins need to recycle multiple times for it to be cost-effective. In order to do that, highly concentrated acids or bases is used for regeneration, however from the environmental point of view, this will generate more toxic waste. It is notable that the synthetic resins have poor water wettability and

thus, they need to be modified and/or pre-treated by activation solvents. Therefore, considering all the points above, ion exchange method is not an option to be applied in our study.

(iv) Adsorption:

The application of adsorbent to remove pollutants via adsorption process has shown an increasing trend in the recent years. This is due to the characteristic of adsorption process, which is convenient in term of synthesis, application and in some cases, it can be cost-effective. In addition, adsorption process can be utilized for various kinds of pollutants such as heavy metal, organic and pharmaceuticals. Various adsorbents for adsorption process has been developed, such as activated carbon (AC) [59], bentonite [60], commercial polymer [61], grafted material [9], resin [62], metal oxide [63], and lignocellulosic material [64] for various kind of pollutants. Adsorption using AC is proven as an effective treatment for organic pollutants in wastewater but has rarely been used in the treatment for mining wastewater, despite the fact that numerous researchers have demonstrated the ability of activated carbons for its removal. For instance, adsorption with AC has been demonstrated for extraction of uranium from monazite [65]. However AC has some disadvantages, some researchers reported that high temperature (around 500 - 700 ºC) is needed during the pyrolysis for the production of AC [59, 65]. Therefore, this makes AC rather costly to be used in large-scale applications, with high-performance AC adsorbents being marketed at market prices of around USD $20-22/kg. In addition, the regeneration of AC is not favourable, which usually requires chemical processes, and certain cases need thermal-induced which is very costly and causes adsorbent loss. Thus, alternative for this is required and researchers are striving to develop more effective adsorbents for the said application.

2.5 Polymer Adsorbent

Adsorption process by polymer adsorbent offers flexibility in design and operation, and can be considered economical as the regeneration of the polymer adsorbent is possible [66]. The adsorption process is proven to produce high-quality treated effluent, and, in some cases, the recovery of the pollutant is undertaken. However, the removal of pollutants from water not an easy task since there are large number of variables have to

be considered. These variables include solution composition, pH of the solution, presence of organic contaminants and many more. In addition, these pollutants usually exist in water at low concentration and often are in complex mixtures. Therefore, robust polymer adsorbent with specificity, but yet have high efficiency towards the removal of pollutants from wastewater must be made available to meet the purpose.

A very high efficiency and selective adsorbent which tailored for specific target species is a huge challenge encountered in the removal of pollutants in wastewater. Even at a very low concentration, contamination of water resource can cause adverse health effect due to its toxicity. Since wide variety of pollutants does not degrade in nature, effective removal from aqueous solutions either physically or chemically is important to protect the environmental quality and public health [67]. There is wide range of polymer adsorbent commercially available in the market, such as amberlite [68] and various researchers have been investigating for more practical and functional polymer adsorbent which varied from physical, chemical, biological and economical properties to meet the purpose. The properties of an adsorbent such as surface morphology, elemental composition, surface area and pore size, and importantly, the functional group incorporated in the adsorbent will affect their adsorption capacity and efficiency relatively. Various adsorbents have been studied, such as AC [69], clay-based adsorbents [60], polymeric-based adsorbents [70], synthetic and natural-based resins [71], metal oxides [63], and lignocellulosic materials [72].

2.6 Development of Ion-Imprinted Adsorbent

Adsorption processes are recognized as among the most effective and inexpensive treatment of contaminants in aqueous solution, attributed to its flexibility in design and operation. Another value-added to this technique is its ability to produce high quality treated effluent. Many researchers have demonstrated the possibility for the regeneration of the adsorbent for cost-saving and in some cases, the recovery of the targeted adsorbate for further use, making it economically feasible [73-75]. A wide range of adsorbents have been investigated for different applications by various researchers. There are several modification techniques for the polymer such as polymerization reactions, grafting, followed by functionalization, copolymer formation, chain extension, crosslinking, branching, and controlled degradation [76]. A summary of various techniques for the synthesis of adsorbent and the comparison of each technique is presented in Table 2.4.

The concept of molecular recognition has been widely investigated, where Wolf and Sarhan first introduced the approach to synthesize molecular imprint polymer (MIP) by covalently preorganized template and monomer in solution prior to polymerization in 1972 and later on detailed out the synthesis and application in 1977 [77]. Following this, another approach was introduced by Mosbach and Arshady in 1981 where they utilized the non-covalent interaction between the template and monomers for the synthesis of MIP [78]. By combining these two methods, another approach known as semi-covalent approach was introduced by several researchers later on, where the strong covalent bonds were utilized in the imprinting step and the non-covalent interactions were being used in the recognition process.

Table 2.4. Existing research on adsorbent and comparison on various synthesis techniques

Synthesis Technique	Experimental Procedures	Advantages	Disadvantages	Ref.
Bulk	• Monomer, crosslinker, solvent and initiator are polymerized together. • Products are ground into fine powder/particles before adsorption.	• Experimental requires fewer steps and fairly easy. • In some cases, free from surfactant.	• Irregularity in shape and size. • Poor purity. • Poor yield. • Hard to explain the mechanism. • Difficult to control polymerization. • In some cases, low surface areas.	[79]
Emulsion (bulk)	• Micelles are stabilized with the addition of surfactants in non-solvent media. • Uniform size of polymer beads is obtained from the dispersion/ suspension of an emulsified solution.	• Uniform polymer, more control on the size, higher yield due to the use of non-solvent media.	• Poor purity due to the addition of surfactant. • Hard to explain the mechanism.	[80]
Precipitate/ Suspension	• Monomer, initiator and solvent are dissolved or dispersed in a media. • The polymer precipitates to form polymer beads. • If mechanical stirring is in use, the polymer beads are suspended from droplets of the solution. • In either case, the use of surfactant is optional.	• Experimental is fairly simple. • In most cases, no surfactant is needed.	• Poor yield. • Very hard to obtain uniform polymer beads. • Hard to explain the mechanism. • Difficult to control polymerization	[81]

Graft polymer	• Monomers are covalently bonded and polymerized onto the main polymer substrate/backbone. In emulsion graft polymerization, water is used instead of the solvent. An initiator is unnecessary in radiation-induced graft polymerization.	• Easy to synthesize. High efficiency. • Good recyclability. • Cost-effective.	• Not selective	[82, 83]
Molecular imprinted polymer (bulk)	• Monomer, crosslinker, solvent and initiator are polymerized together in the presence of a template molecule. The template molecules are removed afterward to leave behind a cavity that is complementary to the template.	• Selective. • In most cases, no surfactant is needed.	• Hard to explain the mechanism. • Difficult to control polymerization.	[17, 84]
Grafted ion-imprinted polymer	• Modification of grafted adsorbent. Cavity is formed by adsorbing the template ion onto the grafted adsorbent, followed by crosslinking.	• Step to step procedure, thus easy to understand the mechanism. • Selective.	• Difficulties to explain the structure of the polymer after crosslinking	This study

Over the past decades, the research on imprinted polymer has undergone tremendous progress. Evolution of the numbers of publication reported on imprinted polymers are increasing every year as shown in Figure 2.2, initially increased significantly since the year 2000 and then fell into saturation at around 1,000 publications/year about five years ago. However, the large number of publications showed the high demand for imprinted polymer and researchers are still struggling to better understand the characteristic, mechanism and properties of imprinted polymers.

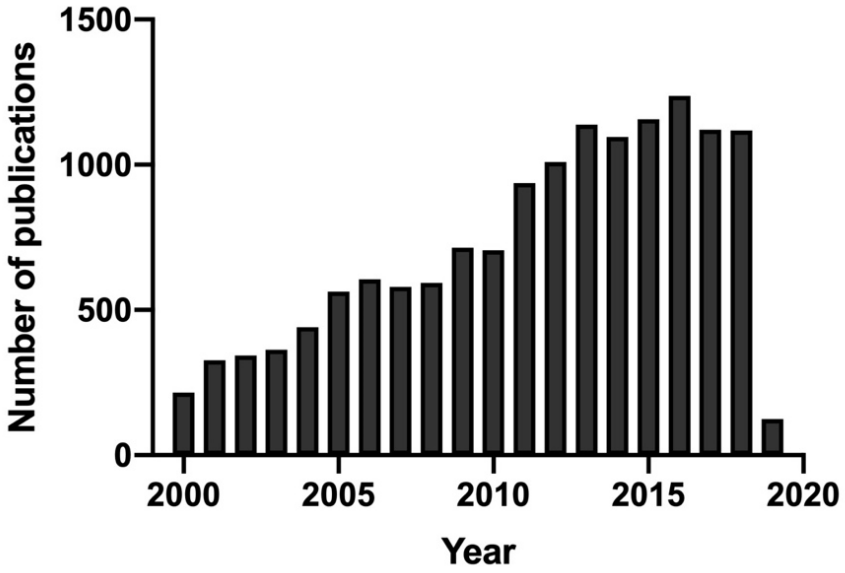

Figure 2.2. The number of publications within the field of the molecular imprinted polymer. Data (until the first half of 2019) were retrieved from the MIP database [85]

2.6.1 Synthesis of Ion-Imprinted Polymer

Although molecular imprinting field is considered a matured technology, the technology for ion imprinting is still in its infancy. Ion-imprinted polymer (IIP) technology is very similar to molecular imprinting technology, only the differences is that while retaining all the characteristics and virtues of MIP, IIP recognize metal ions after imprinting [86]. Generally, IIP is defined as an advanced functional polymer which recognized and highly selective towards certain ion (template ion) in the presence of different competing ions from the same matrices [87]. In addition, IIP also is referred as coordination polymer. In a metal-containing coordination polymer, the metals coordinate with ligands to form complexes. Generally, IIP is synthesized from a combination of

functional monomer or ligand, a template, a crosslinker and in certain cases, an initiator. There are several techniques reported in the literature on the synthesis of metal-containing coordination polymer as follow;

(i) Bulk:

Complexation between the ligand and metal in the backbone, and crosslinking occurs concurrently to form three dimensional network during polymerization [88]. During the complexation process, the ligands simultaneously attach themselves to the metals and form a vast array of structure. At the same time, the complex is surrounded by crosslinker and form a three-dimensional network to serve as cavities.

(ii) Ex-situ:

Polymer containing complexing ligand moieties is pre-prepared. Coordination polymer is formed by chelating the metal ions to the polymer [89]. The binding sites of the ligand capture the metal ions. Subsequently, the chelated polymer is subjected to crosslink giving the structure of network polymer cavities.

(iii) In-situ:

Copolymerization of a ligand that already complex with the metal to another polymer backbone [87]. The complexation is done before the polymerization. Next, the ligands that have already complexed with the metals is polymerized with/onto the polymer backbone.

2.6.2 Types of Polymer Adsorbent

Wide range of adsorbent for different kind of pollutants have been studied and developed over the years by various researchers. Table 2.5 summarized the classification of these adsorbents that are varied from the types of adsorbent, target pollutants and their adsorptive properties.

Table 2.5. List of adsorbents (including imprinted polymer adsorbents) and its corresponding pollutants

Types of pollutant	Target elements	Competitors	Precursors/ Support	Ligands	Initial concentration	Q_e (target element)	Ref.
Heavy metals	Cu(II)	Ni(II), Zn(II)	Bulk	Itaconic acid	10 mg/L	14.8 mg/g	[90]
	Cu(II)	Co(II), Ni(II)	PET film	Acrylic acid	2000 mg/L	55.6 mg/g	[91]
	Cu(II)	Zn(II), Pb(II), Fe(III)	Montmorillonite clay	Diazonium salt	20 mg/L	23.6 mg/g	[92]
	Cu(II)	Pb(II), Fe(III), Ni(II), Cd(II), Co(II)	Lignocellulosic waste (Paper)	Iminodiacetic acid	0.2 mM	0.26 mol/kg	[93]
	Cu(II)	Pb(II), Fe(III), Ni(II), Cd(II), Co(II), Al(III), Zn(II), Ca(II), Mg(II)	Bulk	Thio-semicarbazid	1.0 μg/mL	38.8 mg/g	[90]
	Cu(II)	Zn(II)	Bulk	Alginate/chitosan	50 μg/mL	83.33 mg/g	[94]
	Cu(II)	Co(II), Fe(II), Ni(II), Zn(II)	Bulk	Allylthiourea	100 μg/L	18.5 mg/g	[95]
Radio-active elements	Th(IV)	U(VI), Ce(III), La(III), Zr(IV)	Silica gel	Methacrylic acid	50 μg/mL	33.2 mg/g	[96]
	Th(IV)	La(III), Sr(II), Fe(III), Zn(II), Ni(II), Co(II), Cu(II)	Chitosan	Triethylene tetramine	50 μg/L		[97]

Th(IV)	U(VI), Eu(III), Yb(III)	Bulk	Bis (2-methacryloxyethyl) phosphate	20 mg/L	33.3 mg/g	[98]
Th(IV)	U(VI)	Bulk	Bentonite	2000 ppm	77.7%	[99]
Th(IV)	U(VI), La(III), Ce(III)	Bulk	N-methacryloyl-(l)-glutamic acid	10 mg/L	40.44 mg/g	[100]
Th(IV)	U(VI), La(III), Ce(III), Nd(III)	Magnetic Fe_3O_4 particle	N,N′-bis(3-allyl salicylidene)o-phenylenediamine		42.54 mg/g	[101]
U(VI)	Th(IV)	Polypropylene	Amidoxime	6.73 ppm	8.82 mg/g	[102]
U(VI)	Fe(III), Ca(II), Mg(II), Al(III), Zn(II)	Methacrylic acid	Salicylaldoxime/4-vinylpyridine	50 μg/L	141 mg/g	[103]
U(VI)	-	Vinyltriethoxysilane coated cellulose	4-vinylpyridine	100 mg/L	133.95 mg/g	[104]
U(VI)	-	Bulk	Chitosan	20 μg/L	2.12 mg/g	[105]
U(VI)	V(V)	Polypropylene	S-1-dodecyl-S-(α,α-dimethyl-α-acetic acid) trithiocarbonate	2×10^{-5} mol/L	133.3 mg/g	[106]

2.7 Radiation Processing of Polymers

Innovation in the field of radiation processing remains active in the research and development area which shows a great interest for future commercial use. Radiation processing of polymers offer an environmental-friendly and green method for the preparation of advanced and novel material with value-added properties compared to chemical processing. Chemical processing mostly required high temperature, high pressure for material synthesis or modification. Catalyst is also needed to speed up the reaction. The radiation technologies can initiate chemical reactions at any phase (gas, liquid or solid) without the use of catalyst [107, 108].

Synthesis of polymer can be achieved through various number of polymerization mechanisms. However, many would prefer polymer modification over synthesis of new polymers due to the fact that it is usually less costly and can be achieved more readily. In order to meet specific end-use requirements, tailor-made material is developed through modification of existing polymer by controlling the composition and structure of the polymer molecule. This will determine the performance of the polymer for it to function properly in a given application. Modification will therefore control the properties (chemical, physical, etc) of the polymer. Main approaches for polymer modification are through modification of the composition of the structural units and chemical nature of the trunk polymer which will contributes to the properties of the resultant polymeric products [109].

Crosslinking, degradation, grafting and polymerization are the fundamental radiation processes for polymers [110]. Each process is defined as below;

(i) Crosslinking:

Crosslinking occurs when chains of polymers are joined and formed a network. The natural polymers (such as fibers, cellulosic materials, natural rubber and latex) or the synthetic polymers (such as polyethylene (PE), ethylene-vinyl acetate (EVA) and polyvinylidene fluoride (PVDF) are among the polymers that can be crosslinked by electron beam processing.

(ii) Degradation:

Degradation happens when chain scissioning process reduced the molecular weight of the polymer. Natural cellulose such as chitosan, starch is prone to degradation. Synthetic polymers such as polytetrafluoroethylene (PTFE), and polypropylene (PP) also undergo degradation upon electron beam irradiation.

(iii) Polymerization/Curing:

Electron beam "curing" (as in the case of coatings or composites) is a combination of polymerization and crosslinking using radiation, and it occurs when the monomers are polymerized onto a substrate and create a thin coating layer. Examples of electron beam curable monomers or oligomers include epoxies, acrylates, acrylamides, vinylpyrrolidone, and styrene.

(iv) Grafting:

Grafting is a surface modification that occurs when monomer is "attached" or defined as grafted onto a polymer substrate. Typical example of grafting is modification of natural fibers and cellulose using various acrylate monomers. There are several types of grafting methods, namely chemical grafting, peroxide grafting and radiation grafting.

Grafting process has been more attractive due to fast free radical formations without any toxic chemical intermediates, like initiator or catalyst. These chemicals often need long time to react and high in toxicity. Therefore, grafting is an environmental-friendly method to develop novel material with unique properties. Grafting can be accomplished by electron beam irradiation on common polymers such as PE, PP and natural polymers such cellulosic materials.

2.7.1 Advantages of Radiation Processing

Radiation-induced grafting has several advantages [111]. One of the most promising advantages of radiation grafting is the simplicity and the flexibility of initiating the reaction using various types of high energy radiation source such as gamma radiation, electron beam radiation or ultra-violet. The process can be done in wide range of temperature and in any kind of monomers, such as bulk, solution or emulsion. The polymer substrate also can be in any kind, such as fiber, powder, fabric, or granular beads,

which defined its easy handling. Radiation grafting enables polymer surface modifications with certain distinct properties. With the wide range of monomer varieties, the choice of monomer usually is based on the required properties [82]. Controllable introduction of graft chain with a high density is possible with RAFT-mediated radiation grafting. In addition, graft chains are covalently attached to the polymer substrate assuring long-term chemical stability of introduced chains with the bulk properties unchanged.

The type of radiation utilized in this study is beta radiation emitted from electron beam. A heated cathode produces electron beam radiation in a high vacuum. Then, in an electrostatic field applied between cathode and anode, the electrons emitted from the cathode are accelerated and expedited. The acceleration takes place from the cathode to the anode, where it expedited from negative high voltage potential to the grounded vessel. The accelerated electrons are often focused on the accelerator's window plane through an optical system. The energy gain of the electron beam is proportional to the acceleration voltage and is expressed in electron volts (eV) that represents the energy gained by a particle of unit charge by passing the potential difference of 1V.

The electrons only exit the vacuum chamber if they have sufficient energy to perforate the accelerator's 5-20 μm thick titanium window [112]. The power of the accelerated electrons changed as the electron beam reaches a surface of a material. They lose their energy and decelerate perpetually due to an immensely number of interactions. In an organic material, these include: ionization, excitation and capture of electron [112]. In contradiction to UV, electron beam does not require photo-initiators because the polymerization process initiate and propagate from the free radicals generated by the high-speed electrons. In addition, electron beams can be directed to materials without any thickness restriction [113]. This is done by adjusting the curtain of high-energy electrons to get the desired degree of shielding. Therefore, they are highly appropriate for polymer surface modification.

Electron beam processing offers a number of important advantages over chemical processing, as follows [114]:

(i) Improved properties:

The application of electron beams can boost and strengthen the material properties, which may not be accomplished by chemical processing. In addition, electron beam processing can be used for a wide range of polymers.

(ii) Processing advantages:

Compared to the chemical processing that induces the same type of reaction, electron beam processing induces direct electron-to-electron interactions. This will avoid production of volatile materials during cross-linking and curing, and there are no residues or by-products from the process. In addition, no strict temperature or humidity management is needed, and reactions can be performed directly after processing. The operation is highly controllable, reproducible and precise resulted from the accurate regulation of the accelerator parameters.

(iii) Environmental advantages:

Materials treated with electron beam processing can contain lower or no volatile organic compounds. This process consumes less chemical because it does not need any or using lesser toxic additives. This also will ensure the purity of the product. The process also environmental-friendly in term of it saves energy because it can be carried out at lower temperature and pressure in comparison to chemical processing.

2.7.2 Characterization Techniques

Since grafting is exclusively a surface modification process, the characterization of graft copolymers is mostly depending on surface characterization which consists surface composition, surface mapping and depth profiling. Some of the most common techniques used in surface characterization of polymers are shown in Table 2.6 [115].

Table 2.6. Most common analytical techniques used for characterization of polymer adsorbent

Technique	Probe	Information depth (nm)	Information
Scanning electron microscopy (SEM) and Field emission SEM (FE-SEM)	Electrons	2	Surface topography
Raman Spectroscopy	Light	1000	Surface composition
Optical microscopy	Light	0.1	Surface roughness, structure
Infrared attenuated total reflection (ATR-FTIR)	Infrared light	2000	Surface composition, binding state
X-Ray photoelectron spectroscopy (XPS)	X-rays	5	Chemical composition, binding state
X-ray Absorption Spectroscopy (XAS)	X-rays		Chemical structure
Ellipsometry	Polarized light	0.1	Thin surface layer
Atomic force microscopy (AFM)	Cantilever	0.05	Surface topography, roughness
Surface tension / Contact angle	Liquid drop	0.1	Surface energy
Thermal Gravimetric Analysis (TGA) and Dynamic Scanning Calorimetry (DSC)	Thermal	N/A	Physical and chemical phenomena, thermal stability
X-ray Diffraction (XRD)	X-rays		Crystallographic structure

By far, liquid chromatography mass spectrometry (LC-MS) is the most common method used for separation of the contaminant and the identification of the components that exist in the solution. On the other hand, determination of the concentration of adsorbate in the aqueous solution can be done using atomic absorption spectroscopy (AAS), inductively coupled plasma mass spectroscopy (ICP-MS), UV-Vis spectrophotometry, fluorescence spectroscopy or ion selective electrode (ISE).

2.8 Adsorption Process

Adsorption is a process of mass transfer operation, in which a substance or generally referred as adsorbate is transferred from gas, liquid or dissolved solid to a surface/solid phase or adsorbent [116]. This process will formed a molecular or atomic film with physical and/or chemical interactions on the adsorbent, which differs it from absorption – a process in which the adsorbates dissolved by or permeates the absorbent [116]. In this thesis, the review will be limited only to the case of adsorption between the liquid-solid interfaces.

The terminology of adsorption was first introduced in 1881. Later on, the experiments conducted by Kayser [66] coined in other adsorption term known as "isotherms". Following this, in 1907, Freundlich [117] discovered Freundlich equation or generally known as adsorption isotherm using a mathematical expression. Freundlich adsorption isotherm is useful to quantify the adsorption by unit mass of solid adsorbent at different isothermal variation. Freundlich isotherm has been widely used by researchers and scientists all over the world until now. 10 years later, in 1916, Langmuir [118] introduced a famous theory indicating that a monolayer was formed on the adsorbent surface and the theory is known as Langmuir adsorption theory. The adsorbed amount during an adsorption process can be measured quantitatively by the Langmuir adsorption isotherm. However, a monomolecular layer was not the only cases. This was discovered during an attempt by Brunauer and Emmett [119] to calculate the adsorbent's surface area by N_2 gas. They realized that monolayer coverage did not implied on the adsorption of gases. From the study, they concluded that the surface area can be calculated by utilizing a transition point where the monolayer completed, and the multilayer began to develop. This findings enable them to determine the surface area precisely and later on this theory is known as the famous Brunauer-Emmett- Teller (BET) theory that has been widely used even until now [120]. Since then, different varieties of adsorbents for large range of applications were developed and studied. With the advancement of various adsorption theories, the adsorption mechanism of these adsorbents has been explored.

Adsorption can be classified into two types: (i) physical interaction or physisorption, and (ii) chemical interaction or chemisorption. A comparison of physisorption and chemisorption is shown in Table 2.7 below.

Table 2.7. Comparison of physisorption and chemisorption

Parameters	Physisorption	Chemisorption
Rate of adsorption	Controlled by diffusion	Controlled by surface chemical reaction
Effect of temperature	Almost none	Positive
Enthalpy change	<10	>20
Type of interaction	Reversible	Irreversible
Specificity	Low	High
Activation energy	Small	Large

(i) Physical interaction or physisorption

The interaction of adsorptive forces and adsorbate is comparatively weak in physisorption. In addition, the activation energy is almost zero or negligible [121]. Physisorption is a process where molecular condensation occurred in the capillaries of the solid, which involves weak intermolecular forces of Van Der Waals, hydrogen bonding and dipole-dipole interactions between adsorbate and adsorbent [122]. Physisorption is a reversible exothermic process with a heat of adsorption correspond to the latent heat of condensation. The process is not site-specific and can result in mono-layer or multi-layer. The equilibrium of physisorption is attained quickly, followed by the intra-particle diffusion process of the adsorbate molecules inside the capillary pores of the adsorbent structure. The rate of adsorption varies reciprocally with the square of the diameter but usually increases with the concentration of the adsorbate and the temperature.

(ii) Chemical interaction or chemisorption

Chemisorption represents strong attractive valence forces, either by exchange or sharing electrons which are operative in the formation of new bonds between the adsorbate and the active centres of the adsorbent [122]. The chemisorption can be exothermic or endothermic depending on the magnitude of the energy changes during the adsorption process. It may vary in the range from very small to very large. The site-specific possess irreversible chemical bond involving a significant activation energy. Since the adsorbed molecules are linked to the surface by valence bonds, chemisorption can result in a unimolecular thickness of the adsorbed phase as it proceeds to occupy the

adsorption sites on the surface. Therefore, chemisorption is much stronger than physisorption.

2.8.1 Batch Adsorption

The experimental techniques for adsorption can be categorized into two; namely batch adsorption and continuous adsorption, respectively. Batch adsorption technique is the most common technique and have been employed by researchers to study the performance of adsorbent and its relationship between adsorbate with respect to different parameters. Batch adsorption test is conducted by having a specific volume of solution that contains the adsorbate to remain in contact with a pre-determined quantity of adsorbent until the adsorbate in the aqueous phase achieve the equilibrium. Different parameters such as quantity of adsorbent or contact time are adjusted accordingly to achieve the optimum condition for the adsorption process. For example, contact time to reach equilibrium depends on adsorbent dosage, concentration of adsorbate and for certain cases, agitation speed of the system also have influence on the adsorption capacity. Two important physicochemical aspects for the evaluation of the adsorption process are the equilibrium and the kinetics of the adsorption. Therefore, investigation of these parameters is essential to determine the best condition for the contacting system.

2.8.2 Adsorption Equilibrium

Adsorption equilibrium is a state in which no change can be observed in the concentration of the solute during the adsorption process [123]. Generally, during the adsorption process, the concentration of the solutes continuously changing because the adsorption and desorption of the solutes simultaneously occurs until it reached the equilibrium state. The relation between the amount adsorbed and concentration at a constant temperature can be translated as adsorption isotherm. Table 2.8 listed some of the common equilibrium adsorption isotherm that are frequently used to investigate experimental adsorption data.

Table 2.8. Summary of adsorption systems isotherms [124]

Isotherms model	Equations	Description
Langmuir	$\frac{C_e}{q_e} = \frac{1}{q_{max} b_L} + \frac{C_e}{q_{max}}$ where, C_e is the equilibrium concentration in the liquid phase in $^{mg}/_{L}$, q_{max} and b_L are Langmuir constants related to adsorption capacity and rate of adsorption, respectively.	Involved adsorption on localized sites with no interaction between adsorbate molecules on the surface and that the maximum adsorption occurs when the surface is covered by monolayer adsorbate. Based on several assumptions – the adsorbent has a finite capacity where when the equilibrium is reached, a saturation point is achieved, and no further adsorption can occur. All sites are identical and energetically equivalent The adsorbent is structurally homogenous.
Freundlich	$q_e = K_F C_e^{1/n}$ where, C_e is the equilibrium concentration of the adsorbate in $^{mg}/_{L}$, K_F and $^{1}/_{n}$ are Freundlich constants.	Empirical equation Can be used for non-ideal sorption that involves multi-layer adsorption. Applies to adsorption on heterogenous surfaces with the interaction between adsorbed molecules. No Hendry Law, no saturation limit, not structured, not applicable over a wide range of concentration.
Redlich-Paterson (RP)	$q_e = \frac{K_{RP} C_e}{1 + \alpha_{_{RP} C_e^{\beta}}}$	Capable to represent adsorption equilibria over a wide range of concentration. This equation incorporated the characteristics of Langmuir and Freundlich isotherms into a single equation.

Temkin	$q_e = \left(\frac{RT}{b}\right)\ln(C_e)$ where, ${}^{RT}/_{b} = B$, R is the gas constant (8.31 J/mol.K) and T (K) is absolute temperature. $q_e = q_s exp(-B\varepsilon^2)$	Simple expression Not applicable over a wide range of concentration. Superior in the prediction of gas phase equilibria. Lacking when representing equilibria data in liquid phase adsorption.
Dubinin-Radushkevich (DR)	where, q_s is DR constant and ε can be correlated to $\varepsilon = RT\ln\left(1 + {}^{1}/_{C_e}\right)$. The constant B gives the mean free energy E of adsorption per molecule of adsorbate when it is transferred to the surface of the solid from infinity in the solution and can be computed by using the relationship $E = {}^{1}/_{(2B)^{1/2}}$	Temperature-dependent Violate thermodynamic principle at zero loading or very low concentration Excellent for interpreting organic compounds sorption equilibria in porous solids.

2.8.3 Adsorption Kinetic

Adsorption kinetic study is important to identify the mechanism of adsorption that include the physical and chemical processes in a given system . Kinetic study was carried to determine the required time for obtaining equilibrium concentration of adsorbate, which in most cases the adsorption rate is rapid at the early contact time and then gradually approaching equilibrium. Determination of the best fit kinetic model is the common way to predict the optimum adsorption kinetic expression. Adsorption kinetic model can be divided into diffusion based and chemical reaction based. Since most of the literatures reported on the adsorption of Th(IV) process as a chemical reaction-based process, this study will only focus on this type of adsorption kinetic. The common chemical reaction based kinetic models are tabulated in Table 2.9.

Table 2.9. Chemical reaction based kinetic models [72]

Kinetics model	Equations	Linear Expression
Pseudo first order (PFO) kinetic model	$q_t = q_e(1 - exp^{k_1 t})$ where, k_1 is equilibrium rate constant of pseudo PFO kinetic model adsorption in (l/min).	$\ln(q_e - q_t) = \ln q_e - k_1 t$
Pseudo second order (PSO) kinetic model	$q_t = \frac{t}{\left({}^{1}/_{k_2 q_e^2}\right) + {}^{t}/_{q_e}}$ where, k_2 is equilibrium rate constant of PSO kinetic model adsorption in (g/mg.min).	$\frac{t}{q_t} = \left(\frac{1}{k_2 q_e^2} + \frac{t}{q_e}\right)$
Elovich	$q_t = \frac{1}{\beta}\ln(\alpha\beta) + \frac{1}{\beta}\ln t$ where, α is initial adsorption rate (mg/g.min) and β is desorption constant (g/mg).	$q_t = 1/\beta \ln(\alpha\beta) + 1/\beta \ln t$

CHAPTER 3

PRELIMINARY INVESTIGATION OF AMINE-BASED ADSORBENT AS ION-IMPRINTED POLYMER

3.1 Introduction

Polymeric materials provide good physicochemical properties, reusable, cost effective and easy to handle. Thus, polymeric materials own some advantages in comparison to other materials which favours them to be used as an adsorbent [125]. However, polymeric materials require surface modification in order to give the materials good adsorptive properties. One of the famous technique available for the polymeric material surface modification is radiation induced graft polymerization [126]. Monomer glycidyl methacrylate (GMA, Figure 3.1) are widely used as precursor monomer for surface modification of polymeric materials via radiation induced graft polymerization technique as epoxy group is susceptible to functionalization with various type functional groups [127].

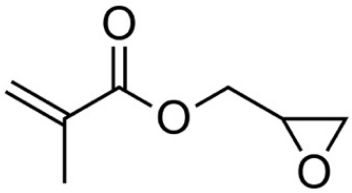

Figure 3.1. Chemical structure of GMA

The key factor to determine the effectiveness of the adsorption process is the effective interaction between adsorbates and the adsorbent's functional groups. Functional groups containing phosphorus (such as phosphoric acid, phosphate, phosphono), groups containing nitrogen (such as amine, amide, imide), and groups containing oxygen (such as hydroxyl, carbonyl, carboxyl) are among the common

functional group used for the synthesis of adsorbent due to their excellent adsorptive properties. Among all the functionalization precursor agents, amine had imposed excellent chelating properties towards transition metals to form strong complexes due to its high reactivity. Previously, numerous substrates such as cellulose [72], polystyrene [128], polyethylene non-woven fabrics [126] and poly(glycidyl methacrylate) (PGMA) [129] have been modified with different amines in order to prepare adsorbent for the removal of heavy metal ions from aqueous solution. Surface functionalization of polymer materials with PGMA were preferred in most of the studies, as PGMA exhibit unique properties. PGMA shows good mechanical strength, high acid-base resistance, high porosity and reactive epoxy group which can be easily modified by various functional groups [127, 129, 130].

Aliphatic amines such as ethylenediamine (EDA), diethylenetriamine (DETA), triethylenetetramine (TETA), and tetraethylenepentamine (TEPA) as shown in Figure 3.2 were commonly used to functionalize PGMA based materials for the removal of metal ions. Numerous studies had been conducted to identify the relationship in between efficiency of metal ions removal with molecular chain length of the aliphatic amines [64, 72, 131]. Studies had been specifically carried out to investigate the role of amine with a longer molecular chain and amine group density on metal ion adsorption capacity [126, 129]. However, despite many studies reported on metal ion adsorption capacity varies on numerous amines, nothing was emphasizing on the enhancement of metal ions selectivity upon crosslinking. Thus, this study focused on selective adsorption of metal ions by adsorbents functionalized with different aliphatic amines. The adsorbents were synthesized by combination of radiation crosslinking and ion recognition polymerization technique. Ion-imprinted polymer (IIP) works based on preorganized functional monomer interaction with imprinted ion via ascertain chemical interface among them by the aid if crosslinking process thereafter [17]. Therefore, recognition of imprinted ion is possible by the present of specific binding sides onto IIP materials which supports the higher selectivity for the rebinding of imprinted ion.

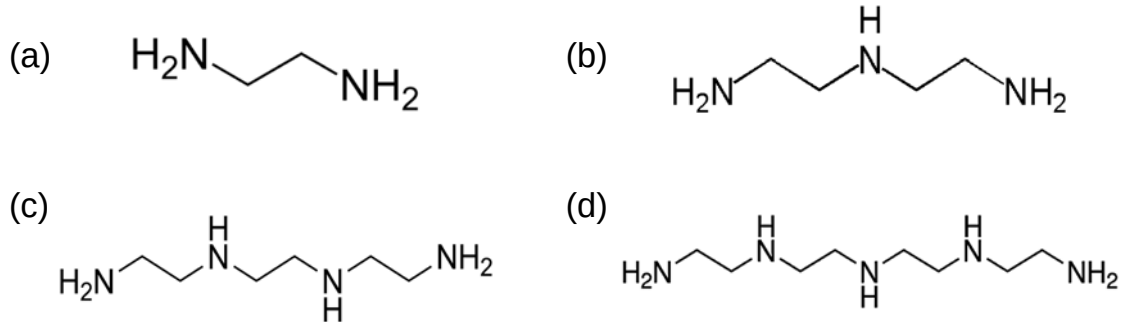

Figure 3.2. Chemical structure of (a) EDA, (b) DETA, (c) TETA, and (d) TEPA

In order to understand the mechanism of the imprinting process, a preliminary investigation was undertaken in this study using polypropylene coated polyethylene non-woven fabrics (PE/PP-NWF) grafted with GMA via radiation graft polymerization technique. Subsequently, the radiation grafted GMA-based adsorbent (GMA-g-NWF) were subjected to chemical functionalization with different aliphatic amines to provide a first impression whether the imprinting ideas conceptualized herein are indeed viable. The amine functionalized GMA-g-NWF were subjected to radiation crosslinking process with divinylbenzene (DVB) for the preparation of ion recognition samples. Prior to radiation crosslinking process, the amine functionalized GMA-g-NWF subjected to adsorption of Cu(II) ion for the preparation of IIP sample. Finally, adsorption of Cu(II) ions was carried out in binary metal ions system in order to examine the selectivity of the IIP sample. The effect of different aliphatic amine onto adsorption capacity and selectivity of the prepared IIP sample was investigate thoroughly.

3.2 Experimental Section

3.2.1 Materials

The polymer trunk, PE/PP-NWF used in this study was obtained from Kurashiki Textile Manufacturing Co. Japan. Monomer, GMA (97% and polyoxyethylene sorbitol ester (TWEEN20) were purchased by Tokyo Chemical Industry Co. LTD. Chemicals: EDA, DETA, TETA, and TEPA used for modification were purchased from Kanto Chemical Co. Inc. Isopropanol (IPA, solvent) used in this study was obtained from Sigma Aldrich. The Cu(II) solutions for metal ions batch adsorption studies were prepared from 1,000 ppm standard stock solution purchased from Merck Chemicals. All chemicals were of analytical grade.

3.2.2 Preparation of Amine Immobilized GMA-g-NWF for Heavy Metal Ion Removal

The GMA-g-NWF and the amine immobilized GMA-g-NWF was prepared. Prior to enhancement of selective adsorptive properties by means of ion imprint polymerization technique, the adsorbent is imposed on selectivity experiment in order to determine the selectivity tendency different aliphatic amine generally. The synthesis of amine immobilized GMA-g-NWF includes the following steps; **(i)** Radiation grafting of GMA onto PE/PP-NWF (denotes as GMA-g-NWF) and **(ii)** Chemical modification (functionalization) of the GMA-g-NWF using different aliphatic amine (denotes as amine immobilized GMA-g-NWF). The complete scheme for preparation amine immobilized GMA-g-NWF shown in Figure 3.3 (i) – (ii). The detailed methodology for the preparation of amine immobilized GMA-g-NWF will be explain briefly hereafter.

3.2.2.1 Preparation of GMA-g-NWF as Adsorbent Substrate

8 × 8 cm (approximately 0.5 g) of PE/PP-NWF sample was packed in polyethylene zipper bag and purged with nitrogen (N_2) gas to eliminate the air trapped inside the pack. Thereafter, the sample embedded in the zipper bag was irradiated with 250 keV and 1.8 mA low energy electron beam accelerator. Total irradiation dose received by PE/PP-NWF samples was around 30 kGy. The monomer, GMA (5 wt%) and surfactant, TWEEN20 (1 wt%) was emulsified with high speed homogenizer until a homogenous solution was attained and purged continuously with N_2 gas. The irradiated PE/PP-NWF was transferred into glass ampoules and vacuumed for 1 minute. The emulsified GMA and TWEEN20 solution were then transferred into glass ampoule which containing irradiated PE/PP-NWF sample. The glass ampoule was placed in water bath at 40 ^{o}C for 15 minutes for grafting process to take place. Finally, the sample was washed thoroughly with distilled water and placed in oven for overnight. The pre-irradiation grafting process parameters were determined in order to obtain final grafting yield (Dg) around 100% referring to our previous study [72] which will also assist to have considerable amount of amine density upon functionalization process with different aliphatic amine, thereafter. The Dg was calculated as in equation 3.1 below;

$$D_g(\%) = \left(W_g - W_0\right)/W_0 \times 100 \quad (3.1)$$

whereas, W_0 is the initial weight of PE/PP-NWF before irradiation and W_g is the weight of PE/PP-NWF after grafting [132].

3.2.2.2 Functionalization of GMA-g-NWF with Aliphatic Amines

Approximately 0.5 g of GMA-g-NWF (Dg≈100%), was placed into 50 ml of prepared amine solution with isopropanol. The different proportion of amine solution with isopropanol was used in order to investigate the effect of amine solution concentration onto amine density (AD). Subsequently, the ampoule was placed in water bath for chemical reaction to take place in due course. The same procedure and experimental conditions were adhered for all the aliphatic amines (EDA, DETA, TETA and TEPA) which been explored in this study. The effect of Dg, reaction temperature and reaction time on amine density in the present of different aliphatic amines were studied as well. Optimum and similar AD should be attained for all the aliphatic amines in order to achieve considerable metal ion removal capacity. The AD, was calculated as in equation 3.2;

$$AD = \frac{\left(\left(Z_i - Z_0\right)/Z_0\right)}{M} \times 1000 \quad (3.2)$$

where Z_i and Z_0 denotes the weight of the GMA-g-NWF after and before functionalization process and M is the molecular weight of amine used [133].

3.2.3 Enhancement of Selectivity Adsorptive Properties of Amine Immobilized GMA-g-NWF by Radiation Crosslinking

Selectivity adsorptive properties of amine immobilized GMA-g-NWF was further enhanced by means of radiation crosslinking to prepare the IIP adsorbent. Following the steps detailed out previously, the IIP sample was synthesized according to the additional following steps; **(iii)** adsorption of template ion (copper) onto amine immobilized GMA-g-NWF from (ii). This will follow by **(iv)** crosslinking of DVB with a complex of amine immobilized GMA-g-NWF and copper (Cu(II)) using electron beam irradiation and **(v)** desorption of template ions. The complete schematic illustration for preparation of IIP sample is shown in Figure 3.3 (iii) – (v).

3.2.3.1 Preparation of IIP by Radiation Crosslinking Process

Amine immobilized GMA-g-NWF, with AD approximately 2.0 – 2.2 mmol/g-ad was subjected to mutual irradiation induced crosslinking process in present of emulsified DVB solution. Prior to radiation crosslinking, the amine immobilized GMA-g-NWF was subjected to adsorption of Cu(II) (10 mg/L, pH 4.0) in aqueous medium which later acknowledged as IIP. Upon completion of adsorption process, the IIP was washed thoroughly with distilled water and dried in oven overnight at 50 ºC. Thereafter, the IIP was retained into zipper pack and filled with emulsified crosslink solution comprising of DVB/TWEEN20 (2:1 ratio) and subsequently purged with nitrogen (N_2) for the removal the dissolved oxygen. The zipper pack filled with IIP and emulsified crosslink solution is exposed to Co-60 gamma source with dose rate of 10 kGy/h. The accumulated dose received by the sample for each irradiation session was around 30 kGy. Sample was placed in water bath at 70 ºC for 2 hours after completion irradiation process. Finally, the samples were washed comprehensively with distilled water and dried in oven at 50 ºC overnight. Then, crosslinking percentage was calculated via gel content method ASTM D 2765-95.

3.2.3.2 Copper Template Removal from IIP by Desorption Process

Upon completion of radiation crosslinking with DVB, desorption of Cu(II) absorbed previously onto amine immobilized GMA-g-NWF sample is vital for the template removal in order to attribute higher selectivity towards Cu(II). 0.1 g of IIP sample was placed into 0.1 M nitric acid (HNO_3) and stirred for 2 hours at room temperature for the removal of Cu(II) template from IIP sample matrix. Finally, the sample was rinsed with distilled water and dried in oven at 50 ºC overnight before subjected to selectivity analysis in binary metal system.

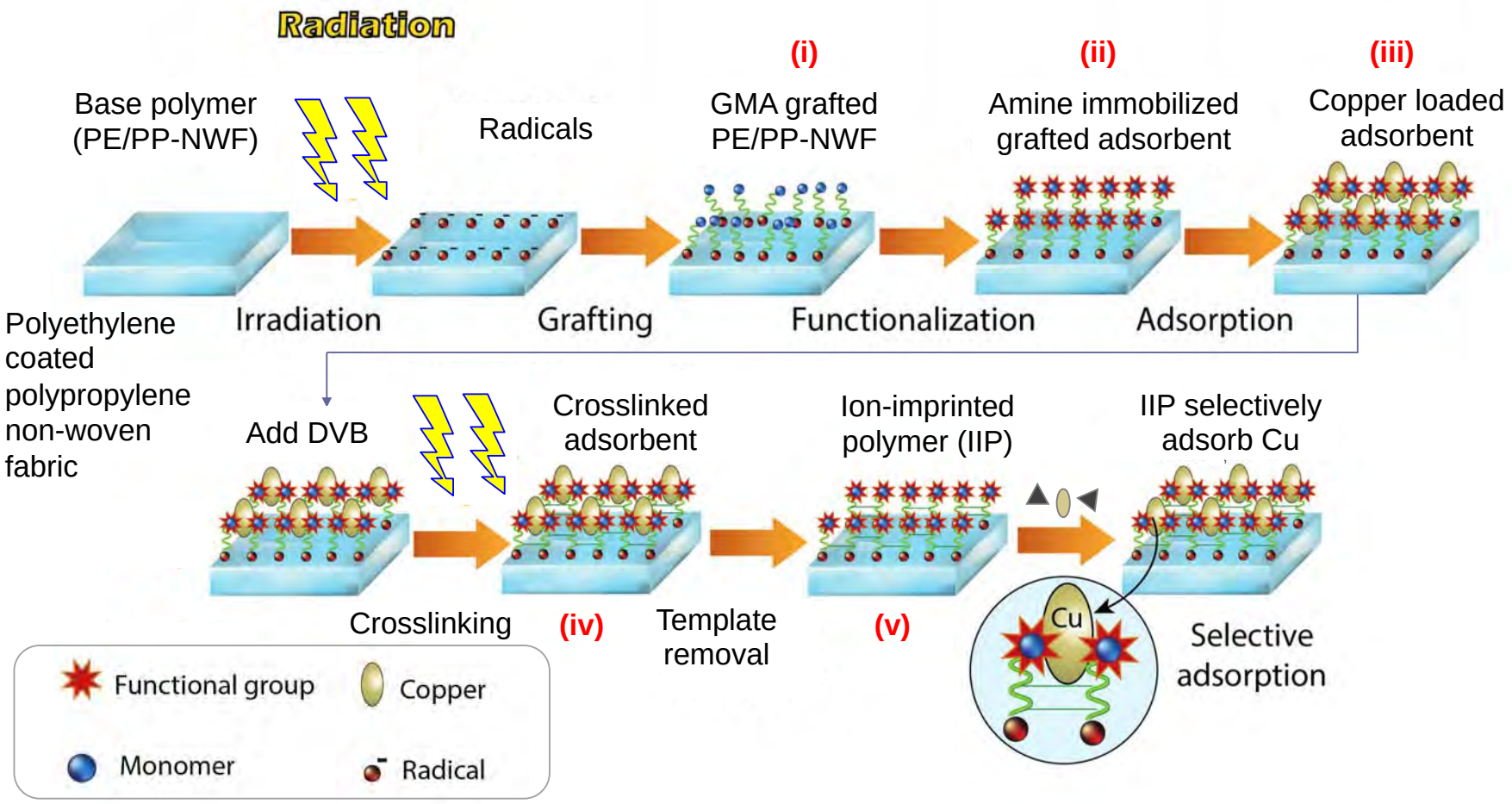

Figure 3.3. Schematic illustration of preparation of amine immobilized GMA-g-NWF and ion-imprinted polymer for copper adsorption

3.2.4 Batch Adsorption of Amine Immobilized GMA-g-NWF and IIP in Binary Metal System

Experimental procedure for adsorption process adhered to batch mode which was performed with a mixed solution of Copper (Cu(II)) and its counter ion, Lead (Pb(II)) with initial concentration of 100 mg/L. Serial dilution was carried out on the metal standard stock solution in order to attain desired concentration, 10 mg/L, concurrently. The adsorption process was conducted in the mixture of metal ion solution to validate the selectivity of amine immobilized GMA-g-NWF and IIP sample towards Cu(II). Approximately 0.05 g of amine immobilized GMA-g-NWF and IIP sample immersed into 50 mL of mixture of metal ion solution, in parallel for 8 hours with continuous stirring. The reaction time was allocated up to 8 hours to ensure equilibrium adsorption for amine immobilized GMA-g-NWF. The same reaction time for IIP was allocated for comparison purpose. The pH of mixture of metal ion solution was fixed to 4.0 for the entire adsorption process. The pH was adjusted with nitric acid with concentration of 0.5 M. The removal of metal ions from metal ion solution was assessed by the aid of Inductively Coupled Plasma - Optical Emission Spectrometry (ICP-OES). The adsorption capacity (q_e) of amine immobilized GMA-g-NWF towards both Cu(II) and Pb(II) was appraised at different time interval. The adsorption capacity (q_e) were calculated via Equation 3.3 displayed below;

$$Adsorption\ capacity\ (q_e) = (C_i - C_f) \times {}^{V}/_{m} \tag{3.3}$$

where C_i and C_e are the initial and equilibrium concentrations (mg/L) of metal ion solution and V (L) is the volume of the metal ion solution and m (g) is the mass of the amine immobilized GMA-g-NWF had been used [134].

Apart from that, the selectivity of amine immobilized GMA-g-NWF and IIP sample towards Cu(II) was also appraised under competitive adsorption in a binary solution of Cu(II) and Pb(II). The distribution coefficient (k_d) is used to assess the physiochemical behaviour of metal ion in the solution (liquid phase) with adsorbent (solid phase), while selectivity (K) is the expression for ratio of a specific ion in the presence of competitor ions. The distribution coefficient and selectivity coefficient were calculated via the equation 3.4 and equation 3.5.

$$k_d = \frac{\text{metal ion on the polymer} \times volume\ of\ the\ solution}{\text{metal ion in solution} \times mass\ of\ the\ polymer} = \frac{C_i - C_f}{C_f} \times \frac{V}{m} \quad (3.4)$$

$$K = {k_{d\ (Cu)}}/{k_{d\ (Pb)}} \quad (3.5)$$

whereby, C_i and C_f are the initial and final concentrations of metal ions (mg L^{-1}), V is the volume of solution (L), and m is the mass of the polymer adsorbent (g). $k_{d\ (Cu)}$ and $k_{d\ (Pb)}$ are the distribution coefficients of copper and lead, respectively [100] . The polymer adsorbent used here is amine immobilized GMA-g-NWF.

3.2.5 Characterizations

3.2.5.1 Field Emission Scanning Electron Microscopy (FE-SEM)

The surface morphology of the amine immobilized GMA-g-NWF and IIP samples were done by FE-SEM (Zeiss, GeminiSem 500) at 10.0 kV and 107.4 µA of voltage and current, correspondingly. The magnifications range of 200 times was used with resolution of 20 nm.

3.2.5.2 Fourier Transform Infrared (FTIR)

The amine immobilized GMA-g-NWF and IIP samples were analyzed with Bruker Tensor II (Germany) FTIR spectrophotometer. The FTIR analysis was performed in order to identify the chemical functionalities present in the corresponding samples. The measurement was carried out in with single reflection diamond universal attenuated total reflection (ATR) mode. The ATR is used in conjunction with the FTIR to enables the samples to be examined directly in the solid or liquid state without further preparation. The samples were scanned under wavenumbers from 4000 to 400 cm^{-1} at resolution of 4 cm^{-1}. The average scan was over 32 times radioed against the background. The relationship between absorbance and transmittance can be calculated using the following mathematical equations [135];

$$Absorbance, A = \log_{10}({1}/{T}) \quad (3.6)$$

According to Lambert Beer's Law;

$$I = I_0 e^{-ax} \quad (3.7)$$

where I is the transmitted radiation intensity, I_0 is the incident radiation intensity, a denotes absorption coefficients and x is the penetration length or depth. The transmittance, T is given by;

$$T = {}^{I}/_{I_0} \tag{3.8}$$

Therefore, by substituting Equation 3.8 to 3.6, the mathematical relationships can be shown as;

$$Absorbance, A = \log_{10}({}^{1}/_{T}) = a \log_{10}(e)x = a'x \tag{3.9}$$

The calculation is applied to all FTIR sample throughout the thesis.

3.2.5.3 X-ray Photoelectron Spectroscopy (XPS)

The adsorptive interaction between Cu ions in IIP samples were observed under XPS (ULVAC-PHI Quantera II). XPS functioned with an X-ray source: 25.6 W operated monochromatic Al − Kα (hν = 1486.6 eV). Samples were fixed after onto holder using double-sided tape. Wide scan analysis was executed using pass energy of 280 eV with 1 eV/step. Narrow scan was performed by using pass energy of 112 eV with 0.1 eV/step. Prior to deconvolution, charge correction was done at C 1s by set binding energies of C-C and C-H to 284.8 eV. The XPS MultiPak version 9.8.0.19 was applied to deconvolute the XPS spectra.

3.2.5.4 X-Ray Absorption Fine Structure (XAFS) Spectroscopy

X-ray absorption experiments were performed at BL5.2 of the Synchrotron Light Research Institute (SLRI), Nakhon Ratchasima, Thailand in order to determine the ligand structural coordination before and after radiation crosslinking process. The storage ring operates at 1.2 GeV and a typical current ranging from 80 to 150 mA. The beamline delivers X-rays with the maximum photon flux between 1.1-1.7 × 10^{11}#photons·s^{-1} employing a bending magnet. The synchrotron radiation was monochromatized by a commercial double-crystal X-ray monochromatic which equipped with Si (111) crystals. Calibration of photon energy was conducted by using a copper foil as a reference. Data were attained in transmission mode using ionization chamber. Spectra were collected from 200 eV before the edge up to k = 13 every 0.03 k with a three second integration

time. XAFS data were analysed using the ATHENA and ARTEMIS programs of the IFFEFIT package [136].

3.2.5.5 Inductively Coupled Plasma - Optical Emission Spectrometry (ICP-OES)

ICP-OES (ThermoFisher Scientific, iCAP 7200) with Solenoid regulation were used. The optimization of the ICP-OES parameters was done by adjusting the Solenoid regulator and the alignment of the mass spectrometer in relation to the torch (x–y adjustment) in order to obtain the maximum production of ions M^+ and minimum signals for M^{++}, MO^+ and background at m/z 220. Argon (purity of 99%) was used.

3.3 Results and Discussion

3.3.1 Radiation-induced Grafting of GMA onto PE/PP-NWF

Radiation-induced grafting of GMA onto PE/PP-NWF was carried out and the degree of grafting (Dg) was determined gravimetrically. Dg obtained based on gravimetric measurement is commonly on practice and also proven to be comparable to other methods such as NMR [137]. The effect of absorbed radiation dose on the Dg was investigated. The other parameters for radiation grafting, such as reaction temperature, reaction time and monomer concentration (including the ratio of monomer to surfactant for the emulsion) was fixed, referring to our previous study [72]. It was found that the Dg increased linearly as the absorbed dose increased from 10 to 100 kGy as shown in Figure 3.4. Since the target Dg in this study is about 100 to 150% by weight of GMA units grafted onto PE/PP-NWF, the absorbed radiation dose of 30 kGy was judged to be sufficient enough to prepare the grafted sample.

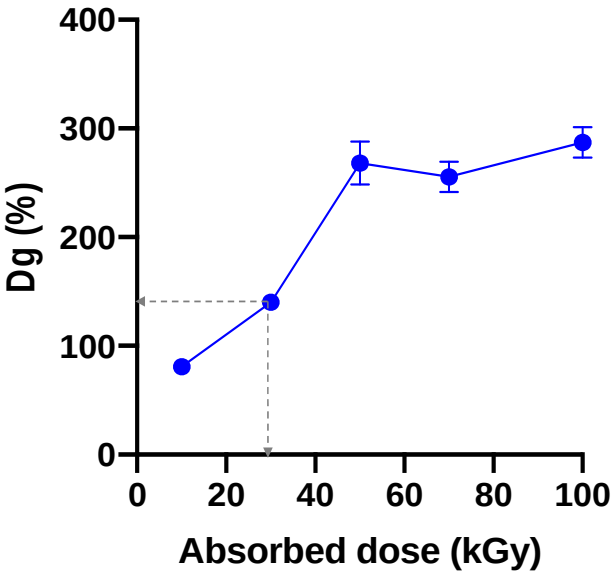

Figure 3.4. Effect of absorbed radiation dose on Dg

The successful grafting of GMA onto PE/PP-NWF was analysed with SEM. Figure 3.5 (a) shows that the surface of ungrafted PE/PP-NWF, while Figure 3.5 (b) shows the surface of grafted PE/PP-NWF with GMA. It was found that the surface of grafted sample was coated with poly-GMA layer and it looked smooth for all fibers, indicating the homogenous coating without any traces of homopolymer. Moreover, PE/PP-NWF fibers have demonstrated obvious morphological changes after grafting of GMA, which exhibited uniform surface coating.

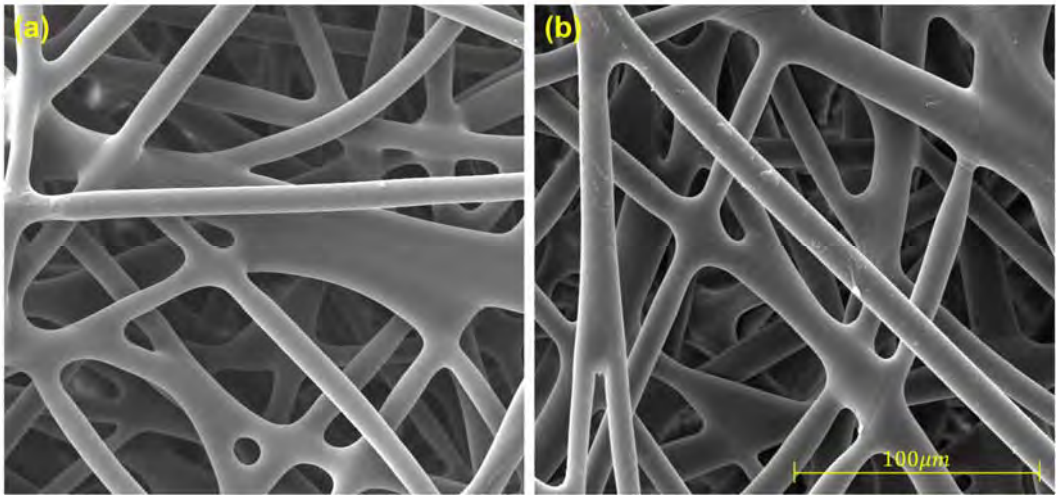

Figure 3.5. Morphological image of (a) PE/PP-NWF and (b) GMA grafted PE/PP-NWF

Initiation step started upon exposure of PE/PP-NWF to electron beam irradiation, where the radicals formed on the surface of PE/PP-NWF backbone. In the presence of GMA monomer in contact with irradiated PE/PP-NWF, the micro radicals were added onto the PE/PP-NWF via the double bond of GMA. This will lead to the formation of covalent bond between the GMA and PE/PP-NWF, which in turn, will grafted the GMA onto irradiated the fibers and consequently will propagate further until termination [82]. The reaction scheme is illustrated in Figure 3.6. Pre-irradiation grafting technique is considered as the most convenient and effective technique because it is easy to create radical sites on polymer backbone. Various functional groups can be introduced to the sites based on the aimed purpose by surface modification [138].

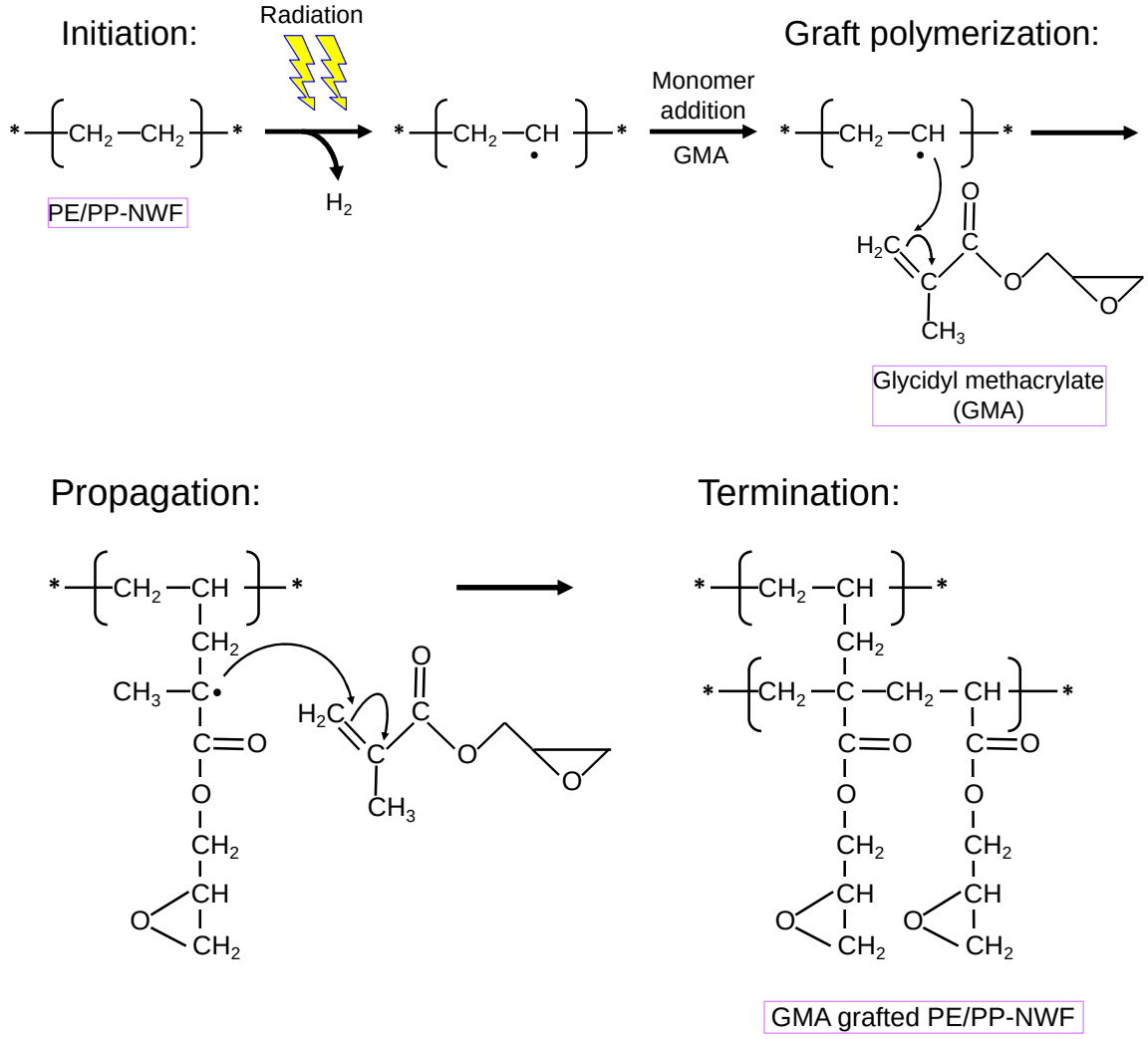

Figure 3.6. Radiation grafting of GMA monomer onto base polymer (PE/PP-NWF)

3.3.2 Optimization of Functionalization Process with Aliphatic Amines

Incorporation of functional moieties which responsible for the chelating of copper ion was carried out by chemical functionalization of different aliphatic amines onto the GMA grafted PE/PP-NWF (denotes as GMA-g-NWF). The functionalization mechanism of ethylenediamine (EDA) onto GMA-g-NWF can be proposed in two schemes as shown below (Figure 3.7). As shown in the proposed scheme, in amine immobilized GMA-g-NWF, the reaction with the epoxy group can either be from the primary amine and/or resulting in the primary amine to form secondary amino group. Same concept is applied for other aliphatic amines as well.

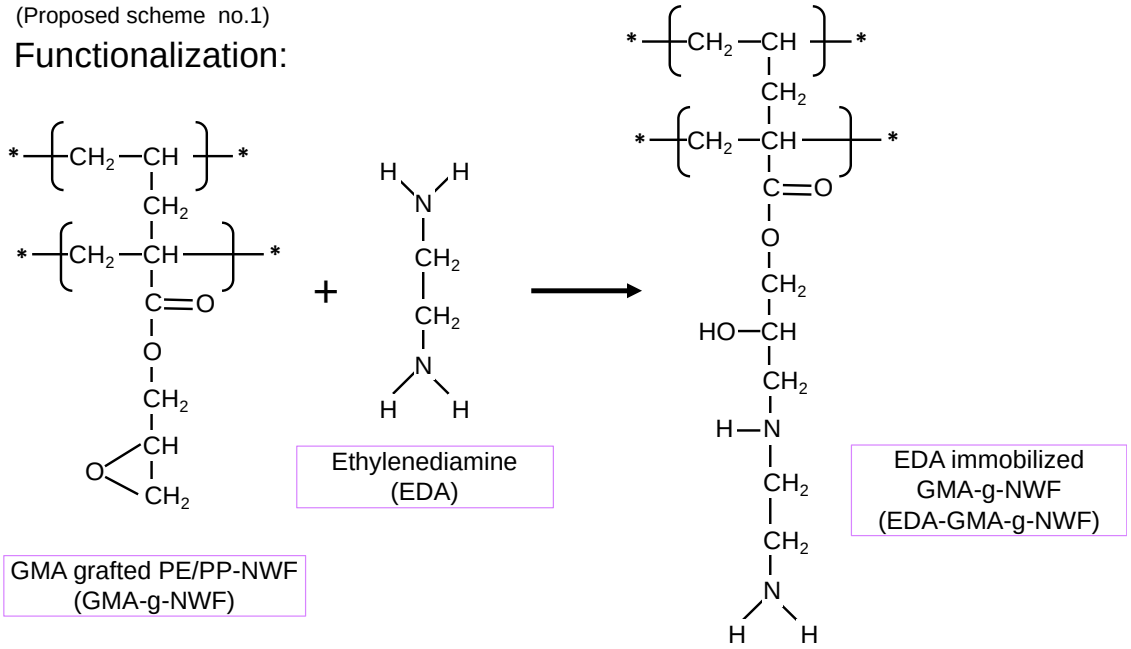

Figure 3.7. Functionalization of EDA onto GMA-g-NWF

(Proposed scheme no.2)

Functionalization:

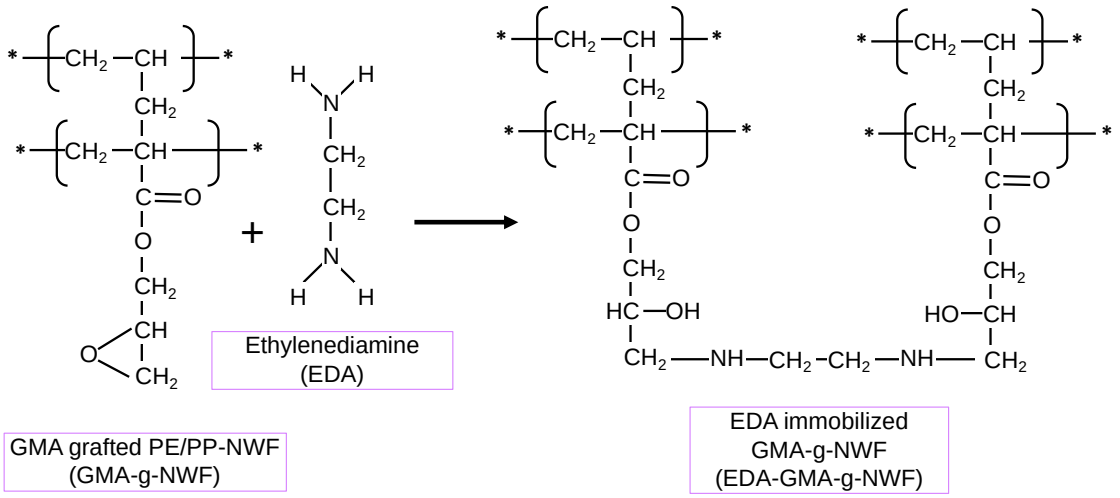

Figure 3.7. Functionalization of EDA onto GMA-g-NWF (continued)

3.3.2.1 Effect of Different Amine Composition onto Amine Density

Amine functionalization process was carried out at different composition of amine and isopropanol solution in order to investigate effect onto amine density. The composition of amine:IPA solution used was 50:50 wt%, 60:40 wt% and 70:30 wt% volume by ratio. The amine density (AD) is calculated according to equation 3.2, and the results attained is tabulated in Table 3.1. Theoretically, as the composition of aliphatic amine increases in the functionalization solution, the overall amine content should increase proportionally. However, as shown in the results, the amine density had demonstrated a descending pattern. The amine density reduces from 5.12 mmol/g-ad to 3.80 mmol/g-ad as the EDA composition increases from 50 to 70 wt%. Similar trend was observed with DETA, TETA and TEPA as well. Solvent usually play a crucial role as good swelling agent at polymer backbone in functionalization process, whereby it helps the easy approach of functional group to active sites [139]. This will eventually promote the functionalization process to take place efficiently. However, as demonstrated in the experiment, the portion of isopropanol which was used as the solvent reduced as the composition of aliphatic amine increased from 50 to 70 wt%. This leads to deceleration in efficiency of the functionalization process, which resulted to lower amine density yield.

Table 3.1. Effect of different ratio on amine density at 60 °C for 2 h, D_g = 107.4%

Aliphatic Amines	AD (mmol/g−ad)		
	50:50	60:40	70:30
EDA	5.12	4.12	3.80
DETA	4.06	3.42	3.39
TETA	3.04	2.98	3.08
TEPA	2.56	2.59	2.58

On the other hand, the number of nitrogen in the amine group of EDA, DETA, TETA and TEPA also influenced the amine density. Taking into consideration the relative amount of amine content to the number of nitrogen, it appears that the amine density immobilized onto GMA-g-NWF indeed is reducing as the number of nitrogen increased. The AD reduced with the sequence of EDA>DETA>TETA>TEPA. At composition of 50% of amine to 50% of isopropanol, EDA had attained amine density around 5.12, DETA = 4.06, TETA = 3.04 and TEPA = 2.56 mmol/g-ad respectively, as shown in Table 3.1. Among all four amines, EDA had shown higher yield of amine density. AD reduced further with the increase in number of nitrogen from EDA (2) to TEPA (5). The molecular weight and structure grow bigger as the number of nitrogen and the chain length increases . This may attribute to steric hindrance effect which prevents the fusion of amine group onto GMA chains [140]. In addition, functionalization process take place by fusion of amine group onto GMA grafted chains upon opening of epoxy group of GMA [141]. Aliphatic amines with longer chains tend to react with more epoxy group. Larger number of amines consumed more sites during the reaction, which eventually reducing the calculated nominal amine density on the GMA-g-NWF. As a result, it leads to lower amine density yield as the molecular weight and structure of EDA, DETA, TETA and TEPA progress further.

3.3.2.2 Effect of Dg onto Amine Density

The Dg of GMA-g-NWF which varies from 100 to 250% was used to examine the effect of different Dg onto amine density with multiple aliphatic amines. The amine density increases constantly as the Dg increases from 100 to 250% for EDA, DETA, TETA and TEPA. The EDA achieve the amine density of 3.35 mmol/g-ad with the Dg of 100% which increases to 4.20 mmol/g-ad while the Dg of GMA-g-NWF increases to

250%. The result obtained illustrated in Table 3.2. The same trend was observed for DETA, TETA and TEPA as well. This phenomena well explained by availability of more of epoxy groups from GMA at higher Dg for the incorporation of amine group will favourably supports the process to occur [142]. Thus, the amine density increases constantly as the Dg increases. On the other hand, amine density decreases steadily as the aliphatic amines chains grows longer from EDA to TEPA. The similar observation was obtained as the changes in Dg of GMA-g-NWF were made. Grow in the bulkiness of the aliphatic amine structure from EDA to TEPA is mainly responsible for the inefficient functionalization process further.

Table 3.2. Effect of different Dg of GMA-g-NWF on amine density at 60 °C for 2 h, 70% amine: 30% isopropanol

	AD (mmol/g-ad)			
Aliphatic Amines	**EDA**	**DETA**	**TETA**	**TEPA**
100% (Dg=105.1%)	3.35	2.36	2.34	1.64
150% (Dg=151.5%)	3.54	3.03	2.53	1.92
200% (Dg=205.6%)	4.01	3.43	2.70	2.00
250% (Dg=251.3%)	4.20	3.64	3.09	2.26

3.3.2.3 Effect of Reaction Temperature onto Amine Density

Amine functionalization process was carried out at different reaction temperature, 60 to 80 ºC in order to study the effect of temperature onto amine density. The temperature variance study was also applied onto the EDA, DETA, TETA and TEPA. The results attained exhibited in

Table 3.3. The amine density increases marginally as the reaction temperature increase from 60 to 80 ºC for EDA, DETA, TETA and TEPA aliphatic amine. The EDA achieve the amine density of 3.85 mmol/g-ad at reaction temperature of 60 ºC which increases to 3.93 mmol/g-ad while the reaction temperature reaches 80 ºC. The similar trend was observed with DETA, TETA and TEPA as well. The thermal energy accelerates the reaction process at a higher temperature which leads to higher migration rate of amine group onto epoxy group of GMA [143]. In contrast, amine density gradually reduces as

the aliphatic amines chains grows longer from EDA to TEPA even with hike in temperature. At reaction temperature of 60 ºC, EDA, DETA, TETA and TEPA had attained amine density around 3.85, 3.31, 2.97 and 2.49 mmol/g-ad respectively. This agrees well with the previous observation at assorted experimental conditions. Conclusively, the bulky structure of aliphatic amine restrains efficiency of the functionalization process predominantly regardless of any of the changes in experimental conditions. Thus, the higher amine density could be achieved by using the smallest and simplest amine, EDA.

Table 3.3. Effect of different reaction temperatures on amine density (2 h, 70% amine: 30% isopropanol, Dg = 105.9%)

Aliphatic amines	**AD (mmol/g-ad)**		
	60 °C	70 °C	80 °C
EDA	3.85	3.90	3.93
DETA	3.31	3.50	3.52
TETA	2.97	3.25	3.28
TEPA	2.49	2.65	2.71

3.3.2.4 Effect of Reaction Time onto Amine Density

The effect of reaction time had been analysed on the assimilation reaction of amine functional group onto GMA-g-NWF. The chosen reaction time was 15, 30, 45, 60, 90 and 120 minutes. The results achieved are shown in Figure 3.8. The amine density increases considerably with reaction time but reaches almost plateau around 30 minutes and thereafter, with insignificant gain was observed in amine density as the reaction increases further. The similar trend was attained for EDA, DETA, TETA and TEPA respectively. EDA had gained amine density of 2.89 mmol/g-ad at 15 minutes of reaction time which increases to 3.80 mmol/g-ad around 30 minutes but the final gain of amine density recorded was around 3.91 mmol/g-ad after 2 hours complete reaction course. Exhaustion of epoxy sites present on GMA-g-NWF is responsible for the insignificant gain in amine density after 30 minutes [133]. Correspondingly, EDA had gained the highest amine density which decreases uniformed as the aliphatic amines chains grows longer. The observation still sustained with the progress in reaction time. EDA with simplest and smallest structure was more promising to attain higher amine density in order to produce effective adsorbent.

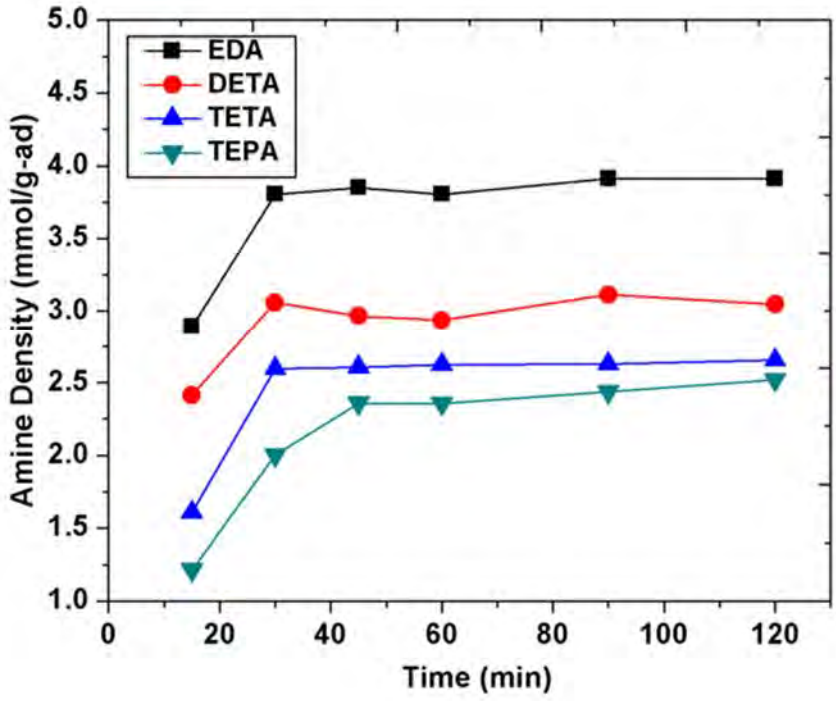

Figure 3.8. Effect of different reaction time on amine density at for 70% amine: 30% isopropanol, 60 ºC, Dg=104.9%.

3.3.3 Characteristics of Amine Immobilized GMA-g-NWF and IIP

3.3.3.1 FE-SEM

Imaging onto amine immobilized GMA-g-NWF and IIP samples which had been functionalized with EDA, DETA, TETA and TEPA, were carried out in order observe the changes in term of morphology before and after crosslinking process, respectively. The images obtained shown in Figure 3.9 – 3.10. The average diameter of pristine sample was around 12.42 µm. The average diameter of GMA-g-NWF sample obviously increased almost up to 13.44 µm. Moreover, the average diameter of GMA-g-NWF samples increased further after functionalization. The average diameter obtained for EDA-GMA-g-NWF, DETA-GMA-g-NWF, TETA-GMA-g-NWF and TEPA-GMA-g-NWF was around 14.07, 18.91, 13.10 and 13.83 µm, respectively. This finding confirms the incorporation of amine group on epoxy group of GMA via functionalization process. Among four types of aliphatic amine, DETA had shown the highest gain in term of average diameter. On the other hand, all the IIP samples shown a slight reduction in

average diameter in comparison to amine immobilized GMA-g-NWF after the crosslinking process. The average diameter obtained for EDA-IIP, DETA-IIP, TETA-IIP and TEPA-IIP was around 12.45, 12.48, 13.06 and 13.71 µm, respectively. The decrease in average diameter after crosslinking process attributed from removal of unreacted aliphatic amine. The differences in average diameter of EDA-IIP, DETA-IIP, TETA-IIP and TEPA-IIP was almost insignificant as the crosslinking process was conducted merely in the present of very small amount of crosslinking agent.

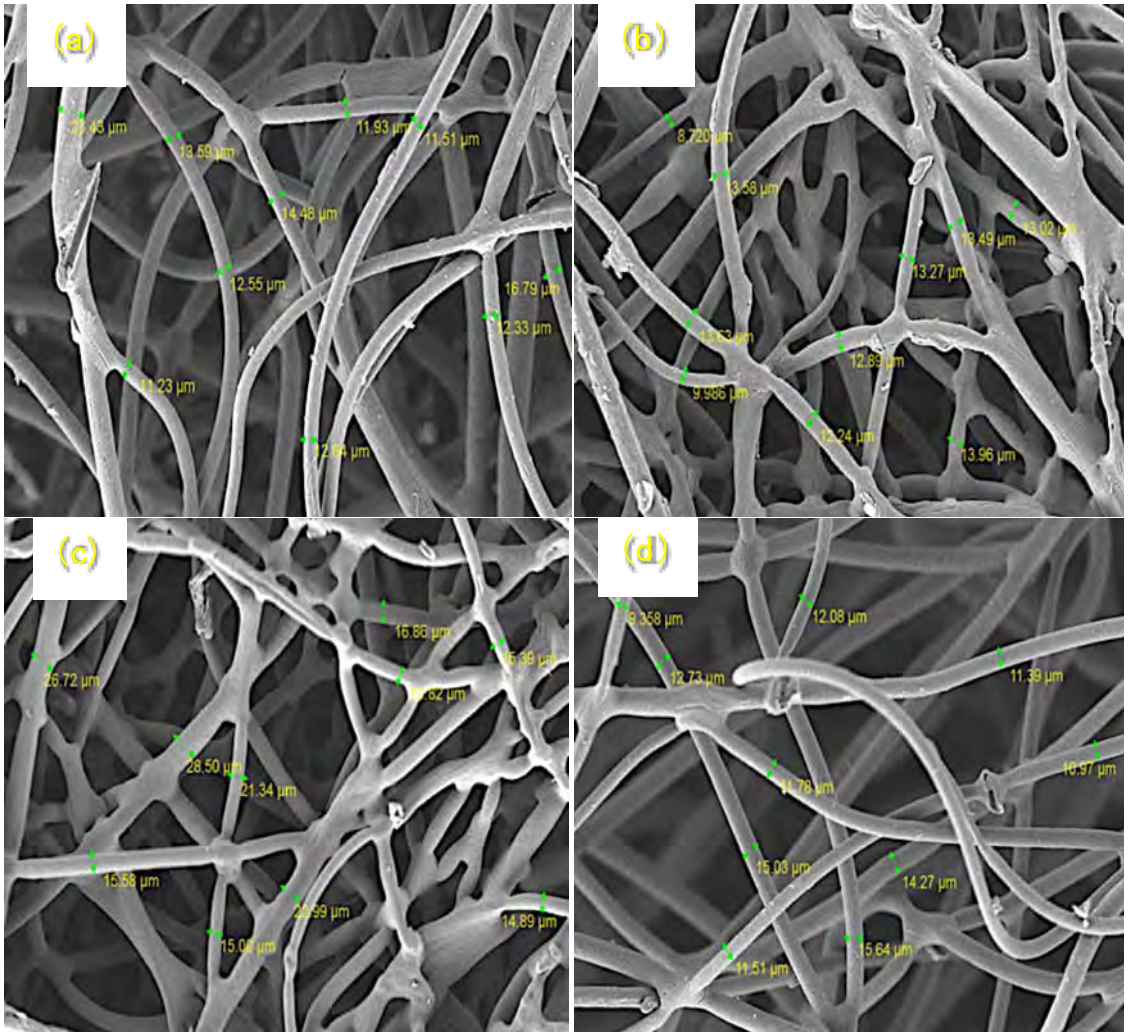

Figure 3.9. FE-SEM imaging of (a) EDA-GMA-g-NWF, (b) EDA-IIP, (c) DETA-GMA-g-NWF, (d) DETA-IIP, (e) TETA-GMA-g-NWF, (f) TETA-IIP, (g) TEPA-GMA-g-NWF and (h) TEPA-IIP at experimental condition of 70% amine: 30% isopropanol, 60 ^{o}C, Dg≈100% and 2h

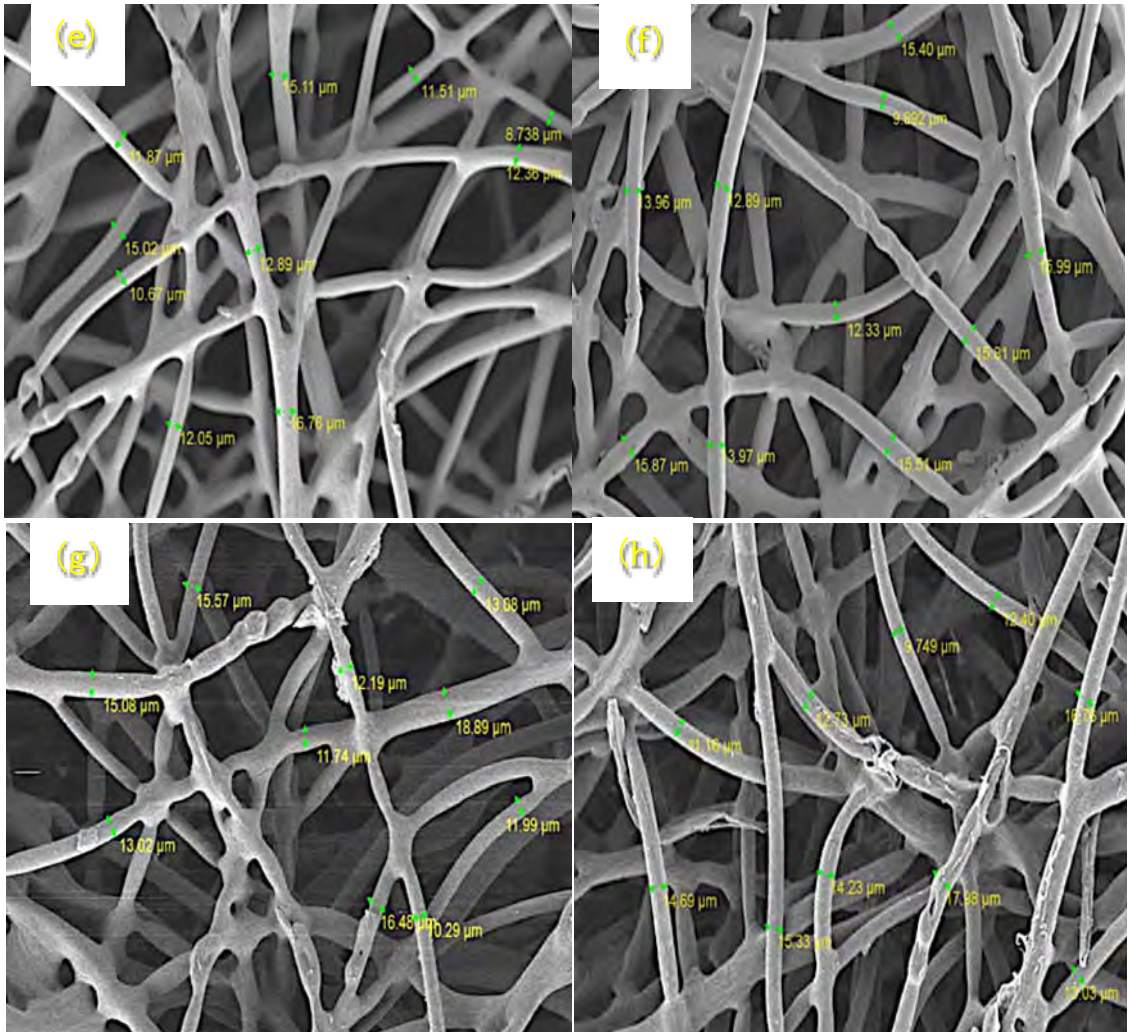

Figure 3.10. FE-SEM imaging of (a) EDA-GMA-g-NWF, (b) EDA-IIP, (c) DETA-GMA-g-NWF, (d) DETA-IIP, (e) TETA-GMA-g-NWF, (f) TETA-IIP, (g) TEPA-GMA-g-NWF and (h) TEPA-IIP at experimental condition of 70% amine: 30% isopropanol, 60 ºC, Dg≈100% and 2h (continued)

3.3.3.2 FTIR

Amine immobilized GMA-g-NWF (EDA-GMA-g-NWF, DETA-GMA-g-NWF, TETA-GMA-g-NWF & TEPA-GMA-g-NWF) and IIP (EDA-IIP, DETA-IIP, TETA-IIP & TEPA-IIP) samples were also subjected to FTIR analysis in order to identify the functional group present on the each samples, respectively. The result obtained for EDA immobilized GMA-g-NWF is illustrated in Figure 3.11 – 3.12. Both GMA-g-NWF and IIP samples exhibits common stretching for PE/PP at 2913 cm^{-1}, 2843 cm^{-1}, 1464 cm^{-1}, 1370 cm^{-1} and 718 cm^{-1} which attributed to C-H stretch (PP), C-H stretch (PE), CH_2 stretch (PP & PE), symmetric CH_3 deformation stretch (PP) and CH_2 stretch (PE) respectively [144]. Additional stretching detected at 1732cm^{-1} and 1140cm^{-1} assigned for C=O and C-O vibration which originates from –COO– ester group of GMA [145]. However, additional stretching was found, such as N-H stretching at 3201cm^{-1}, N-H bending at 1524cm^{-1}, C-N alkyl group stretching at 1256cm^{-1} and 1156cm^{-1} in the EDA-GMA-g-NWF, which attributed from aliphatic amine groups [142], after the functionalization process. Besides that, additional peaks at 831 cm^{-1} (as circled in Figure 3.12), which presented on the IIP sample is attributed to C-H stretch from crosslinking process with DVB [146]. For the other amine immobilized GMA-g-NWF samples (DETA-GMA-g-NWF, TETA-GMA-g-NWF & TEPA-GMA-g-NWF) and IIP samples (DETA-IIP, TETA-IIP & TEPA-IIP), similar peaks can be seen in all samples.

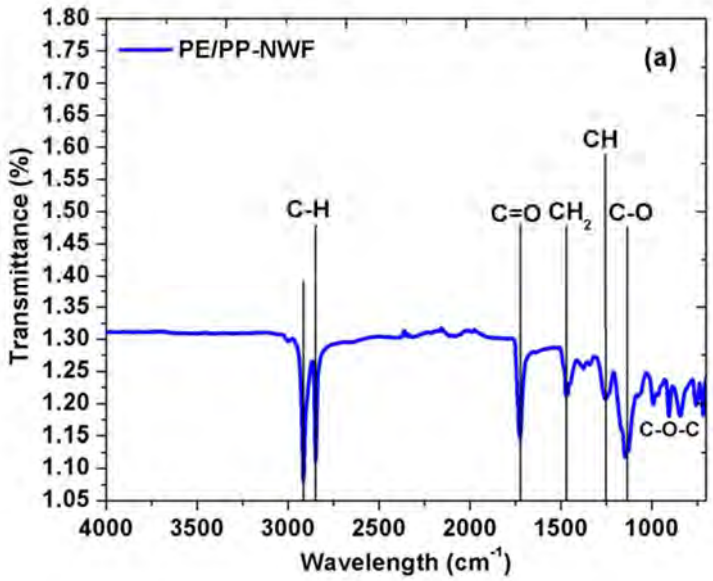

Figure 3.11. FTIR spectra of (a) PE/PP-NWF, (b) EDA-GMA-g-NWF & (c) IIP-EDA at experimental condition of 70% amine: 30% isopropanol, 60 ºC, Dg≈100% and 2h

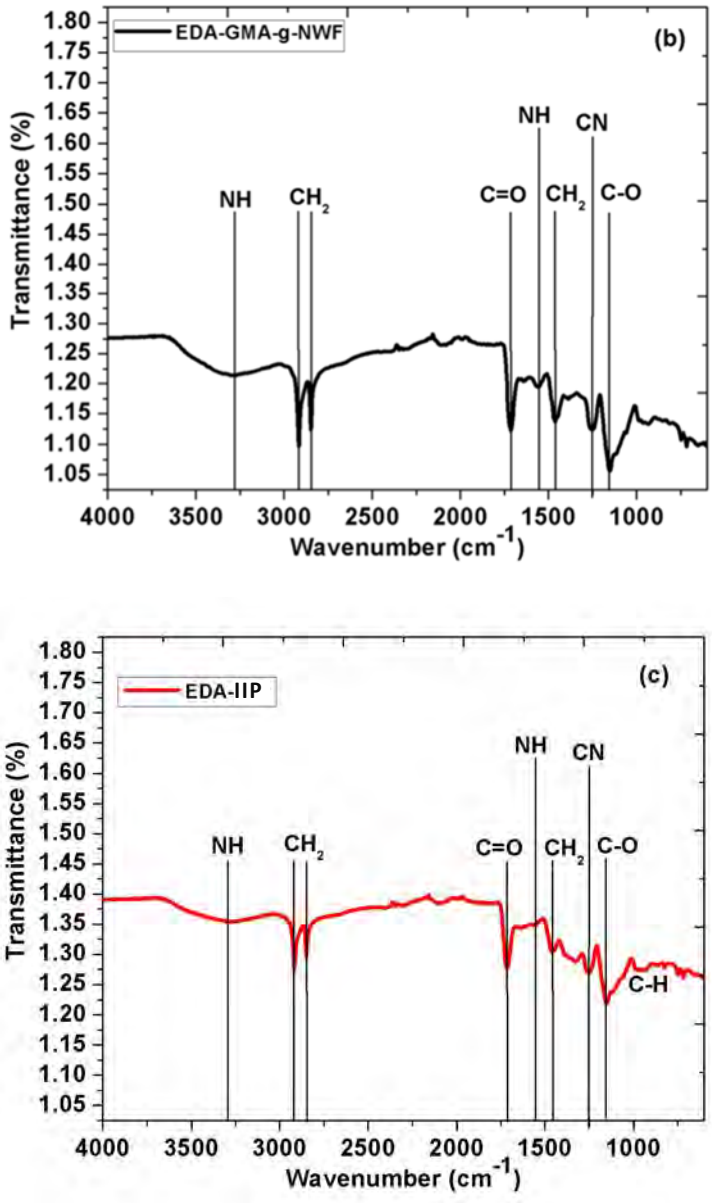

Figure 3.12. FTIR spectra of (a) PE/PP-NWF, (b) EDA-GMA-g-NWF & (c) IIP-EDA at experimental condition of 70% amine: 30% isopropanol, 60 ºC, Dg≈100% and 2h (continued)

3.3.3.3 XPS

X-ray photoelectron spectra onto IIP samples after adsorption of copper ion was had reported in this paper in order to verify the presence of metal ion into polymer matrix. Thus, only IIP samples subjected to XPS analysis. O1s and N1s orbitals were detected in IIP-EDA, IIP-DETA, IIP-TETA and IIP-TEPA samples. The result obtained showed in Figure 3.13 (a) – (d).

(a) IIP-EDA (amine density: 2.0 – 2.2 mmol/g-ad)

(i) O1s

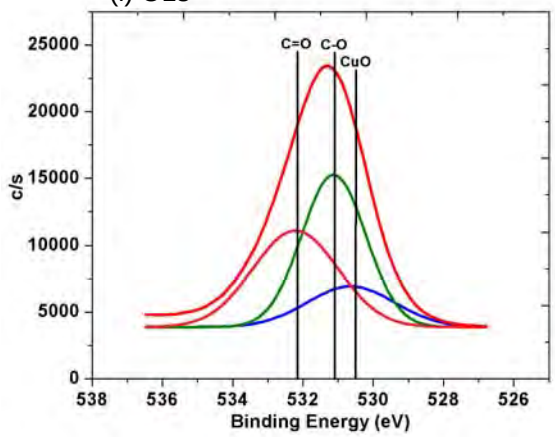

(ii) N1s

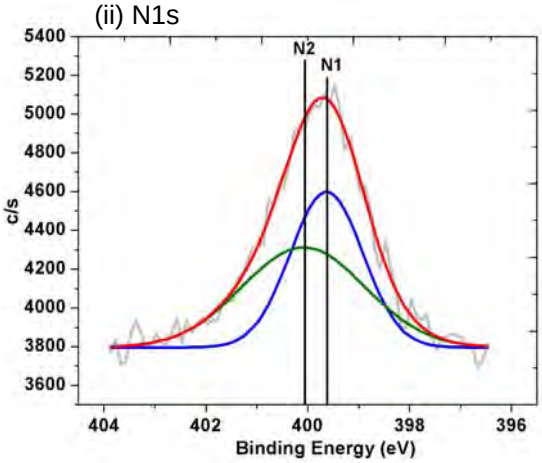

(b) IIP-DETA (amine density: 2.0 – 2.2 mmol/g-ad)

(i) O1s

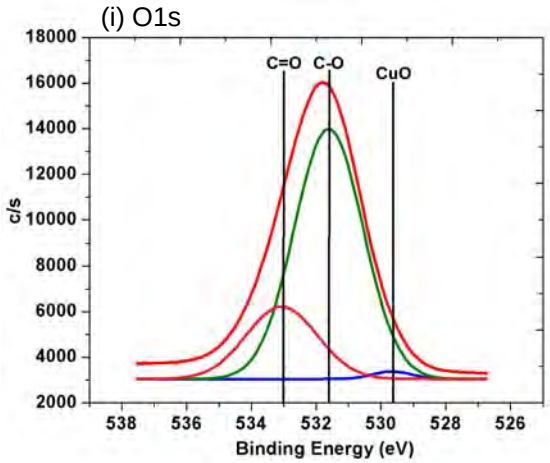

(ii) N1s

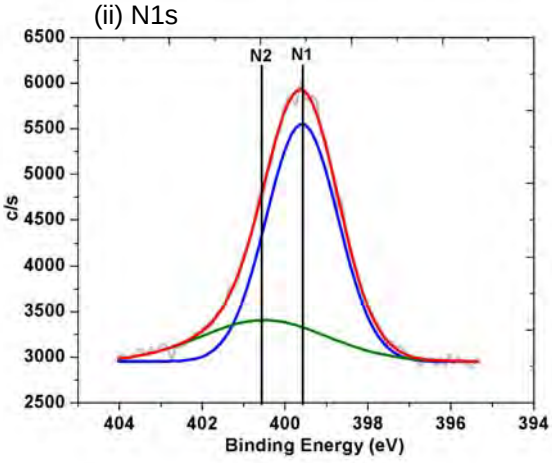

(c) IIP-TETA (amine density: 2.0 – 2.2 mmol/g-ad)

(i) O1s

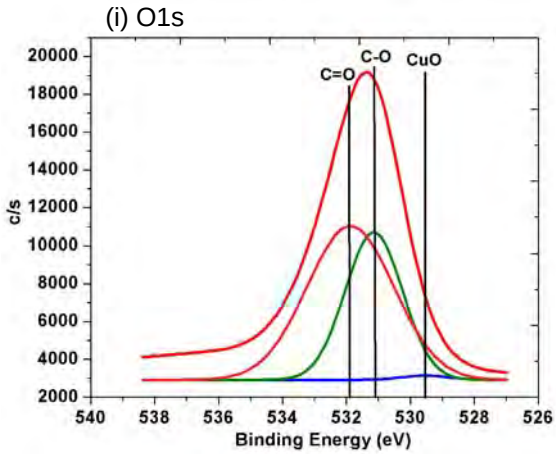

(ii) N1s

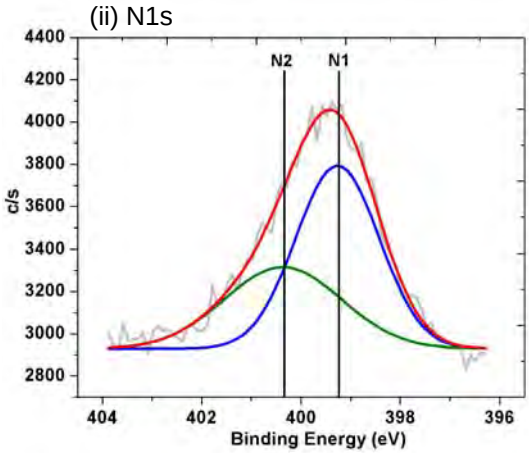

(d) IIP-TEPA (amine density: 2.0 – 2.2 mmol/g-ad)

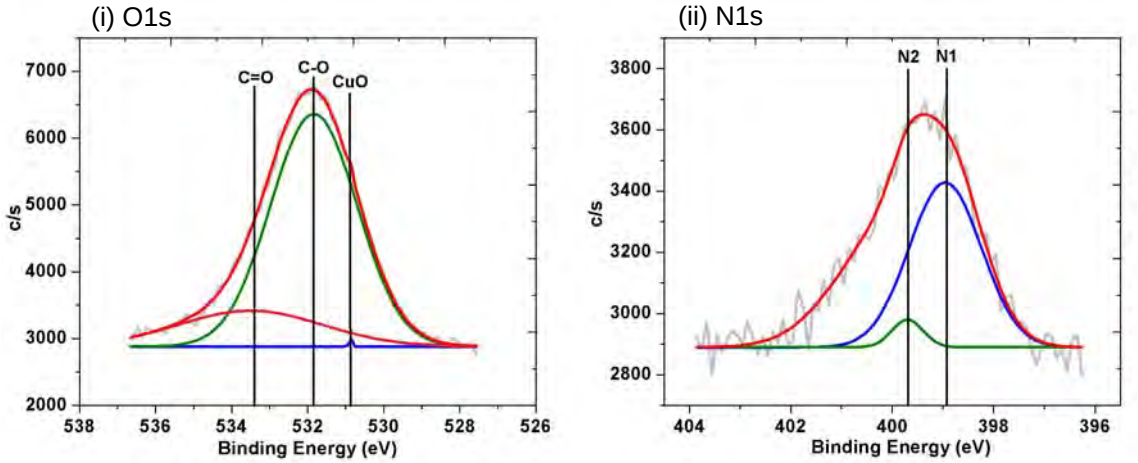

Figure 3.13. XPS spectra of (a) IIP-EDA, (b) IIP-DETA, (c) IIP-TETA and (d) IIP-TEPA

Strong peak was observed at 399.48 and 400.37 eV in the N1s and N2s which indicates primary and secondary amine groups of EDA, DETA, TETA and TEPA, respectively [147]. The O1s spectrum of IIP-EDA, IIP-DETA, IIP-TETA and IIP-TEPA samples shows presence of oxygen bonding as such C-O and C=O at binding energy of 531.70 and 533.22 eV, originating from the functional monomer, GMA [148]. The O1s spectrum of the all IIP samples exhibit a broad distribution at higher binding energy due to the presence of oxygen bonded carbon and copper concurrently in the IIP samples. The main peak at 531.70 eV attributes to the present of C-O along with binding energy at 530.30 eV indicates the existence of CuO. The XPS performed onto IIP samples had verify the chemical composition of the samples after adsorption of copper ion into polymer matrix. Conclusively, clear evidence was obtained on adsorption of copper ions onto IIP samples which attribute to detection of CuO that allowed carbonyl groups from GMA to bond with.

3.3.3.4 XAFS Spectroscopy

The local coordination environment of metal ions can be investigated with XAFS spectroscopy [149]. XAFS is also capable of determining distances, the coordination number, and the types of atoms surrounding the metal centers [150]. This XAFS information on metal system could be interpreted by fitting structurally well-characterized model complexes as a reference XAFS experimental data [151]. In this

study, XAFS was used to investigate the molecular structure of surface complexes of Cu (II) adsorbed onto both amines immobilized GMA-g-NWF and IIP samples which had been modified with a different aliphatic amine, EDA, DETA, TETA, and TEPA, respectively. The structural parameters of both amine immobilized GMA-g-NWF and IIP complexes were determined from the EXAFS spectra and reported in Table 3.4.

The main purpose of this analysis was to observe the structural changes in metal complexes after radiation crosslinking process with DVB along with different aliphatic amine. Fourier transform (FT) of EXAFS spectra obtained were exhibited in Figure 3.14 and Figure 3.15 for both amine immobilized GMA-g-NWF and IIP samples, respectively. Based on the fitting of EXAFS spectra, the Cu-O (at $\sim 4.2^{\circ}$A) and Cu-N (at $\sim 2.0^{\circ}$A) shells were observed in the Cu (II) adsorbed onto for both amine immobilized GMA-g-NWF and IIP samples. This observation indicating the formation of inner-sphere complexes on amine immobilized GMA-g-NWF and IIP samples surfaces. Different fitting values obtained for ΔR, indicate similar path for both amine immobilized GMA-g-NWF and IIP complexes, Cu-O and Cu-N. Moreover, the ΔR defined for the two axial Cu–O and Cu-N paths for all the amine immobilized GMA-g-NWF and IIP complexes. It is clear from Figure 3.14 and Figure 3.15 that Cu-O and Cu-N paths have effective contributions to the experimental EXAFS data. This finding agrees with XPS results of IIP samples in 3.3.3.3. The outcome from this study supported by another study which reported on EXAFS investigation on Cu(II) complexes [131, 152].

Table 3.4. Structural parameters of both amine immobilized GMA-g-NWF and IIP complexes from EXAFS spectra

Sample	Shell	N [a]	R [b] (Å)	σ^2 [c] (Å^2)	E_0 [d] (eV)
IIP-EDA	Cu-O	4.000	4.061	0.029	7.622
	Cu-N	6.000	2.014	0.008	3.501
IIP-DETA	Cu-O	4.000	4.085	0.004	7.100
	Cu-N	6.000	2.038	0.012	3.749
IIP-TETA	Cu-O	4.000	4.001	0.020	7.600
	Cu-N	6.000	2.014	0.010	2.652
IIP-TEPA	Cu-O	4.000	3.999	0.025	7.501
	Cu-N	6.000	2.038	0.014	4.709
EDA-GMA-g-NWF	Cu-O	4.000	4.205	0.004	4.045
	Cu-N	4.000	1.999	0.003	4.058
DETA-GMA-g-NWF	Cu-O	4.000	4.218	0.004	4.124
	Cu-N	4.000	1.993	0.003	3.882
TETA-GMA-g-NWF	Cu-O	4.000	4.253	0.004	4.253
	Cu-N	4.000	1.973	0.005	1.657
TEPA-GMA-g-NWF	Cu-O	4.000	4.240	0.007	4.240
	Cu-N	4.000	1.968	0.004	0.197

a) Coordination number, **N** is the number of atoms coordinated with Cu ion within the detection range of the photoelectron scattering.
b) Bond length, **R** is determined within 0.01 Å error range.
c) Debye-Waller factor, σ^2 is determined within 10% error range.
d) The threshold energy shift, E_0 is referred as the energy of the maximum derivative of absorption coefficient, μ as a function of energy.

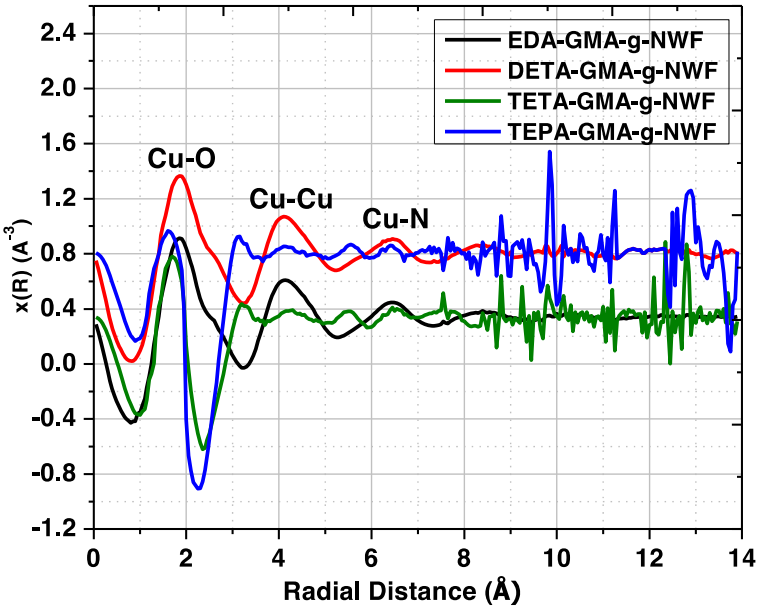

Figure 3.14. FT of EXAFS spectra of amine immobilized GMA-g-NWF prepared at experimental condition of 70% amine: 30% isopropanol, 60 ºC, Dg≈100% and 2h

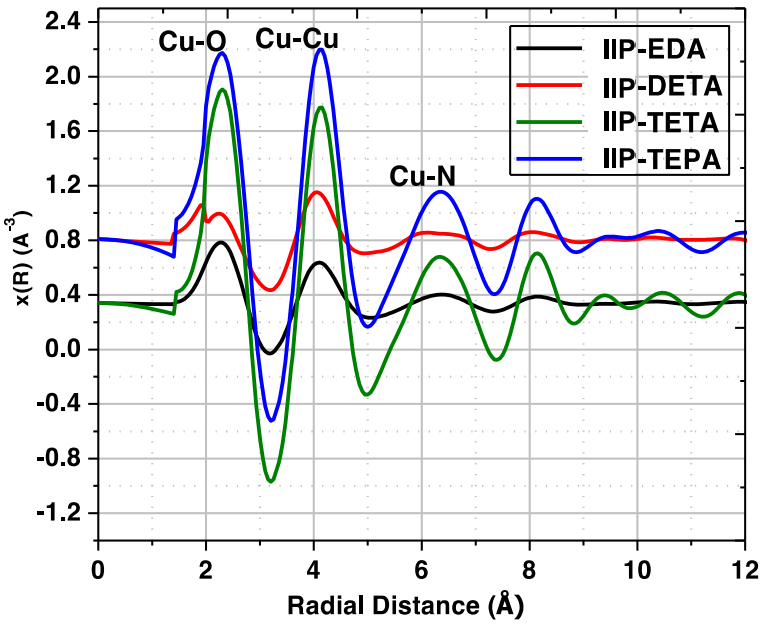

Figure 3.15. FT of EXAFS spectra of IIP prepared at experimental condition of 70% amine: 30% isopropanol, 60 ºC, Dg≈100% and 2h

3.3.4 Metal Ions Adsorption Performance

3.3.4.1 Adsorption Capacity of Amine Immobilized GMA-g-NWF and IIP Towards Copper

Amine immobilized GMA-g-NWF were subjected to adsorption of Cu(II) and Pb(II) ions in order to investigate the effect of different aliphatic amines on the adsorption capacity of copper in binary metal system. Besides that, IIP samples were used for the adsorption to investigate the effect of ion recognition technique via crosslinking process on adsorption capacity, as well. The result obtained is shown in Figure 3.16 – 3.17 (a) – (d). The experimental conditions of amine functionalization process were predetermined in order to attain amine density, (AD) approximately 2.0~2.2 mmol/g-ad provided standardized condition was applied for adsorption experiment.

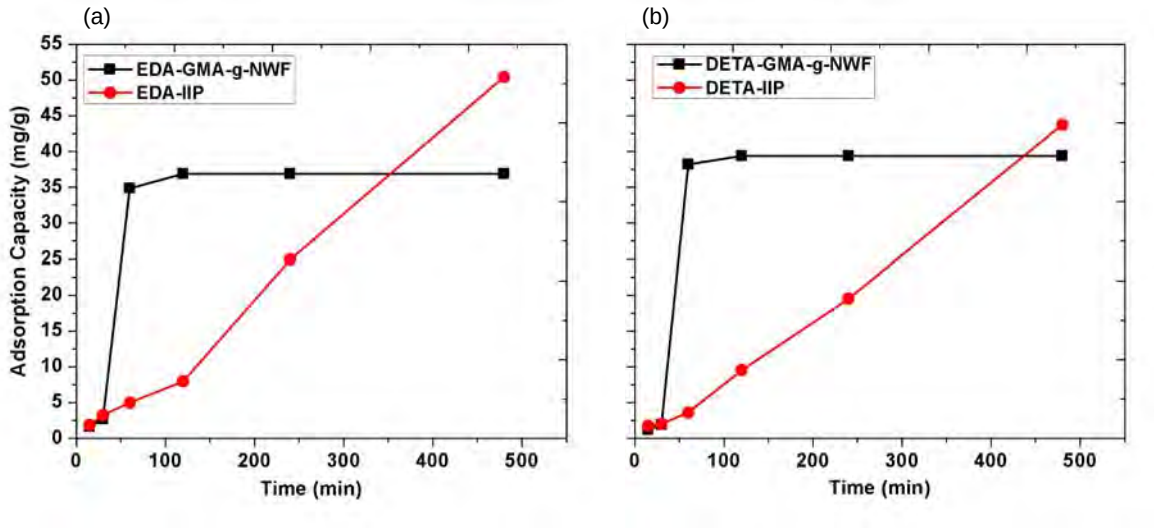

Figure 3.16. Adsorption capacity of Cu(II) versus time by amine immobilized GMA-g-NWF and IIP at experimental condition of initial copper concentration: 10 mg/L, adsorbent dose: 0.02 g, temperature: 30 ºC, amine density: 2.0 – 2.2 mmol/g-ad, stirring speed: 200 rpm and solution volume: 100 ml.

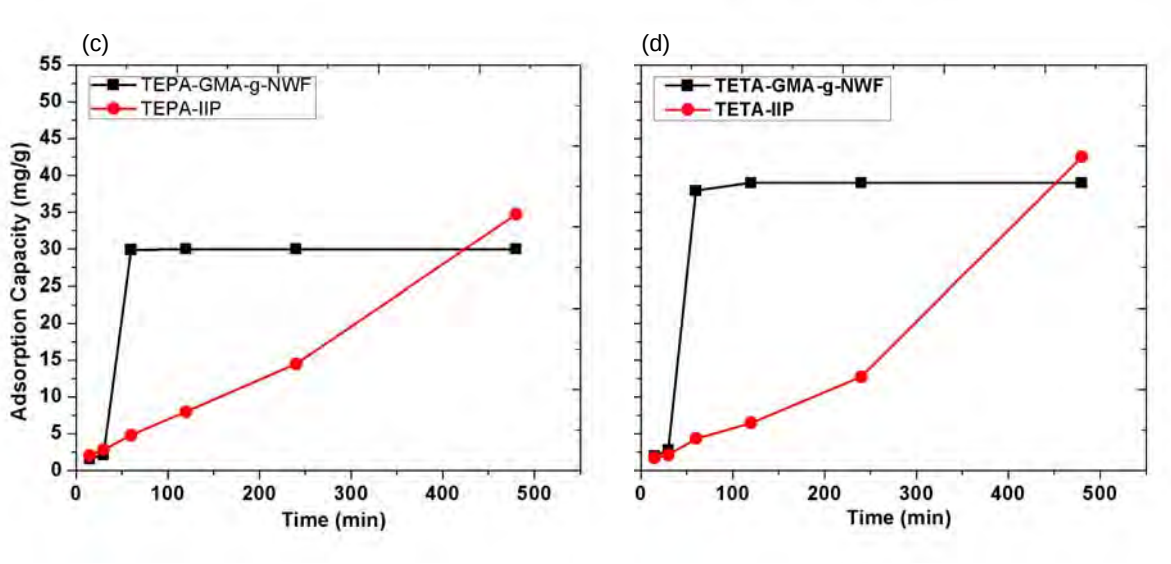

Figure 3.17. Adsorption capacity of Cu(II) versus time by amine immobilized GMA-g-NWF and IIP at experimental condition of initial copper concentration: 10 mg/L, adsorbent dose: 0.02 g, temperature: 30 ºC, amine density: 2.0 – 2.2 mmol/g-ad, stirring speed: 200 rpm and solution volume: 100 ml (continued)

As shown in the figure, the adsorption capacity of both amine immobilized GMA-g-NWF and IIP samples were measured against adsorption time. The adsorption capacity of amine immobilized GMA-g-NWF samples decreased, with a trend of EDA-GMA-g-NWF> DETA-GMA-g-NWF> TETA-GMA-g-NWF> TEPA-GMA-g-NWF. These findings strongly related to the size of aliphatic amines. Since the EDA possesses the smallest size, thus the migration of Cu onto the active sites is easier to take place abundantly in comparison to other aliphatic amines [126]. Another main reason for the reduction of adsorption capacity towards Cu ion as the number of amines increased from 2 to 5 is related to the covalent interactions relative to the ionic interactions during the competitive adsorption between Cu and Pb. Wang F. et al. [153] discussed the effect of the covalent index in their study, and they found out that Pb has a larger covalent index of 6.41 than Cu (2.64), which resulted to Pb having stronger interaction to the nitrogen and oxygen atoms to form complexes than Cu. This explained the reason of reduction in adsorption capacity towards Cu as aliphatic amines chain grows greater. The adsorption capacity of EDA-GMA-g-NWF towards copper ion increases significantly for initial 60 minutes, but thereafter, the adsorption capacity reaches almost plateau. The adsorption

capacity EDA-GMA-g-NWF at first 15 minutes of adsorption was around 1.60 mg/g which increases up to 34.85 mg/g after 60 minutes of the process. The active sites present onto EDA-GMA-g-NWF more likely actively occupied by Cu(II) ions during the initial stage of the adsorption process. However, subsequent saturation in adsorption of Cu(II) ion merely takes place due to the exhaustion of active sites onto EDA-GMA-g-NWF [154]. The saturation is attributed from the simultaneous adsorption of Pb, suggesting possible competitive effect towards the active sites between Cu and Pb. A similar trend was attained for DETA-GMA-g-NWF, TETA-GMA-g-NWF and TEPA-GMA-g-NWF samples as well.

However, all the IIP samples had shown different trend from amine immobilized GMA-g-NWF on adsorption capacity with time. The EDA-IIP sample had shown ascending trend with time for adsorption capacity of Cu ion. The adsorption capacity increases from 1.82 mg/g to 50.41 mg/g while the adsorption time increases from 15 minutes to 480 minutes, respectively. Although the adsorption reaches the maximum of 480 minutes, the adsorption capacity of the EDA-IIP sample still did not show any sign for saturation. The EDA-IIP samples initially exhibit a slower adsorption rate which leads to higher Cu ion intake capacity. The three-dimensional network formed through cross-linked imprinted polymeric material enables specific sites for designated ions which gives higher adsorption capacity at a slower adsorption rate [155]. Since the adsorbent did not reach saturation, it is anticipated that there are more available active sites for Cu, which leads to higher Cu ion intake capacity. Due to the slow adsorption rate, the IRP does not reach a plateau as consequences of insufficient contact time between the solute and the adsorbent. A similar trend was attained for DETA-IIP, TETA-IIP and TEPA-IIP samples as well. Meanwhile, IIP samples also illustrated a descending trend for adsorption capacity with aliphatic amines chain growth. The adsorption capacity towards Cu ion reduces with trend of EDA-IIP> DETA-IIP> TETA-IIP> TEPA-IIP. The size of aliphatic amine plays a major role in the adsorption performance of both amine immobilized GMA-g-NWF and IIP samples.

3.3.4.2 Selectivity of Amine Immobilized GMA-g-NWF and IIP in Binary Metal Species System

Both amine immobilized GMA-g-NWF and IIP samples were subjected to selectivity experiment in binary metals system which consist of both copper and lead ions. The main aim of the study is to investigate the selectively of the prepared polymeric material which enacted with ion recognition technique in term of different aliphatic amines. The result obtained shown in Figure 3.18 and Figure 3.19. The experimental conditions of amine functionalization process were predetermined in order to attain AD approximately 2.0 – 2.2 mmol/g-ad provided standardized condition was applied for selectivity experiment. The selectivity of both amine immobilized GMA-g-NWF and IIP samples towards copper ions were measured against time. The selectivity of EDA-GMA-g-NWF towards copper ion increases for initial 60 minutes, but thereafter, no significant changes was observed. The highest selectivity attained for EDA-GMA-g-NWF was around 1.1, which is almost insignificant. DETA-GMA-g-NWF, TETA-GMA-g-NWF and TEPA-GMA-g-NWF samples were also showing insignificant selectivity towards copper ion as well. Amine-functionalized adsorbent possess good adsorption capacity for copper ions in single metal ion system as published by several researchers [131, 156, 157], however, due to competition of interfering ions, EDA-GMA-g-NWF, DETA-GMA-g-NWF, TETA-GMA-g-NWF and TEPA-GMA-g-NWF own very poor selectivity towards copper ion in binary metal system.

On the other hand, EDA-IIP sample exhibited very good selectivity towards copper ion in the binary metal system. The selectivity of EDA-IIP increases from 44.6 to 113.7 while the experimental time increases from 15 minutes to 480 minutes, respectively. The selectivity of EDA-IIP sample still haven't reaches plateau even after maximum time of 480 minutes. This is attributed from the multilayer adsorption process, which requires a longer time to reach the equilibrium. This may further be confirmed by sorption isotherm data [158] in a future study. This observation complimentary with adsorption capacity of EDA-IIP towards Cu(II) as shown previously. DETA-GMA-g-NWF, TETA-GMA-g-NWF and TEPA-GMA-g-NWF samples were also showing similar outcome. The IIP samples own some cavities which are complimentary to imprinted copper ion in term of size and coordination geometry. Meanwhile, amine immobilized GMA-g-NWF shows random distribution of functionalities in polymeric network without any rebinding

affinities specificity [159]. Therefore, amine immobilized GMA-g-NWF randomly adsorb the any metal ions which present in the absorption system without being selective towards copper. The improvement on selectivity is limited as the equilibrium state was not achieved within the experimental duration. However, the selectivity still shows improvement almost 100 times by ratio. This is considered as very good which align with previous findings [155]. The selectivity of IIP samples decreases based as the aliphatic amines chain grows greater. The selectivity towards copper ion reduces slightly with trend of EDA-GMA-g-NWF> DETA-GMA-g-NWF> TETA-GMA-g-NWF> TEPA-GMA-g-NWF. The chain length and size of aliphatic amine plays important factor in this, where complex structural coordination with longer aliphatic amine chains may inhibit diffusion of Cu ions into template cavities.

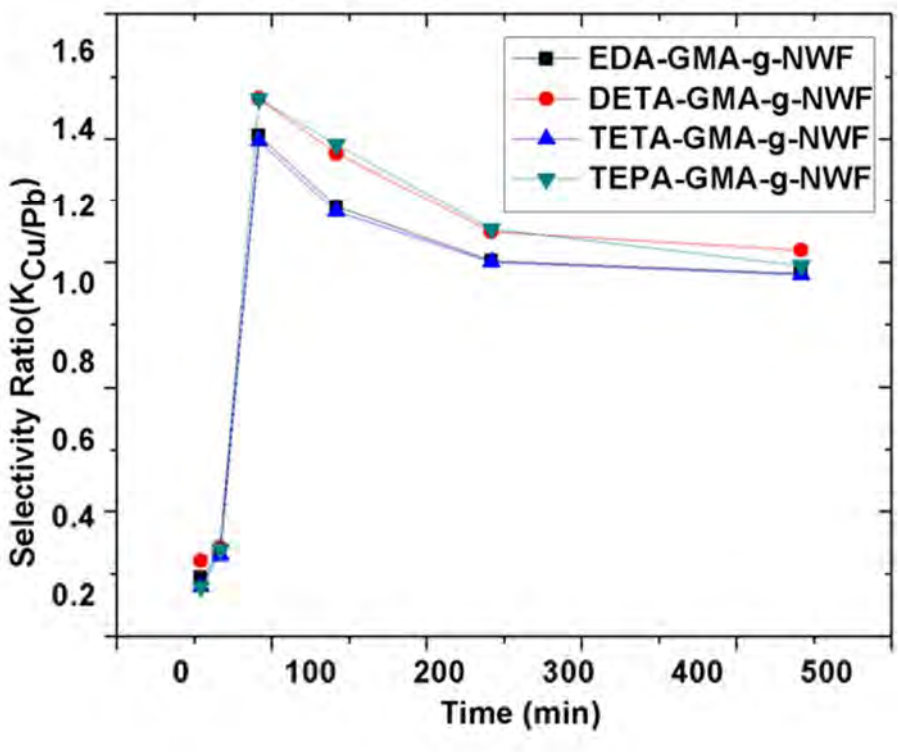

Figure 3.18. Selectivity ratio of amine immobilized GMA-g-NWF samples versus time at experimental condition of initial copper concentration: 10 mg/L, adsorbent dose: 0.02 g, temperature: 30 ºC, amine density: 2.0 – 2.2 mmol/g-ad, stirring speed: 200 rpm and solution volume: 100 ml

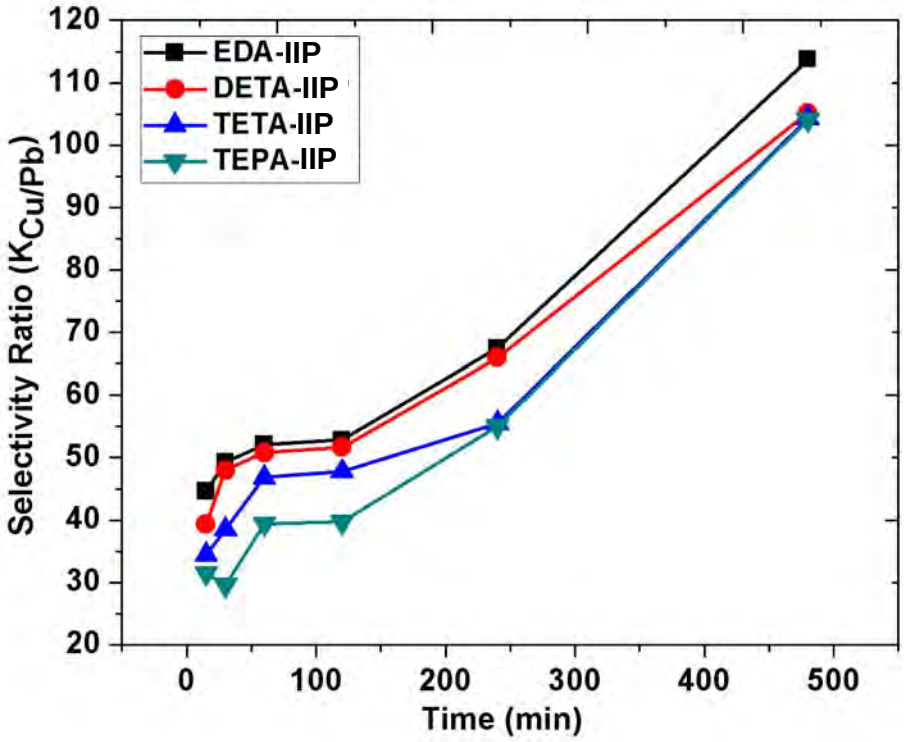

Figure 3.19. Selectivity ratio of IIP samples versus time at experimental condition of initial copper concentration: 10 mg/L, adsorbent dose: 0.02 g, temperature: 30 ºC, amine density: 2.0 – 2.2 mmol/g-ad, stirring speed: 200 rpm and solution volume: 100 ml (continued)

3.4 Conclusion

The effect of different aliphatic amine as the functionalization agent in both amine immobilized GMA-g-NWF and IIP samples in order to investigate the selectivity towards copper ion were investigated in this study. Functionalization of GMA-g-NWF with different aliphatic amines, EDA, DETA, TETA and TEPA were extensively optimized with different experimental condition. The amine composition had imposed major effect onto amine density yield. However, the amine density reduces as the aliphatic amine chain grows longer, from EDA to TETA. The addition molecular weight and bulky structure further attribute steric hindrance which obstructs the corporation of amine group onto GMA. The similar trend observed in all other experimental condition which had been investigated. The differences in amine immobilized GMA-g-NWF and IIP samples were

extinguished by using various characterization tools. The structural coordination of GMA-g-NWF and IIP samples were analysed with XPS and EXAFS spectroscopy. The complexation of copper ion with prepared adsorbent take place dominantly by the binding of Cu-O. The structural coordination of IIP samples remains the same even after crosslinking process. The adsorptive capacity and selectively of both amine immobilized GMA-g-NWF and IIP samples were compared at similar experimental conditions. The IIP samples had exhibited superior adsorptive capacity and selective in comparison to amine immobilized GMA-g-NWF. Meantime, the adsorption capacity of both amine immobilized GMA-g-NWF and IIP samples reduces slightly as the aliphatic amines grows longer form EDA to TEPA. However, the selectivity of the IIP samples still sustained for all the aliphatic amines, EDA, DETA, TETA and TEPA, respectively. Noteworthy that the results from this study will be served as the empirical evidences to support the arguments for further investigation in the next chapter as follow;

(i) For the synthesis of IIP, the aliphatic amine is most beneficial at its simplest form. In this study, EDA has shown the highest efficiency and selectivity. This finding will be a reference towards the selection of monomer in the next chapter.

(ii) The structural coordination of the polymer adsorbent remains the same even after crosslinking process. Therefore, it can be assumed that any degradation or chain scission that might happened (if any) during the radiation crosslinking did not have any profound effect on the adsorption efficiencies.

CHAPTER 4

SYNTHESIS AND CHARACTERIZATION OF AMINE-BASED ADSORBENT AS ION-IMPRINTED POLYMER

4.1 Introduction

Chapter 3 has concluded that grafted adsorbent has the ability to retain metallic ions from an aqueous media. However, previously demonstrated approaches have relied on multi-step routes to introduce functional moieties. In addition, the adsorption capacity of amine-based adsorbent does not show any significant reduction (only reduces slightly) as the aliphatic amines grows longer, which indicates that neither the length of the amines contributes to the structural of IIP nor the adsorption capacity. A simpler alternative, which will be demonstrated in this chapter, is therefore to directly graft a simple nitrogen-containing methacrylate to the substrate. Nitrogen-containing methacrylate have been used widely as monomers for graft polymerization owing to its interesting functional properties. 2-(dimethylamino)ethyl methacrylate (DMAEMA, MF= $C_8H_{15}NO_2$, MW= 157.2 g/mol) is a weak polybase methacrylate which is soluble at neutral pH or in acidic media due to protonation of the tertiary amine [160]. DMAEMA is a common monomer used for the preparation of grafted adsorbent for heavy and toxic metals [70, 161, 162]. DMAEMA contains two different functional groups, carboxyl and tertiary amino groups which will enhance the sorption capacity of the grafted adsorbent.

The concept of ion-imprinted polymer (IIP) materials implicates preorganized interaction of functional monomer towards imprinted ion through definite chemical interaction between them with the presence of enormous quantity of cross-linking agent for intended polymerization process [17]. The specific binding sides that are present on the imprinted polymeric materials enable the recognition of the template ion and with that, the material exhibit higher selectivity for the rebinding of that particular ion [163, 164]. Crosslinker is responsible to set functional monomers around ion templates and therefore

creating a highly cross-linked rigid polymer's cavity even after removal of ion template [165]. Thus, optimization of crosslinking process parameter is vital to attain viable adsorption capacity.

In this present study, the functional group covalently bonded onto the polymer substrate through graft polymerization and followed by formation of functional monomer and template ion. Afterwards, polymerization with crosslinker was carried out onto the substrate to form the cavity and finally the template was removed. To better understand the effect of DMAEMA as the monomer precursor and the viability of the proposed imprint technique, a thorough investigation on the effect of process parameters towards the synthesis of the polymer adsorbent were carried out at every stage (for both grafted adsorbent and crosslinked IIP). This is to ensure a clear understanding on the technique and to evaluate the properties of the prepared adsorbents. Several polymer characterization techniques such as Scanning Electron Microscope (SEM), Fourier Transform Infrared (FTIR), X-ray Photoelectron Spectroscopy (XPS), X-ray Diffraction (XRD) and Thermogravimetric Analysis (TGA) were used to evaluate the physical, chemical and structural properties of the adsorbent. This chapter will solely focus on the synthesis and characterization of the materials, while the adsorption behaviour of DMAEMA grafted adsorbent and the imprinted polymer will be discussed in Chapter 5.

4.2 Experimental Section

4.2.1 Materials

Polyolefin non-woven fabric which contains a polypropylene (PP) core and a polyethylene (PE) sheath (denotes as PE/PP-NWF) used as trunk polymer was obtained from Kurashiki Textile Manufacturing Co., Japan. 2-(Dimethylamino)ethyl methacrylate (DMAEMA, 98%) was purchased by Tokyo Chemical Industries Co. LTD, Japan. Ultrapure water was obtained from Elix Milipore ultrapure water system at 14.6 MΩcm resistivity. Polyoxyethylene sorbitol ester (TWEEN20) and divinylbenzene (DVB, 80%) were purchased from Sigma Aldrich. All chemicals were of analytical grade and used as received, unless stated otherwise.

4.2.2 Characterizations

4.2.2.1 Fourier Transform Infrared (FTIR)

FTIR spectroscopic analysis was carried out using Perkin Elmer Frontier for PE/PP-NWF and DMAEMA-grafted PE/PP-NWF (denotes as P-DMAEMA). Meanwhile, ion-imprinted polymer (IIP) and non-imprinted polymer (NIP) were analysed with FTIR (BRUKER, Tensor II) in order to identify the chemical functionalities, present in respective samples. All samples were scanned under wavenumbers from 4000 cm^{-1} to 400 cm^{-1} at resolution of 4 cm^{-1} with single reflection diamond universal attenuated total reflection (ATR). The averaged scan was over 32 times.

4.2.2.2 Scanning Electron Microscope (SEM)

Morphological structure of PE/PP-NWF and P-DMAEMA samples were examined using a SEM with energy dispersive x-ray (SEM-EDX, Hitachi SU3500/Horiba) spectroscopy. Meanwhile, the surface morphology of IIP and NIP samples was completed with field emission SEM (FE-SEM, Zeiss Gemini SEM500) at 3.0 kV and 107.4 µA of voltage and current, respectively. The magnifications range of 500 times was used with resolution of 10 nm. The samples were coated with thin layer of Aurum (Au) before imaging.

4.2.2.3 Thermogravimetric Analysis (TGA)

TGA was conducted with Rigaku Thermoplus TG 8120 TGA analyser at heating rate of 10 °C/min to investigate the thermal stability of PE/PP-NWF and P-DMAEMA. All samples were kept in a bottle containing silica gel for 24 hours before measurement to keep it in dry condition. On the other hand, the IIP and NIP samples were tested with TGA (Perkin Elmer Pyris 1). The samples were heated at the heating rate of 4 °C/min, from room temperature to 500 ºC. Nitrogen flow was maintained at a rate of 50 mL/min.

4.2.2.4 X-ray Photoelectron Spectroscopy (XPS)

The adsorptive interaction between thorium ions in IIP samples were observed with XPS (ULVAC-PHI Quantera II). XPS analysis was operated using similar settings and parameters as in 3.2.5.3. The XPS MultiPak version 9.8.0.19 was applied for the deconvolution of the XPS spectra.

4.2.2.5 X-ray Diffraction (XRD)

XRD (PanAnalytical X'Pert Pro) patterns of all samples were substantiated with CuKα (α=1.542A) at 40kV and 30mA. Data were collected from 2θ of 10 º to 30 º at rate of 1 º/min. Crystal structure, crystallite size, and crystallinity degree were derived from the experimental X-ray diffraction patterns.

4.2.3 Synthesis of Radiation Modified Amine-based Adsorbent

4.2.3.1 Preparation of DMAEMA Grafted PE/PP-NWF

Radiation induced graft polymerization was done as described in previous chapter. Small piece of PE/PP-NWF (5 cm x 5 cm) was set in polyethylene zipper pack and purged with nitrogen (N_2) to eliminate the air trapped inside the pack. The zipper pack which contains PE/PP-NWF was exposed to electron beam irradiation at dry ice temperature. The sample was irradiated at doses ranging from 10 to 100 kGy. Most appropriate electron beam irradiation condition was chosen in order to achieve vital Dg. The irradiated PE/PP-NWF was moved into a glass ampoule and vacuumed for 1 minute. The emulsified monomer solution consists of monomer, DMAEMA and surfactant, TWEEN20 with 1:0.6 ratio was moved into the glass ampules which filled with irradiated NWF. The choice of surfactant and the ratio was dictated by results obtained after many studies trials in the laboratory and according to previous study. Subsequently, the glass ampoule was located into water bath at predetermined temperature and time for grafting reaction to occur. Lastly, the DMAEMA-grafted PE/PP-NWF (denotes as P-DMAEMA) was washed thoroughly with distilled water and placed in a vacuum oven at 35 ºC overnight. The Dg was calculated according to equation 3.1 as described in Chapter 3.

4.2.3.2 Preparation of Radiation Crosslinked P-DMAEMA Adsorbent

In order to prepare radiation crosslinked samples, the P-DMAEMA (Dg≈100%) were subjected to adsorption of thorium prior radiation crosslinking in the present of DVB. 0.1 g of P-DMAEMA immersed into 50 mL of 25 mg/L of thorium (pH 3.0 - 3.5) in aqueous medium at stirring mode for 120 minutes. Thereafter, the samples were filtered, and the aliquot was tested with ICP-MS. P-DMAEMA were subjected to irradiation induced crosslinking at two different states, namely IIP and NIP. P-DMAEMA adsorbed with thorium (25 ppm, pH 3.1 - 3.3) was term as IIP. After adsorption, the IIP was washed with distilled water and placed in an oven at 50 ºC overnight for drying. Thereafter, the IIP was placed into polyethylene zipper pack and filled with emulsified crosslink solution consists of DVB/TWEEN20 (2:1 ratio) and subsequently purged with nitrogen (N_2) to remove the dissolved oxygen. The polyethylene zipper pack filled with IIP and emulsified crosslink solution exposed to 2MeV and 10 mA electron beam irradiation (EPS 3000 Nissin High Voltage, Japan) at room temperature. The sample was irradiated with 60 kGy absorbed radiation dose in order to attain required crosslinking yield.

On the other hand, NIP was prepared with the same manner, excluding the thorium adsorption process prior to irradiation induced crosslinking. After irradiation, the samples were kept in water bath at 60 ºC for 120 minutes. Finally, the samples were washed comprehensively with distilled water and dried in oven at 50 ºC overnight. Crosslinking percentage was calculated via gel fraction analysis method ASTM D 2765-95. Measured samples were put into a test tube, 20 mL of xylene were added and heated in the thermostatic oil tank set at the temperature of 120 °C for 24 hours. The extracted samples were dried in oven at the temperature of 100 °C until constant weight was obtained. The percentage of crosslinking was defined as gel fraction or gel content and calculated as;

$$Gel\ content\ (\%) = {W_t}/{W_0} \times 100 \quad (4.1)$$

where, W_0 and W_t are the weights of the dried samples before extraction and after extraction, respectively.

Desorption of thorium absorbed onto IIP sample is essential for the template removal which attribute thorium selectivity nature onto IIP sample. 0.1 g of IIP sample was immersed into 0.1 M of HNO_3 and stirred for 120 minutes at room temperature. Upon completion of desorption process, IIP samples was filtered and the aliquots subjected to analysis in order verify the desorption efficiency. After desorption, the IIP sample is ready for the selectivity analysis in binary and individual solution. Both IIP and NIP will be tested for selectivity for thorium at different parameters. The overall route for the preparation of IIP was illustrated in Figure 4.1.

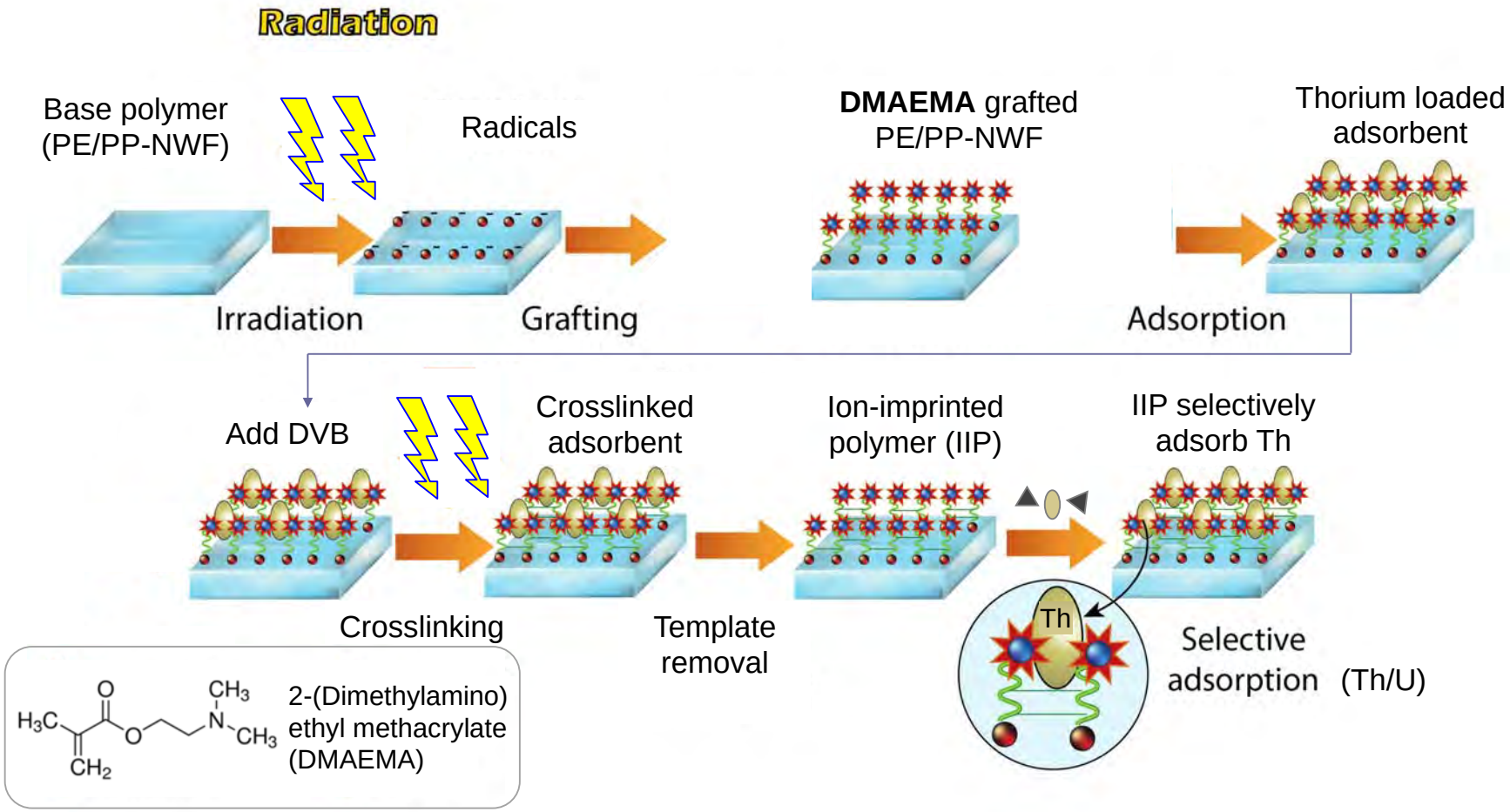

Figure 4.1. Overall route for the preparation of ion imprint polymer via single-step grafting

4.3 Results and Discussion

4.3.1 Synthesis of Radiation Grafted Amine-based Adsorbent

In this chapter, PE/PP-NWF was functionalized by radiation grafting of DMAEMA onto PE/PP-NWF to impart adsorptive properties for Th(IV) removal. The effect of process parameters such as absorbed radiation dose, monomer concentration, time and temperature onto the Dg were investigated and optimized.

4.3.1.1 Effect of Absorbed Radiation Dose

Effect of absorbed radiation dose on Dg was studied using 7 wt% DMAEMA monomer concentration emulsified with TWEEN20 with ratio of monomer-surfactant = 1:0.6. The PE/PP-NWF was irradiated at different doses and then reacted with monomer/surfactant/water emulsion at 40°C for different time interval. As shown in Figure 4.2, the results follow the typical trends of radiation graft polymerization, where the Dg increases with the increase of irradiation dose. This indicates that higher irradiation doses lead to formation of more free radicals in the PE/PP-NWF, which consequently increase the availability for grafting reaction of monomer onto the substrate. These results are in good agreement with the results obtained by Madrid *et al.* [70] who observed a rapid increase in Dg of DMAEMA onto non-woven PE/PP with absorbed dose. Typically, the Dg increases with the reaction time. At temperature 40°C which can be considered as low temperature, the grafting reaction proceed slowly and take longer time to complete the reaction, thus increment of Dg can be seen with time. As shown in Figure 4.2, Dg for P-DMAEMA follows the general trend where the Dg percentage gradually increases with the augment of reaction time.

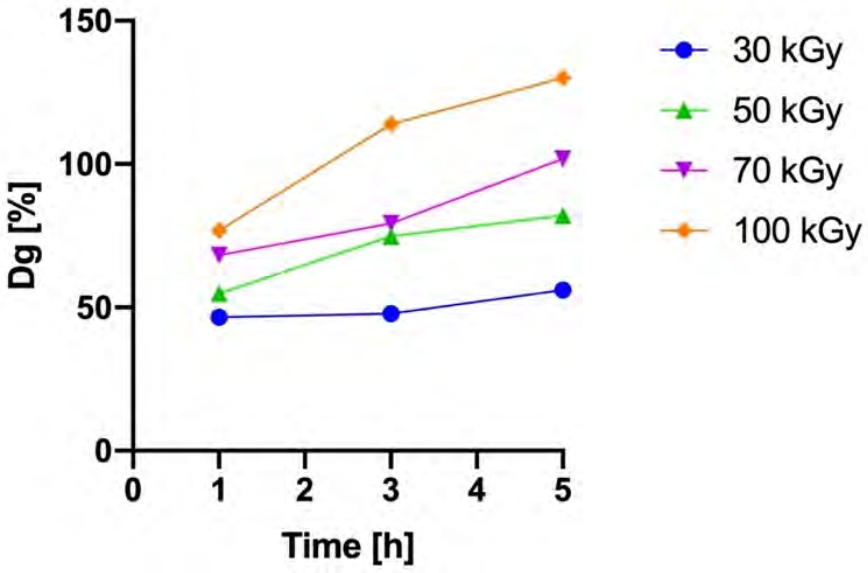

Figure 4.2. Dose dependence of grafting of DMAEMA at various time interval

4.3.1.2 Effect of Monomer Concentration

For the adsorbent to be suitable for the collection and recovery of metal ions, Dg of 100% by weight of monomer units was targeted in this study. The effect of monomer parameter on Dg was studied using DMAEMA emulsified with TWEEN20 at various monomer-surfactant ratio and monomer concentration. Reaction time of 3 hours and absorbed radiation dose of 100 kGy remained constant for all samples. As shown in Table 4.1, P-DMAEMA shows a stable graft polymerization within range 103% to 114% at all monomer-surfactant ratio, with slightly higher Dg at 1:0.6 monomer-surfactant ratio. Examination of monomer–surfactant solution by dynamic light scattering confirmed very weak light scattering and unimer sizes with trace amount of loose aggregates for DMAEMA-TWEEN20 at 1:0.2 and 1:1 monomer-surfactant ratio (Table 4.1). However, DMAEMA-TWEEN20 produced much more intense light scattering when the ratio is increased to 1:0.6, due to more stable solution with formation of aggregates with average diameter around 132.86 nm. Thus, this ratio is used for further investigation.

Table 4.1. Dg and particle size of DMAEMA at different monomer-surfactant ratio

Monomer to surfactant ratio	Avg. Dg (%)	Std. Dev.	Avg. particle size (nm)	Std. Dev.
1: 0.2	105.88	3.56	14.4	14.2
1: 0.6	112.76	1.81	132.86	2.59
1: 1	109.62	4.34	9.03	7.18

Figure 4.3 shows the effect of various monomer concentration on the Dg. The Dg increases with increased concentration of DMAEMA monomer in all cases. The Dg is still increasing after 3 hours because at high concentration of monomer, the monomer is readily available for the reaction to continuously occurs.

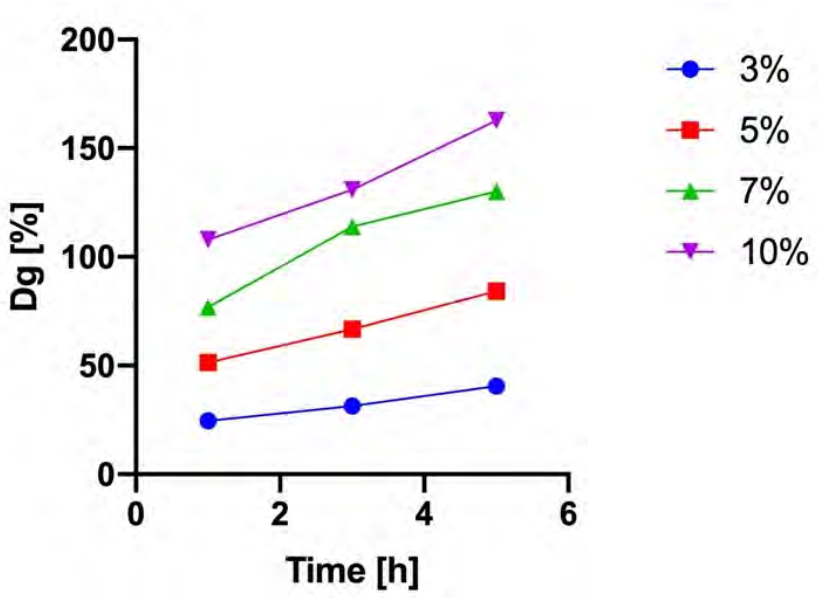

Figure 4.3. Effect of monomer concentration on percentage of Dg at various time interval

4.3.1.3 Effect of Time

The Dg increases proportionally with reaction time as shown in Figure 4.3. This observation may denote to rapid interaction in between free radicals onto PE/PP-NWF and DMAEMA monomers as the time increases, which upholds the Dg higher. The highest Dg obtained was around 162% using 10 wt% monomer concentration at 5 hours reaction time.

Although many researchers have reported kinetic data of grafting reaction [166-168], investigation on how the structure of the nitrogen-containing ester side influences

the kinetics of radiation grafting for DMAEMA is not yet fully investigated. The relation of the rate of grafting reaction to the function of monomer concentration and the absorbed radiation dose were determined using equation 4.2 as described by Naser M. M. *et al.* [166] as below.

$$R_g = k\,[M]^m[D]^n \tag{4.2}$$

where, *Rg* is the initial rate of grafting, *M* is the monomer concentration (wt%), *D* is the absorbed radiation dose (kGy) and *k* is the grafting rate constant.

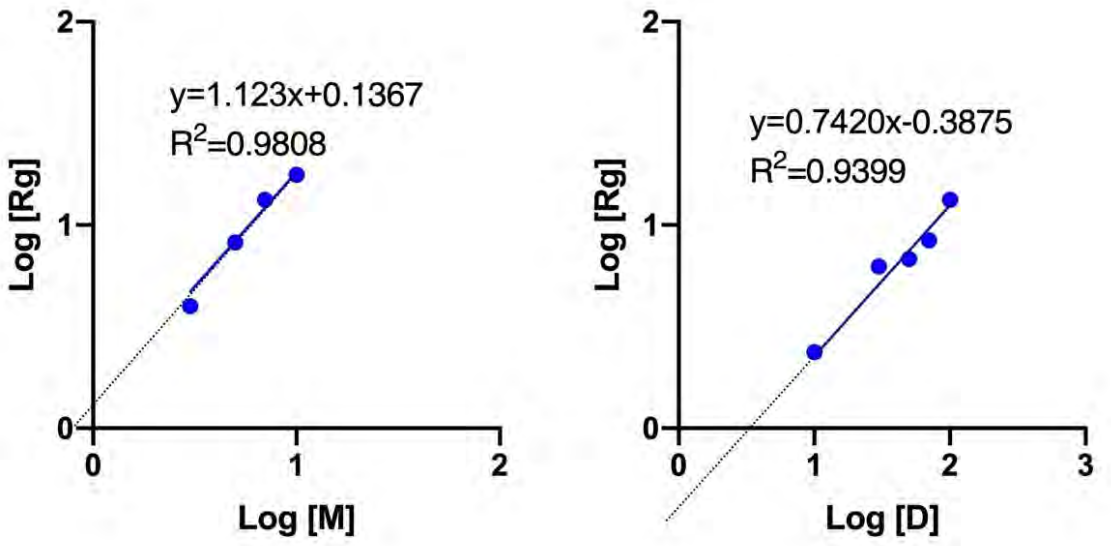

Figure 4.4. Logarithmic plot of rate of grafting versus radiation dose

The value of parameter *m* and *n* can be experimentally determined by plotting logarithmic form of the equation for various monomer concentration and absorbed radiation doses. Rg is obtained from the slope of the graph depicted in Figure 4.2 and Figure 4.3. The slope of the log graph plotted in Figure 4.4 indicates that the rate of grafting was proportional to the 1.12 power of DMAEMA concentration and increases parabolically with the absorbed radiation dose (n = 0.74). The grafting rate equation for the grafting of DMAEMA onto PE/PP-NWF can be written as:

$$R_g = k\,[M]^{1.12}[D]^{0.74} \tag{4.3}$$

Equation 4.3 demonstrates that grafting kinetics for DMAEMA system does not only depends on the absorbed radiation dose, which reflects the amount of efficient

trapped radicals but also on the concentration of the monomer in the grafting sites, which will determine the rate of monomer diffusion.

4.3.1.4 Effect of Temperature

In typical graft polymerization, an increase in Dg can be seen at higher reaction temperature due to increase mobility of monomer molecules and their collision with backbone polymer resulting in faster rate of reaction [169].

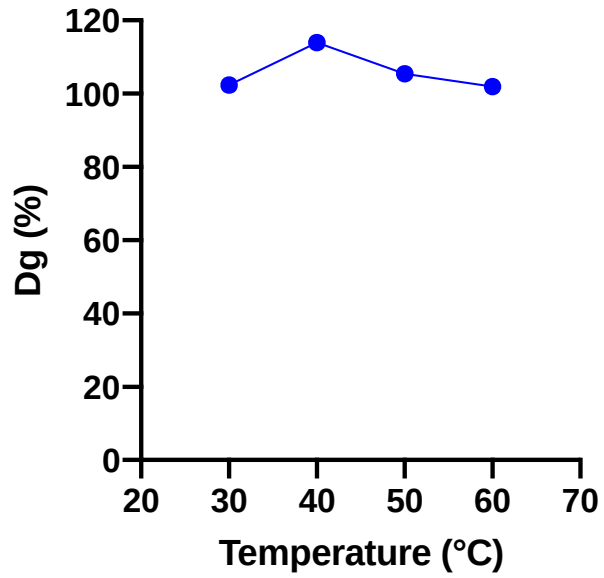

Figure 4.5. Percentage Dg for grafting of DMAEMA at various temperature

As shown in Figure 4.5, the result for grafting of P-DMAEMA shows higher Dg at low temperature, with maximum grafting occurs at 40°C. This is due to the behaviour of DMAEMA monomer, which is soluble below low critical solution temperature (LCST) and insoluble beyond it. It is reported in literature that the LCST of DMAEMA is in the range of ca. 40-50°C [170, 171]. Above this transition temperature, the solubility of DMAEMA monomer decrease to certain extend. From the results, the activation energy value for each temperature can be determined by reaction rate constants at different temperatures using the Arrhenius equation as below;

$$\log {}^{k_2}/_{k_1} = {}^{E_a}/_{R} \times \left({}^{1}/_{T_1} - {}^{1}/_{T_2}\right) \quad (4.4)$$

where, E_a is the activation energy of the reaction in J/mol, R is the ideal gas constant = 8.31 J/K·mol, T_1 and T_2 are absolute temperatures, k_1 and k_2 are the reaction rate constants at T_1 and T_2.

The calculated values are summarized in Table 4.2. Activation energy is the amount of energy that needs to be supplied in order for a reaction to proceed. Thus, it can be concluded that the grafting of DMAEMA onto PE/PP-NWF needs higher energy when the temperature increases. This result is in agreement with the findings by F. Ranogajec for pre-irradiation grafting of styrene on polyethylene [172]. He evidently described that the amount of graft polymer after a sufficiently long reaction time is less at higher temperature and subsequently when nearing its termination. The activation energy of termination was found to be higher than that of propagation during the reaction process.

Table 4.2. Activation energy value at various temperature for DMAEMA

Monomer	***Ea* (kJ mol^{-1}) (T = 313 – 323 K)**	***Ea* (kJ mol^{-1}) (T = 323 – 333 K)**
DMAEMA	84.52	89.88

4.3.2 Synthesis of Crosslinked P-DMAEMA as Ion-Imprinted Polymer

This section focused on the preparation of ion recognition adsorbent through ion imprint technique to enhance the selectivity properties of the adsorbent. P-DMAEMA with the Dg≈100% was chosen for further investigation based on the results discussed earlier. Thorium, Th(IV) was chosen as template ion.

4.3.2.1 Effect of Crosslinker Concentration

P-DMAEMA (Dg≈100%) was used to determine the optimum crosslinking polymerization process condition with DVB. Both IIP and NIP samples were optimized for crosslinking polymerization process in order to examine the influence of thorium which present on IIP samples towards crosslinking polymerization process. The initial concentration of DVB (10, 15 and 20 wt%) in emulsion state with TWEEN20 was evaluated in terms of amount crosslinking (%) via gel content analysis at absorbed radiation dose of 60 kGy, temperature 70 ºC and time 120 minutes. Both IIP and NIP samples had shown linear increment with DVB concentration, but NIP samples show slightly higher crosslinking in comparison to IIP samples as shown in Figure 4.6. IIP

samples demonstrated a crosslinking degree of 83.71, 88.70 and 90.72% at 10, 20 and 30% of DVB concentration, respectively. However, NIP samples reached higher crosslinking degree of 91.24, 94.85 and 96.90% at 10, 20 and 30 wt% of DVB concentration, respectively. This result is attributed to the abundant availability of DVB which promotes more crosslinking to take place within the samples [173]. Moreover, DVB is highly reactive which helps to increase the activation energy of polymerization and also the reaction rate. Therefore, it promote higher crosslinking percentage as the concentration increases. Similar observation was attained in the study performed on development of novel route for the synthesis of cross-linked polystyrene copolymer beads with guar and xanthan gums [174]. In this system, DVB acts as a precursor to form a cross-linkage to the DMAEMA grafted chains with PE/PP-NWF. The presence of thorium in IIP samples resulted in relatively lower crosslinking compared to the NIP samples.

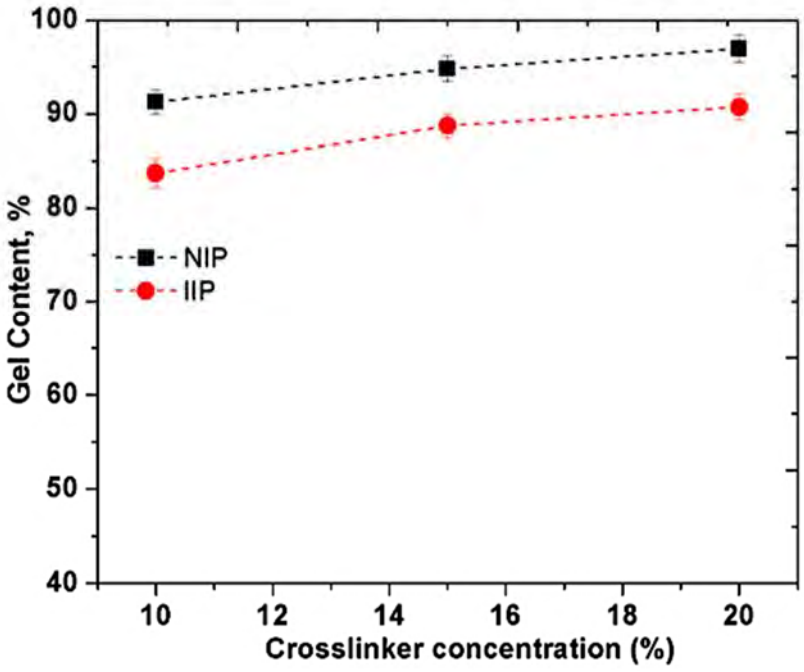

Figure 4.6. Effect of crosslinking polymerization onto DVB concentration

In general, abundant availability of DVB promotes more crosslinking to take place within the samples [20]. In this system, DVB act as a precursor to crosslink DMAEMA grafted chains among themselves and also with PE/PP-NWF. Presence of thorium in IIP samples makes those samples to have slightly lower crosslinking than NIP samples.

4.3.2.2 Effect of Th(IV) Concentration

Next, P-DMAEMA (Dg≈100%) was impregnated with different concentration of thorium as template ion, 25, 50 and 100 ppm, respectively and the effect on the crosslinking degree was assessed. It was found that the crosslinking percentage reduced significantly as the concentration of thorium increased. The crosslinking degree drops to 59.43 from 83.71% as the concentration of thorium increases from 20 to 100 ppm as shown in Figure 4.7. Amount of crosslinking mainly depends on the competition between the crosslinker and template for interaction with functional monomer. According to Shoravi S. *et al*. [175] the capacity of a crosslinker to compete with coordination of the template along with interaction of functional monomer is merely weak. Thus, high loading capacity of thorium template had hindered the crosslinking process due to high competition between template and crosslinker which had led to reduction in crosslinking. Furthermore, at given circumstance, the formation of homopolymers is very much substantial at recognition sites and this is well agreed by Sibrian-Vazquez M. *et al*. as well [176].

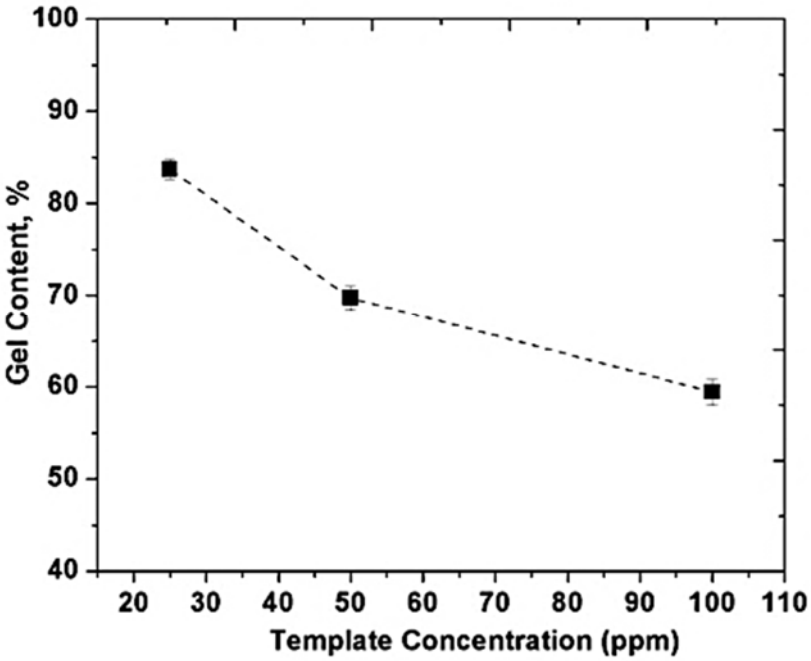

Figure 4.7. Effect of crosslinking polymerization onto thorium imprints concentration

4.3.2.3 Effect of Dg

P-DMAEMA with different Dg, (10, 50 and 100%) was subjected to radiation crosslinking process for both IIP and NIP samples. The results obtained exhibited in Figure 4.8. The crosslinking percentage decreases slightly as the Dg increases for both IIP and NIP samples respectively. The crosslinking amount for NIP sample with Dg 10 and 100% was around 94.05 and 91.24%, respectively. A similar trend was observed with the IIP samples as well. Sample with higher Dg will have longer grafted-DMAEMA chains in comparison to those samples with lower Dg. Thus, samples with longer grafted-DMAEMA chains possess better prospect for higher crosslinking. But the results obtained are contradicted with this notion since in the proposed experimental scheme based on covalent imprinting approach. Covalent imprint approach involves formation of covalent bond in between the monomer and the template before the crosslinking process, and also in between the binding sites and the analyte during the recognition process [177]. Furthermore, the hydrophilic nature of the functional monomer, DMAEMA and hydrophobic DVB crosslinker are also responsible for the interfacial repulsion that negatively impacts the crosslinking process efficiency [178].

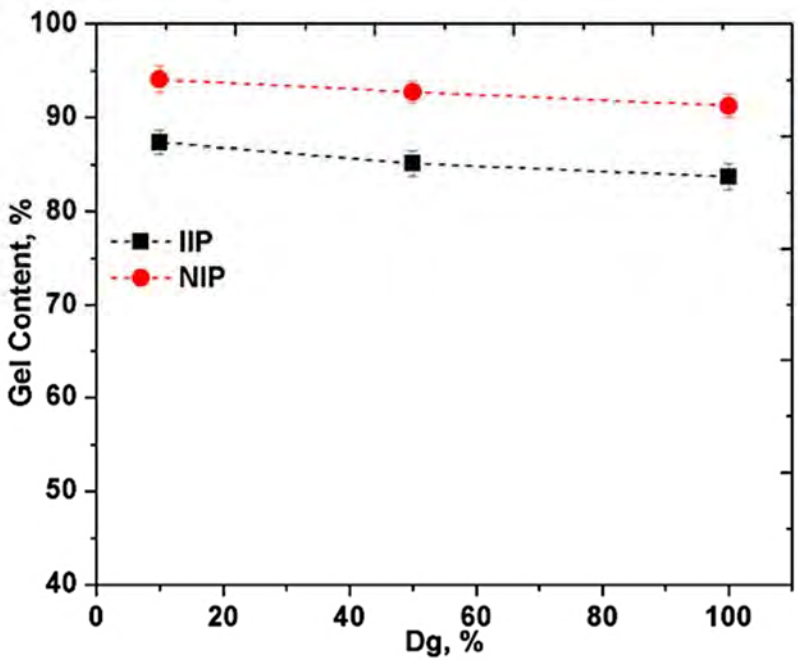

Figure 4.8. Effect of crosslinking polymerization onto Dg

4.3.2.4 Effect of Absorbed Radiation Dose

Both IIP and NIP samples were crosslinked at different absorbed radiation doses, 30, 60, 90 and 120 kGy respectively. The result obtained is shown in Figure 4.9. The crosslinking was directly proportional to absorbed radiation dose. The crosslinking percentage obtained for NIP samples were 43.30, 70.61, 80.57 and 83.71% at absorbed radiation dose of 30, 60, 90 and 120 kGy respectively. The same pattern was achieved on IIP samples too. The crosslinking process initiated by electron beam irradiation which operates based on free radical mechanism. Generally, the degree of crosslinking is governed by concentration of free radicals formed in the system. Increase in absorbed radiation dose will lead to increase in concentration of free radicals formed in trunk polymer and also co-monomer [179, 180]. The formation of radicals on the grafted DMAEMA chains will act as the point of initiation for the side chains. Consequently, the grafted DMAEMA chains will be added to the double bond of the DVB forming covalent bonding among them. Moreover, radiation dose had been classified as one of the most prominent factor in radiation crosslinking process [181]. Thus, substantial investigation pertaining to the effect of radiation dose on crosslinking process is vital.

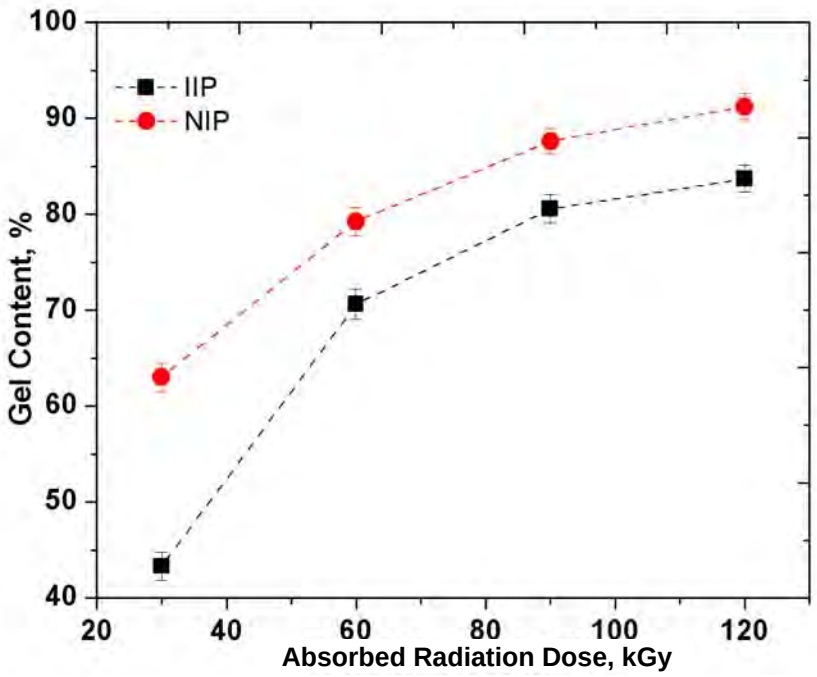

Figure 4.9. Effect of crosslinking polymerization onto absorbed radiation dose

4.3.2.5 Effect of Temperature

The effect of temperature onto crosslinking process had been investigated in this study. After exposure to radiation, both IIP and NIP were placed in water bath for 120 minutes at three different temperatures, 60C, 70 and 80 ºC. The results obtained shown in Figure 4.10. The crosslinking process accelerates with temperature. NIP samples were cross-linked up to 93.92, 95.24 and 97.71% when reacted at 60, 70 and 80 ºC respectively. Rate of crosslinking increases with increase in process temperature [180]. This significantly contributes towards higher crosslinking percentage by enhancing the kinetics of the reaction. Moreover, thermal condition too, does influence the diffusion of crosslinker in solution. Thus, crosslinker will have better access to the active sites formed by radiation onto the surface of the polymer substrate. It can be concluded that process temperature determines the final effect on radiation crosslinking process.

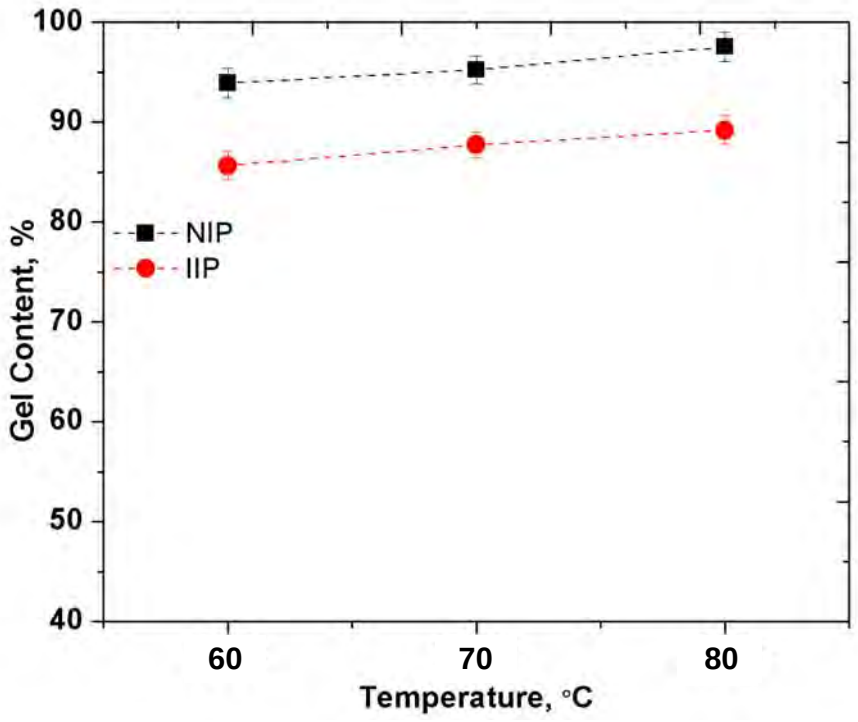

Figure 4.10. Effect of crosslinking polymerization onto process temperature

4.3.3 Evaluation of Characteristic Properties

4.3.3.1 SEM

The morphology of the PE/PP-NWF, P-DMAEMA, IIP and NIP samples are portrayed in Figure 4.11. Basically, the PE/PP-NWF possess unoriented fibrous-structured surface which is observed at microscopic scales. The individual fibril of PE/PP-NWF sample is approximately 10 μm which notably increased with DMAEMA grafting. P-DMAEMA had demonstrated obvious morphological changes which exhibited some coating that covers the surface with more bulk and uniform coating. A thin layer of DMAEMA coating is observed on every PE/PP fibrils of the NWF after the irradiation grafting process. This observation had proven the occurrence of successful grafting of DMAEMA onto PE/PP-NWF. In the study on grafting of glycidyl methacrylate onto hyacinth fibers by Madrid *et al* [182], the SEM analysis had given an identical outcome parallel to this study. Apparently, the diameter of individual fibril further increases in size for both IIP and NIP samples. This observation supports the claim of attachment of DVB onto P-DMAEMA due to crosslinking. Nevertheless, the crosslinking process which had taken place on both IIP and NIP samples could not be clearly indicated through SEM analysis. The IIP and NIP samples are subjected to further characterization using different techniques in order to ascertain crosslinking process.

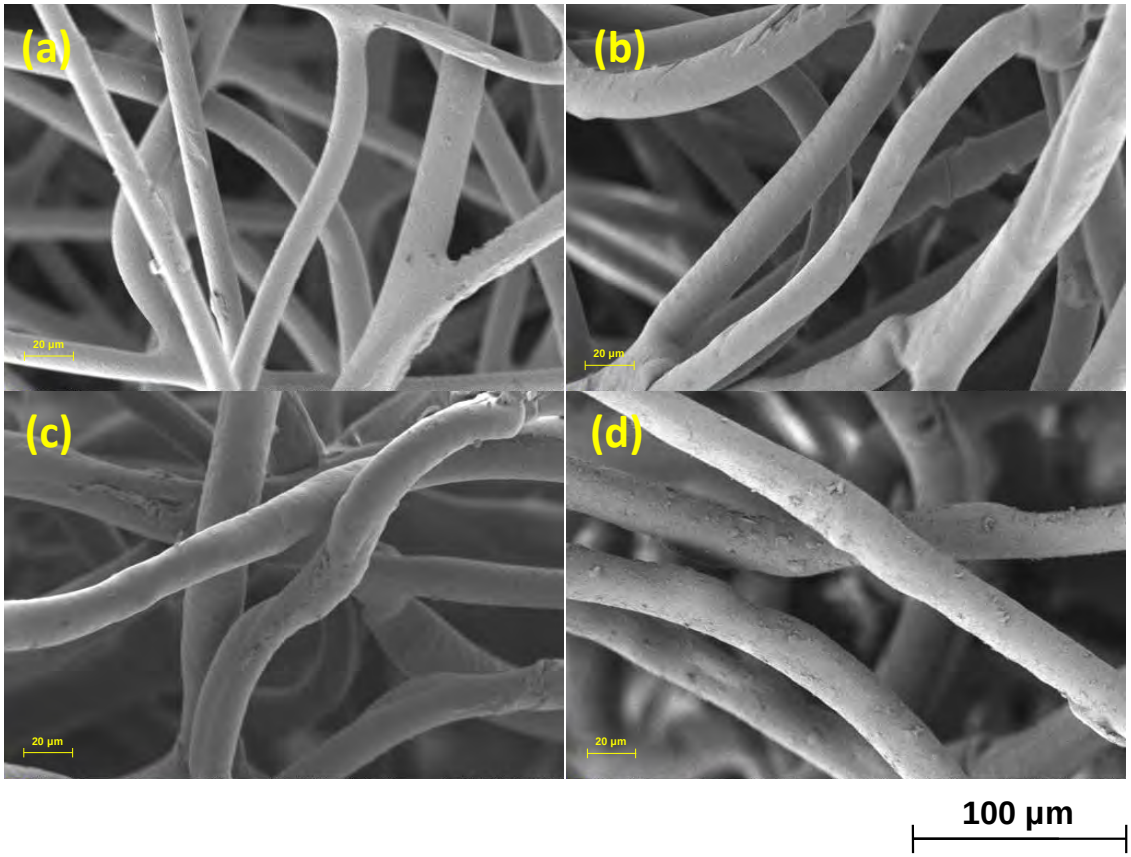

Figure 4.11. FE-SEM imaging (a) PE/PP-NWF; (b) P-DMAEMA (Dg≈100%); (c) IIP (Gel content: 83%); and; (d) NIP (Gel content: 90%) with magnification of 500x

4.3.3.2 FTIR

The FTIR spectra of the samples are shown in Figure 4.12, in which certain similarities were observed clearly among all PE/PP-NWF, P-DMAEMA, IIP and NIP samples. The characteristic band at 2913 cm^{-1}, 2843 cm^{-1}, 1464 cm^{-1}, 1370 cm^{-1} and 718 cm^{-1} found onto PE/PP-NWF samples attributed to C-H stretch (PP), C-H stretch (PE), CH_2 stretch (PP and PE), symmetric CH_3 deformation stretch (PP) and CH_2 stretch (PE) respectively. Additional characteristic band at 1731 cm^{-1} and 1147 cm^{-1} which found onto P-DMAEMA, IIP and NIP samples attributed to C=O stretch and C-N stretch (aliphatic) from DMAEMA via radiation grafting process. This finding supports the claim grafting of DMAEMA onto PE/PP-NWF samples. Characteristic band at 905 cm^{-1}, 831 cm^{-1} and 779 cm^{-1} which presents onto IIP and NIP samples attributed to C-H stretch from crosslinking process with DVB. The appearance of a new band in the region 1326 cm^{-1} and 1141 cm^{-1} IR spectra that corresponded to the νTh-O supports the formation of Th-O bonds in the system.

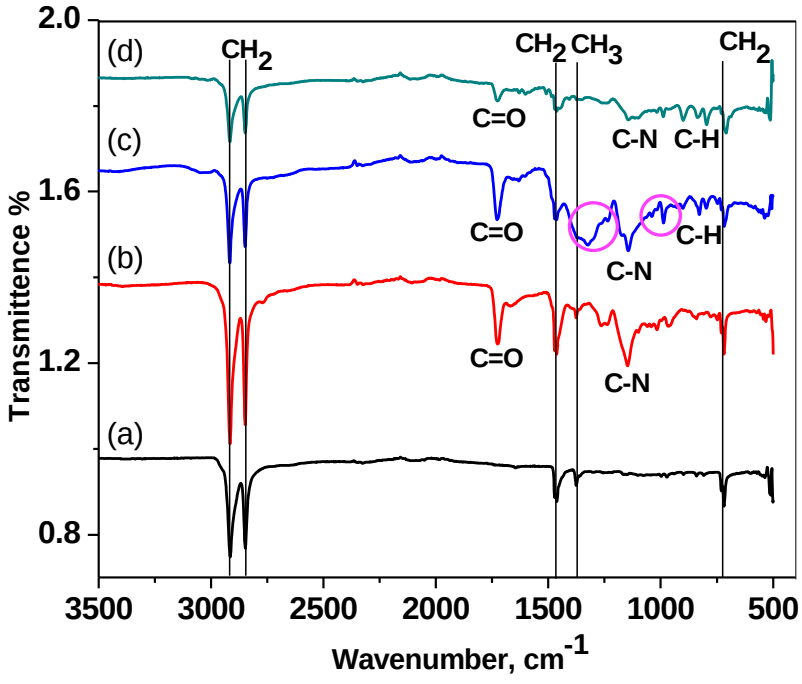

Figure 4.12. FTIR spectra (a) PE/PP-NWF; (b) P-DMAEMA (Dg≈100%); (c) IIP (Gel content: 83%); and; (d) NIP (Gel content: 90%).

4.3.3.3 TGA

Figure 4.13 describes the TGA curves obtained for ungrafted sample (PE/PP-NWF), grafted sample (P-DMAEMA), and IIP sample. The selected heating profile of the samples was from room temperature to 500 ºC with heating rate of 4 ºC/min. PE/PP-NWF samples displays one-step thermal degradation with decomposition temperature at 450 ºC which was closely in agreement with [183] and [184]. The degradation process had started at 283 ºC and ended at 498 ºC. This is in good agreement with other researchers who examined the thermal degradation of pristine non-woven PE/PP fabrics [70, 185]. P-DMAEMA sample, on the contrary, had shown show two-step degradation process which indicates the decomposition of the grafted material and the trunk polymer that signifies incorporation of DMAEMA onto PE/PP-NWF. Notably, the initial weight loss in P-DMAEMA, and IIP is estimated around ~7 % within the temperature range of 29 to 60 °C is associated with the loss of water from the samples [186]. The weight loss of the first step started at 159 ºC and ended at 283 ºC with an accompanying weight loss of 23%. As the graft chain contains 100% by weight of DMAEMA chains, the weight loss agrees very well with the loss of DMAEMA units. The second step of degradation started around 292 ºC and ended at 496 ºC with the weight loss of 76%. The former weight loss was due to the degradation of the DMAEMA graft chains, and the latter was due to the degradation of the DMAEMA graft chains as well as the PE/PP-NWF. It can be concluded that the grafted PE/PP-NWF exhibited decreased thermal stability, in comparison with the ungrafted PE/PP-NWF. IIP sample exhibits similar weight loss pattern as P-DMAEMA. Since IIP sample comprises of 100% by weight of DMAEMA units of grafted chain on top of NWF surface, therefore, IIP sample exhibits two stage degradation similar to those of P-DMAEMA.

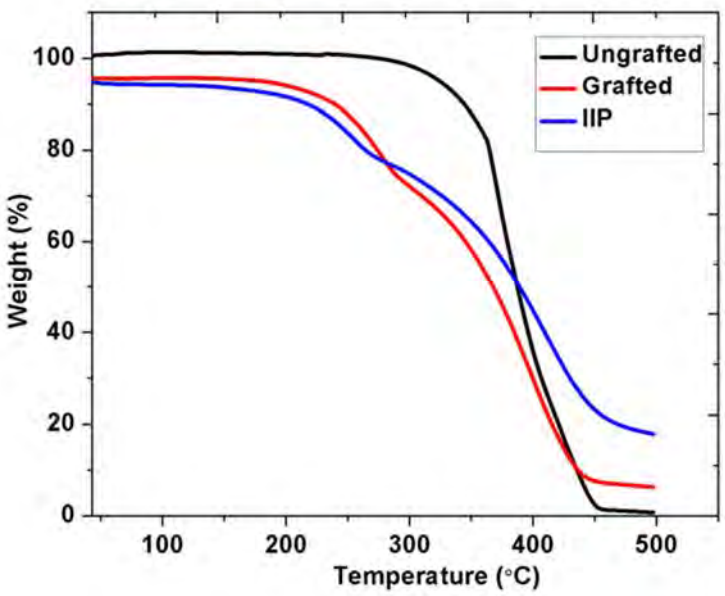

Figure 4.13. Thermogravimetric curves of PE/PP-NWF; P-DMAEMA (Dg≈100%); IIP (Gel content: 83%); and; NIP (Gel content: 90%).

4.3.3.4 XPS

Figure 4.14 – 4.15 (a) – (d) exhibit C1s, O1s and N1s XPS spectra measured onto PE/PP-NWF, P-DMAEMA, IIP and NIP samples respectively. The C1s components were detected onto PE/PP-NWF (ungrafted) sample at 284.73 eV binding energy which corresponds to aliphatic carbon (CAC). O 1s and N 1s orbital was found on DMAEMA-grafted-NWF, IIP and NIP samples, but not on ungrafted NWF sample. Strong peaks were observed at 399.49 eV and 402.75 eV in the N 1s indicating primary and secondary amine group from DMAEMA [147]. But the intensity of strong peak of primary amine at 402.75 eV binding energy slightly shifted in IIP samples, possibly due to incorporation of thorium. The O1s spectrum of P-DMAEMA, IIP and NIP samples shows presence of oxygen bonding as such C-O and C=O at binding energy of 532.45 and 533.44 eV, originating from the functional monomer (DMAEMA) and crosslinker (DVB). The O1s spectrum of the NIP sample exhibit a broad distribution at higher binding energy due to the presence of oxygen bonded carbon and thorium concurrently in the IIP sample. The main peak at 532.38 eV attributes to the present of C-O along with binding energy at 530.68 eV indicates the existence of ThO2. In addition, the change in the binding energy

of O1s was 0.07 eV is found to be lower than that of N1s which amounted to 0.22 eV, implying that the chemical affinity for oxygen is stronger than nitrogen for thorium ion adsorption. The finding thru XPS for IIP sample spectra is as predicted and XPS also verify the chemical composition of the samples at each step of the whole process. Conclusively, clear evidence was obtained on adsorption of thorium ions onto IIP samples which attribute to detection of ThO2 that allowed carbonyl groups from DMAEMA to react with.

(a) XPS spectra, C1s of PE/PP-NWF (ungrafted)

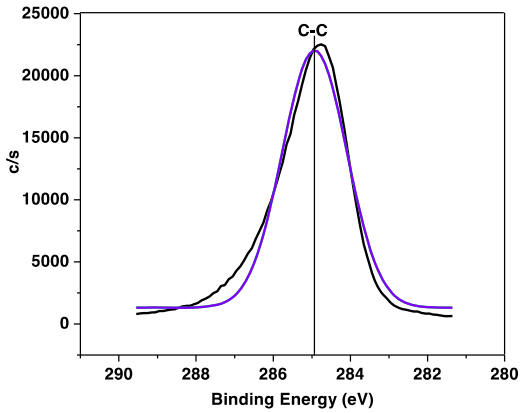

(b) XPS spectra of P-DMAEMA (grafted, with 100% grafting yield)
(i) O1s and (ii) N1s

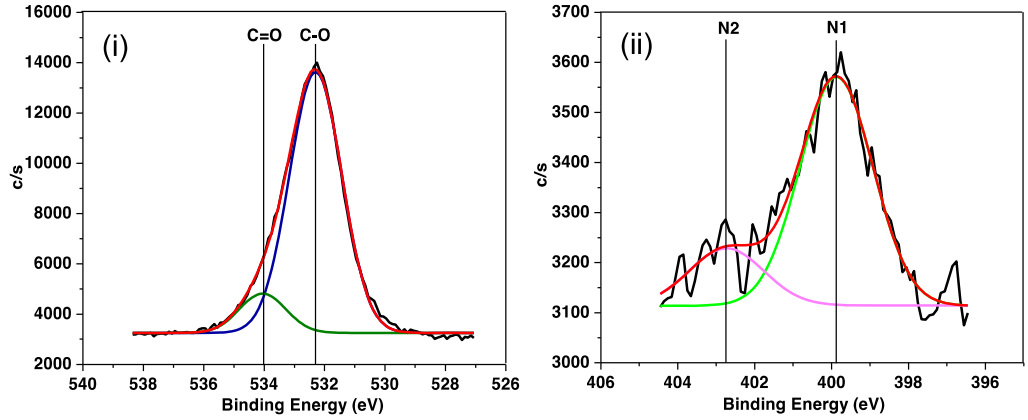

Figure 4.14. C1s, O1s and N1s XPS spectra of (a) PE/PP-NWF, (b) P-DMAEMA, (c) IIP and (d) NIP samples respectively

(c) XPS spectra of IIP (Gel content: 83%), (i) O1s and (ii) N1s

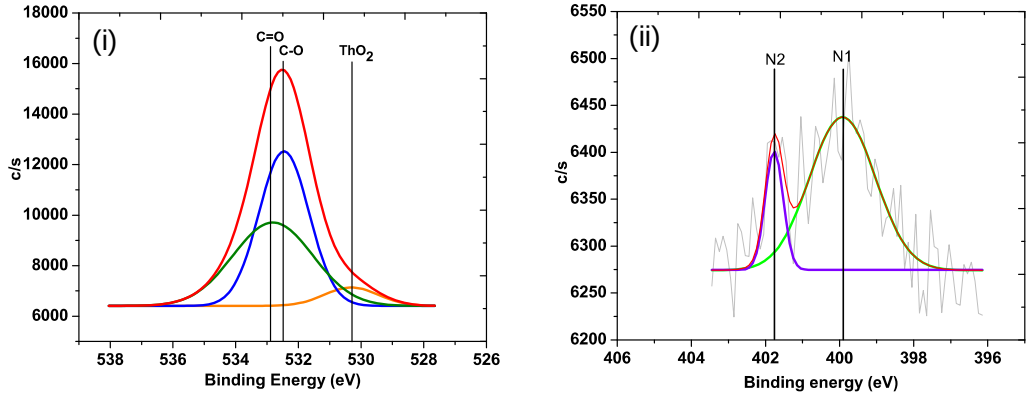

(d) XPS spectra of NIP (Gel content: 90%), (i) O1s and (ii) N1s

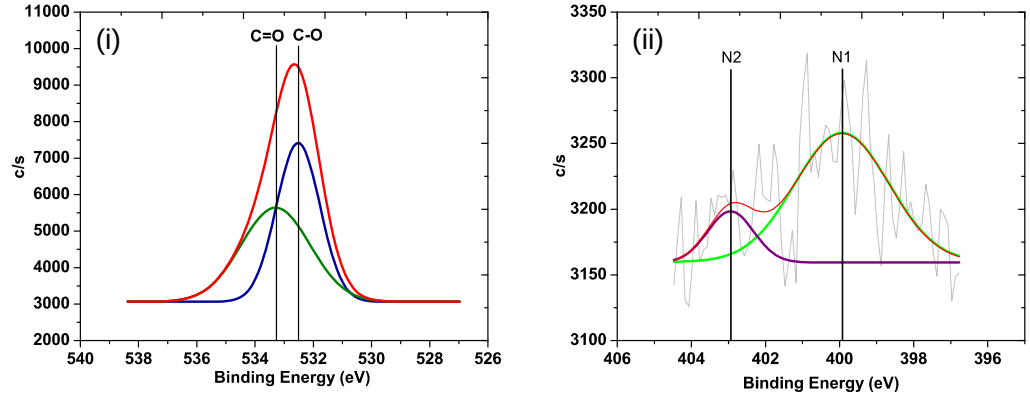

Figure 4.15. C1s, O1s and N1s XPS spectra of (a) PE/PP-NWF, (b) P-DMAEMA, (c) IIP and (d) NIP samples respectively (continued)

The reaction mechanism for the synthesis of IIP samples in this study was summarized into four steps: (i) radiation grafting of DMAEMA monomer onto base polymer (PE/PP-NWF); (ii) impregnation of Th(IV) template via adsorption; (iii) crosslinking of linear polymer chains to form a three-dimensional crosslinked network; and (iv) removal of the template ions and regeneration of the polymer. The mechanism for synthesis of IIP samples can be schematically represented by Figure 4.16 (a) – (c). For radiation grafting, upon exposure to electron beam irradiation, radicals formed on the surface of the PE/PP-NWF backbone which is known as the initiation step. In the presence of DMAEMA monomer in contact with irradiated PE/PP-NWF, the micro radicals were added onto PE/PP-NWF via the double bond of DMAEMA. This will lead to the formation of covalent bond between the DMAEMA and PE/PP-NWF which, in turn, will

propagate grafting onto irradiated fibers [82]. The reaction mechanism of radiation grafting is similar as prescribed in Chapter 3. Irradiation grafting technique is considered as the most convenient and effective technique because it is easy to create radical sites on the polymer backbone. Various functional groups can be introduced to the active sited based to aimed purpose by surface modification technique [138].

Upon completion of polymerization process, impregnation of template ion (thorium) were performed via adsorption process. Thorium ion forms polydentate ligand with functional monomer, DMAEMA [187]. Formation of polydentate ligand occurs by creation of ring structures that include the thorium ion and the two-ligand atoms, O and N which are attached to the thorium as shown in Figure 4.16 (a). N and O atoms which contain lone pairs of electrons, function as donor atom leading to the formation of covalent bond coordination [188]. This was further confirmed by the outcome from XPS analysis which is exhibited in Figure 4.15. Furthermore, monomer–template ion complex was copolymerized with the presence of a cross-linker (DVB) via irradiation technique which establishes a three-dimensional polymeric matrix around the template ion (Figure 4.16 (b)). After co-polymerization, the template is removed and a target specific recognition cavity for thorium ion was formed in the polymeric matrix permanently [155]. The final product (polymer adsorbent) is referred as IIP.

Template impregnation:

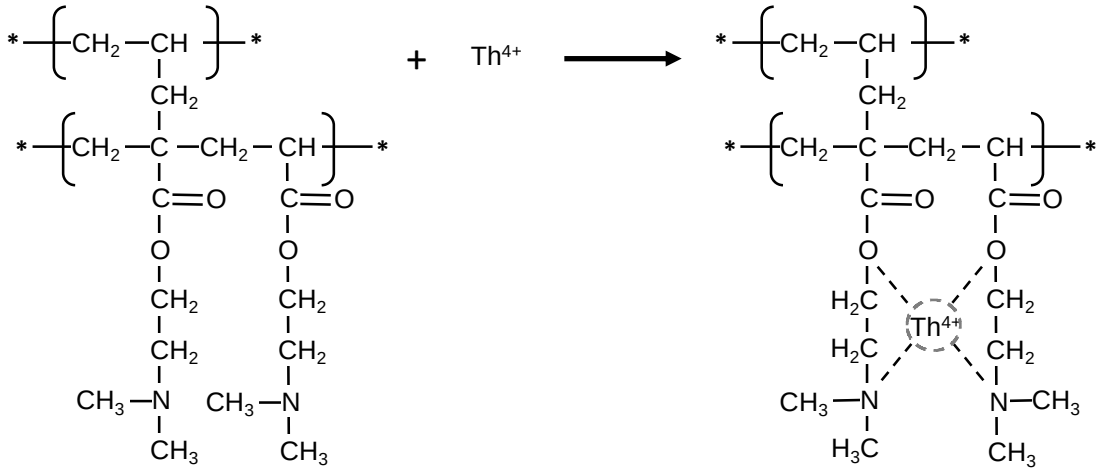

Figure 4.16. (a) Impregnation of Th(IV) template via adsorption

Crosslinking:

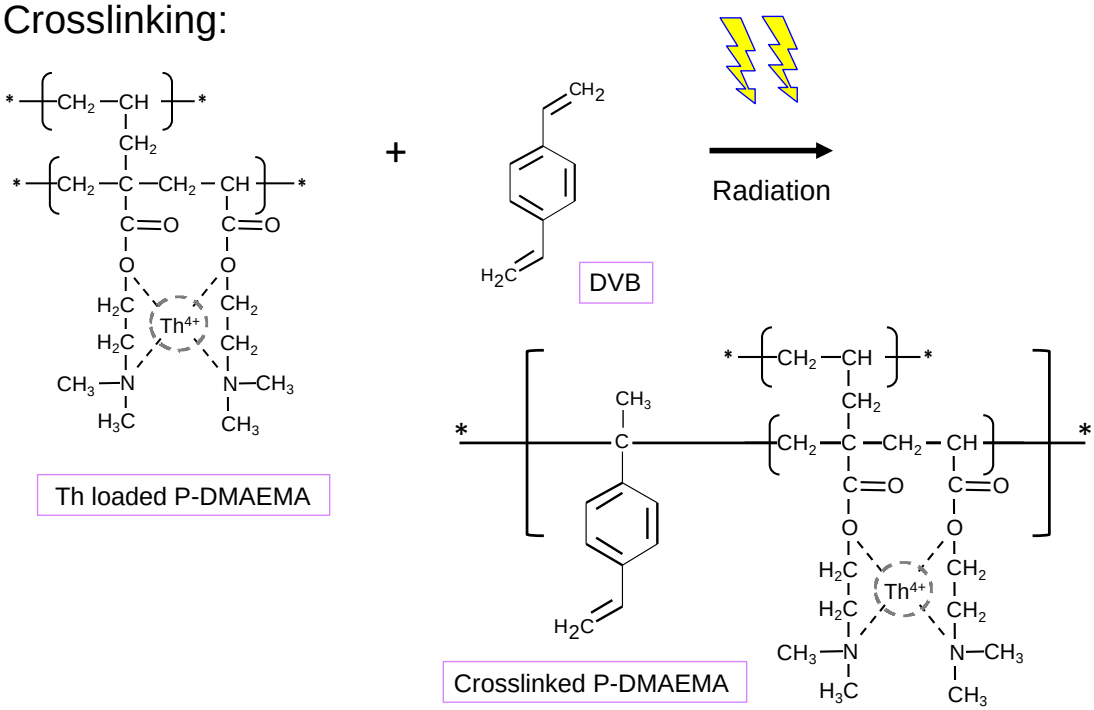

Figure 4.16. (b) Crosslinking of linear polymer chains to form a three-dimensional crosslinked network

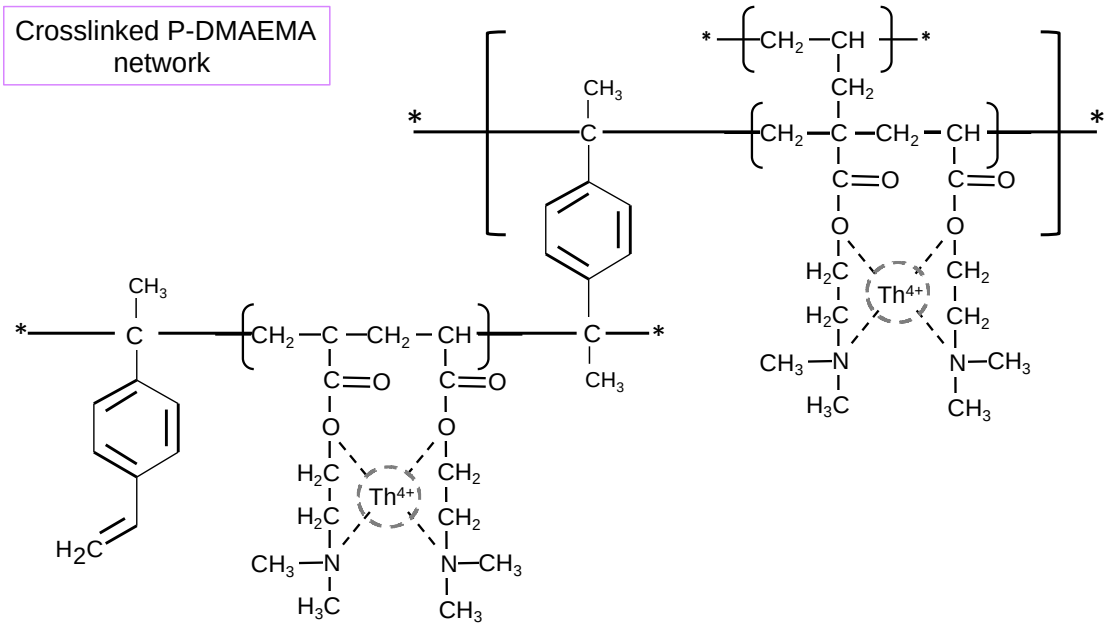

Figure 4.16. (b) Crosslinking of linear polymer chains to form a three-dimensional crosslinked network (continued)

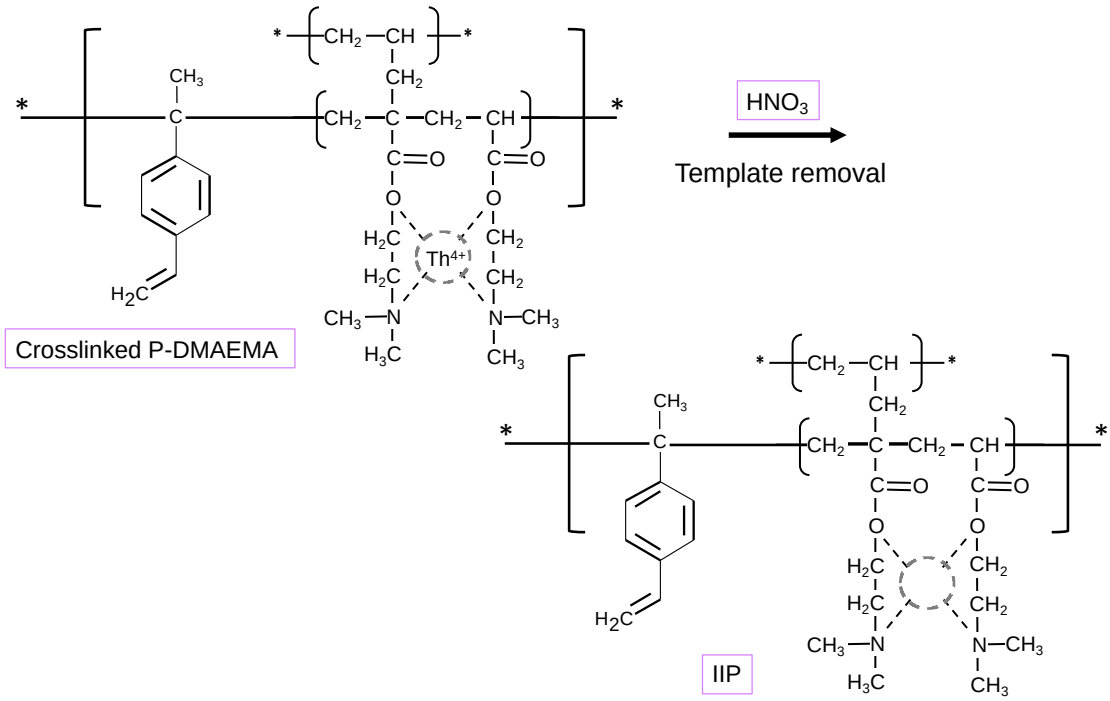

Figure 4.16. (c) Removal of the template ions

4.3.3.5 XRD

Figure 4.17 shows the XRD spectrum of P-DMAEMA, IIP and NIP in which each spectrum has a diffraction peak at 13.78°, 13.49°, 13.69°, and 13.43° respectively, corresponding to the peak for the PE/PP-NWF. The layer spacing increases which is clearly indicated by the shift of the diffraction peak to lower 2θ [189]. The reduction in peak intensity in DMAEMA-grafted PE/PP-NWF, IIP and NIP samples signifies the interaction presents between monomer and template [190]. The equation 4.5 is used to determine the crystal size, L;

$$L = \frac{K\lambda}{\beta cos\theta} \tag{4.5}$$

where, K is the Scherrer constant (usually 0.9), λ is the X-ray's wavelength of, β is the full width at half-maximum (FWHM), and θ is the diffraction peak.

A summary of measured 2θ, calculated d-spacing, and calculated FWHM, crystal size and crystallinity degree are presented in Table 4.3. Crystallinity (%) of the samples had been calculated by using equation 4.6.

$$Crystallinity\ (\%) = \frac{F_c}{F_c + F_a} \times 100\% \tag{4.6}$$

whereby, F_c is the domain of crystal and F_a is the domain of non-crystal.

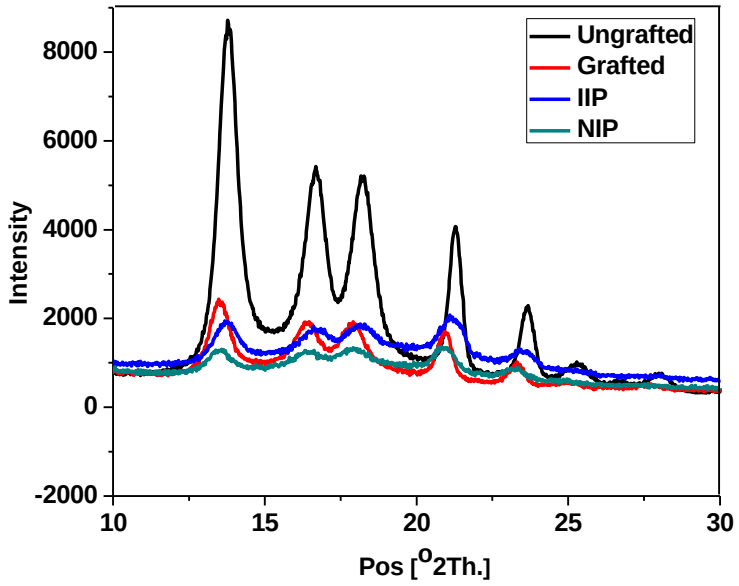

Figure 4.17. XRD spectra PE/PP-NWF (ungrafted); P-DMAEMA (grafted, Dg≈100%); IIP (Gel content: 83%); and; NIP (Gel content: 90%)

Table 4.3. Analysis on XRD patterns of PE/PP-NWF; P-DMAEMA (Dg≈100%); IIP (Gel content: 83%); and; NIP (Gel content: 90%)

Samples	2θ (º)	d-spacing (Å)	FWHM (º)	Crystal Size (Å)	Crystallinity (%)
PE/PP-NWF	13.78	6.42	0.85	3.26	50.04
P-DMAEMA	13.49	6.55	0.87	1.60	29.23
IIP	13.69	6.46	1.16	1.20	10.41
NIP	13.43	6.57	0.97	1.40	13.74

The XRD diffraction patterns as exhibited in Figure 4.17 for PE/PP-NWF, P-DMAEMA, IIP and NIP samples had proved the existence of mixture of crystal and amorphous phases, qualitatively. The crystallinity degree obtained as tabulated in Table 4.3 supports that the polymer used in this study is semi crystalline, quantitatively. IIP samples show the lowest crystallinity degree as more chemical bonds and interactions are present on those samples particularly.

4.4 Conclusion

P-DMAEMA adsorbent precursors by radiation induced grafting of DMAEMA onto PE/PP-NWF was successfully prepared. Incorporation of the carbonyl and amino functional group from DMAEMA onto PE/PP-NWF were strongly evidenced by FTIR analysis. Thermal properties investigated by TGA showed that the grafted materials exhibited a decreased in thermal stability, in comparison to the pristine PE/PP-NWF. A reduction of crystallite size and percentage of crystallinity can be seen from XRD results. The kinetic behaviour of grafting rate showed the order of dependence of the rate of grafting on the DMAEMA monomer concentration and absorbed radiation dose. Radiation grafting of DMAEMA onto PE/PP-NWF needed higher activation energy when the temperature was increasing in the range of 313 – 333 K.

An extensive investigation on the synthesis of ion-imprinted P-DMAEMA by using electron beam irradiation towards thorium has been conducted. The chosen parameters for the preparation of IIP were crosslinking percentage of 80 – 90% grafted P-DMAEMA using 2:1 ratio of DVB to TWEEN20 at 60 kGy absorbed radiation dose. Both IIP and NIP samples were prepared. Characterizations performed on IIP and NIP samples evidently proven the ion-imprinted and non-imprinted process was accomplished.

TGA result indicates that both IIP and NIP samples exhibits two-stage degradation and similar weight loss pattern as P-DMAEMA. The crystallinity degree obtained from XRD supports that the polymer used in this study is semi crystalline, with IIP samples show the lowest crystallinity degree in comparison to NIP, P-DMAEMA and pristine PE/PP-NWF. In order to evaluate the effectiveness of the prepared adsorbent polymer, the assessment of adsorptive properties of P-DMAEMA, IIP and NIP will be discussed in detail in Chapter 5.

CHAPTER 5

ASSESMENT OF ADSORPTION PERFORMANCE AND SELECTIVE REMOVAL OF THORIUM USING AMINE-BASED IIP

5.1 Introduction

The synthesis and characterizations of amine-based adsorbent, and subsequently, further modification using crosslinking has been explained in detail in Chapter 4. Accordingly, this chapter presents the result of adsorption experiments in batch studies according to different parameters, which determined the performance of the modified adsorbents. Batch adsorption performances was performed, and the adsorption kinetics and equilibrium were also studied to investigate the effect of the process parameters and the relevant adsorption behaviour towards radioelements, namely thorium and uranium. Subsequently, the selectivity of crosslinked adsorbent towards thorium was appraised under competitive adsorption in a binary solution. The effect of process parameters towards the adsorption capacity and selectivity was evaluated.

Although there are considerable amount of literature reported on removal of Th(IV) using other grafted adsorbent such as hydrogel [191], amidoximated polyolefin [102, 192], nanocomposite [193, 194] and graphene [195, 196], all these studies were conducted using conventional method by varying one factor at a time (OFAT) whilst maintaining all other factors constant. The OFAT method of investigating each factor separately is time consuming. In addition, the OFAT method are not capable to process multi-variables, and if several variables influence the response, their interactive effects between two or more variables in the system would not be observable despite the fact that several factors dominating the response. Design of experiment (DoE) is a statistical method that applies factorial concept and use the modelling to predict the behaviour of the predetermined process variables [197]. Therefore, Response Surface Methodology (RSM)-based Box-Behnken model DoE was employed in one of the sub-sections in this

chapter to statistically determine the optimum reaction conditions for Th(IV) adsorption. RSM can avoid the limitations of OFAT method and reduce lead time and improve efficiency. Furthermore, the interaction between the process variables can be explained based on the RSM prediction and experimental data obtained from the experiment. In addition, no effort was conducted to optimize the economical usage of fibrous grafted adsorbent for removal of thorium from aqueous solution using Box-Behnken method. In this study, Box-Behnken response surface methodology was employed to optimize the effects of process parameter on the adsorption capacity and to observe the correlation when the adsorbent dosage was set to minimum. All analyses were studied in detail for a better understanding of the overall adsorption mechanism occurred during the Th(IV) adsorption process.

5.2 Experimental Section

5.2.1 Materials

1000 mg/L thorium, Th(IV) in 2% HNO_3 standard solution was purchased from Perkin Elmer (UK). The standard solution was subjected to series of dilution in order to attain desired concentration using 2% nitric acid (HNO_3, 65%). pH adjustment was done using concentrated HNO_3 or ammonia (NH_3).

5.2.2 Batch Adsorption Studies

Batch equilibrium tests were carried out in term of effect of solution pH, effect of Dg, initial adsorbate concentration and contact time towards the adsorption capacity of adsorbent. The adsorbent with known weight was added to 100 mL of predetermined Th(IV) concentration. The mixture was then stirred for a definite period of time. The solution was filtered using a syringe filter (Whatmann 0.45 μm nylon filter) prior to analysis. The removal percentage of Th(IV) ions and adsorption capacity of adsorbent was calculated using the equations below.

$$Removal\ (\%) = {(C_f - C_i)}/{C_i} \times 100 \quad (5.1)$$

$$Adsorption\ capacity\ (q_e) = (C_i - C_f) \times {V}/{m} \quad (5.2)$$

whereby, C_i and C_f are the initial and final concentrations of elements (mg/L), V is the volume of solution (mL), and m is the mass of the adsorbent.

5.2.2.1 Response Surface Method of Th(IV) Adsorption by P-DMAEMA

Response surface method (RSM) is one of the statistical techniques of DoE that employed a regression analysis from a collective data to identify the best process performance, interaction effect, and significance of factors for optimization [197, 198]. There are two main types of RSM, namely; Central Composite Design (CCD) and Box-Behnken Design (BBD). The CCD approach can test extreme conditions of up to 5 levels per factor, which can fit a full quadratic model. Conversely, the BBD has fewer design points compared to the axial points of the CCD, which is similar to the face-centred composite design (alpha=1). Therefore, the BBD requires fewer experimental runs for similar numbers of factors, which makes it less expensive and time saving compared to CCD. Box-Behnken design involves 3 factors; adsorbent dosage (X_1), initial concentration (X_2) and time (X_3). Three levels (low (-1), medium (0) and high (+1)) of each factor were used in this study to optimize the efficiency of Th (IV) adsorption. Process factors and their levels are given in Table 5.1.

Table 5.1. Process factors with 3 levels of Box-Behnken

Factors	**Levels of Box-Behnken**		
	Low (-1)	Medium (0)	High (+1)
Adsorbent dosage (g) (X_1)	0.002	0.0035	0.005
Initial concentration (mg/L) (X_2)	1	5.5	10
Time (h) (X_3)	8	16	24

In due consideration of the economical use of the adsorbent, the adsorbent dosage was set to minimum and the reaction time was extended explicitly beyond the standard practice to ensure complete equilibrium. This will guarantee that the effect of time will have the least influence on the system during the experiments. In the optimization process of RSM, linear or quadratic models are commonly used. To optimize the adsorption capacity, quadratic model was chosen and is given below;

$$y = \alpha_0 + \alpha_1 X_1 + \alpha_2 X_2 + \alpha_3 X_3 + \alpha_{12} X_1 X_2 + \alpha_{13} X_1 X_3 + \alpha_{23} X_2 X_3 + \alpha_{11} X^2{}_1 + \alpha_{22} X^2{}_2 + \alpha_{33} X^2{}_3 \quad (5.3)$$

where y is the predicted response variable, α_0 is the constant regression, α_i, α_{ii}, α_{ij} represents the linear coefficient, quadratic coefficient, and the interaction coefficient, respectively. X_i is the coded variable level and i or j is the number of independent variables. Each fitted model was examined to ensure that it gives an accurate

approximation to the true system in order to empirically assess the usefulness of the predictive capabilities of the model and to verify that the model satisfies the assumptions of the analysis of variance (ANOVA).

5.2.3 Selectivity Studies

The selectivity of IIP and NIP towards thorium was appraised under competitive adsorption in a binary solution of Th(IV): Other REEs (interfering ions) (U(VI), Ce(IV), La(III), Sm(III) and Pr(III)). Besides, the selectivity experiments were carried out under non-competitive adsorption mode as well. The adsorption was carried by stirring 0.1 g of IIP and NIP in 50 mL of binary or individual solutions at pH 3.0 for 180 minutes. Subsequently, the IIP and NIP were filtered, and the aliquots were tested with XRF in order to quantify the elements. The adsorbed amount of elements onto the samples was calculated by the difference between initial and final solution. The distribution coefficient (k_d) is calculated according to equation 3.4, meanwhile the selectivity (K) and relative selectivity coefficient (K') were calculated via the equation below;

$$K_{IIP} = \frac{k_{d\,(thorium)}}{k_{d\,(interfering)}} \tag{5.4}$$

$$K_{NIP} = \frac{k_{d\,(thorium)}}{k_{d\,(interfering)}} \tag{5.5}$$

$$K' = {K_{IIP}}/{K_{NIP}} \tag{5.6}$$

whereby, $k_{d\,(thorium)}$ and $k_{d\,(interfering)}$ are the distribution coefficients of thorium and interfering element, respectively. K_{IIP} and K_{NIP} are selectivity coefficients of both IIP and NIP, respectively.

5.2.4 Analytical Procedures

5.2.4.1 Thorium Concentration Measurement

To evaluate the adsorption behaviour of each adsorbent, adsorption test was performed using thorium ions as adsorbate in batch adsorption system. The initial concentration of thorium solution and the concentration in remaining solution after the adsorption process was measure with ICP-OES (Spectro Arcos, Germany) spectrometer.

5.2.4.2 Multi Elements Concentration Measurement

ICP-MS spectrometer, Perkin Elmer (model NEXION 350x) with pneumatic nebulization (cross-flow nebulizer), a Scott-type nebulization chamber and a Gilson peristaltic pump were used. An injector alumina tube with the diameter of 1.3 mm was used inside the torch. The optimization of the ICP-MS parameters was done by adjusting the nebulizer gas flow and the alignment of the mass spectrometer in relation to the torch (x–y adjustment) in order to obtain the maximum production of ions M^+ and minimum signals for M^{++}, MO^+ and background at m/z 220. Argon (purity of 99.9%) was used.

5.2.4.3 pH Measurement

The effect of pH was studied by performing adsorption test in different initial pH (1, 1.5, 2, 2.5, 3 and 3.5) in room temperature. The pH was adjusted with HNO_3 and/or NH_3 as required. The pH of thorium solution was recorded by pH meter (Mettler Toledo, Germany). The effect of pH on the adsorbent was observed by swelling test. To determine the swelling ratio, the dried samples were immersed into buffer solution of pH ranging from 2 to 12 for 180 minutes. The excessive solution was gently wiped with tissue and the samples were weighed. The swelling ratio was determined gravimetrically as follows;

$$Swelling\ Ratio\ = {W_s}/{W_d} \tag{5.7}$$

where, W_d is initial (dry) weight of sample and W_s is the weight of swollen sample, respectively.

5.3 Results and Discussion

5.3.1 Adsorption Equilibrium

In the adsorption process, adsorbates are simultaneously being adsorb and desorb as it proceeds until an equilibrium state is achieved. In this study, adsorption at equilibrium was carried out in order to determine the amount of Th(IV) adsorbed per unit mass of adsorbent used. Amine-based adsorbents, P-DMAEMA as described in Chapter 4, section 4.4.1 was evaluated. The effect of operational parameters such as solution pH and the effect of Dg towards the adsorption capacity was investigated. Subsequently, the adsorbent was subjected to further study on adsorption kinetics, isotherms and thermodynamics for better understanding of the overall adsorption mechanism occurs during the adsorption in single-metal system for Th(IV) and U(VI) respectively. The focus of this study is to have complete understanding of adsorption behaviour of the prepared adsorbent in single metal system before the incorporation with ion recognition imprinted technique. This knowledge serves as a basic platform to predict the adsorption mechanism for IIP in binary metal system.

5.3.1.1 Effect of Solution pH

DMAEMA is hydrophilic in both its protonated and non-protonated states, but sensitive to both temperature and pH changes. The swelling behaviour of grafted PE/PP-NWF was investigated as a function of pH at room temperature. As shown in Figure 5.1, P-DMAEMA swells when protonated to low pH, which associated with the positive charge repulsion of tertiary amine moieties [199]. Investigation by V. Bütün *et al.* revealed that DMAEMA has a pK_a of about 7.0 [200]. Therefore, as shown in the figure, swelling ratio decreased significantly above pH 7 due to deprotonation. This result is in agreement with findings by Burillo *et al.* [170] which revealed that DMAEMA exist in hydrophilic phase at acidic condition (ca. pH 2) and hydrophobic phase at pH 6 or more. Thus, to ensure the hydrophilicity for both of the grafted PE/PP-NWF, adsorption was done in acidic condition.

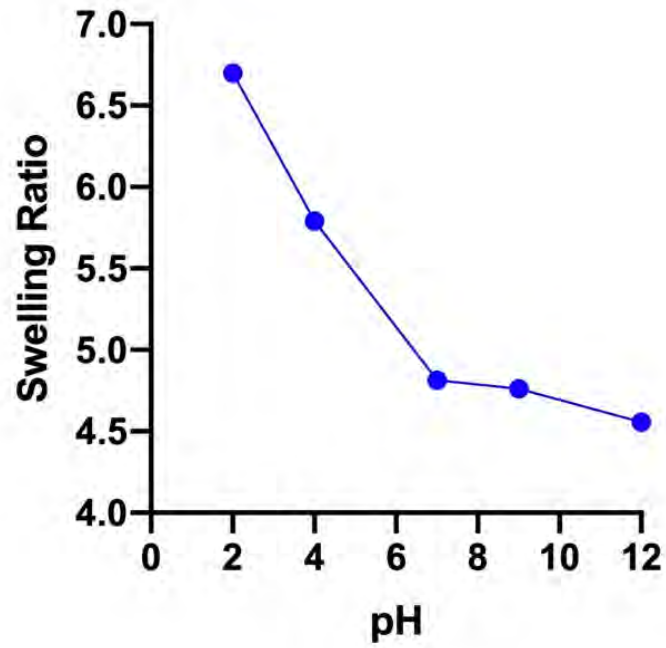

Figure 5.1. Swelling ratio as function of pH for P-DMAEMA

The influence of pH on the thorium ions adsorption onto grafted P-DMAEMA was studied using pH 1 to pH 3.5 at room temperature. As shown in Figure 5.2, the pH was limited to pH 3.5 based on the reason that below pH 3.5, the predominant thorium ion would be positively charged, while at pH > 3.5, Th(IV) ions undergo extensive hydrolysis with water and form hydrolytic species [71, 201]. Thus, adsorption studies pH > 3.5 is avoided to ensure that the stability of thorium ions as tetrapositive ions.

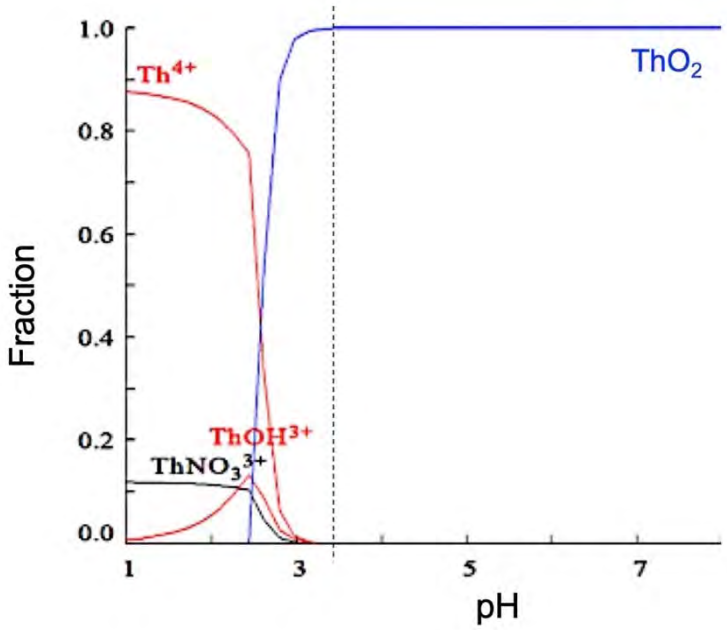

Figure 5.2. Thorium species in HNO_3 as function of pH

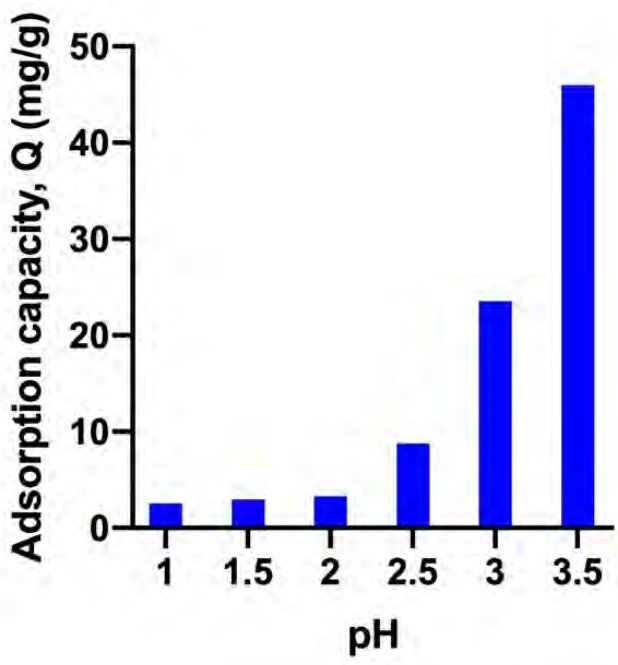

Figure 5.3. Adsorption capacity as function of pH for P-DMAEMA

Batch adsorption test was carried out at pH 1 to 3.5 for 8 hours to evaluate the effect of pH on the adsorption capacity. Each sample was punch-cut into 5 mm in diameter pieces with average Dg used in the experiments was 114%. As shown in Figure 5.3, at pH 1 and pH 2, the amino active sites become highly protonated and the protonated N sites repel with the positively charged Th (IV) ions. Due to this electrostatic repulsion, no appreciable uptake of thorium ions was seen at this pH. However, at pH > 3, deprotonation starts to occur resulting to increase of thorium ions uptake.

5.3.1.2 Effect of Dg

In general metal ions adsorption process, the adsorption capacity of metal ions will increase as the graft yield increases, due to more functional groups which are grafted onto the substrate are available for the interaction to take place. The effect of Dg on the adsorption amount of thorium ions was studied by performing batch adsorption experiments in the Dg range 20 to 120% (pH 3.5, 8 hours reaction time). Each sample was prepared as mentioned earlier. The results are shown in Figure 5.4. The adsorption capacity for Th (IV) ions increased with the increase of Dg for P-DMAEMA.

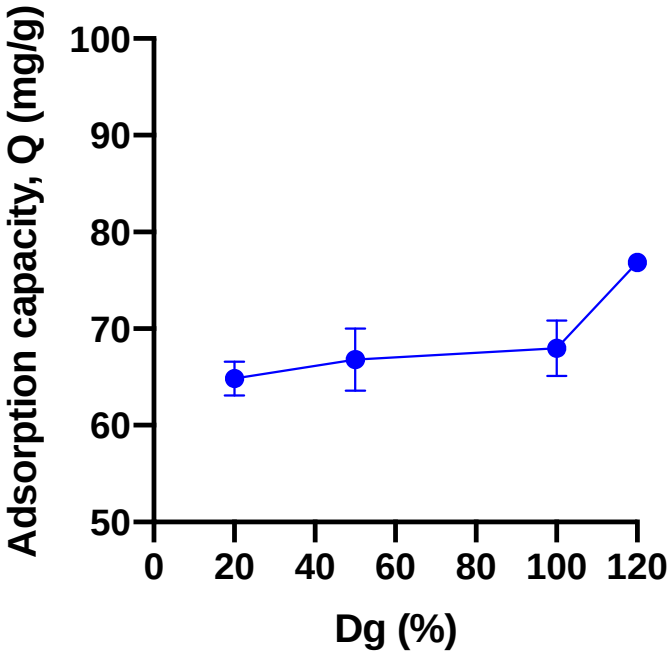

Figure 5.4. Effect of Dg on the adsorption capacity of Th (IV) by P-DMAEMA in aqueous solution

Bhardwaj *et al.* summarized in a guideline [202] that grafting yields should be tailored-made depending on its intended application. Sekine A. *et al.* [133] and Ma H. *et al.* [156] reported in their studies that Dg greater than 100% is sufficient for preparation of metal ions adsorbent. Therefore, Dg of 100% by weight of monomer units was targeted in this study.

5.3.2 Adsorption of Th(IV) and U(VI) in Single-metal System

5.3.2.1 Effect of Initial Concentration

Figure 5.5 shows the effect of different initial concentration of Th(IV) towards the adsorption capacity and removal percentage using P-DMAEMA. It was observed that as the initial concentration increases from 25 to 300 mg/L, the amount of adsorbates adsorbed by the adsorbent increased. This is due to enhanced interaction between the adsorbates and adsorbents as the initial concentration increasing, which give an indication of a finite binding sites on the adsorbent. A linear increment can be seen for U(VI), while a saturation trend can be observed for Th(IV) at 200 mg/L onwards. At low concentration, the ratio of surface-active sites to total Th(IV) and U(VI) ions are high, resulting in high

percentage of removal. Vice versa, at high concentration the removal percentage is low. This is because with the increase of initial concentration, the number of active sites on the adsorbent become fewer to accommodate the adsorbates and thus reduces the removal performance [203]. In order to further understand the distribution of Th(IV) and U(VI) during the adsorption process using P-DMAEMA, the equilibrium of the adsorption is measured and can be expressed by the isotherm models.

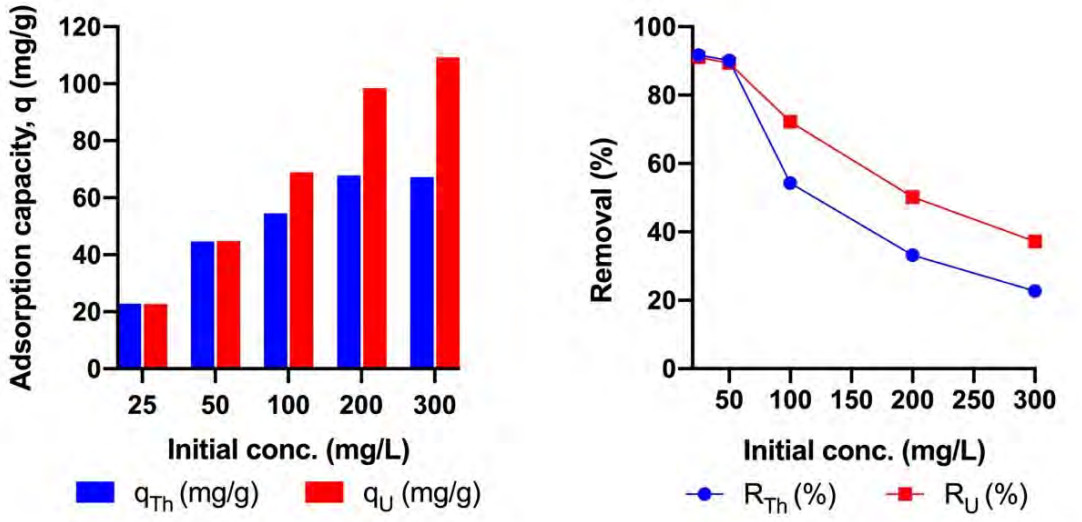

Figure 5.5. Effect of initial concentration on (a) adsorption capacity, and (b) percentage of removal of Th(IV) and U(VI) by P-DMAEMA

5.3.2.2 Isotherm Model Analysis

In order to have a better understanding of the correlation between the distribution of Th(IV) and U(VI) with P-DMAEMA adsorbent in the adsorption process, two-parameters isotherm models namely Freundlich and Langmuir were investigated. These models describe the adsorption isotherms and explain the experimental results and real adsorption behaviour by relating the adsorption capacity at equilibrium, $q_e\ (mg/g)$ to the concentration at equilibrium, $C_e\ (mg/L)$ [204]. Langmuir isotherm model is the most common model used in mono-layer homogeneous surfaces. The isotherm is expressed by equation as follows;

$$q_e = q_{max} \frac{K_L C_e}{1+K_L C_e} \quad (5.8)$$

whereby, $q_e\,(mg/g)$ is thorium adsorption at equilibrium, $C_e\,(mg/L)$ is the concentration of thorium solution at equilibrium, $K_L(L/g)$ are Langmuir adsorption constant. The isotherm constants can be obtain using the linearized equation below;

$$C_e/q_e = \left(C_e/q_{max}\right) + \left(1/K_L q_{max}\right) \quad (5.9)$$

On the other hand, the Freundlich isotherm model describes adsorption at multi-layers heterogenous surfaces and is expressed by equation as follows;

$$q_e = K_F C_e^{1/n} \quad (5.10)$$

whereby, $q_e\,(mg/g)$ is thorium adsorption at equilibrium, $C_e\,(mg/L)$ is the concentration of thorium solution at equilibrium, $K_F(mg/g)(L/mg)^{1/n}$ is Freundlich adsorption constant related to adsorption capacity and *n* is the heterogeneity factor indicating the adsorption intensity [205]. The isotherm constants can be obtain using the linearized equation below;

$$ln\ q_e = ln\ K_F + (1/n)\ ln\ C_e \quad (5.11)$$

The best fitting model was determined using mathematical error functions to validate each isotherm model. The fit of the model to the data is assessed using the standard deviation (SD), coefficient of variation (CV), average relative error (ARE) and linear coefficient correlation (R^2), whereby *CV* <1 indicates a low variance of distribution and the better fit is evaluated when R^2 is closer to 1 [206]. The mathematical equations are as follows;

$$SD = \left[\left\{\sum\left(q_{exp} - q_{mean}\right)^2\right\}/(x-1)\right]^{0.5} \quad (5.12)$$

$$CV = SD/q_{mean} \quad (5.13)$$

$$ARE = \frac{100}{x}\sum_{i=1}^{x}\left|\frac{q_{exp}-q_{theory}}{q_{exp}}\right|_i \quad (5.14)$$

where, q_{exp} are the actual experimental data points and q_{mean} are the mean of the experimental data. q_{theory} is the calculated data and *x* is the number of experiments conducted. The adsorption isotherms describing the Th(IV) and U(VI) adsorption onto P-DMAEMA, along with the correlation coefficients are presented in Table 5.2.

Table 5.2. Adsorption isotherm parameters of Th(IV) and U(VI) adsorption

	Th(IV)	**U(VI)**
$q_{exp}\,(mg/g)$	68.60	109.27
Langmuir		
$q_{max}(mg/g)$	68.97	114.94
$K_L(L/mg)$	0.18	0.081
R^2	0.998	0.997
SD	22.26	40.18
CV	0.45	0.59
ARE	12.11	12.34
Freundlich		
$K_F\left((mg/g)(1/mg)^{1/n}\right)$	24.87	20.95
n	5.04	3.00
R^2	0.834	0.943
SD	19.42	39.37
CV	0.38	0.57
ARE	12.65	11.86

Langmuir isotherm model shows high coefficient correlation (R^2) for both Th(IV) and U(VI) as shown in the results. This confirms the applicability of Langmuir isotherm model to describe both adsorption of Th(IV) and U(VI) onto P-DMAEMA via the R^2 value. This indicates that the adsorption was a monolayer adsorption onto the adsorbent surface, without the interaction between the adsorbed molecules on adjacent sites. In order to further analyse whether the adsorption system is favourable or not, the separation factor, R_L is calculated as below to further describe the characteristic of Langmuir isotherm.

$$R_L = 1/(1 + K_L C_0) \tag{5.15}$$

where C_0 is the initial concentration (mg/L). The value of R_L indicates the type of the isotherm to be either favourable ($0<R_L$), linear (R_L=1), irreversible (R_L=0) or unfavourable (R_L>1) [207].

R_L for Th(IV) and U(VI) adsorption for all concentrations were found to be $0<R_L<1$. Thus, it can be concluded that both Th(IV) and U(VI) adsorption onto P-DMAEMA is favourable and best fit to the Langmuir adsorption isotherm model. The predicted data and the experimental data were compared by data fitting to the isotherm equations, as shown in Figure 5.6.

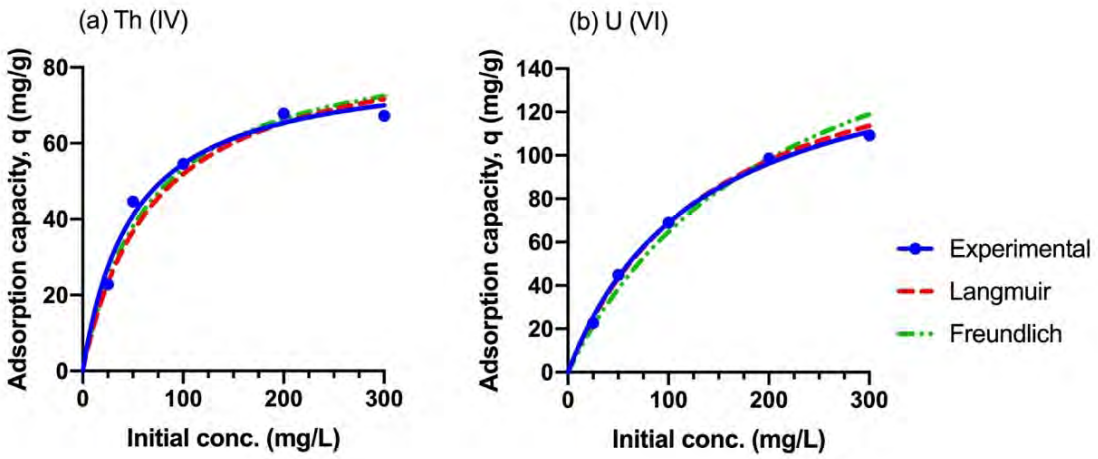

Figure 5.6. Isotherm model analysis for (a) Th(IV) and (b) U(VI) adsorption

It was observed that the Langmuir model showed good fitting of the adsorption isotherm, in comparison to Freundlich model. Freundlich model showed lower R^2 value, but the value is fairly high (0.83 for Th(IV) and 0.94 for U(VI)) and the fitting does not deviate much from the experimental value. This means that the adsorption for both Th(IV) and U(VI) ions underwent from monolayer to multilayer adsorption and P-DMAEMA encompassed of a mixture of homogeneous and heterogeneous adsorption sites on the surfaces [208]. A value of *n* ranging from 2 to 10 is considered favourable, thus the high value of *n* (*n*=5.04) from Freundlich indicates a relatively uniform surface on P-DMAEMA for Th(IV) adsorption. On the other hand, although still within the range, the low *n* value (*n*=3.00) for U(VI) adsorption compared to Th(IV) adsorption indicates the existence of high energy active sites on P-DMAEMA where high adsorption at low concentration could be achieved.

5.3.2.3 Effect of Temperature

Figure 5.7 shows the effect of different temperature on the adsorption capacity of Th(IV). The temperature investigated in this study is 30°C to 50°C. It was observed that the adsorption of Th(IV) and U(VI) ions increased accordingly to higher temperature, from 30°C to 50°C. The adsorption capacity increased with temperature, which probably due to the increase of kinetic energy in the aqueous solution that contributes to the number of collisions between the ions with the active sites of the adsorbent. Similar observation was reported by other researchers where the adsorption capacity increases as the

temperature increased [72, 209]. In order to further understand the performance of Th(IV) and U(VI) adsorption with respect to temperature, the thermodynamic parameters were analysed according to Gibbs expression.

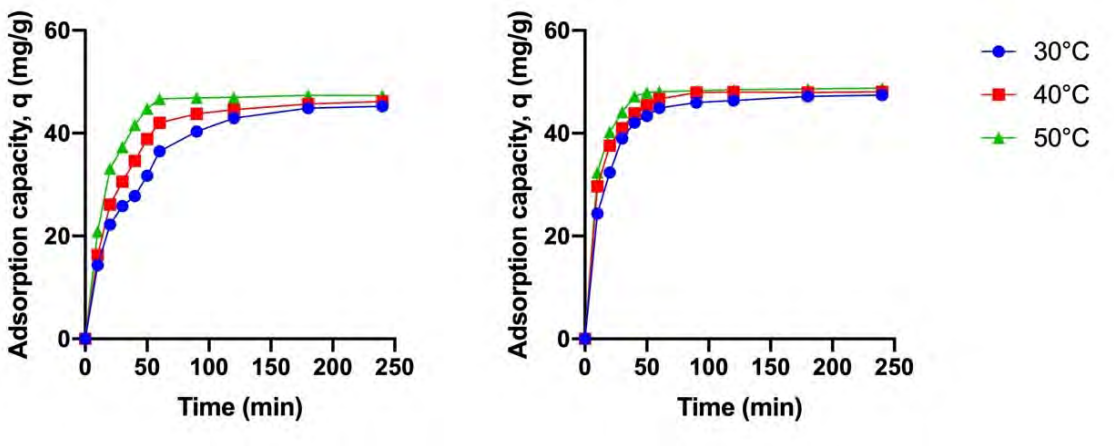

Figure 5.7. Effect of temperature on the adsorption capacity of (a) Th(IV) and (b) U(VI)

5.3.2.4 Thermodynamic Properties

The Gibbs free energy which based on the adsorption related to the equilibrium classical Van Hoff [210], is expressed as shown in Equation 5.17 based on the thermodynamic parameters such as free energy (ΔG^0), enthalpy (ΔH^0) and entropy (ΔS^0). Additionally, the Gibbs free energy was calculated as shown in Equation 5.18;

$$\Delta G^0 = \Delta H^0 - T\Delta S^0 \quad (5.16)$$

$$\Delta G^0 = -RT \ln K_D \quad (5.17)$$

The combination of above equations gives;

$$\ln K_D = \frac{\Delta S^0}{R} - \frac{\Delta H^0}{RT} \quad (5.18)$$

where, R is the universal gas constant (8.314 J/K mol), T is the absolute solution temperature (K), K_D is the distribution coefficient. K_D (*dimensionless*) is calculated from $K_D = \frac{q_e}{C_e} \cdot \frac{m}{V}$, where q_e is the amount of metal adsorbed at equilibrium (mg/g), C_e is the retained concentration of each metal at equilibrium (mg/L), m is the mass of adsorbent (g) and V is the volume of adsorbate solution (L).

Table 5.3. Thermodynamic properties of Th(IV) and U(VI) adsorption onto P-DMAEMA

Adsorbates	ΔG^0**(kJ/mol)**			ΔH^0	ΔS^0
	303 K	313 K	323 K	**(kJ/mol)**	**(J/mol K)**
Th(IV)	-2.126	-3.041	-3.955	25.58	91.45
U(VI)	-3.856	-5.006	-6.155	30.97	114.88

The results are tabulated in Table 5.3. When Th(IV) and U(VI) is chemisorbed onto the surface of P-DMAEMA, the surface energy is minimized, and the entropy changed due to the changes in the structure of the adsorbent. Since a large value for the change of entropy was observed, negative value of ΔG^0 was perceived, which confirms the adsorption is exothermic. The negative values of ΔG^0 ensures the spontaneous nature of the adsorption for both Th(IV) and U(VI) onto P-DMAEMA. The value decreased as the temperature increased indicating that the adsorption processes are more favourable at higher temperature. The positive value of ΔS^0 indicated some structural changes occur on the adsorbent during the interaction between the active sites and metal ions [134]. The higher value of ΔS^0 for U(VI) adsorption indicated that interaction between the active sites and U(VI) ions at the solid/liquid interface are more random during the adsorption process in comparison to Th(IV) adsorption.

5.3.2.5 Effect of Contact Time

Contact time plays a vital role in adsorption to determine the rate of adsorption process under various conditions. Generally, adsorption can be categorized into two stages, the initial rapid phase and the slower second phase (saturation). From Figure 5.7, it can be seen that the adsorption rate was rapid for the first one hour, and the gradually slowing until it reached saturation for both Th(IV) and U(VI). This is due to the adsorption on the exterior surface at the initial stage and it became slow when the ions entered into the interior surface. In addition, the slower second phase of adsorption may imply other adsorption mechanisms such as microprecipitation or complexation [211]. U(VI) adsorption shows higher adsorption rate than Th(IV) where it increased rapidly and reached saturation after 1.5 hours. On the other hand, Th(IV) adsorption increased rapidly for the first one hour and gradually increased until it reached its equilibrium after 2 hours. The adsorption rate of Th(IV) shows higher tendency as the temperature

increased. However, the results suggested that after the equilibrium time, no further adsorption occurred for both Th(IV) and U(VI) for all temperatures.

5.3.2.6 Kinetic Model Analysis

Generally, solid-liquid adsorption process involves the adsorption of adsorbates by active sites of adsorbent via physical and chemical interaction (physisorption or chemisorption) [212, 213]. Several researchers have proposed different models to identify and predict the adsorption process, mainly by describing the adsorption kinetic steps using either physical or chemical based models in order to obtain insight of the adsorption mechanism on the adsorbent surfaces. In this study, two models, namely pseudo-first order (Lagergren model) [214] and pseudo-second order (Ho and Mckay model) [215, 216] kinetic were investigated to identify the mechanism of Th(IV) and U(VI) adsorption kinetic in single-metal system. The linearized equations are as follow;

Pseudo First Order (PFO):

$$\ln(q_{e1} - q_t) = \ln q_{e1} - k_1 t \tag{5.19}$$

Pseudo Second Order (PSO):

$$t/q_t = \left(1/k_2 q_e^2\right) + \left(t/q_{e2}\right) \tag{5.20}$$

Table 5.4. Kinetic parameters for thorium adsorption onto P-DMAEMA in single metal system (Initial concentration = 50 mg/L, pH 3.5)

	Th(IV)			**U(VI)**		
	30°C	40°C	50°C	30°C	40°C	50°C
$q_{exp}\,(mg/g)$	45.2	46.17	47.32	47.41	48.08	48.78
PFO						
$q_{theory}(mg/g)$	41.388	36.343	47.465	26.576	37.713	44.036
$k_1(1/min)$	0.02414	0.02893	0.05592	0.03169	0.05537	0.08088
$h_0(mg/g \cdot min)$	41.3518	38.2110	125.985	22.382	78.750	156.838
$t_{1/2}$	1.001	0.951	0.377	1.187	0.479	0.281
R^2	0.9925	0.9605	0.9899	0.9149	0.9858	0.9881
PSO						
$q_{theory}(mg/g)$	49.32	48.85	49.01	48.74	49.05	49.39
$k_2(mg/min)$	0.00095	0.00158	0.00315	0.00325	0.00321	0.00317
$h_0(mg/g \cdot min)$	2.3213	3.7622	7.5758	7.722	7.722	7.722
$t_{1/2}$	21.2471	12.9843	6.4693	6.312	6.352	6.396
R^2	0.9884	0.9949	0.9976	0.9987	0.9993	0.9996

It was found that the kinetics adsorption of P-DMAEMA for both Th(IV) (Figure 5.8) and U(VI) (Figure 5.9) correlated well with PSO kinetic model in contrast to that of PFO kinetic model. This shows the adsorption is more inclined towards chemisorption. Th(IV) and U(VI) and surface of P-DMAEMA intact by chemical bond formation by metal complexation [217]. Furthermore, the experimental maximum adsorption capacity found to be in good agreement with theoretical maximum adsorption capacity for Th(IV) and U(VI).

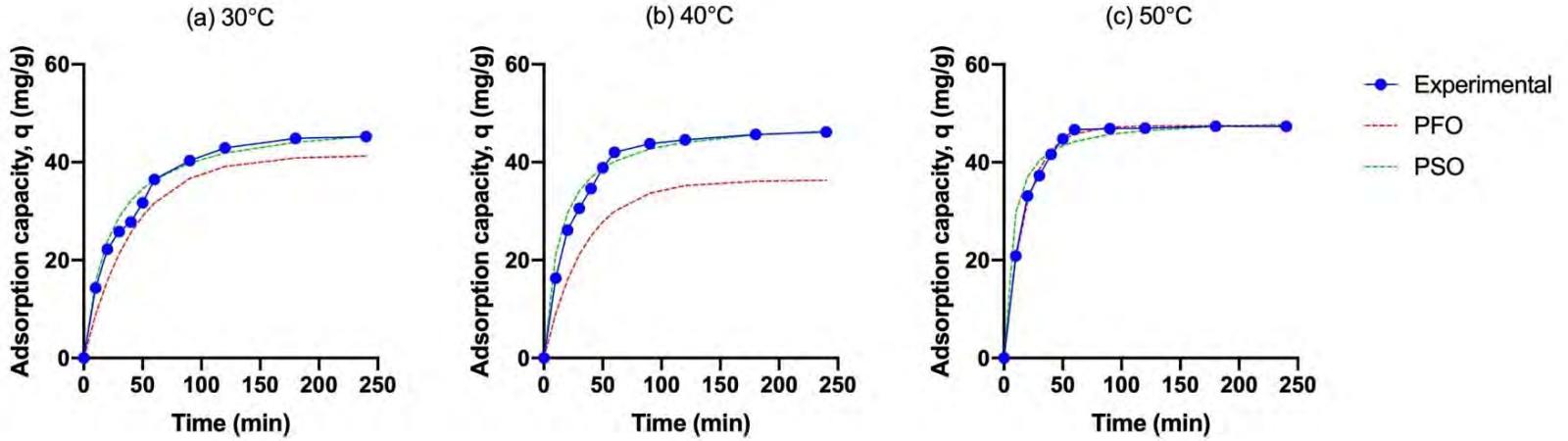

Figure 5.8. Fitting of adsorption kinetic data of Th(IV) at (a) 30°C, (b) 40°C and (c) 50°C

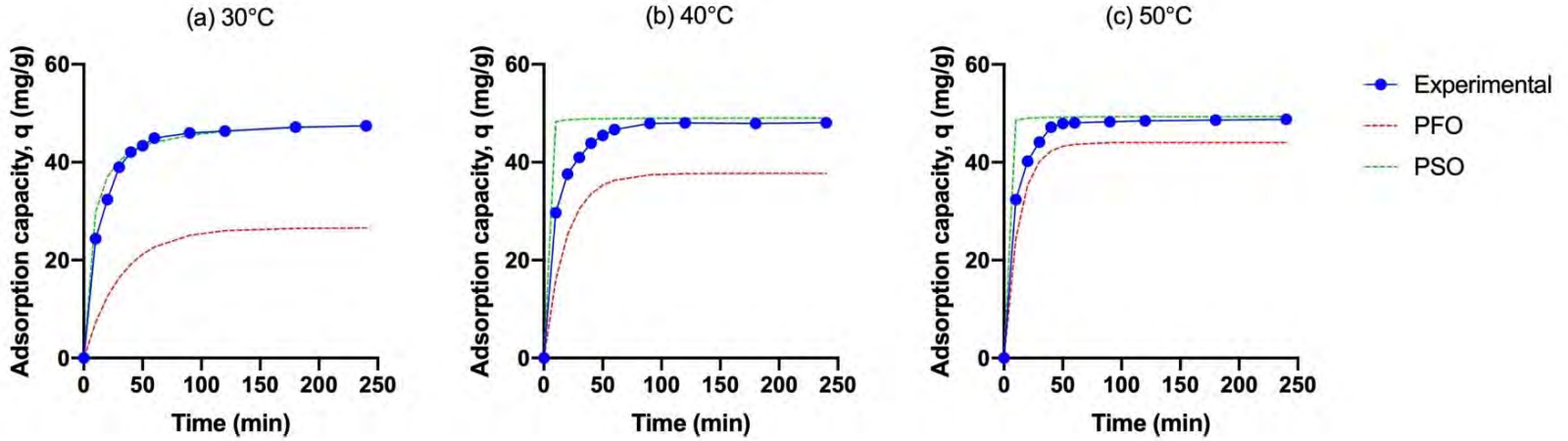

Figure 5.9. Fitting of adsorption kinetic data of U(VI) at (a) 30°C, (b) 40°C and (c) 50°C

5.3.3 Application of Response Surface Modelling to Economically Maximize Thorium (IV) Adsorption

Optimization of adsorption parameters of Th (IV) onto P-DMAEMA was undertaken to ensure an efficient adsorption capacity over the experimental ranges applied. Investigation by Hadjittofi *et al.* on effect of pH revealed that pH 3.5 is the most suitable pH to achieve highest adsorption capacity [69] of Th(IV) and Dg >100% is enough to be used as adsorbent. However, there are other parameters that influence adsorption capacity in the adsorption process such as time, temperature, adsorbent dosage etc. To investigate all of these factors using conventional method by varying one factor whilst maintaining constant all other factors (or also known as OFAT) are time-consuming and the interactive effects between those factors could not be determined [218]. Therefore, response surface method (RSM) was employed to determine the optimum process parameters or regions that satisfied given operational specifications or system. RSM design and analysis were performed with the software package Design Expert version 9. A total of 17 batch adsorption experiments were carried out using RSM with three-factorial Box-Behnken experimental design that consists of three-levels (refer to Table 5.1). Analysis of variance was applied to establish a prediction model for each response. The experimental design with experimental data and predicted response were tabulated in Table 5.5.

Table 5.5. Experimental design with observed and predicted responses for adsorption of Th ions

	Factor 1	**Factor 2**	**Factor 3**	**Observed Response**	**Predicted Response**
Run	X_1: Adsorbent dosage	X_2: Initial concentration	X_3: Time	Adsorption capacity	Adsorption capacity
	g	mg/L	hour	mg/g	mg/g
1	0.002	1	16	18.85	18.55
2	0.002	10	16	22.29	22.20
3	0.0035	1	8	11.38	11.55
4	0.0035	5.5	16	15.77	16.29
5	0.002	5.5	24	24.87	25.13
6	0.005	10	16	12.58	12.89
7	0.0035	10	24	13.35	13.18
8	0.0035	5.5	16	16.26	16.29
9	0.0035	10	8	18.54	18.49
10	0.005	1	16	8.58	8.67
11	0.0035	1	24	12.20	12.24
12	0.005	5.5	8	18.11	17.85
13	0.0035	5.5	16	16.72	16.29
14	0.005	5.5	24	12.66	12.52
15	0.0035	5.5	16	15.71	16.29
16	0.002	5.5	8	24.29	24.42
17	0.0035	5.5	16	16.96	16.29

The sequential model sum of squares and the model summary statistics tests were conducted to evaluate the adequacy of the models for the adsorption of Th (IV) by P-DMAEMA. The corresponding results are shown in Table 5.5. The sequential model sum of squares results suggested that quadratic model provided a good description of the experimental data with "Predicted R^2" of 0.9724 in good agreement with the "Adjusted R^2" of 0.9882. Furthermore, the larger magnitude of F-value (110.45) and smaller p-value (<0.0001) indicate that this model is highly significant and was found to be the most appropriate model for further analysis. An empirical relationship between the response and the independent variables in the coded units based on the experimental results can be expressed by quadratic equation as below;

$$Adsorption\ capacity_{Th(IV)} = 16.29 - 4.80X_1 + 1.97X_2 - 1.15X_3 + 0.14X_1X_2 - 1.51X_1X_3 - 1.50X_2X_3 + 2.70{X_1}^2 - 3.41{X_2}^2 + 0.99{X_3}^2 \quad (5.21)$$

Table 5.6. Sequential model sum of squares and model summary statistics

Source	Sum of squares	Df	Mean square	F-value	p-value prob.>F	Remarks
Linear	225.69	3	75.23	9.82	0.0012	
2FI	18.19	3	6.06	0.74	0.5496	
Quadratic	79.72	3	26.57	110.45	< 0.0001	Suggested
Cubic	0.44	3	0.15	0.47	0.7186	Aliased
Residual	1.24	4	0.31			
Total	4908.34	17	288.73			
Source	**Std. Dev.**	**Predicted R^2**		**Adjusted R^2**	**R^2**	**Remarks**
Linear	2.77	0.3630		0.6232	0.6938	
2FI	2.85	-0.2694		0.5996	0.7497	
Quadratic	0.49	0.9724		0.9882	0.9948	Suggested
Cubic	0.56	0.3630		0.9847	0.9962	Aliased

Table 5.7. ANOVA for response surface quadratic model for Th adsorption

Source	Sum of Squares	df	Mean Square	F Value	p-value Prob > F
Model	323.60	9	35.96	149.43	< 0.0001
***X_1* - Adsorbent dosage**	184.04	1	184.04	764.88	< 0.0001
***X_2* - Initial concentration**	30.99	1	30.99	128.81	< 0.0001
***X_3* - Time**	10.65	1	10.65	44.27	0.0003
X_1X_2	0.081	1	0.081	0.33	0.5809
X_1X_3	9.10	1	9.10	37.84	0.0005
X_2X_3	9.00	1	9.00	37.41	0.0005
X_1^2	30.77	1	30.77	127.89	< 0.0001
X_2^2	48.98	1	48.98	203.57	< 0.0001
X_3^2	4.15	1	4.15	17.24	0.0043
Residual	1.68	7	0.24		
Lack of Fit	0.44	3	0.15	0.47	0.7186
Pure Error	1.24	4	0.31		
Cor Total	325.28	16			
R^2 = 0.9948	**$R^2_{adjusted}$ = 0.9882**		**$R^2_{predicted}$ = 0.9724**		
Adeq. Precision = 43.754					

As presented in Table 5.7, the results of analysis of variance (ANOVA) for the quadratic model suggests that the model was statistically significant where the F-value was found to be 149.43 with the F-statistics probability value less than 0.0001. In this model, X_1, X_1^2, X_2 and X_2^2 were highly significant factors while X_3 was also found to be significant. All other interactions between process parameters were significant except for the interaction between adsorbent dosage and initial concentration (X_1X_2), which was found to be not significant. The correlation between observed experimental value and predicted value of adsorption capacity is given in Figure 5.10. The actual values were reasonably distributed near the straight line, with R^2=0.9948, indicating a good agreement of the model with the experimental data. It can be seen in Figure 5.11 that the residuals were distributed normally in the normal residual plot. Results for diagnostic case analysis are tabulated in Table 5.8. The value for predicted and actual response indicates no significant differences, which is evidence of close correlation between the modelled and measured data. The leverage value was within 0 to 1. Internally studentized residuals measure the number of standard deviations separating actual and predicted values. From the table, no lurking or unusual variables were detected in data of the internally studentized residuals. Difference in fits or DFFITS is calculated by measuring the influence of actual value on its predicted value. The DFFITS was found to be between +2 and -2, indicating absence of any treatments with overly large influences on predictions or regression coefficients. Cook's distance did not detect any data points that could be considered outliers, confirming that there is no unusual change in regression. Therefore, it can be concluded that the analysis of diagnostic case statistics of data showed that the model fits well to optimize the adsorption capacity for Th adsorption.

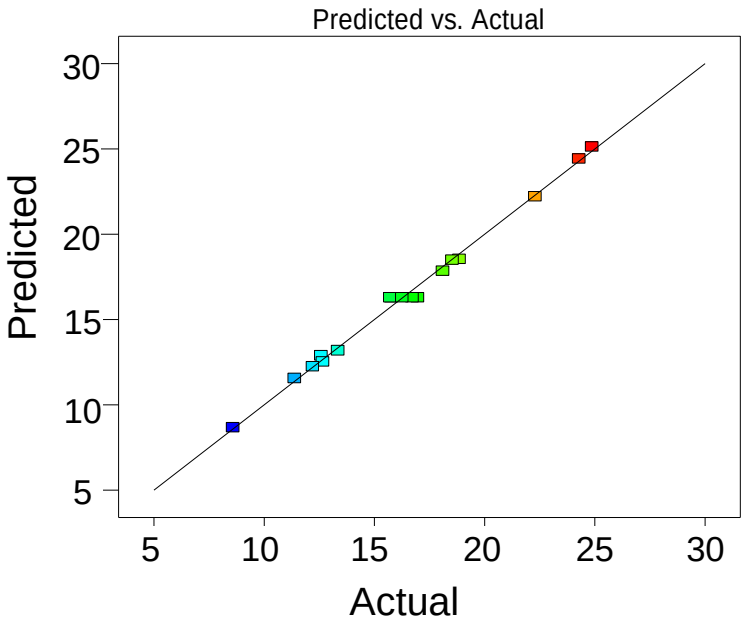

Figure 5.10. The relationship between the actual and the predicted value

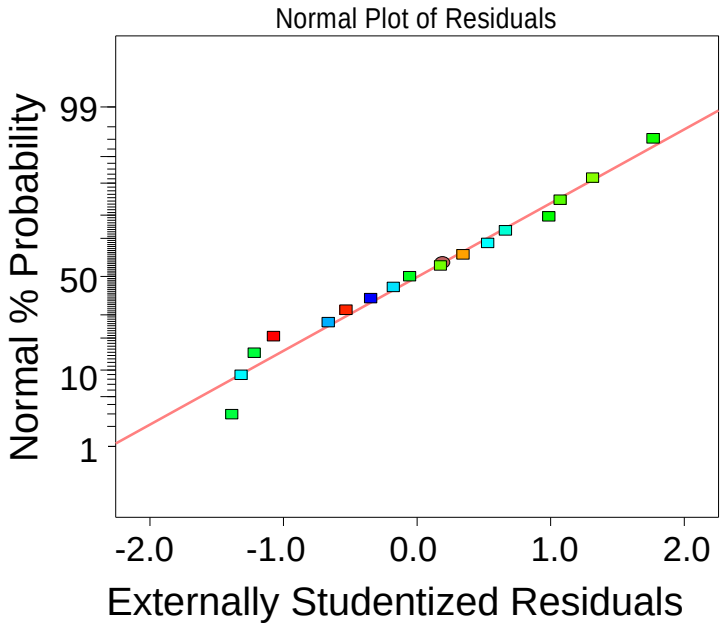

Figure 5.11. Normal plot of studentized residuals

Table 5.8. Diagnostic case analysis

	Actual Value	Predicted Value	Residual	Leverage	Internal Studentized Residual	External Studentized Residual	Cook's	DFF-ITS
1	18.85	18.55	0.31	0.750	1.251	1.315	0.470	2.278
2	22.29	22.20	0.091	0.750	0.370	0.346	0.041	0.599
3	11.38	11.55	-0.17	0.750	-0.691	-0.663	0.143	-1.148
4	15.77	16.29	-0.52	0.200	-1.177	-1.217	0.035	-0.608
5	24.87	25.13	-0.26	0.750	-1.061	-1.073	0.338	-1.858
6	12.58	12.89	-0.31	0.750	-1.251	-1.315	0.470	-2.278
7	13.35	13.18	0.17	0.750	0.691	0.663	0.143	1.148
8	16.26	16.29	-0.026	0.200	-0.059	-0.054	0.000	-0.027
9	18.54	18.49	0.047	0.750	0.190	0.177	0.011	0.306
10	8.58	8.67	-0.091	0.750	-0.370	-0.346	0.041	-0.599
11	12.20	12.24	-0.047	0.750	-0.190	-0.177	0.011	-0.306
12	18.11	17.85	0.26	0.750	1.061	1.073	0.338	1.858
13	16.72	16.29	0.43	0.200	0.990	0.988	0.024	0.494
14	12.66	12.52	0.14	0.750	0.560	0.531	0.094	0.919
15	15.71	16.29	-0.57	0.200	-1.303	-1.386	0.042	-0.693
16	24.29	24.42	-0.14	0.750	-0.560	-0.531	0.094	-0.919
17	16.96	16.29	0.68	0.200	1.549	1.769	0.060	0.884

5.3.3.1 Optimization of Process Variables for Economical Usage of P-DMAEMA

Using the model acquired, a numerical optimization procedure for any combination of four goals, namely adsorbent dosage, initial concentration, time and adsorption capacity of Th can be conducted. Different criteria for the independent variables (adsorbent dosage, initial concentration, time) and dependent variable (adsorption capacity of Th) can be set accordingly. Therefore, with the objective to find maximum adsorption capacity by utilizing the minimum adsorbent dosage, the criteria of the procedure in this study was set as “minimum” for adsorbent dosage, “in range” for initial concentration and time and “maximum” for adsorption capacity. The effect of adsorbent dosage (g) with initial concentration of Th (mg/L) and time (h) on Th adsorption capacity (mg/g) is shown in contour plot (Figure 5.12(a) to (c)).

In Figure 5.12, the contour plot shows how variable A: Adsorbent dosage (g/L), variable B: Initial concentration (mg/L) and variable C: Time (hour) affect the quality (contours) of adsorption capacity (mg/g). The darker regions (red) identify higher adsorption capacity. The graphs suggested that when setting the adsorbent dosage to a minimum, time and initial concentration both have significant effects on the adsorption capacity. It was shown in Figure 5.12(a) and Figure 5.12(b) that by increasing the reaction time and initial concentration, the maximum adsorption capacity can be achieved while keeping the adsorbent dosage constant at 0.002 g. In this case, the value of 0.002 g set as the adsorbent dosage was sufficient. Therefore, the predicted adsorption capacity is in good agreement with the experimental value of 24.87 mg g^{-1}, when the process variables are set according to the optimal values. In Figure 5.12(a), interaction between adsorbent dosage and initial concentration at a constant time of 24 hours suggested that an increase in adsorbent dosage at a given initial concentration did not result in higher adsorption capacity. This may due to the effect of overlapping or screening of the dense outer layer when the number of active sites are beyond optimal [66]. An increase of adsorption capacity with time can be seen in Figure 5.12(b). However, higher adsorbent dosage is needed to achieve the maximum adsorption capacity at extended time as shown in the figure. This is due to a larger number of adsorbing species will need a larger number of surface sites to accommodate the Th ions. On the other hand, the interaction between the initial concentration and time at a constant adsorbent dosage of 0.002 g was

considered less significant, based on Figure 5.12(c). It suggested that increase of decrease beyond the optimum level of time and initial concentration at a constant adsorbent dosage did not result in higher adsorption capacity. This support the earlier observation of interaction between adsorbent dosage and time.

Overall, the graphs suggested that while setting the adsorbent dosage to minimum, the significant factor for adsorption capacity are time and initial concentration. It was shown that maximum adsorption capacity can be achieved by increasing reaction time and initial concentration, while keeping the adsorbent dosage constant at 0.002 g. This predicted adsorption capacity was in good agreement with the experimental value of 24.87 mg/g, when the process variables were set according to the optimal values given. Keshtkar *et al.* used central composite design (CCD) RSM to optimize the process parameters for Th (IV) removal using commercial product, Amberlite IR-120 and IRA-400 [219]. The adsorption capacities of Th (IV) onto IR-120, IRA-400 and IR-120+IRA-400 under optimized conditions were found to be 24.15, 2.43 and 13.11 mg/g, respectively. Therefore, it can be concluded that P-DMAEMA used in this study is comparable to those of commercially available resins.

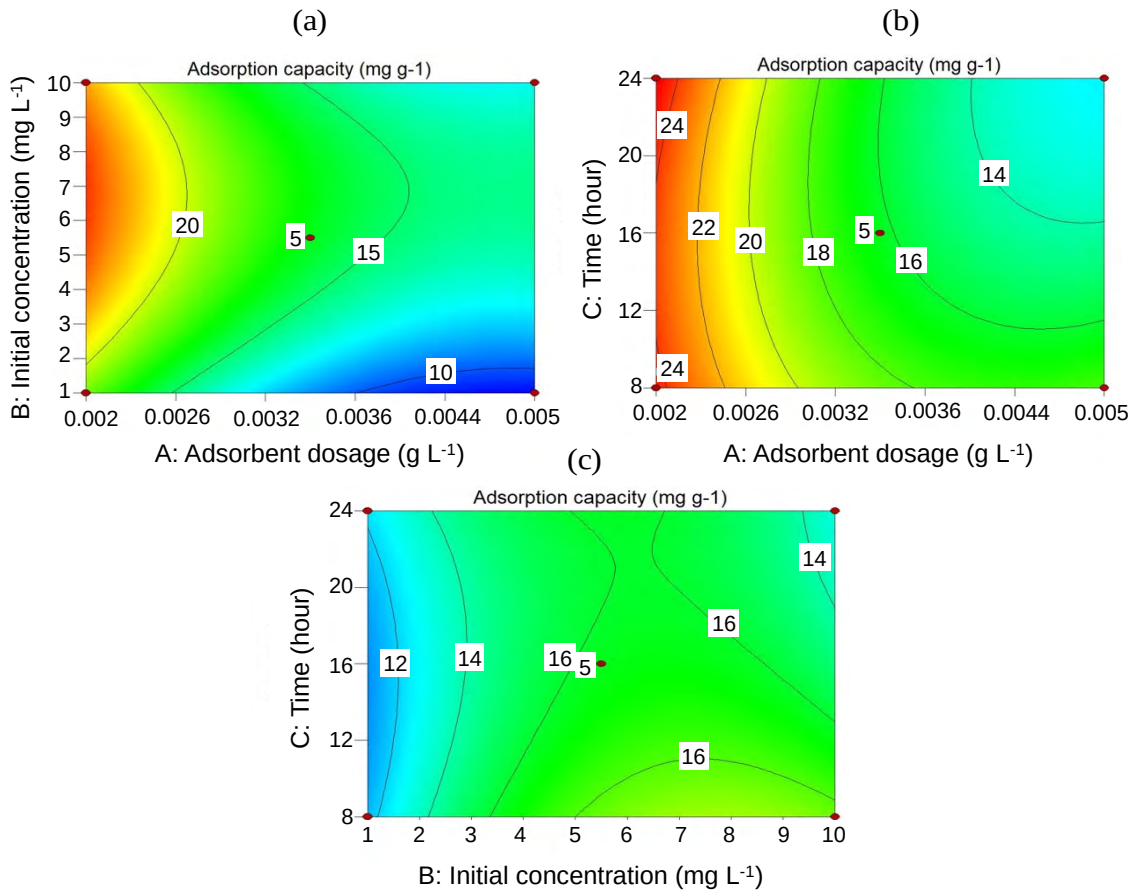

Figure 5.12. Effect of interaction between (a) absorbent dosage and initial concentration, (b) absorbent dosage and time, and (c) initial concentration and time

As mentioned previously, radiation-induced grafting of DMAEMA onto fibrous non-woven fiber for removal of Th has not been previously reported in the literature. However, DMAEMA is a common monomer used for the preparation of grafted adsorbent for heavy and toxic metals [70, 161, 162] Previous research works on DMAEMA-grafted adsorbent showed that high adsorption capacity could be observed for a metal ion with a smaller ionic radius, as presented in Table 5.9. Many researchers have explained the sequence of the adsorption process, which typically starts from the hydrolysis reaction of metal ions in aqueous solutions. The adsorption of the metal ions on the adsorbent will follow right after the hydrolysis. More significant ions are hydrolysed compared to smaller ions; and therefore, have lower adsorption capacities compared to the smaller ions.

Table 5.9. Comparative adsorption capacities of different DMAEMA grafted adsorbents

Precursors/ Support	Target Elements	Ionic Radii (Å)	Initial Concentration	Q_e / pH	Ref.
PP films	Phosphate, PO_4^{3-}	2.38*	25 ppm	2.85 mg g^{-1} at pH 7.2	[220]
PP films	Nitrate, NO^{3-}	1.79*	25 ppm	3.4 mg g^{-1} at pH 7.2	[220]
PE/PP non-woven fabric	Thorium, Th^{4+}	1.08	5.5 ppm	24.87 mg g^{-1} at pH 3.5	**This study** (at minimal adsorbent dosage)
PE/PP non-woven fabric	Thorium, Th^{4+}	1.08	50 ppm	47.32 mg g^{-1} at pH 3.5	**This study** (at optimal adsorbent dosage)
PE/PP non-woven fibers	Arsenic, As^{5+}	0.60	10 ppm	83.33 mg g^{-1} at pH 7	[221]
Silica	Arsenic, As^{5+}	0.60	100 ppm	44.3 mg g^{-1} at pH 7	[222]
Cellulose microsphere (CMS)	Chromium Cr^{6+}	0.58	100 ppm	78.8 mg g^{-1} at pH 4	[223]
Silica	Chromium Cr^{6+}	0.58	100 ppm	51.9 mg g^{-1} at pH 5	[222]

*Thermochemical radii

The findings of Igwe and Abia [124] support the observation that adsorption capacity increases with decreasing ionic radii as follows; Zn^{2+}(0.74Å)> Cd^{2+}(0.97Å)>Pb^{2+}(1.20Å). As observed, the adsorption capacity of the adsorbent prepared in this study for Th ions is comparable with data in the literature. However, the rate of adsorption varies in terms of the selected experimental conditions. Therefore, it is difficult to directly compare P-DMAEMA adsorbent in this study to others reported in the literature.

5.3.4 Selectivity Study

P-DMAEMA proves to be good adsorbent for both thorium and uranium. However, based on the previous findings, it can be concluded that P-DMAEMA is more favourable towards U(IV) than Th(IV), and P-DMAEMA did not show any selectivity towards only one single element. Therefore, further attempt was made to modify the adsorbent to be selective towards Th(IV) by additional process of crosslinking of P-DMAEMA (denotes as IIP) with the aid of crosslinker, DVB. The selectivity properties of IIP was evaluated in binary metal system. The effect of operational parameters such as template concentration, percentage of crosslinking and initial adsorbate concentration were investigated in batch adsorption experiment.

5.3.4.1 Effect of Initial Concentration

The competitive selectivity of both IIP and NIP samples which imprinted with thorium were investigated at different concentrations in the presence of both uranium and thorium ions simultaneously. The metal ion bound by the IIP and NIP samples were summarized in Table 5.10 in term of selectivity. It was noted that the selectivity of IIP towards thorium is higher in comparison to NIP samples. Meanwhile, NIP samples had shown higher selectivity towards uranium. IIP samples consist of cavities which is complimentary to the imprinted thorium ion in terms of size and coordination geometry while NIP samples exhibits the random distribution of the ligand functionalities in polymeric network without any rebinding affinities specificity [224]. Therefore, NIP samples randomly adsorb the uranium ions dominantly without being selective while the IIP samples selectively adsorb more thorium ions. Besides, the selectivity coefficient, K_{IIP} displayed ascending trend whereas K_{NIP} had shown descending trend. This observation strongly suggests that the IIP samples imprinted with thorium impose higher selectivity towards thorium ions. Anyhow, the distribution coefficient, k_d reduces for IIP and NIP samples as the metal concentration increases. Reduction in binding capacity of both IIP and NIP samples as the metal concentration increases results in lower k_d values. Exhaustion of metal binding sites onto IIP and NIP samples as the metal concentration increases leads to reduction on binding capacity [225].

Table 5.10. k_d, K, K' values of uranium with respect to thorium at different concentration

Metal Concentration (mg/L)	**Distribution coefficients (k_d)** Th(IV)		**Distribution coefficients (k_d)** U(VI)		K_{IIP}	K_{NIP}	K'
	IIP	NIP	IIP	NIP			
10	0.94	0.86	0.90	0.98	1.05	0.87	1.20
20	0.92	0.69	0.85	0.92	1.08	0.75	1.45
30	0.87	0.69	0.79	0.94	1.10	0.73	1.51
40	0.71	0.59	0.63	0.93	1.12	0.64	1.74
50	0.58	0.39	0.49	0.89	1.18	0.44	2.68

5.3.4.2 Effect of Crosslinking

The selectivity imposed by IIP which is imprinted with thorium and NIP samples were evaluated at different crosslinking percentage in the presence of both uranium and thorium ions simultaneously. The metal ion bound by the IIP and NIP samples were summarized in Table 5.11 in term of selectivity. The result obtained strongly indicates that the IIP samples possess higher selectivity towards thorium in comparison to NIP samples. However, the distribution coefficient, k_d reduces as the crosslinking percentage increases. Although, k_d reduces with crosslinking percentage, the IIP samples still exhibits higher selectivity towards thorium. This observation strongly suggests that binding capacity of the both IIP and NIP samples reduces as the crosslinking percentage increases. In contrast, the selectivity coefficients, K_{IIP} and K_{NIP} displayed descending trend as well. Generally, type and amount of crosslinking agent used to impose greater influence onto binding capacity of imprinted polymerization system [226]. Crosslinking agents holds significant role in template complexation of imprint polymerization system [175]. Crosslinking gives rigidity to the polymer matrix and preserve the shape of the binding cavities formed. However, excessive crosslinking can cause the polymer to be too rigid and thus, restricts the interaction of functional monomer with template thereafter. This is well-explained by the reduction in binding capacity as the crosslinking percentage increases. Therefore, balance in between the equilibrium of the polymerization systems and the binding capacity are crucial for the IIP to perform as a selective adsorbent.

Table 5.11. *kd, K, K'* values of uranium with respect to thorium at different crosslinking percentage

Crosslinking Percentage (%)	**Distribution coefficients (k_d)** Th(IV)		**Distribution coefficients (k_d)** U(VI)		K_{IIP}	K_{NIP}	K'
	IIP	NIP	IIP	NIP			
20 ± 10	0.93	0.26	0.30	0.97	3.09	0.27	11.41
60 ± 10	0.69	0.18	0.27	0.91	2.53	0.20	12.27
80 ± 10	0.44	0.11	0.24	0.80	1.83	0.13	13.17

5.3.4.3 Effect of Template Concentration

In this study, the effect of different concentration of thorium ion-imprinted onto IIP samples were assessed against the extent of selectivity nature of both IIP and NIP samples in the mixture of binary metal ion solution. At these circumstances, the IIP samples was imprinted with different concentration of thorium ion in order to observe the selectivity towards thorium and the results obtained were displayed in Table 5.12. It was very clear that IIP samples still holds higher selectivity towards thorium even in coexisting with uranium which is specified by higher k_d values for IIP samples towards thorium. Both of the selectivity coefficients, K_{IIP} and K_{NIP} reduces as the imprinted thorium ion concentration increases but the K_{IIP} is still greater than K_{NIP} which strongly claims the higher selectivity of IIP samples towards thorium. Thorium cavity imprinted onto NWF together with the DMAEMA ligand capable to match the charge, coordination number, coordination geometry and size to thorium ion. The imprinted sites number onto the trunk polymer play important role in ionic recognition. Increase in number of imprinted sites onto polymer trunk leads to more thorium cavity to be occupied during selectivity analysis and eventually favours the selectivity towards thorium [100].

Table 5.12. k_d, *K, K'* values of uranium with respect to thorium at different imprint concentration

Template, Th(IV) Concentration (mg/L)	**Distribution coefficients (k_d)** Th(IV)		**Distribution coefficients (k_d)** U(VI)		K_{IIP}	K_{NIP}	K'
	IIP	NIP	IIP	NIP			
5	0.73	0.68	0.38	0.93	1.92	0.73	2.64
20	0.77	0.60	0.55	0.93	1.40	0.64	2.20
30	0.79	0.57	0.61	0.94	1.30	0.60	2.18
50	0.83	0.54	0.71	0.96	1.17	0.57	2.08

5.3.4.4 Effect of Different Metal Concentration

Competitive selectivity of thorium with couple of mixture were performed in batch mode in order to investigate the selectivity of thorium over any other element coexisting. Thorium/Cerium, Thorium/Lanthanum, Thorium/Samarium and Thorium/Praseodymium was chosen as competitive elements as thorium, cerium, lanthanum and samarium often co-exist in natural ore. Due to similar behaviour of these elements, separation of thorium alone is quite difficult. Table 5.13 summarizes k_d, *K* and *K'* values of Ce(IV), La(III), Sm(III) and Pr(III) with respect to Th(IV). The k_d values of IIP samples regards to thorium is obviously higher than NIP samples. k_d values express the adsorption affinity of recognition for imprinted thorium ions. The outcome obtained strongly claims the higher selectivity of IIP samples towards thorium in comparison to other binary elements coexisted. Imprinted sites onto polymer trunk play a vital role in ion recognition based on coordination number and ionic radius. The higher selectivity of IIP samples towards thorium is mainly due to variation in coordination numbers of Ce(IV), La(III), Sm(III) and Pr(III) with Th(IV) [227]. Moreover, the ionic radius of Ce(IV), La(III), Sm(III) and Pr(III) is larger compared to Th(IV). Competitive selectivity studies between Th(IV)/Ce(IV), Th(IV)/La(III), Th(IV)/Sm(III) and Th(IV)/Pr(III) had proven that, IIP samples are only selective towards thorium even in the presence of Ce(IV), La(III), Sm(III) and Pr(III) ions.

Table 5.13. k_d, K, K' values of Ce, La, Sm and Pr with respect to thorium at different imprint concentration (C_0 = 50 mg/L)

Different Binary Elements	Distribution coefficients (k_d) Th(IV)		Distribution coefficients (k_d) Binary Element		K_{IIP}	K_{NIP}	K'
	IIP	NIP	IIP	NIP			
Ce/Th	0.86	0.43	0.67	0.83	1.19	0.52	2.28
La/Th	0.92	0.90	0.93	0.95	0.99	0.95	1.04
Sm/Th	0.92	0.85	0.92	0.91	0.99	0.93	1.06
Pr/Th	0.93	0.81	0.91	0.97	1.02	0.84	1.22

5.4 Conclusion

In this chapter, the adsorption behaviour of P-DMAEMA and IIP towards Th(IV) and U(VI) was experimentally and analytically examined. P-DMAEMA adsorbent was synthesized as in Chapter 4 via single-step pre-irradiation grafting and IIP was prepared by radiation crosslinking of P-DMAEMA with the presence of crosslinker, DVB. On the other hand, the NIP sample was prepared with similar conditions without the presence of thorium template.

The kinetic adsorption data obtained of P-DMAEMA on Th(IV) adsorption obeyed PSO kinetic model which is approved by the higher coefficient value, R^2>0.99. Adsorption data obtained were analysed with Langmuir and Freundlich adsorption isotherm models as well. Equilibrium adsorption of Th(IV) and U(VI) both obeyed the Langmuir adsorption model, and it can be seen that the adsorption capacity increases with temperature. The adsorption process for both Th(IV) and U(VI) were favourable which was indicated by the separation factor obtained in the range of $0<R_L<1$. The results revealed a good agreement between q_{exp} (Th(IV)=68.6 and U(VI)=109.3 mg/g) and q_{max} (Th(IV)=68.9 and U(VI)=114.9 mg/g) values.

The present study also revealed that even though the adsorbent dosage was set to minimum in due consideration of the economical use of the adsorbent, P-DMAEMA was effective in the removal of Th (IV) from an aqueous solution. The uptake capacity and economical usage of the adsorbent were optimised using Box-Behnken Design by adapting the desirability function. The optimal adsorption capacity of 25.13 mg/g was predicted at an initial concentration of 5.5 mg/L, the reaction time of 24 hours, and

adsorbent dosage of 0.002 g. This predicted adsorption capacity was in good agreement with the experimental value of 24.87 mg/L. However, from the overall results of P-DMAEMA adsorption, it can be seen that P-DMAEMA is more favourable towards U(IV) than Th(IV), thus IIP was utilized to improve the selectivity of Th(IV) adsorption.

In conclusion, based on the overall findings, IIP samples are predominantly selective towards thorium in comparison to NIP samples at all circumstances. Initial concentration of Th(IV) had imposed greater effect onto selectivity of IIP samples. Meantime, effect of crosslinking percentage and imprint concentration imposed adverse effect onto selectivity of IIP samples. However, based on the overall results, the selectivity ratio is still not satisfactory. This might be due to DMAEMA can be easily protonated at acidic condition. Also, it was found that the k_d was relatively low, which affect the low selectivity ratio. Therefore, Chapter 6 will explore a different monomer, phosphoric acid methacrylate which is suitable in acidic condition. Additionally, in order to maximize the formation of the labile complex of template and monomer, the polymerization conditions should be precisely determined to minimize non-specific binding sites.

CHAPTER 6

SELECTIVE REMOVAL OF THORIUM USING PHOSPHORUS-BASED ADSORBENT

6.1 Introduction

In the previous chapter, the functional monomer was covalently bonded onto the polymer substrate through graft polymerization and followed by impregnation of template through adsorption process. Subsequently, polymerization with crosslinker was carried out onto the template-embedded substrate to form a cavity of the template. This method is identified as *'ex-situ'* approach. The advantage of this method is that the amount of template attach to the polymer can be quantified, which can be translated to the amount of cavity on the polymer substrate. However, the *'ex-situ'* method suffers several limitations such as; i) the amount of cavity produced is limited since it depended solely on the adsorption of the template, ii) the long polymer chains might interrupt the formation of template cavity during crosslinking, and iii) repulsive forces between the polymers may hinder the reaction. Therefore, another approach which is defined as '*in-situ*' approach (Figure 6.1) is introduced to form a cavity onto the polymer substrate. This method, which will be detailed out in this chapter, used spontaneous polymerization of template complexation with crosslinker on the surface of the substrate. This method provides advantages over the previous method, whereby more cavity formation is achievable since the complexation solution can infiltrate and crosslink between polymer better.

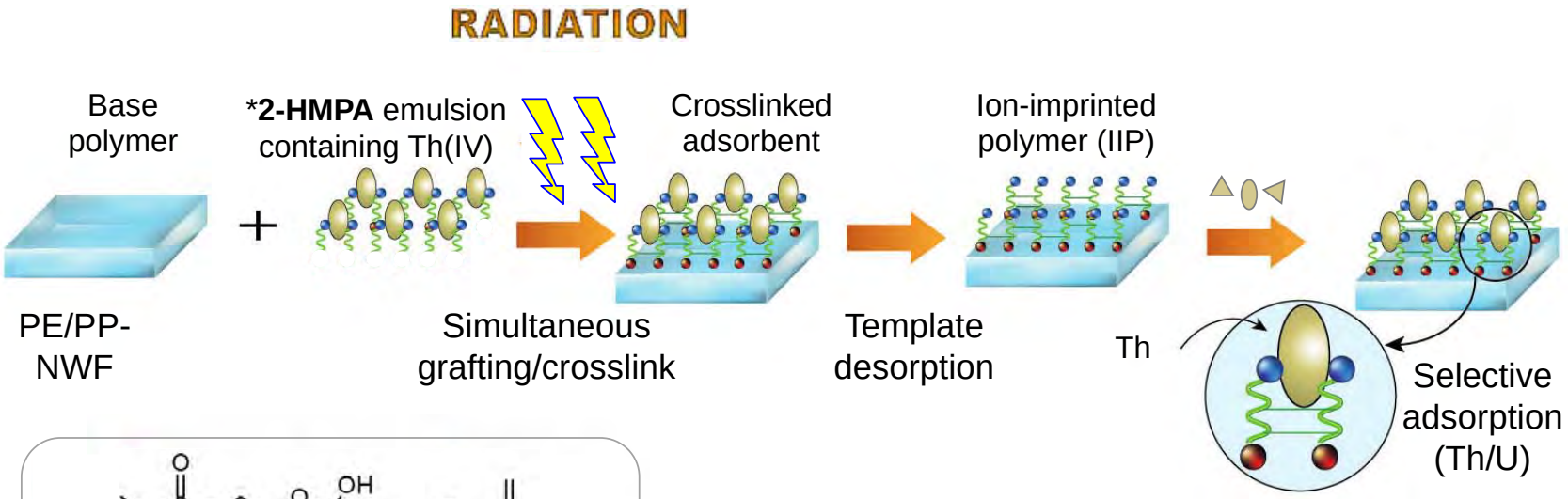

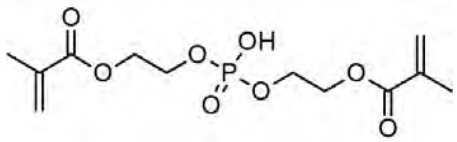

2-hydroxyethyl methacrylate phosphoric acid (2-HMPA)

***TWEEN20** is used as a surface-active agent in the emulsion

Figure 6.1. Schematic representation for the preparation of ion-imprinted polymer adsorbent using '*in-situ*' approach

Specific preference shown by the ligand/functional monomer towards one analyte in the presence of two or more analytes concurrently is defined as selectivity. On the other hand, ratio of distribution coefficients which defined the equilibrium analyte in the polymer and in the solution, is quantitatively expressed by ratio of selectivity. Practise of chelating ligands in selectivity of ion is quite common by optimizing the stability of the ligand towards targeted metal ion. Ligands are capable of forming strong coordination compounds with targeted metal ions which widely applied in many sectors such as waste water treatment, medical field, separation industries, recycling processes and fundamental research on living cells [228]. Preparation of surface imprinted polymer for selective separation of thorium was reported in literature and most of the works were incorporated onto the surface of polymer in the form of particle [20]. For example, functional monomer such as N-(o-carboxyphenyl) maleamic acid [229], 1-phenyl-3-methylthio-4-cyano-5-acrylicacidcarbamoyl-pyrazole [230], 3-methyl-1-phenyl −4-(cis-acylbutenoic acid)-2-pyrazolin-5-one [231], methacrylic acid [96] and acryloyl-β-cyclodextrin [232] were imprinted onto silica gel using azobisisobutyronitrile as radical initiator. In another study, thorium surface imprinted adsorbent was synthesized by complexing N,N'-bis(3-allyl salicylidene)o-phenylenediamine as functional agent onto magnetic Fe_3O_4 particle [233] and polymerization was also initiated by azobisisobutyronitrile. On the other hand, radiation-induced polymerization technique uses high energy radiation, for example, electron beam or gamma emission, to induce the process of polymerization [202]. One of the advantages of the radiation-induced polymerization technique is the absence of a chemical initiator since the radiation can generate the radicals needed to initiate the polymerization reaction [202]. The use of ion-imprinted polymer (IIP) has gained more attention in recent years due to its high selectivity in the separation of metal ions [17, 234-236]. Generally, the preparation of an ion-imprinted polymer requires the design of an artificial receptor with predetermined selectivity and specificity for a given analyte [17].

As mentioned in the previous chapter, the general concept upon preparing imprinted polymers are by creating a three-dimensional network from the polymerization of functional monomer and crosslinker [237]. The 3-D network preserves the structure of the cavity, which profoundly influences the recognition ability of the imprinted polymer [238]. The general procedure for IIP requires three steps; firstly, the complexation of the template metal ions with the polymerizable ligand/monomer [239]. Next, template ions

are trapped by creating a three-dimensional crosslinked network surrounding the complex. This is done by copolymerization of the metal-ligand complexation with a crosslinker that will act as a matrix-forming monomer. The final step is to leach out the template ion, leaving a cavity of the template in terms of the shape, size, and interaction for further adsorption usage [237].

The stability of the emulsion significantly influences the process of polymerization [240]. It is necessary to produce a stable emulsion before radiation polymerization because emulsion stability reportedly affects the quality and functionality of the copolymer [241-243]. Polymerization in the emulsion generally involves a reaction in a disperse system comprising water as a medium, a hydrophobic monomer, and a surfactant which acts as an emulsifier [244]. Seko *et al.* [241] observed the connection between the diameter of micelles and the grafting yield, of which surfactant concentration was observed as significant. They found that smaller micelles in the emulsion contributed to effective reactions, which leads to higher degree of polymerization.

There is no work reported on the use of emulsion in the synthesis of surface ion-imprinted polymer incorporating radiation to initiate the grafting and crosslinking of a fibrous substrate to produce a thorium-imprinted polymer adsorbent. In this study, we report the radiation copolymerization of 2-hydroxyethyl methacrylate phosphoric acid-thorium ion complex with the presence of crosslinker, ethylene glycol dimethacrylate (EGDMA) or divinylbenzene (DVB) onto the surface of polyethene-coated-propylene fibers for the preparation of a new thorium-selective ion-imprinted polymer adsorbent. The use of 2-hydroxyethyl methacrylate phosphoric acid (2-HMPA), which has a phosphoric acid functional group, is likely to impart high adsorption properties onto the adsorbent. The stability of 2-HMPA emulsion containing Th (IV) template required to achieve optimum Dg was investigated. For this purpose, the particle size and particle size distribution of the emulsion as a function of monomer/surfactant ratio were investigated using dynamic light scattering (DLS). The effect of the pH of the grafting medium to synthesize the ion-imprinted polymer was also determined by DLS. The successful preparation of Th (IV) imprinted polymer was verified with fourier transform infra-red (FTIR) and x-ray photoelectron spectroscopy (XPS). The morphology of the polymer was observed by scanning electron microscope (SEM). The effects of reaction parameters such as the concentrations of monomer and crosslinker, types of crosslinker and absorbed

dose on the adsorption properties of IIP were analysed in comparison with a non-imprinted polymer. The characterization of the newly synthesized IIP was also described and discussed. Association of imprint with radiation technique for the removal of pollutants like pharmaceutical compounds [245], pesticides [146] and metals ions [246, 247] from aqueous solution were quite prevalent earlier. But this study holds uniqueness by imposing both the grafting and imprinting processes by the aid of electron beam irradiation. The utilization of emulsion polymerization in the imprinting system and further incorporation of high energy radiation to initiate the simultaneous grafting and crosslinking onto a substrate to produce thorium imprinted polymer adsorbent has not been reported elsewhere in the literature. The aim of this work is to elucidate the role of the emulsion graft polymerization in the synthesis of ion-imprinted polymer adsorbent.

6.2 Experimental Section

6.2.1 Materials

The 1000 mg/L of standard stock solution of thorium, Th(IV) and uranium, U(V) was purchased from Perkin Elmer. Standard solution for thorium template and adsorption test was prepared by appropriate step dilutions of the stock standard solution with 0.5% nitric acid (HNO_3). 2-hydroxyethyl methacrylate phosphoric acid consists of 50% di-ester and 50% mono-ester, denotes as 2-HMPA (MF= $C_{12}H_{29}O_8P$, MW= 332.33 g/mol) was purchased from Kyoeisha Chemical Co. Ltd., Japan and used without further purification. Crosslinker: divinylbenzene (DVB) and ethylene glycol dimethacrylate (EGDMA), surfactant: polyoxyethylenesorbitan monolaurate (TWEEN20) were purchased from Sigma Aldrich, Malaysia. 65% HNO_3 and methanol of analytical grade were purchased from Merck, Germany. PE/PP non-woven fabric used as trunk polymer was obtained from Kurashiki Textile Manufacturing Co., Japan.

6.2.2 Analysis

6.2.2.1 Characterizations

The FTIR spectra of the samples were obtained in ATR mode using the Bruker Tensor II (Germany) FTIR spectrophotometer. The morphological properties of the surface of the adsorbent was analysed using SEM (FEI Quanta 400, USA) at different

magnifications. The adsorbent was pre-coated with conductive gold onto the surfaces before observing the microstructure at 20 kV. XPS (ULVAC-PHI Quantera II) was employed to observe the interactive adsorption of the thorium ions with the imprinted polymer for comparison with the non-imprinted samples. The settings and parameters for XPS analysis is similar to 3.2.5.2. The samples were placed on the sample holder by means of two-sided tape. The wide scan investigation was accomplished by means of a 280 eV with 1 eV/step pass energy. However, the narrow scan (chemical state analyses) was accomplished by means of a 112 eV with 0.1 eV/step pass energy. The emulsion droplet size was determined by DLS (NANOPHOX, Sympatech Germany) and particle size distribution was calculated using a relative refractive index of 1.46. Experiments were conducted immediately on the freshly prepared samples.

6.2.2.2 Crosslinking Analysis

Crosslinking percentage was calculated via gel content analysis method according to ASTM D 2765-95 as detailed out in equation 4.2 in Chapter 4. Polymers that are not crosslinked and still present in water after the irradiation process is defined as soluble fraction, *s*, according to below equation;

$$s = 1 - gel\ content \tag{6.1}$$

GelSol95 software (available at http://mitr.p.lodz.pl/biomat/gelsol.html) was used to evaluate the crosslinking extend by measuring the insoluble fraction (gel content). The calculation is based on the Charlesby-Pinner [248] equation as below;

$$s + s^{1/2} = p_0/q_0 + 2/(q_0 \cdot u_w \cdot D) \tag{6.2}$$

where p_0 is the average number of main chain scissions per monomer unit and per unit dose, q_0 is the monomer unit crosslinked per unit dose proportion, u_w is initial weight of polymerized fraction and *D* is the absorbed radiation dose.

However, in most cases, ionizing radiation-assisted reaction does not obey Charlesby-Pinner equation. Thus, a modified equation, Charlesby-Rosiak [249] was introduced later for measurement where possibility of chain scission and crosslinking occurs simultaneously during irradiation, as below;

$$s + \sqrt{s} = p_0/q_0 + (2 - p_0/q_0)\left(\frac{D_v+D_g}{D_v+D}\right) \quad (6.3)$$

where D_g is the dose at the point where first crosslinking occurs in kGy and D_v is the virtual dose. The value for chain scission and crosslinking, p_0/q_0 were obtained from the slopes of the logarithmatic plots of *s* versus D_g.

From the value of D_g and p_0/q_0 obtained using equation 6.3, and the molecular weight of initial polymer before radiation process, M_w, the number of crosslinked units formed per 100 eV of absorbed energy, *G(x)* can be calculated using equation 6.4 and number of chain scission units formed per 100 eV of absorbed energy, *G(s)* can be calculated using equation 6.5.

$$G(x) = \frac{4.8\times10^5}{M_w \cdot D_g} \quad (6.4)$$

$$G(s)/G(x) = 2\,p_0/q_0 \quad (6.5)$$

6.2.3 Preparation of Emulsion Systems Containing Thorium (IV)

The aqueous phases were prepared by mixing 10 ppm of thorium solution prepared from series of dilution of the 1000 ppm thorium standard stock solution and TWEEN20 as a surfactant in 0.5% HNO_3 at room temperature in a stirrer for 60 minutes Next, the solutions were left standing at 4°C for 24 h to ensure complete dispersion. The resulting mixtures were adjusted to the desired pH using NaOH (1 M). The emulsions were prepared by the mixing aqueous solution and monomer to obtain the desired volume fraction of 2-HMPA monomer in the final emulsion. The mixtures were then mixed by the high-speed homogenizer (Daihan Scientific, Korea) operated at 600 rpm for 30 minutes to make the pre-emulsions, which were further homogenized at 1,000 rpm for 5 minutes to gain fine emulsions.

6.2.4 Radiation Grafted of Emulsion Containing Th (IV) Template

The synthesis of IIP was done by mixing the emulsion with crosslinker, DVB using high speed homogenizer until a homogeneous solution was attained. Same procedure was done using different crosslinker, EGDMA to substitute DVB. Then, the mixture solution was transferred into glass vial and 1 cm (W) x 5 cm (H) PE/PP non-woven fabric was immersed inside the solution. The solution was purged with nitrogen to eliminate any dissolved oxygen. The glass vial was then irradiated using 3 MeV and

2mA electron beam accelerator model EPS-3000 (NHV, Japan). The absorbed dose was varying in the range of 0 to 100 kGy depending on the exposure time. The absorbed radiation dose was set to 10 kGy per pass for uniformity. After irradiation, the IIP was washed by stirring in hot water and the washed again repeatedly using methanol in order to remove excess solution. After drying overnight in oven, the IIP was treated using 1 M HNO_3 to remove Th (IV). Finally, the IIP was cleaned with distilled water and then dried under 60 °C for 12 hours. Non-imprinted polymer (NIP) was also prepared by repeating above procedure without addition of Th (IV). The percentage of grafting yield was determined by the percent increase in the weight as describe in equation 3.1 in Chapter 3 and denoted as Yield (%).

6.2.5 Th(IV) Template Removal

Upon completion of radiation grafting as mention in 6.2.4, desorption of Th(IV) template is vital for the template removal in order to attribute higher selectivity towards Th(IV). 0.1 g of IIP sample was placed into 0.1 M of HNO_3 and stirred for 2 h at room temperature for the removal of Th(IV) template from IIP sample matrix. Finally, the sample was rinsed with double distilled water and dried in oven at 50 ºC overnight before subjected to selectivity analysis in binary metal system.

6.2.6 Adsorption Performance of IIP for Th(IV) and U(VI) in Binary Metal Species System

Batch adsorption was performed in duplicate, and all measurements were done using the same instruments for consistency. All of experiments were carried out in the 50 mg/L of Th(IV) solution under the presence of competing ion, U(VI) (50 mg/L) with approximately 0.10 g of IIP adsorbent for 5 hours at room temperature. U(VI) was chosen as the competitor ion due to the fact that U(VI) has almost similar atomic radius and ionic radii to Th(IV). The pH of the solutions was fixed at 3.5. After the equilibrium, the remaining solution were filtered and subjected to ICP-MS analysis. NexION 350X ICP-MS system (Perkin Elmer, UK) with a concentric nebulizer was used for analyte determination. The percentage of removal, R (%) of Th(IV) by IIP adsorbent was calculated according to equation 5.1. Meanwhile, the distribution coefficient (k_d),

selectivity (K) and relative selectivity coefficient (K') were calculated according to equation (5.4 – 5.6) as exhibited in Chapter 5.

6.2.7 Regeneration Study

The feasibility of regenerating spent adsorbent was performed using 0.1 M HNO_3 in batch system. Initially, batch adsorption was carried out in the 50 mg/L of thorium solution with approximately 0.02 g IIP for 3 hours. The initial solution pH was kept at 3.5 and the reaction was performed in room temperature. After attaining equilibrium, the IIP was removed and the concentration of the residual was determined using ICP-MS. The adsorption capacity of this residual is calculated according to equation 3.3 in Chapter 3 and denotes as q_i, which indicates the adsorption capacity of the initial used IIP. The spent IIP was washed thoroughly with double-distilled water to remove any excess Th(IV) and dried in oven for overnight. Then, desorption was performed on the IIP saturated with Th(IV) by shaking the adsorbent in 0.1 M HNO_3 in room temperature for 2 hours. After desorption process, the IIP was removed, rinsed in ample double-distilled water and then dried in oven. It was then re-used for the next adsorption run and the regeneration was repeated 4 times in order to observe the adsorption and regeneration efficiencies. The adsorption capacity for each adsorption cycle is denotes as q_r. The regeneration efficiency, RE is calculated using equation 6.6.

$$RE(\%) = 100 \times q_r/q_i \tag{6.6}$$

where, q_r is the adsorption capacity of the regenerated adsorbent and q_i is the adsorption capacity of the initial used adsorbent.

6.3 Results and Discussion

6.3.1 Functionalization of Polymer Substrate through Radiation-induced Grafting of 2-HMPA

Radiation processing of materials to impart new functionalities has been widely investigated [169]. The selection of base polymer to be used is very important in this process. Cellulosic fibers are abundance in nature and can be easily modified via radiation grafting. Rapid localization of the absorbed energy within the cellulose molecules can produce highly reactive intermediate radicals which further facilitate the process

thereafter [83]. However, they are also prone to degradation up to certain level. On the other hand, synthetic fibers are commercially available and possess much better physical properties then cellulosic fibers. Yet, synthetic fibers are lack of functional groups for a target function. The purpose of the study in this section is to choose a suitable base polymer for radiation modification of 2-HMPA. The chosen polymer will be used as base polymer for further development as ion-imprinted polymer (IIP) adsorbent. 2-HMPA is chosen as monomer because phosphorylated adsorbent is commonly used in the extraction of radioactive waste because of high affinity in acidic condition.

6.3.1.1 Radiation grafting of 2-HMPA onto kenaf fiber and PE/PP-NWF

The procedures for radiation-induced grafting onto the base polymer, kenaf fiber and PE/PP non-woven fiber respectively were in accordance to the method detailed out in section 3.2.2.1. Degree of grafting, Dg was calculated according to equation 3.1. As shown in Figure 6.2, the Dg increased steadily proportional to the increasing of reaction time during the course of grafting using PE/PP as base polymer. On the other hand, grafting of 2-HMPA onto kenaf fiber exhibited increasing trend until 3 hours reaction time, then the Dg levelled off with additional augment of time.

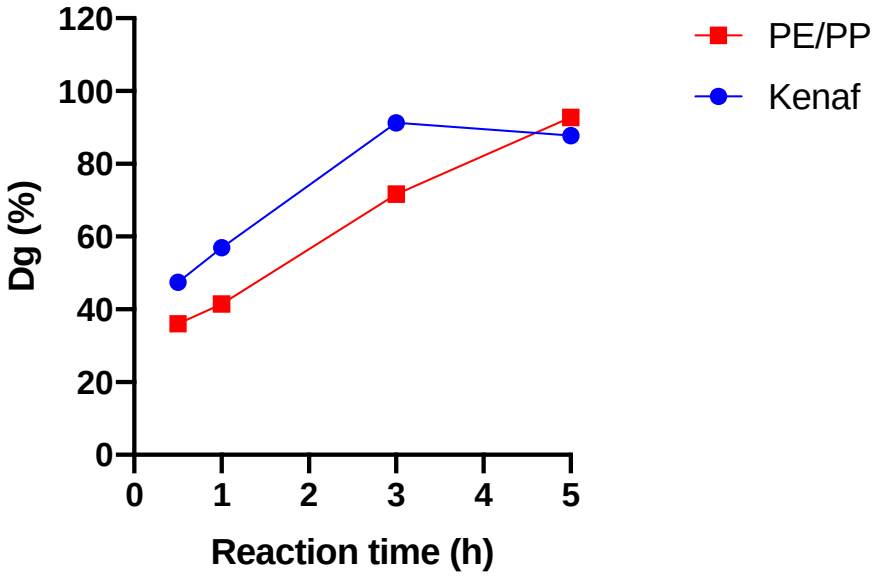

Figure 6.2. Dg against reaction time, with 40 ºC reaction temperature and absorbed radiation dose of 50 kGy and 10% 2-HMPA concentration

Higher value of Dg can be seen for grafting of 2-HMPA onto kenaf fiber. This is due to the swelling of the backbone which enhanced the mobility of radicals generated to active sites on the kenaf fiber. Kenaf fiber is naturally hydrophilic, and thus it is easier to swell in solution in comparison to synthetic fiber. Therefore, grafting is easier to take place in short time. However, the swelling cause loose bond between cellulose hydrogen and promote the formation of water-cellulose-monomer complex [250]. This will lead to the increase of homopolymer and therefore decrease the Dg at longer period of reaction time. In that sense, grafting of 2-HMPA onto PE/PP-NWF exhibited more durability over time. These observations will be a reference for the selection of base polymer in the next section.

6.3.2 Simultaneous Grafting of 2-HMPA Emulsion Containing Th (IV) Template

In the previous chapters, pre-irradiation grafting technique was employed in the preparation of IIP. In the pre-irradiation grafting technique, the base polymer is irradiated first to produce free radicals and subsequently submerge the irradiated polymer in a monomer solution. However, considering for more practical industrial application, a simpler process which is the simultaneous grafting process is proposed here. The simultaneous grafting technique is a one-pot process, whereby the base polymer is immersed in the monomer and irradiated simultaneously with the monomer solution. Radicals is generated at the base polymer surface or in the monomer, and the radicals allow for polymerization of the monomer and the polymer. Considering the nature of the simultaneous grafting technique, the formation of homopolymer is prominent with cellulose rather than in PE/PP upon exposure to radiation, which might reduce the availability of active sites on the polymer backbone for grafting to proceed. This will adversely affect the grafting yield. Therefore, selection of PE/PP-NWF as the base polymer will give better grafting yield at optimal experimental condition. Accordingly, the condition for the monomer solution need to be fine-tuned as well, since the monomer is also subjected to radiation at the same time.

6.3.2.1 Stability of 2-HMPA Emulsion

The process of radiation graft polymerization is highly dependent on the micelle size as explained by Mohamed *et al.* [242] in their study on the radiation graft

polymerization of 4-chloromethylstyrene emulsion onto kenaf fiber. Therefore, it is essential to produce an excellent emulsion with the lowest possible particle size and the highest stability in this study. Emulsion tends to break down over time, which could result in a minimized contact area. To avoid such an unfavourable and unstable emulsion system, the effect of monomer/surfactant ratio on the emulsion stability was studied by dynamic light scattering (DLS) to observe the particle size distribution. Typically, the surfactant decreases the surface tension of the water/oil interface and acts as a bridge for the monomer to have contact with the substrate and stabilize the emulsion during the reaction [241]. Tamada *et al*. [251] explained that dispersing a monomer in water with a surfactant increased the yield of graft polymerization by ten-fold. Nasef and Sugiarmawan [166] emphasized the importance of surfactant concentration in emulsion systems towards the micelle size and ultimately the grafting yield. Therefore, a suitable ratio of monomer/surfactant plays an essential role in the formation of micelles and thus affect the degree of polymerization. The effect of monomer to emulsifier ratio was studied using the monomer/surfactant ratios of 1:3, 1:1, 3:2 and 3:1. The emulsions were prepared using 10 ppm metal ion concentration without the presence of a crosslinker. The emulsion stability study aimed to identify the suitable ratio of monomer to surfactant. Identifying the most suitable ratio is important to achieve a suitable monomer and surfactant composition for the complexation of the template metal ions, and subsequently for radiation polymerization. However, the following discussion is limited to the freshly prepared emulsion. Hence, the effect of time on the phase separation of the emulsion was not considered. This is because the graft polymerization is conducted through the simultaneous radiation-induced technique. Thus, time is not considered a critical parameter in this study.

Table 6.1. Particle size at different monomer concentrations

Monomer/surfactant ratio	**Yield (%)**	**d_{10} (nm)**	**d_{50} (nm)**	**d_{90} (nm)**	**VMD/ SMD**
1:1	36.7	137.17	163.43	194.23	1.017
1:3	30.0	162.62	185.34	211.16	1.009
3:1	65.0	120.19	142.78	169.56	1.017
3:2	18.8	247.89	283.68	322.97	1.010

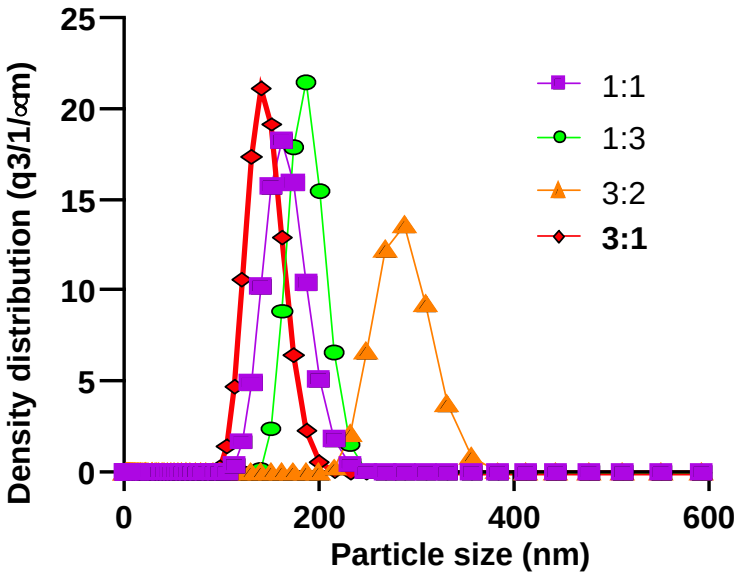

Figure 6.3. Particle size distribution at different monomer to surfactant ratio

As observed in Table 6.1, the volume means diameter (VMD) represents the average diameter based on the unit volume area of a particle, whereas the surface mean diameter (SMD) represents the average diameter based on the unit surface of a particle. The proximity of VMD and SMD give an indication of the shape of the droplets. The closer the value of VMD/SMD to 1 indicates that the droplets are near to spherical form. All VMD/SMD values tabulated in the table are near to 1, which indicates that all emulsions are nearly spherical. The existence of two-particle populations can be seen based on the density distribution graph in Figure 6.3. The emulsion prepared at ratio 1:1, 1:3 and 3:1 clearly shows one narrow peak indicating fine micelles with particle size of ~200 nm was formed. However, for ratio 3:2, an increment in the particle size can be observed. More coarse droplets with average particle size of ~300 nm is visible in the particle size distribution.

The schematic representation of the reaction process during graft polymerization is illustrated in Figure 6.4. As depicted in the figure, the monomer binds thorium to form a metal-ligand complexation. Typically, majority of the monomer-thorium complexation is concentrated in the micelle [252]. The rest is in the monomer droplets and little is dissolved in water. The graft polymerization proceeds once exposed to high energy radiation, where it is initiated by the addition reaction of the monomer dissolved in water with the polymer radicals on the surface of the base polymer and it propagates

continuously. When all monomer dissolved in the water are consumed by grafting, monomer in the droplets would diffuse to the water phase. When the all monomer in the droplets are consumed, monomer in the micelles would diffuse to the water phase to keep the equilibrium concentration in water. A three-dimensional network was developed from the polymerization, whereby this will preserve the structure of the cavity for thorium recognition. It is predicted that smaller micelles could cover a wider surface area of trunk polymer. Thus, the grafting efficiency was experimentally enhanced, as shown in Table 6.1. The imprinted polymer adsorbent prepared using the monomer/surfactant ratio of 3:1 yielded ~65% of grafting. Based on this, the monomer ratio of 3:1 was chosen as the best composition between the monomer and surfactant for further investigation.

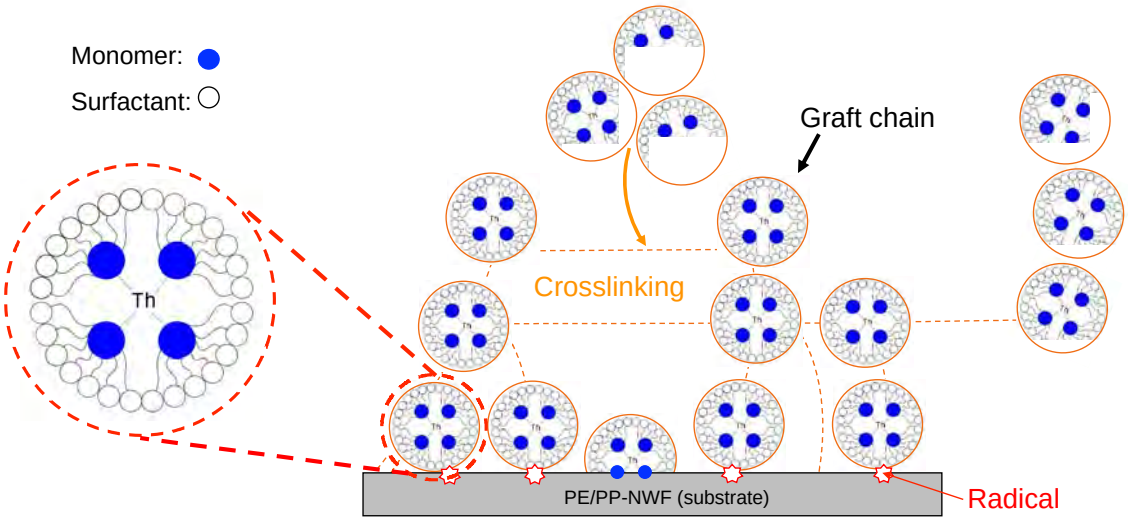

Figure 6.4. Proposed model of emulsion and illustration of emulsion graft polymerization

6.3.3 Effect of Absorbed Radiation Dose and Type of Crosslinker

Irradiation is one of the most critical processes in the synthesis of imprinted polymer required to create the crosslinked network. The selected crosslinker also plays a vital role in shaping the recognition ability of the polymer [18]. Therefore, two different types of crosslinkers, namely; divinylbenzene (DVB) and ethylene glycol dimethacrylate (EGDMA) were used. DVB is rigid and hydrophobic, while EGDMA is hydrophilic and flexible. In order to study the effect of absorbed radiation dose on the degree of crosslinking, the changes in percentage yield (increase in weight), and the gel content of IIP were determined at different electron beam irradiation doses (10 kGy to 100 kGy).

Figure 6.5 shows the effect of absorbed radiation dose on weight increase of IIP in the presence of DVB and EGDMA, respectively. The process parameters used were 15 wt% monomer (2-HMPA), 5 wt% surfactant (TWEEN20), and 5 wt% crosslinker (DVB or EGDMA). As observed in Figure 6.5, the IIP prepared by using DVB as crosslinker (denotes as IIP (DVB)) shows an increasing trend in yield with absorbed radiation dose. On the other hand, the yield of IIP prepared by EGDMA as crosslinker (denotes as IIP (EGDMA)) increased until 50 kGy and gradually decreased with the increase of irradiation dose. Another important observation was the brittleness of the IIP, which was higher for the PE/PP non-woven fibers that were modified using DVB as a crosslinker. As the radiation dose increased beyond 60 kGy, the IIP (DVB) became brittle and fragile. The increase in the percentage of yield with radiation dose is attributed to radiation-induced polymerization and crosslinking of the monomer that occurred upon exposure of the electron beam radiation to the system [18]. Therefore, based on the observation, the radiation dose is limited up to 60 kGy.

The decrease in weight gain of IIP (EGDMA) beyond 50 kGy is associated with the occurrence of other secondary radiation-induced reactions, such as degradation and oxidation at higher radiation doses. The same phenomenon was observed by Flores-Rojas *et al.,* [253] where the grafting yield of the EGDMA-*co*-GMA increased with the increasing absorbed dose until 30 kGy but showed no increment thereafter. Another contributing factor is the nature of EGDMA required to compete with the functional monomers and bind the template. This could decrease the availability of EGDMA as a crosslinker, which could potentially affect the formation of the crosslinked network for the imprinted polymer. This finding is in agreement with Muhammad *et al.* [238], who suggested that the selection of the crosslinker should be based on the strength of the interaction with the template. This phenomenon will be further explained in the next section.

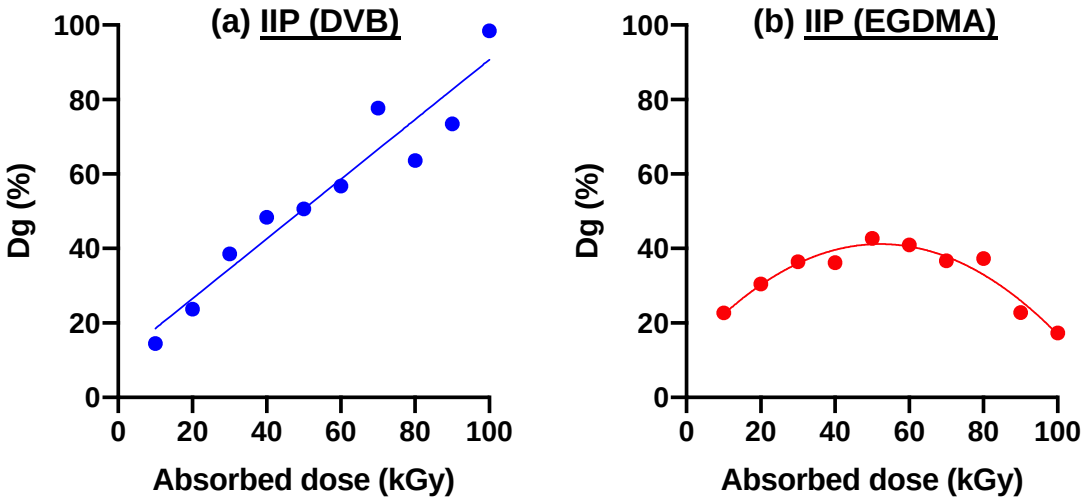

Figure 6.5. Effect of absorbed dose on grafting yield of (a) IIP with DVB as a crosslinker and (b) IIP with EGDMA as crosslinker

6.3.3.1 Effect of Absorbed Dose on Crosslinking

Modification of polymer via high-energy radiation usually will be resulting in crosslinking or degradation, or both simultaneously if the chain scission occurs in tandem with the crosslinking [254]. In order to optimize the designing of imprinted polymer, this phenomenon should be fully understood. Therefore, sol-gel analysis was performed, based on gravimetric determination of sol and gel fractions after irradiation. In order to calculate the soluble fraction, gel content analysis was performed on both samples according to ASTM D2765-95. The result is presented in Figure 6.6.

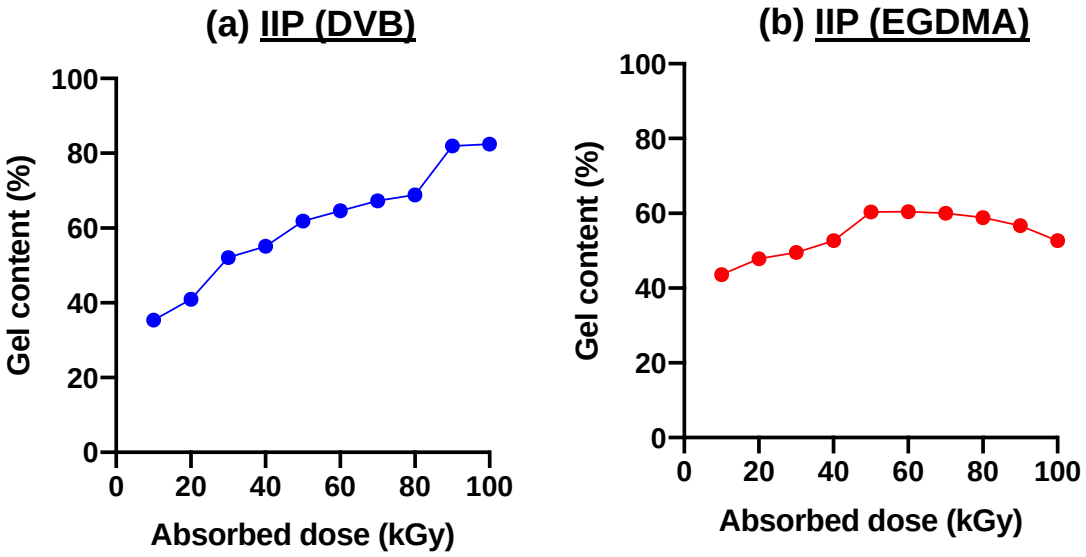

Figure 6.6. Gel content analysis of (a) IIP (DVB) and (b) IIP (EGDMA). Samples were boiled with xylene at (120±2) ºC for 24 hours according to ASTM D2765-95

From the gel content results, soluble fraction, *s* is calculated according to Equation 6.1. Graph of *s* versus absorbed radiation dose (kGy) were plotted as shown in Figure 6.7 and Charlesby-Rosiak equation (Equation 6.3) was used to measure the crosslinking extent.

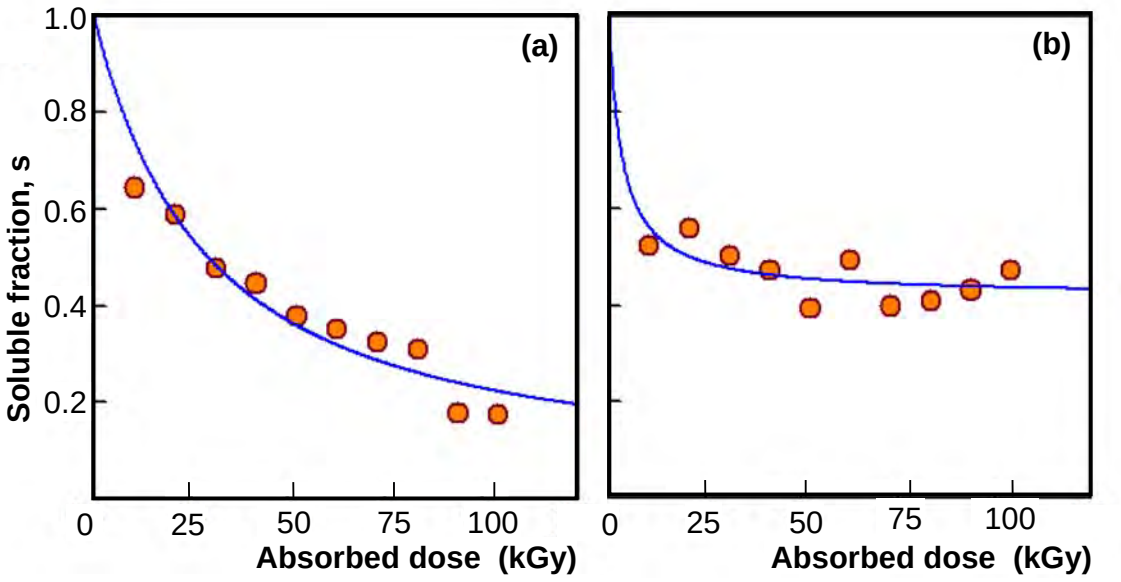

Figure 6.7. Gel fraction data according to Charlesby-Rosiak equation. The plots were drawn using GelSol95 program. (a) IIP with DVB as a crosslinker and (b) IIP with EGDMA as crosslinker

The value for chain scission to crosslinking, p_0/q_0 was obtained from the slopes of the logarithmic plots of *s* versus absorbed radiation dose. The slopes are dependent on the chain scission rate and therefore, this enables to evaluate the simultaneous chain scission and crosslinking phenomenon. If the $p_0 = q_0$, the probabilities of crosslink formation are equal to chain scission. If $p_0 < q_0$, the crosslink bound to be dominant than chain scission and if $p_0 > q_0$, the chain scission is predominant. Based on the graphs, gelation dose for IIP with DVB as a crosslinker is 6.79 kGy, with $p_0/q_0 = 0.75$. The calculated G value for chain scission, G(s) is 2.21×10^{-5} mol/J, while the G value for crosslinked units, G(x) is 3.32×10^{-5} mol/J. From the results, it can be concluded that crosslinking is the determining factor in IIP (DVB) system. On the other hand, for IIP with EGDMA as a crosslinker, the gelation dose was found to be 2.4 kGy with $p_0/q_0 = 1.08$. The calculated G(s) is 1.35×10^{-4} mol/J, while the G(x) is 6.26×10^{-5} mol/J. While crosslinking is the preferred reaction pathway for IIP(EGDMA), the chain scission yield value, G(s) is higher than crosslinking yield value, G(x). This is due to the properties of EGDMA which consist of carbonyl moiety that are more vulnerable to high energy radiation in comparison to DVB that consists of a benzene ring, thus the chain scission is bound to take place in the EGDMA system. This is the main contribution towards the decrease in weight gain of IIP (EGDMA) beyond 50 kGy, as observed in section 6.3.3.

6.3.3.2 Effect of Absorbed Dose on Th(IV) Removal

The effect of absorbed radiation dose on gel fraction and percentage of thorium removal by IIP (DVB) and IIP (EGDMA) in binary metal system of Th(IV) and U(VI) are presented in Figure 6.8 (a) and (b), respectively. The IIP (DVB) shows an increasing trend to reach the highest gel fraction of 89% with 100 kGy absorbed radiation dose. The acceleration of the crosslinking process occurs as the radiation dose increases resulting in a higher yield of gel fraction. This corresponds with the earlier results, where the percentage yield increases with increasing doses. Similar to the yield (%) trend, the gel fraction for IIP (EGDMA) increased until 50 kGy but decreased thereafter. However, it can be observed that thorium removal is more efficient at a lower percentage of gel content. This is because there is more flexibility at lower gel fraction, therefore metal ion can penetrate into the interior of the crosslinks more easily, thereby giving effective interaction between the ligand in the three-dimensional network and metal ions in

aqueous medium. This will result in higher complexation values. Furthermore, the IIP (DVB) shows higher thorium removal in comparison to the IIP (EGDMA). This is due to the crosslinker, DVB is more inert towards thorium. On the other hand, EDGMA has moderate interactions with thorium. The crosslinker that displays a lower binding of the template is preferable because it generates an imprinted polymer with a lower non-specific binding and a higher imprinting factor [17]. The higher thorium removal efficiency of IIP (DVB) suggests that DVB is a preferable crosslinker compared to EGDMA. Thus, DVB will be used for further investigation in this study.

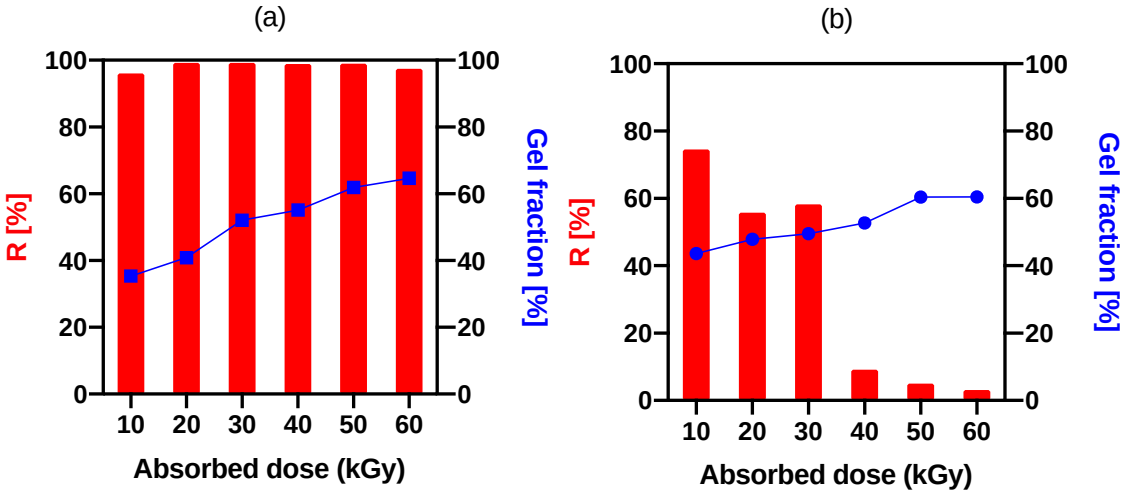

Figure 6.8. Effect of dose on gel fraction (%) and removal percentage of thorium, R (%) by (a) IIP (DVB) and, (b) IIP (EGDMA). Process parameter = 10 wt% 2-HMPA, 5 wt% TWEEN20

The graft polymerization of 2-HMPA emulsion onto PE/PP-NWF is portrayed in the SEM images as shown in Figure 6.9. For normal surface modification, the morphology is commonly investigated by an increase in the diameter of the trunk polymer fiber or an increase in the roughness of the surface or swelling of the trunk fiber as indicators. However, as shown in the figure, the most notable observation for IIP is the presence of globular morphology attached to the surface and distributed across the fibrous surface of the fiber. Some of the particles were also found clustered together, and it can be observed that the PE/PP fiber is coated with thick layers of 2-HMPA copolymer. This unusual observation is reportedly associated with the homo-polymerization of 2-HMPA, which is a multi-functional monomer typically used to promote radiation-induced

crosslinking. Therefore, there is a possibility that precipitation (homopolymer) is formed during the irradiation and subsequent bonding of the formed polymer microspheres to the PE/PP-NWF substrate. However, this phenomenon is rarely reported in the literature. Thus, subsequent studies are needed to support this contestation.

Elemental analysis was carried out by energy dispersive x-ray (EDX) point identification analysis to observe the presence of thorium in IIP and the percentage of elements in the polymers (Figure 6.10). The results show that only carbon and oxygen are present in the pristine PE/PP non-woven fabric with the percentage of mass 80.9% and 19.1%, respectively. However, for IIP, in addition to carbon and oxygen, phosphorus from the 2-HMPA monomer and thorium from the template were detected. The composition was; 43.3% carbon, 36.9% oxygen, 15.1% phosphorus and 4.8% thorium. This proves the integration of thorium template into the system.

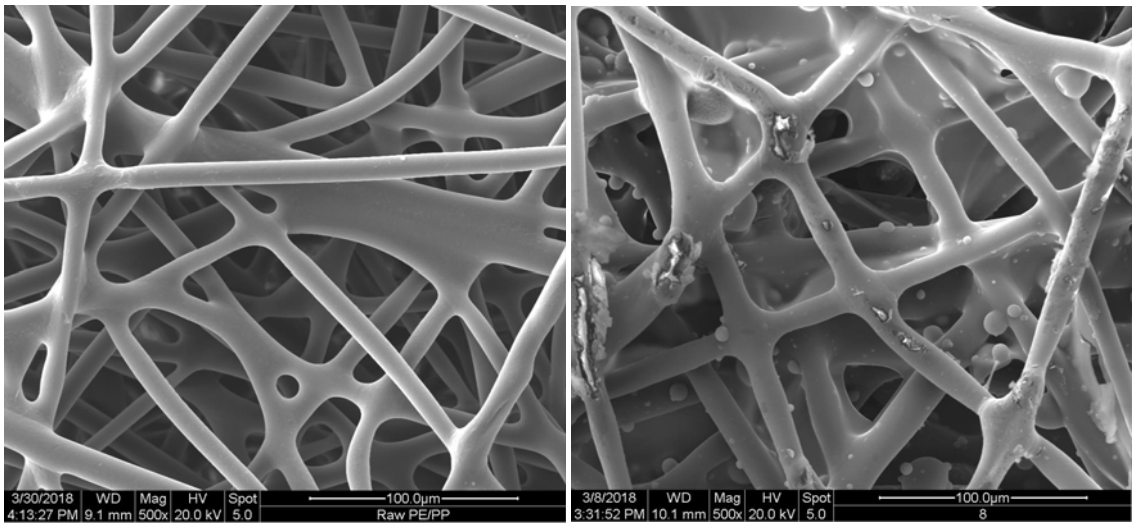

Figure 6.9. SEM images of (a) pristine PE/PP non-woven fiber and (b) IIP (Process parameter = 10 wt% 2-HMPA, 5 wt% TWEEN20, 5 wt% DVB, 60 kGy radiation dose)

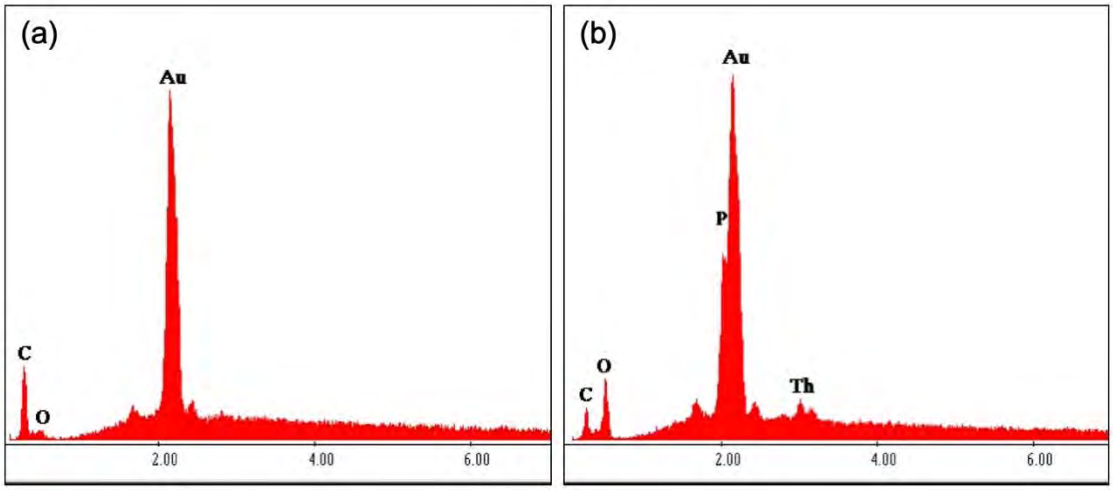

Element	Pristine PE/PP(wt %)	IIP (wt %)
Carbon	80.94	43.26
Oxygen	19.06	36.91
Phosphorus	-	15.05
Thorium		4.79

Figure 6.10. EDX images of (a) pristine PE/PP non-woven fiber and (b) IIP (Process parameter = 10 wt% 2-HMPA, 5 wt% TWEEN20, 5 wt% DVB, 60 kGy radiation dose)

The tendency for homo-polymerization of the 2-HMPA upon irradiation could be associated with the poor solubility of both 2-HMPA and DVB in water. Although the surfactant TWEEN20 was added to the aqueous solution, it did not form a stable emulsion, resulting in phase separation. Among the literatures that have highlighted this phenomenon, the work done by Chandler-Temple [255] has gained a lot of attention. The author observed that the granular microstructure of the grafted copolymer and homopolymer of methoxy acryl ethyl phosphate onto poly(tetrafluorethylene). The conclusion was that the granular morphology is attributed to the poor solubility of the graft copolymer in the solvent, 2-butanone. This also explains why the percentage removal of thorium decreases at higher gel content, as indicated in Figure 6.8. The radiation-induced precipitation polymerization increases as absorbed radiation dose increases, resulting in a higher percentage of gel content along with the formation of the microspheres. As the formation of the microspheres predominates, the surface area reduced drastically, resulting in a decrease in the extraction performance [256, 257].

6.3.4 Interaction Mechanism

The pattern of metal ion complexes is governed by the interaction of the 2-HMPA functional groups with the Th^{4+} ions in the solution during the synthesis of IIP. Thus, to validate the computational theory, IR analysis is used to detect the functional groups available. In addition, it is used to identify the surface complexation that occurs in the samples. The FTIR spectra of the pristine PE/PP non-woven fiber and pristine 2-HMPA monomer are shown in Figure 6.11. The characteristic peaks of PE/PP-NWF (2915, 2848, 1462, 718 cm^{-1}) can be seen in the pristine PE/PP-NWF. Meanwhile, for pristine 2-HMPA, significant peaks at 1715 cm^{-1} correspond to C=O stretching vibration in ester (-COOR) and phosphate groups, 1243 cm^{-1} (P=O) and 1160 cm^{-1} (O-P-O) are identified in the spectra. In addition, peak at 2929 cm^{-1} indicates the -CH_2 stretching vibration and the O-H bending vibration at 1454 cm^{-1} associated with the hydroxyl groups, which are able to interact with Th^{4+} ions. The presence of these peaks can be seen in both the FTIR spectra of IIP using EGDMA and DVB as crosslinkers (Figure 6.11 (b)). After the addition of thorium during the synthesis, the sharp band at 1715 cm^{-1} of the pristine 2-HMPA associated with C=O stretching vibrations was shifted to 1731 cm^{-1} in the complex, suggesting that the carbonyl oxygen is involved in the coordination with Th^{4+}. This is in accordance with Li and Barron [258] who explained that σ donation removes electron density from the oxygen atom to the metal ion. Hence, this leads to increased electronegativity and a consequent increase in C-O vibration frequency on metal complexation [258].

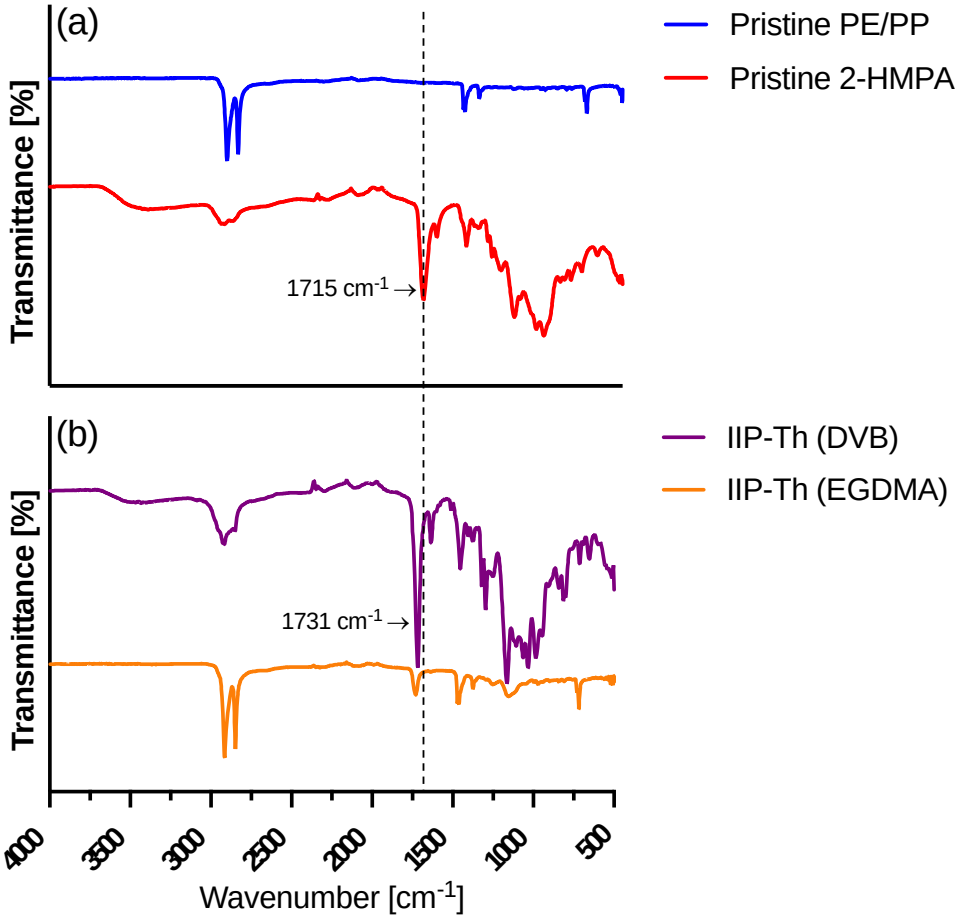

Figure 6.11. FTIR spectra of (a) Pristine PE/PP non-woven fiber and pristine 2-HMPA monomer, and (b) IIP with DVB as a crosslinker and IIP with EGDMA as crosslinker

In addition, the results are supported by XPS findings in Figure 6.12. The wide scanning plot for the raw PE/PP, IIP and non-imprinted polymer (NIP) samples are shown in Figure 6.12 (a) – (c). The raw PE/PP samples exhibit peaks at 284.34, 531.32, and 977.01, which correspond to C1, O1s, and O KLL and the elements present on the PE/PP non-woven fabrics. The NIP samples reveal components at 284.34, 531.32, 977.01 and 1000.48, which correspond to C1, O1s, and O KLL, respectively. Additional peaks were detected at 190.21 and 132.98 that correspond to P1s and P2p. The phosphate (P=O) group is the functional group responsible for the subsequent adsorption of thorium ions. This observation supports the claim that the functionalization process occurred effectively. Meantime, the IIP sample exhibits components at 284.34, 531.32, 977.01 and 1000.48

that correspond to C1, O1s, and O KLL, respectively. Additional peaks for phosphorus were detected at 190.21 and 132.98, which correspond to P1s and P2p accordingly. The presence of thorium was observed, and the Th4f spectrum in Figure 6.12 (d) shows two peaks at 346.76 eV and 350.52 eV, which are assigned to $Th4f_{5/2}$ and $Th4f_{7/2}$, respectively. These values are consistent with Th(IV) ions in the literature [259].

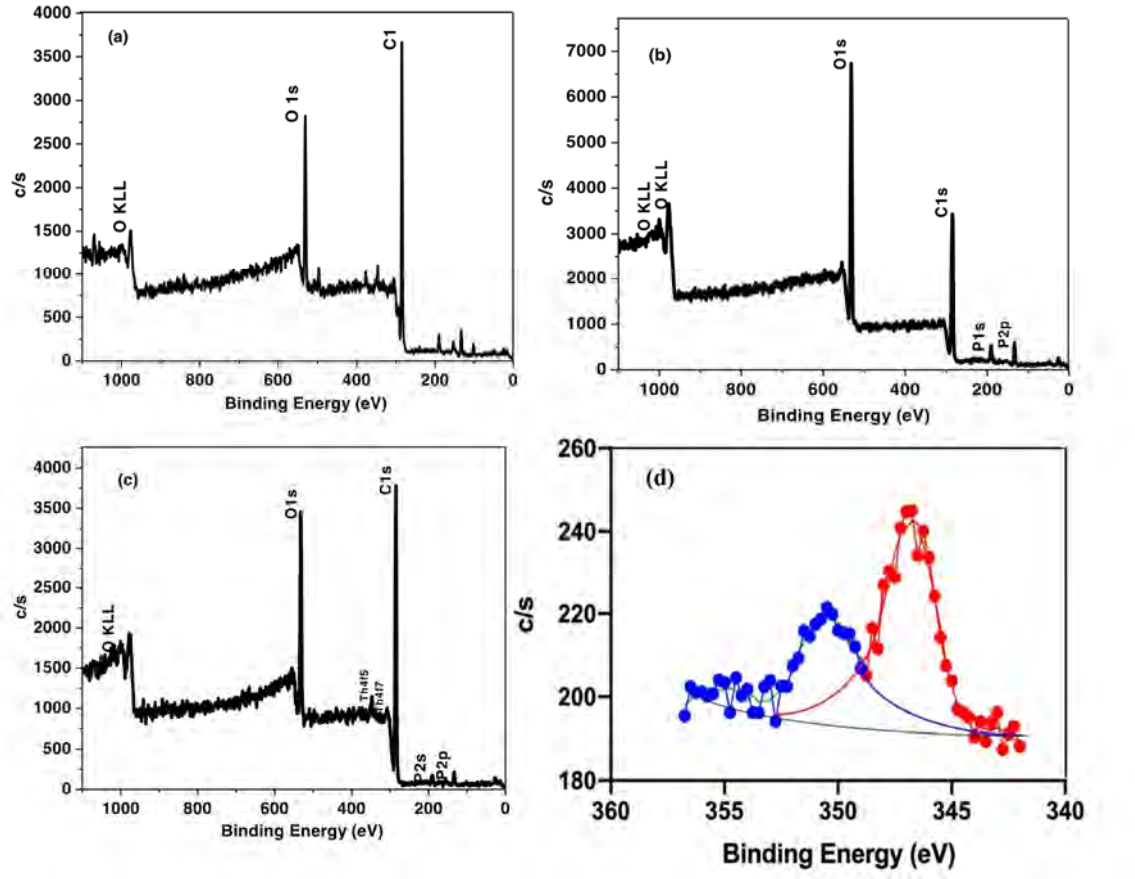

Figure 6.12. XPS wide scanning plot of (a) Pristine sample, (b) NIP sample, (c) IIP sample, and (d) High-resolution XPS spectra of Th4f

The theory of ion imprinting technology onto polymers relies within interaction of functional monomer towards imprinted ion via definite chemical interaction among them with the presence of reasonable quantity of cross-linking agent for anticipated polymerization process thereafter [17]. The most promising aspect of ion imprint technique is their high selectivity and affinity towards targeted ion which is used for imprinting process [260]. The specific binding sites formed onto imprinted polymeric materials by the aid of complexation in between imprinted ion and functional monomer which enables the recognition of printed ion by rebinding of the printed ion [261]. Therefore, based on the findings, a schematic representation of the interaction mechanism during the synthesis of IIP is proposed, as shown in Figure 6.13.

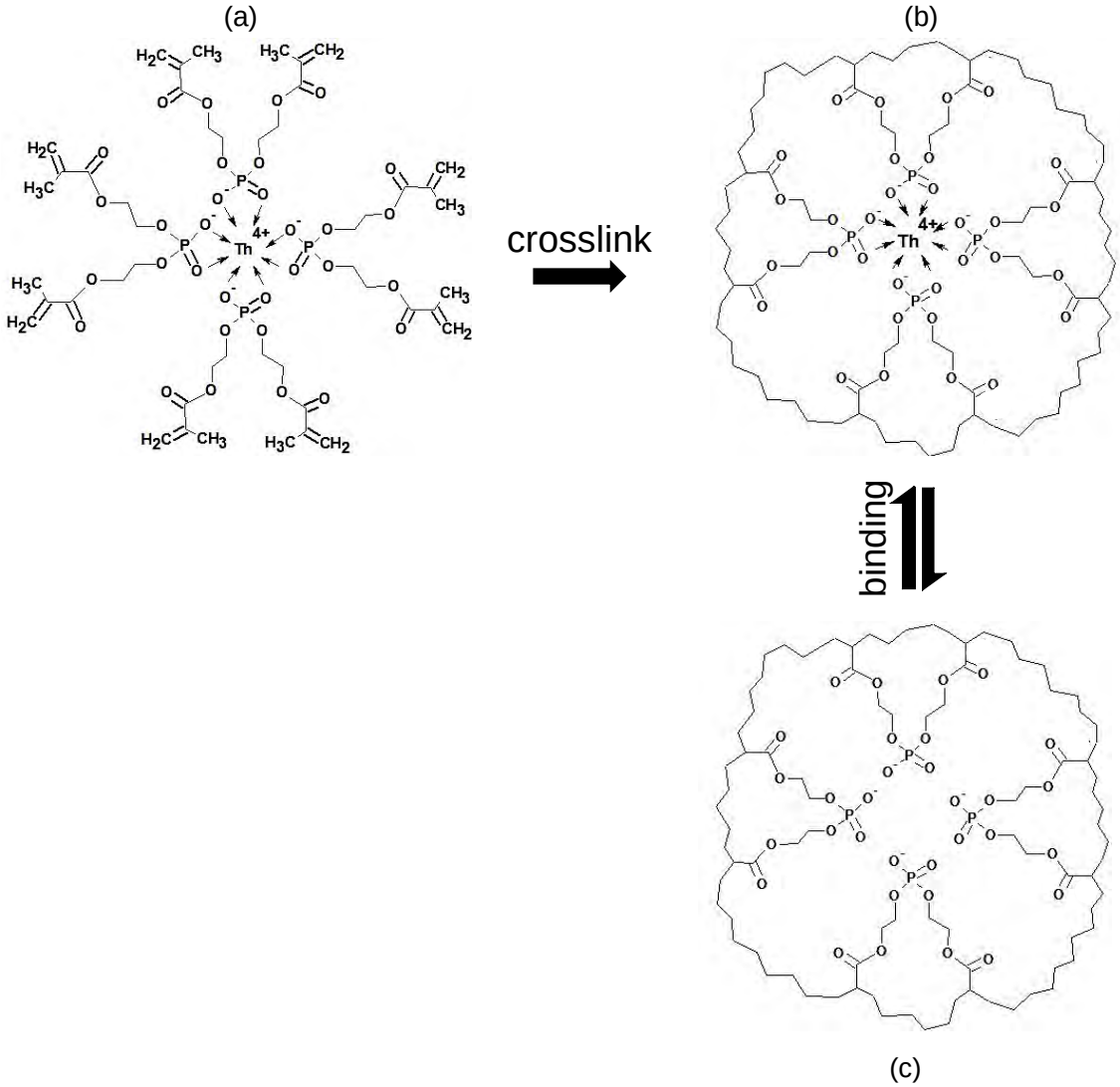

Figure 6.13. Schematic representation of the synthesis of IIP. (a) Metal-ligand complex (b) Template ions are trapped by creating three-dimensional crosslinked network surrounding the complex. (c) Template ion is removed from the three-dimensional crosslinked network, leaving behind a cavity that is morphologically similar to target ion

6.3.5 Kinetic Study of Th(IV)/U(VI) Adsorption in Binary Metal Species

Contact time plays a vital role in adsorption to determine the rate of the process under various conditions. Generally, adsorption can be categorized into two stages, the initial rapid phase and the slower second phase (saturation) [123]. From Figure 6.14, it can be seen that the adsorption rate was rapid for the first one hour, and then gradually slowing until it reached saturation for both Th(IV) and U(VI). The rapid adsorption occurred on the exterior surface at the initial stage, but as the ions entered into the interior surface, it slowed down. The Th(IV) adsorption shows higher adsorption capacity than U(IV). This is because the IIP consists of a mixture of specific binding sites and unspecific binding sites, where the specific binding sites in IIP combine effectively with Th(IV). This makes it more selective towards Th(IV) over U(VI). On the other hand, the randomly distributed unspecific binding sites in the IIP can also combine with U(VI), leading to a reasonable amount of adsorption capacity of U(VI). The distribution coefficient of Th(IV) was found to be higher than that of U(VI) as shown in Table 6.2 (full results are tabulated in Table D1, Appendix D), with the highest selectivity ratio, K of Th(IV) over U(VI) was found to be 9.5. The distribution coefficient of Th(IV) shows an ascending trend over time and occasionally deviating from trend line. This is due to the possibility of layer of Th(IV) may be physically adsorbed on top of the underlying chemisorbed layer. Therefore, as the contact time pursued, Th(IV) that was held by the weak physical forces on the adsorbent surface may be desorbed and adsorbed repeatedly. This explains the slight reduction in selectivity of Th(IV) over U(VI) after 5 hours of adsorption from 9.5 to 6.7. Another possibility is due to the limited number of specific binding sites, which selectively and effectively combine with Th(IV) as the time increases until all the specific binding sites are all occupied. When all the specific binding sites have been occupied, the unspecific binding sites combine with both Th(IV) and U(VI) without any preferences. Although the value is not significant, this will lead to the increase of U(IV) uptake. Subsequently, the difference of distribution coefficient between Th(IV) and U(VI) becomes smaller, resulting in lower selectivity ratio at higher length of time. The same phenomenon was experienced by Lee, J.Y. *et al.* [262] in an adsorption experiment of Cu^{2+} and Pb^{2+} in a binary metal system. They observed a significant leaching of Cu^{2+} ions from the adsorbent at extended contact time. They explained that

the adsorbates rearrange the functional group coordinating system as the adsorption proceeds, resulting to the release of the extra metal ions into the solution as the equilibrium is reached.

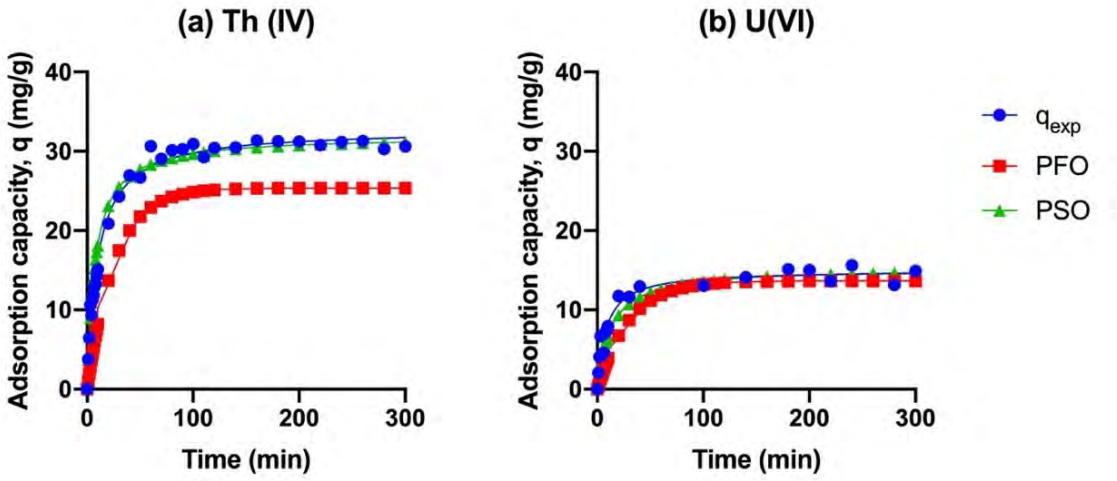

Figure 6.14. Effect of time on the adsorption of Th(IV) and U(VI) and kinetic model fitting

Table 6.2. Selective adsorption properties of IIP in binary metal species at 90, 150 and 300 minutes. Full selective adsorption data is tabulated in Appendix D

Time (min)	k_dTh	k_dU	K (Th/U)
90	3.293	0.347	9.49
150	3.876	0.589	6.58
300	3.462	0.513	6.75

Two adsorption kinetic models, namely pseudo-first-order (PFO, Lagergren model) [214] and pseudo-second-order (PSO, Ho and Mckay model) [215, 216] kinetic were investigated to identify the mechanism of Th(IV) and U(VI) adsorption kinetics in the binary-metal system. All values were calculated using the linearized equations as shown in equation 5.20 and 5.21 in Chapter 5. The results are tabulated in Table 6.3. From the results, the Th(IV) adsorption showed a good correlation with the PSO kinetic model ($\boldsymbol{R^2}$=0.99), which describes the process of chemisorption. This result is evident because the adsorption of IIP involves valence forces through sharing or exchange of electrons between the adsorbent and adsorbate. On the other hand, the correlation coefficient ($\boldsymbol{R^2}$=0.95) and the predicted $\boldsymbol{q_{theory}}$ value showed that PSO fits better to the experimental data for U(VI) adsorption. As seen in Figure 6.14, even though PFO, an indication of

physisorption mechanism, is a good fit to the experimental data for U(VI) adsorption, but it failed to predict the percentage of U(VI) adsorbed. Clearly, the value for q_{theory} deviated too far from q_{exp} ,thus PFO model is unfavourable. The deviation of correlation coefficient, R^2=0.95 for U(VI) species in comparison to R^2=0.99 for Th(IV) species in PSO kinetic model might be due to the competitive effect of the two adsorbates in the binary system. Initial adsorption rate constant, h_0 exhibits the trend Th(IV)>U(VI) at the fixed initial concentration, indicating that Th(IV) sorption system process reached equilibrium faster than U(VI) using IIP.

Table 6.3. Kinetic parameters for thorium adsorption onto IIP in binary metal system (Initial concentration = 50 mg/L, pH 3.5)

	Th(IV)	**U(VI)**
$q_{exp}\,(mg/g)$	31.353	16.915
	PFO	
$q_{theory}(mg/g)$	25.356	13.656
$k_1(mg/min)$	0.039	0.034
$h_0(mg/g \cdot min)$	25.266	6.378
$t_{1/2}$	1.004	2.141
R^2	0.9599	0.8959
	PSO	
$q_{theory}(mg/g)$	31.156	15.314
$k_2(1/min)$	0.00410	0.00514
$h_0(mg/g \cdot min)$	4.189	1.205
$t_{1/2}$	7.626	12.711
R^2	0.9987	0.9518

6.3.6 Regeneration Studies

The cavities that are developed during crosslinking will preserve a coordination geometry designated specifically to the template, and if these cavities are still intact and undisturbed or destroyed during the desorption, they would have a memory effect resulting in specific rebinding during the regeneration study. To determine the commercial viability and practicality of the adsorbent, regeneration is essential. In this analysis, the possibility and efficiency of regeneration was done by exposing the adsorbent to adsorption/desorption process over multiple cycles. The results are shown in Figure 6.15.

The regeneration efficiency decreased 19.1% after four cycles. The decrease in value is due to some Th(IV) that might have been 'trapped' or bounded through stronger interactions in the system, and as a result, a small portion of Th(IV) not recoverable. Thus, the adsorption efficiency is reduced in the subsequent cycles. In addition, the tendency of the IIP to rebind again is relatively lower compared to their initial complexation. One of the reasons might due to distortion of the crosslinked network or the ligand system from their initial position during each desorption cycle that might affect the cavities.

According to literature, surface grafted Fe_3O_4/chitosan ion-imprinted polymer were reported to retained 70% of adsorption efficiency over cadmium after five cycles of adsorption/desorption process [263]. On the other hand, Shafizadeh, F. and co-workers evaluated the regeneration of palladium ion-imprinted polymer and they concluded that the polymer adsorbent could be used repeatedly at least five times without any significant decrease in the adsorption capacity [264]. Therefore, the ability of IIP to maintain 78% of regeneration efficiency after four cycles is considered fair, in comparison to the literature.

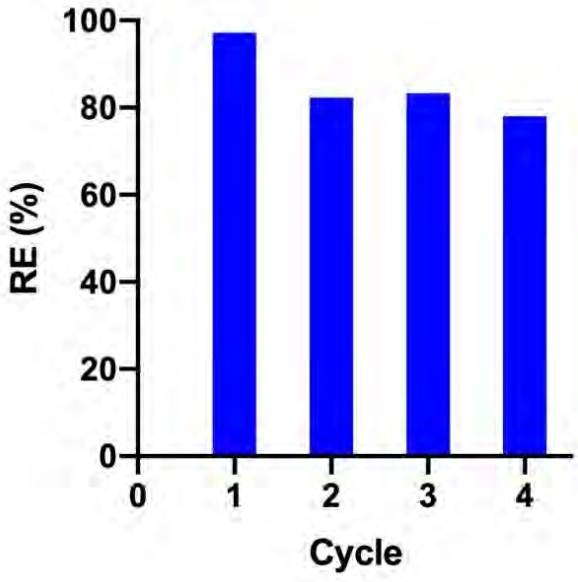

Figure 6.15. Regeneration of IIP on Th(IV) adsorption performance

6.4 Conclusion

2-HMPA emulsion containing Th(IV) as template ion was successfully grafted onto PE/PP-NWF substrate to obtain IIP for selective adsorption of Th(IV) in binary metal system. The IIP synthesized using DVB as crosslinker showed better thorium removal up to 99%, in comparison to the IIP synthesized using EGDMA, which only managed to remove 75% of Th(IV). The optimum parameters for the synthesis of IIP were 10 wt% 2-HMPA concentration, 5 wt% TWEEN20 concentration, and 5 wt% DVB concentration at 60 kGy absorbed radiation dose. The selectivity ratio of thorium over uranium decreases with the increase in the absorbed radiation dose, which corresponds to the higher gel content of IIP. The high degree of radiation-induced crosslinking affects the rigidity of the polymer adsorbent. In addition, too high crosslinking also will be resulting in drastic reduction in surface area, which will limit the adsorption. Therefore, crosslinking percentage at around 50% - 60% was enough to give high removal of Th(IV). Carbonyl and phosphate active sites were found to be predominant to construct the metal ion-monomer complex, giving a coordination type of bonding during the complexation reaction. Based on the findings, a schematic representation of the interaction mechanism during the synthesis of IIP is elucidated and proposed.

Batch adsorption tests were performed to evaluate the adsorption efficiency and selectivity of IIP. The IIP achieved maximum distribution coefficient of 3.29 L/g and selectivity ratio (Th(IV)/U(VI)) of 9.5 at 90 minutes of contact time under acidic conditions (pH=3.5). The adsorption kinetics of IIP showed good fitting and obeyed the PSO kinetic model for both Th(IV) and U(VI) adsorption. The regeneration studies confirmed that after four cycles of adsorption/desorption process, the IIP still maintain its ability to sorb Th(IV) ions with only 19% reduction of performance in comparison to the initial efficiency. Since the adsorbent does not need to be replaced in every cycle, it will help to save costs and increase its viability to treat larger volumes of wastewater.

CHAPTER 7

CONCLUSIONS AND RECOMMENDATIONS

7.1 Conclusions

Ion-imprinted polymer adsorbents were synthesized and modified with the aid of radiation processing. The use of high energy radiation enables the polymer to be synthesized with the absence of catalyst, or initiator. Systematic investigations on the metal ion complexation with incorporated ligands and the effect between the variables of parameters in the design of ion-imprinted polymer was carried out in the present study. In general, the nature of the monomers and the relative rigidity and flexibility of the crosslinking has a significant effect on the complexing ability of the developed imprinted polymer. In Chapter 3, the fabrication of the imprinted polymer adsorbent was carried out involving preliminary grafting of the GMA, which followed by subsequent chemical functionalization with aliphatic amines and radiation crosslinking process. The crosslinked amine immobilized GMA grafted samples (denoted as IIP) had exhibited superior selectivity in comparison to uncrosslinked amine immobilized GMA grafted samples. The results from this investigation proved the viability of the imprinting concept proposed in this course of work. Further investigations were made to improvise the design of IIP, aiming for the enhancement of selectivity performance of targeted ion.

In order to obtain significant improvement in the design of the imprinted polymer adsorbent, two approach have been utilized, namely '*in-situ*' and '*ex-situ*' technique. The results of the both approaches are summarized here;

(i) Synthesis of amine-based ion-imprinted polymer adsorbent using '*ex-situ*' approach.

This study included two parts: the synthesis of P-DMAEMA and crosslinked P-DMAEMA (denoted as IIP), which was detailed out in Chapter 4 and the investigation of the adsorbents' adsorption behaviour towards Th(IV) and U(VI) in Chapter 5. Generally, it was found that the modified adsorbents showed significant physicochemical changes than the pristine substrate (PE/PP-NWF). The chosen parameters for the preparation of IIP were crosslinking percentage in the range of 80% - 90% of grafted P-DMAEMA, using 2:1 ratio of DVB to TWEEN20 at 60 kGy absorbed radiation dose. Both IIP and NIP samples were prepared, and characterizations was performed on IIP and NIP samples, which had evidently proven the accomplishment of ion-imprinted and non-imprinted process.

Chapter 5 investigated the adsorption performance of both P-DMAEMA and IIP towards Th(IV) and U(IV). Based on the results of batch adsorption system, process parameters such as pH, grafting yield, initial solution concentration, reaction temperature and contact time were having a profound effect on the adsorption capacities. The adsorption mechanism of P-DMAEMA was explained by modelling the isotherm and kinetics. The adsorption of Th(IV) and U(VI) both followed the Langmuir isotherm, while the kinetic adsorption data obtained revealed that the adsorption obeyed PSO kinetic model which is approved by the higher coefficient value, R^2>0.99. The adsorption process was also thermodynamically spontaneous, and negative value of $\Delta \boldsymbol{G^0}$ was perceived, which confirms the adsorption is exothermic. However, based on the findings, it can be concluded that P-DMAEMA is either equally or more favourable towards U(IV) than Th(IV), and P-DMAEMA did not show any selectivity towards only one single element. Therefore, further attempt was made to modify the adsorbent as IIP to be selective towards Th(IV) by additional process of crosslinking with the aid of crosslinker, DVB. Comparison of adsorption behaviour was made in term of selectivity efficiency at various operational variables. It was observed that the increase in number of imprinted sites and the rigidity of the crosslinked polymer adsorbent leads to more thorium cavity to be occupied during selectivity analysis and eventually favours the selectivity towards thorium. Competitive selectivity studies between Th(IV)/Ce(IV), Th(IV)/La(III), Th(IV)/Sm(III) and Th(IV)/Pr(III) had proven that, IIP samples are only selective towards

thorium even in the presence of Ce(IV), La(III), Sm(III) and Pr(III) ions. However, since amino group can be easily protonated at acidic condition, the k_d was relatively low, which affect the selectivity and resulted in low ratio. Therefore, a different monomer, phosphoric acid methacrylate which is more suitable in acidic condition is used in the '*in-situ*' approach.

(ii) Synthesis of phosphorus-based ion-imprinted polymer adsorbent using '*in-situ*' approach.

The '*in-situ*' approach, which is more applicable for the industry due to its simplicity, was carried out at various operational variables. Complexation of the template metal ions with the polymerizable ligand/monomer is the most important part in this approach. The complexation solution infiltrated the substrate and crosslinked, whereby the crosslinked network preserved the structure of the cavity, which profoundly influences the recognition ability of the imprinted polymer. The findings revealed that complexation emulsion prepared at pH 2.5 with the monomer/surfactant ratio of 3:1 showed fair stability and recorded the highest percentage of grafting yield. A schematic representation of the interaction mechanism during the synthesis of IIP is proposed. Carbonyl and phosphate active sites were found to be predominant to construct the metal ion-monomer complex, giving a coordination type of bonding during the complexation reaction.

It was observed that the removal efficiency of Th(IV) were found to be higher at lower percentage of crosslinking. Furthermore, the IIP that was crosslinked in the presence of DVB showed higher thorium removal in comparison to those of EGDMA as crosslinker. The adsorption data analysis showed that the adsorption of Th(IV) followed PSO model, suggesting a monolayer adsorption with a finite number of identical sites and predominantly through the chemisorption interaction. However, the PFO model showed good fitting on the initial part of the adsorption, which indicates that an asymmetric physisorption interaction can also occur on the adsorbent surface. Based on the regeneration studies, it was concluded that the prepared adsorbent can be repeatedly use up to four cycles.

Both approaches have its own advantages and disadvantages, as shown in Table 7.1. Thus, in deciding on which approach should be used in preparing IIP, the final application and economical aspect should be taken into consideration. Based on the results in this study, '*in-situ*' approach has been demonstrated a better system for thorium-selective IIP. However, if the targeted ion is changed to different element, the selection of the approach should be reconsidered. Overall, the findings of this study will help in predicting and selecting adsorbents for future application in radioactive wastewater research. However, only binary elements were used in selective study on thorium, thus, it is our best interest to report on multiple elements on selectivity comprehensively in our future studies.

Table 7.1. Comparison between '*In-situ*' approach and '*Ex-situ*' approach

	Advantages	**Disadvantages**
'*Ex-situ*' approach	(i) Pre-organized: Fix template in place before crosslink (ii) Material flexibility: Can be carried out in any type of adsorbent (iii) Good recovery: Easy to remove template from polymer	(i) Material integrity: Require 2-times exposure to radiation (ii) Limitation on number templates that can be imprinted
'*In-situ*' approach	(i) Pre-assembly: Complexation of large number of templates (ii) Simple process : Carried out simultaneously (iii) Material integrity: Only require one-time exposure to radiation	(i) Low recovery: Can be difficult to remove template from polymer (ii) Inability to pre-organized template in place during polymerization

7.2 Recommendations and Future Work

The approach used in this study has given promising results. However, there are a few limitations that is unavoidable in this study. Under the Atomic Energy Licensing (Radioactive Waste Management) Regulations of Malaysia, the control limit of activity concentration for naturally occurring radionuclides from ^{238}U and ^{232}Th decay series in raw material and waste is 1 Bq/g, which is equivalent to 81 ppm (81×10^{-6} g-U/g) and 246 ppm (246×10^{-6} g-Th/g), respectively. Therefore, adsorption of radioelements was performed in synthetic standard stock solution with initial concentration of 1,000 mg/L. Series of dilution were performed to achieve the desired concentration. Therefore, it is not expected to accurately represent the behaviour of the radioelements in the actual wastewater. Should this work be continued in the future, the use of real wastewater will be preferable. In addition, a few recommendations are presented to be included for future research as follow;

(i) The research included studies of single and binary-component adsorption of Th(IV), however, competitive adsorption between Th(IV) and other metal ions in ternary or higher system should be observed. This will reveal a better understanding of competitive adsorption, and the effect of interfering ions during the adsorption.

(ii) The study of surface complexation of Th(IV) and 2-HMPA ligand should be extended to more sophisticated X-ray absorption spectroscopy (XAS) techniques, such as X-ray Adsorption Near Edge Structure (XANES) and extended X-ray Absorption Fine Structure (EXAFS) . This will provide a better insight on atom's coordination geometries and inter-atomic distances.

APPENDICES

Appendix A Adsorption isotherm model analysis of Th(IV) and U(VI) using P-DMAEMA

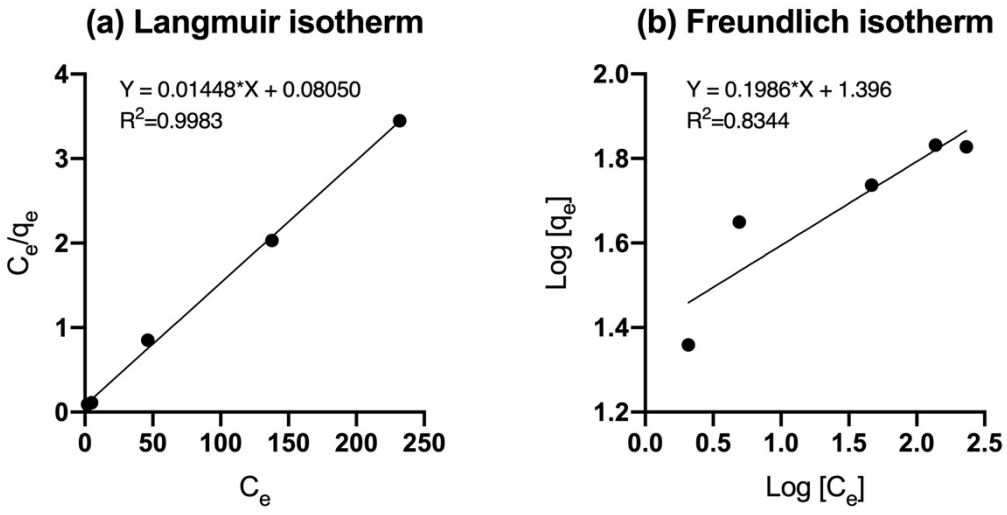

Figure A 1. (a) Langmuir and (b) Freundlich isotherm plot for Th(IV) adsorption

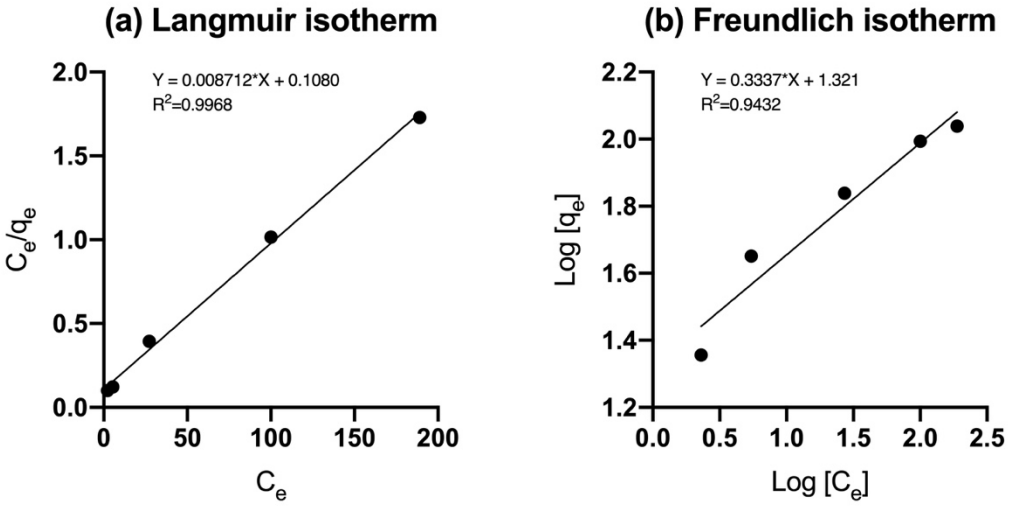

Figure A 2. (a) Langmuir and (b) Freundlich isotherm plot for U(VI) adsorption

Appendix B The plots of first-order and second-order kinetic models for Th(IV) and U(VI) adsorption using P-DMAEMA

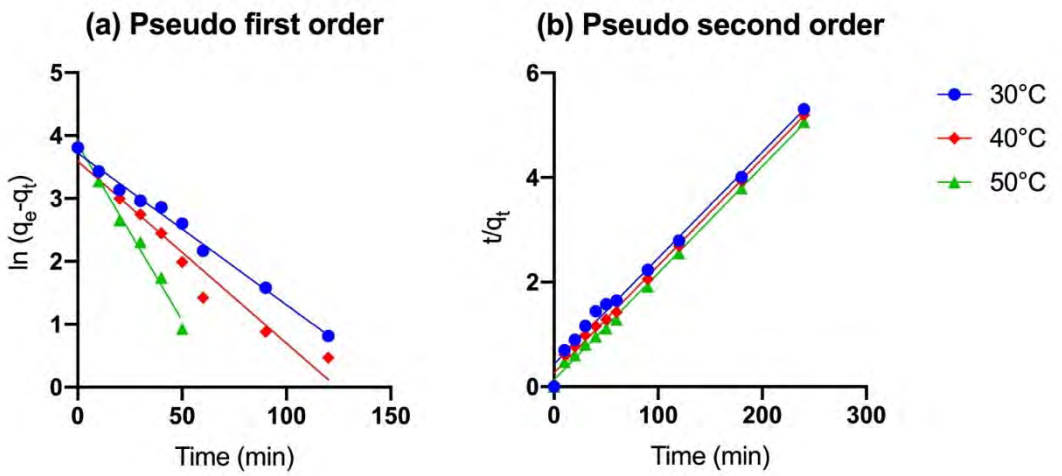

Figure B 1. (a) Pseudo first order and (b) Pseudo second order kinetic plot for Th(IV) adsorption

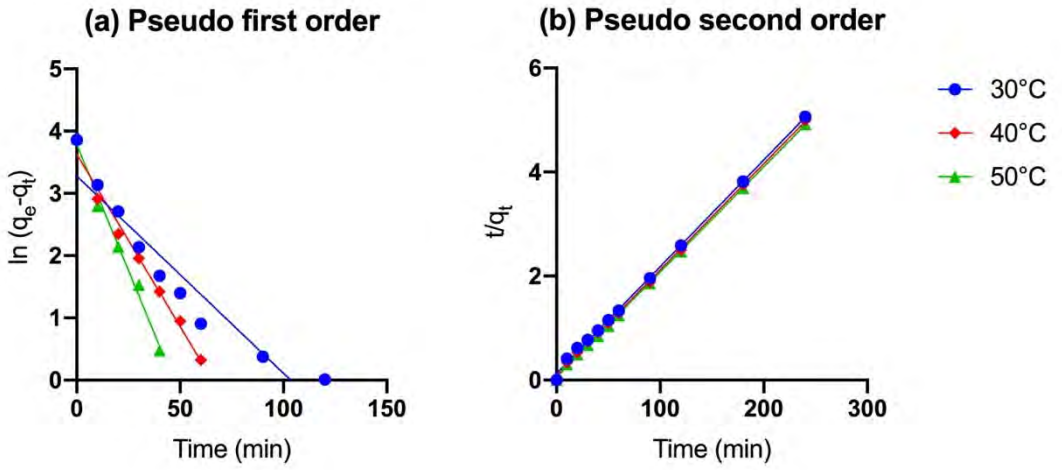

Figure B 2. (a) Pseudo first order and (b) Pseudo second order kinetic plot for U(VI) adsorption

Appendix C The plots of first-order and second-order kinetic models for Th(IV) and U(VI) adsorption using IIP

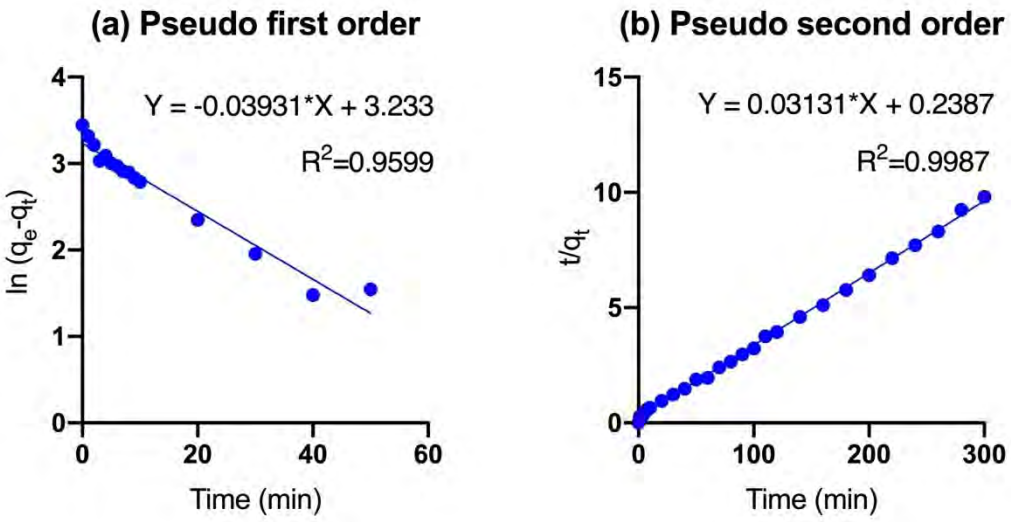

Figure C 1. (a) Pseudo first order and (b) Pseudo second order kinetic plot for Th(IV) adsorption

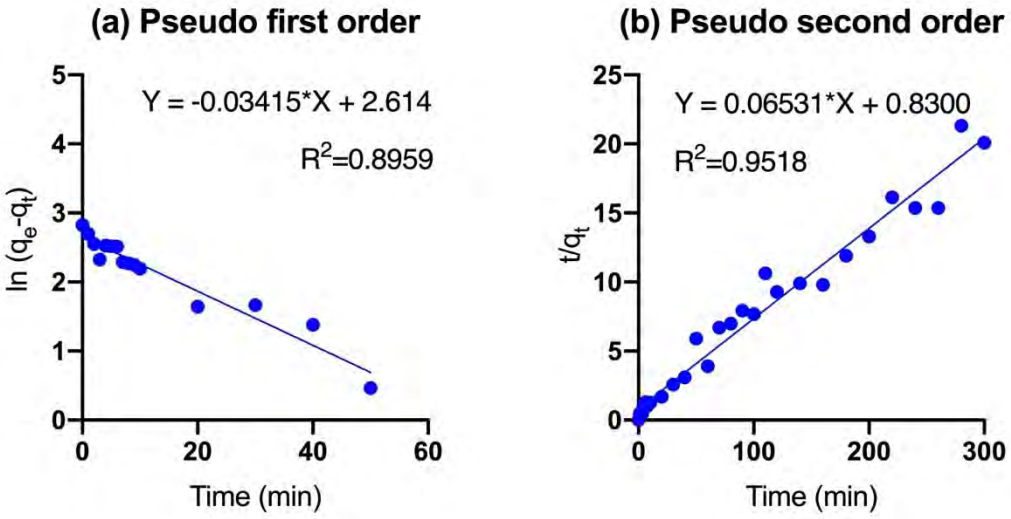

Figure C 2. (a) Pseudo first order and (b) Pseudo second order kinetic plot for U(VI) adsorption

Appendix D Selective adsorption properties of IIP in binary metal species

Table D 1. Selective adsorption properties of IIP in binary metal species at different time intervals

Time (min)	Adsorption capacity, q (mg/g)		Distribution coefficients		$K\ (Th/U)$
	q_tTh	q_tU	k_dTh	k_dU	
0	0.0000	0.0000	0.0000	0.0000	0.0000
1	3.7811	2.0896	0.1056	0.0498	2.1229
2	6.4677	4.0796	0.1954	0.1020	1.9158
3	10.6468	6.6667	0.3684	0.1783	2.0667
4	9.3532	4.3781	0.3097	0.1103	2.8084
5	11.2438	4.4776	0.3973	0.1131	3.5138
6	11.8408	4.5771	0.4275	0.1159	3.6890
7	12.9353	7.0647	0.4863	0.1909	2.5469
8	13.2338	7.2637	0.5032	0.1974	2.5493
9	14.3284	7.4627	0.5686	0.2039	2.7886
10	15.1244	7.9602	0.6199	0.2205	2.8111
20	20.8955	11.7413	1.1234	0.3635	3.0905
30	24.2786	11.6418	1.5973	0.3593	4.4453
40	26.9652	12.9353	2.1572	0.4159	5.1865
50	26.6667	8.4577	2.0833	0.2376	8.7691
60	30.6567	15.3234	3.4877	0.5339	6.5323
70	29.0547	10.4478	2.7937	0.3109	8.9846
80	30.1294	11.4428	3.2328	0.3510	9.2100
90	30.2587	11.3433	3.2926	0.3469	9.4917
100	30.9154	13.0348	3.6243	0.4205	8.6195
110	29.2537	10.3483	2.8680	0.3071	9.3399
120	30.4179	12.9353	3.3685	0.4159	8.0989
140	30.4876	14.1294	3.4026	0.4726	7.2005
160	31.3532	16.3184	3.8756	0.5891	6.5786
180	31.2338	15.1244	3.8044	0.5233	7.2695
200	31.2040	15.0249	3.7869	0.5181	7.3092
220	30.7861	13.6318	3.5550	0.4484	7.9279
240	31.1343	15.6219	3.7466	0.5501	6.8112
260	31.2935	16.9154	3.8397	0.6242	6.1515
280	30.2886	13.1343	3.3066	0.4251	7.7792
300	30.6070	14.9254	3.4623	0.5129	6.7505

Appendix E List of Publications

Publications:

1. **Nor Azillah Fatimah Othma**n, Sarala Selambakkannu, Ting Teo Ming and Zulhairun Abdul Karim "Modification of Kenaf Fibers by Single Step Radiation Functionalization of 2-Hydroxylethyl Methacrylate Phosphoric Acid (2-HMPA)" *SN Applied Sciences* **1** (3), 220 (2019).

2. Sarala Selambakkannu, **Nor Azillah Fatimah Othman**, Wilfred S. Paulus, Nur Aqilah Sapiee and Rahman Yaccup "A Selective Removal of Thorium by Ion Imprinted Poly(Bis [2-Methacryloyloxy) Ethyl] Phosphate)-Grafted Non-Woven Fabrics" *ALTA URANIUM-REE Proceedings*, p. 205-217 (2019).

3. **Nor Azillah Fatimah Othman**, Sarala Selambakkannu, Ting Teo Ming, Nor Hasimah Mohamed, Takeshi Yamanobe and Noriaki Seko "Application of Response Surface Modelling to Economically Maximize Thorium (IV) Adsorption" *Desalination and Water Treatment* (2019). (Accepted)

4. **Nor Azillah Fatimah Othman**, Sarala Selambakkannu, Ting Teo Ming, Azian Hashim and Tuan Amran Tuan Abdullah "Integration of Phosphoric Acid onto Radiation Grafted Poly (Glycidyl Methacrylate) -PP/PE Non-woven Fabrics Aimed Copper Adsorbent via Response Surface Method" *Journal of Polymer Research* **26** (12) 283 (2019).

5. **Nor Azillah Fatimah Othman**, Sarala Selambakkannu, Tuan Amran Tuan Abdullah, Hiroyuki Hoshina, Suchinda Sattayaporn and Noriaki Seko "Selectivity of Copper by Amine-Based Ion Recognition Polymer Adsorbent with Different Aliphatic Amines" *Polymers* **11** (12) 1994(1)-1994(21) (2019).

6. **Nor Azillah Fatimah Othman**, Sarala Selambakkannu, Azian Hashim, Chantara Thevy Ratnam, Takeshi Yamanobe, Hiroyuki Hoshina and Noriaki Seko "Synthesis of Surface Ion-imprinted Polymer for Specific Detection of Thorium under Acidic Conditions" *Polymer Bulletin* (2020). (Accepted)

Presentations:

1. **Nor Azillah Fatimah Othman**, Zulkafli Ghazali, Tuan Amran Tuan Abdullah, Nor Azwin Shukri, and Sarala Selambakkannu (2017). "An Improved Method of Producing Adsorbent for Metal Removal using Radiation Induced Graft Polymerization" (Oral presentation), *International Conference on Applications of Radiation Science and Technology (ICARST-2017)*. IAEA Headquarters, Vienna, Austria (24 – 28 April 2017).

2. **Nor Azillah Fatimah Othman**, Sarala Selambakkannu, Azian Hashim, Chantara Thevy Ratnam, Takeshi Yamanobe, Hiroyuki Hoshina, and Noriaki Seko (2018). "Ion-Imprinted Polymer for Selective Recognition of Thorium in Acidic Condition" (Poster Presentation), *12th SPSJ International Polymer Conference (IPC2018)*. International Conference Center Hiroshima, Hiroshima, Japan (4 – 7 December 2018)

3. **Nor Azillah Fatimah Othman**, Sarala Selambakkannu, Tuan Amran Tuan Abdullah, and Zulhairun Abdul Karim (2018) "Characterization of Radiation-induced Ion-imprinted 2-HMPA/DVB Crosslinked Polymer" (Oral presentation), *2nd National Congress on Membrane Technology (NATCOM2018)*. Universiti Teknologi Malaysia, Johor, Malaysia (30 – 31 October 2018)

4. **Nor Azillah Fatimah Othman**, Sarala Selambakkannu, Ting Teo Ming, Hafizal Yazid and Zulhairun Abdul Karim (2019) "Characterization of Radiation-induced Ion-imprinted Copolymer using Small Angle X-Ray

Scattering (SAXS)" (Oral Presentation), *International Conference of Sustainable Environmental Technology 2019 (ISET2019)*. DoubleTree by Hilton Hotel, Johor, Malaysia (20 – 22 August 2019)

5. **Nor Azillah Fatimah Othman**, Sarala Selambakkannu, and Tuan Amran Tuan Abdullah (2019) "Computational Studies of Functional Monomer for Thorium Imprinted Polymer Adsorbent using Density Functional Theory" (Oral Presentation), *International Nuclear Science, Technology and Engineering Conference (INuSTEC2019)*, Universiti Kebangsaan Malaysia, Selangor, Malaysia (29 – 31 October 2019)

REFERENCES

1. Ramasamy, D.L., A. Wojtuś, E. Repo, et al., *Ligand immobilized novel hybrid adsorbents for rare earth elements (REE) removal from waste water: Assessing the feasibility of using APTES functionalized silica in the hybridization process with chitosan.* Chemical Engineering Journal, 2017. **330**: p. 1370-1379.
2. Saad, D.M., E.M. Cukrowska, and H. Tutu, *Functionalisation of cross-linked polyethylenimine for the removal of As from mining wastewater.* Water SA, 2013. **39**(2): p. 257-264.
3. Saad, D.M., E.M. Cukrowska, and H. Tutu, *Modified cross-linked polyethylenimine for the removal of selenite from mining wastewaters.* Toxicological & Environmental Chemistry, 2013. **95**(3): p. 409-421.
4. Mahfoudhi, N. and S. Boufi, *Nanocellulose as a novel nanostructured adsorbent for environmental remediation: a review.* Cellulose, 2017. **24**(3): p. 1171-1197.
5. Siti, N., H. Mohd, L.K. Md, et al., *Adsorption process of heavy metals by low-cost adsorbent: a review.* World Applied Sciences Journal, 2013. **28**(11): p. 1518-1530.
6. Singh, N., G. Nagpal, and S. Agrawal, *Water purification by using adsorbents: a review.* Environmental Technology & Innovation, 2018. **11**: p. 187-240.
7. Ju, W., A. Bagger, G.-P. Hao, et al., *Understanding activity and selectivity of metal-nitrogen-doped carbon catalysts for electrochemical reduction of CO 2.* Nature communications, 2017. **8**(1): p. 944.
8. Liu, C., Y. Huang, N. Naismith, et al., *Novel polymeric chelating fibers for selective removal of mercury and cesium from water.* Environmental science & technology, 2003. **37**(18): p. 4261-4268.
9. Gu, S., L. Wang, X. Mao, et al., *Selective Adsorption of Pb (II) from Aqueous Solution by Triethylenetetramine-Grafted Polyacrylamide/Vermiculite.* Materials, 2018. **11**(4): p. 514.
10. Goh, E. and S. Effendi, *Overview of an effective governance policy for mineral resource sustainability in Malaysia.* Resources Policy, 2017. **52**: p. 1-6.
11. Minerals, M. *Guidelines to doing mining business in Malaysia*. The Gateway to Malaysia's Resource Industry 2016 28 April 2019]; Available from: http://malaysianminerals.com/.
12. Hamzah, Z., *Determination of Heavy Minerals in 'Amang' From Kampung Gajah Ex-mining Area.* Malaysian Journal of Analytical Sciences, 2009. **13**(2): p. 194-203.
13. Hamzah, Z., A. Saat, Z.A. Bakar, et al. *Anthropogenic heavy metals, U-238 and Th-232 profiles in sediments from an abandoned tin mining lake in Malaysia*. in *Proceedings of 3rd International Conference on Chemical, Biological and Environmental Engineering, Singapore*. 2011.
14. Legislation, F.S., *Environmental Quality Act 1974 [ACT 127]*. Environmental Quality (Sewage and Industrial Effluents) Regulation, 1979.

15. Rao, T., P. Metilda, and J. Gladis, *Preconcentration techniques for uranium(VI) and thorium(IV) prior to analytical determination—an overview*. Talanta, 2006. **68**(4): p. 1047-1064.
16. Kones, J., N. Azhar, N.A. Sapiee, et al., *Alkaline Fusion of Malaysian Monazite and Xenotime for The Separation of Thorium and Uranium.* Jurnal Sains Nuklear Malaysia, 2019. **31**(1): p. 37-41.
17. Branger, C., W. Meouche, and A. Margaillan, *Recent advances on ion-imprinted polymers.* Reactive and Functional Polymers, 2013. **73**(6): p. 859-875.
18. Pustam, A.N. and S.D. Alexandratos, *Engineering selectivity into polymer-supported reagents for transition metal ion complex formation.* Reactive and Functional Polymers, 2010. **70**(8): p. 545-554.
19. Mafu, L.D., T.A.M. Msagati, and B.B. Mamba, *Ion-imprinted polymers for environmental monitoring of inorganic pollutants: synthesis, characterization and applications*. Environmental Science and Pollution Research, 2013. **20**(2): p. 790-802.
20. Hande, P.E., A.B. Samui, and P.S. Kulkarni, *Highly selective monitoring of metals by using ion-imprinted polymers.* Environ Sci Pollut Res Int, 2015. **22**(10): p. 7375-404.
21. Gao, B. and Y. Zhang, *Preparation of Fe(III) ion surface-imprinted material for removing Fe(III) impurity from lanthanide ion solutions.* Journal of Industrial and Engineering Chemistry, 2015. **24**: p. 351-358.
22. Chang, X. and Y. Cui, *Solid-phase extraction of iron(III) with an ion-imprinted functionalized silica gel sorbent prepared by a surface imprinting technique.* Talanta, 2007. **71**(1): p. 38-43.
23. Jiang, N. and Z. Hu, *Selective solid-phase extraction of nickel(II) using a surface-imprinted silica gel sorbent.* Analytica Chimica Acta, 2006. **577**(2): p. 225-231.
24. Fallah, N., M. Taghizadeh, and S. Hassanpour, *Selective adsorption of Mo(VI) ions from aqueous solution using a surface-grafted Mo(VI) ion imprinted polymer.* Polymer, 2018. **144**: p. 80-91.
25. Ting, T.M., M.M. Nasef, and P. Sithambaranathan, *Kinetic investigations of emulsion- and solvent-mediated radiation induced graft copolymerization of glycidyl methacrylate onto nylon-6 fibres.* Journal of Radioanalytical and Nuclear Chemistry, 2017. **311**(1): p. 843-857.
26. Koki, I.B., S.M. Zain, K.H. Low, et al., *Development of water quality index of ex-mining ponds in Malaysia.* Malaysian Journal of Fundamental and Applied Sciences, 2019. **15**(1): p. 54-60.
27. Ali, B.N.M., C.Y. Lin, F. Cleophas, et al., *Assessment of heavy metals contamination in Mamut river sediments using sediment quality guidelines and geochemical indices.* Environmental monitoring and assessment, 2015. **187**(1): p. 4190.
28. Meor Yusoff, M., M. Kaironie, K. Nursaidatul, et al., *An Alternative Alkaline Fusion Process for the Production of Heavy Rare Earth, Thorium, Uranium and Phosphate from Malaysian Xenotime.* 2015.
29. *Rare earth reserves worldwide as of 2016, by country (un 1,000 metric tons REO).* 2017, Statista: Statista 2017.
30. Badrulhisham, A.A., Meor Yusoff, M.S. , *Mid-stream sector*, in *Blueprint for the establishment of rare earth-based industries in Malaysia: A starategic new*

source for economic growth. 2014, Akademi Sains Negara: Kuala Lumpur. p. 52-64.
31. Ali, S., *Social and environmental impact of the rare earth industries.* Resources, 2014. **3**(1): p. 123-134.
32. Al-Areqi, W.M., A.A. Majid, and S. Sarmani. *Thorium, uranium and rare earth elements content in lanthanide concentrate (LC) and water leach purification (WLP) residue of Lynas advanced materials plant (LAMP)*. in *AIP conference proceedings*. 2014. AIP.
33. Al-Areqi, W., A.M. Amran, and S. Sukiman, *Digestion Study of Water Leach Purification (WLP) Residue for Possibility of Thorium Extraction.* Malaysian Journal of Analytical Sciences, 2014. **18**(1): p. 221-225.
34. Sulaiman, M., M. Yusoff, N.S. Kamaruzaman, et al. *Standardless EDXRF Analysis Methods of U and Th in Malaysian Tin Slag Waste*. in *Materials Science Forum*. 2016. Trans Tech Publ.
35. Sun, H. and T.M. Semkow, *Mobilization of thorium, radium and radon radionuclides in ground water by successive alpha-recoils.* Journal of Hydrology, 1998. **205**: p. 126−136.
36. Lung, M. and O. Gremm, *Perspectives of the thorium fuel cycle.* Nuclear Engineering and Design, 1998. **180**: p. 133-146.
37. Sakai, N. and M. Yoneda, *Potential Health Risk of Heavy Metals in Malaysia*, in *Environmental Risk Analysis for Asian-Oriented, Risk-Based Watershed Management*. 2018, Springer. p. 19-32.
38. Tokonami, S., H. Yonehara, S. Akiba, et al., *Natural radiation levels in Tamil Nadu and Kerala, India*, in *Radioactivity in the Environment*. 2005, Elsevier. p. 554-559.
39. Taylor, C.D., *Mineralogy of Uranium and Thorium (RJ Lauf)*. Economic Geology, 2018. **113**(6): p. 1448-1449.
40. Sanusi, M., A. Ramli, N. Basri, et al., *Thorium distribution in the soils of Peninsular Malaysia and its implications for Th resource estimation.* Ore Geology Reviews, 2017. **80**: p. 522-535.
41. Al-Areqi, W.M., A. Ab Majid, and S. Sarmani. *Thorium, uranium and rare earth elements content in lanthanide concentrate (LC) and water leach purification (WLP) residue of Lynas advanced materials plant (LAMP)*. in *International Nuclear Science, Technology and Engineering Conference 2013: Advancing Nuclear Research and Energy Development, iNuSTEC 2013*. 2014. American Institute of Physics Inc.
42. Al-Areqi, W.M., C.N.A.C.Z. Bahri, A.A. Majid, et al., *SOLVENT EXTRACTION OF THORIUM FROM RARE EARTH ELEMENTS IN MONAZITE THORIUM CONCENTRATE*. Malaysian Journal of Analytical Sciences, 2017. **21**(6): p. 1250-1256.
43. Ruf, M.I.F.M., C.N.A.C.Z. Bahri, W.M. Al-Areqi, et al. *Standardless EDXRF application for quantification of thorium (Th), uranium (U) and rare earth elements (REEs) in various Malaysian rare earth ores*. in *AIP Conference Proceedings*. 2016. AIP Publishing.
44. AL-Areqi, W.M., A.A. Majid, S. Sarmani, et al. *Thorium: Issues and prospects in Malaysia*. in *AIP Conference Proceedings*. 2015. AIP Publishing.

45. Alnour, I., H. Wagiran, N. Ibrahim, et al. *Determination of the elemental concentration of uranium and thorium in the products and by-products of amang tin tailings process*. in *AIP Conference Proceedings*. 2017. AIP Publishing.
46. Baharim, N.B., *Spatial and Temporal Distributions of Water Physicochemical, Sediment Quality and Sedimentation in Sembrong Reservoir*. 2015, Universiti Teknologi Malaysia.
47. Azhar, G., *Managing Malaysian water resources development.* Buletin Kesihatan Masyarakat Isu Khas, 2000. **200**: p. 40-58.
48. Prasanna, M., S. Praveena, S. Chidambaram, et al., *Evaluation of water quality pollution indices for heavy metal contamination monitoring: a case study from Curtin Lake, Miri City, East Malaysia.* Environmental Earth Sciences, 2012. **67**(7): p. 1987-2001.
49. Shazili, N.A.M., K. Yunus, A.S. Ahmad, et al., *Heavy metal pollution status in the Malaysian aquatic environment.* Aquatic Ecosystem Health & Management, 2006. **9**(2): p. 137-145.
50. Chan, N.W., *Managing urban rivers and water quality in Malaysia for sustainable water resources.* International Journal of Water Resources Development, 2012. **28**(2): p. 343-354.
51. Sapiee, N.A., K.M. Takip, R. Hazan, et al. *Extraction of thorium from Malaysian xenotime for preparation of nuclear grade thorium*. in *AIP Conference Proceedings*. 2019. AIP Publishing.
52. Bejan, D. and N.J. Bunce, *Acid mine drainage: electrochemical approaches to prevention and remediation of acidity and toxic metals.* Journal of Applied Electrochemistry, 2015. **45**(12): p. 1239-1254.
53. Kulkarni, S.J., *An Insight into Electro-dialysis for Water Treatment.* International Journal of Scientific Research in Science and Technology, 2017. **2**(3): p. 506-509.
54. Frioui, S., R. Oumeddour, and S. Lacour, *Highly selective extraction of metal ions from dilute solutions by hybrid electrodialysis technology.* Separation and Purification Technology, 2017. **174**: p. 264-274.
55. Torosyan, V.F., E.S. Torosyan, P. Sorokin, et al. *Updating of sewage-purification facilities of electroplating enterprises with counterflow ion-exchange filters*. in *IOP Conference Series: Materials Science and Engineering*. 2015. IOP Publishing.
56. Zhang, X., P. Gu, and Y. Liu, *Decontamination of radioactive wastewater: State of the art and challenges forward.* Chemosphere, 2019. **215**: p. 543-553.
57. He, J. and A. Kappler, *Recovery of precious metals from waste streams.* Microbial biotechnology, 2017. **10**(5): p. 1194-1198.
58. da Silva Queiroz, C.A., J.A. Seneda, and W.d.R.P. Filho, *Preparation of High Purity Neodymium Oxide from Brazilian Monazite by Ion Exchange.* Journal of Energy and Power Engineering, 2015. **9**: p. 616-621.
59. Namasivayam, C. and D. Sangeetha, *Removal and recovery of vanadium (V) by adsorption onto ZnCl 2 activated carbon: kinetics and isotherms.* Adsorption, 2006. **12**(2): p. 103-117.
60. Yin, Z., D. Pan, P. Liu, et al., *Sorption behavior of thorium (IV) onto activated bentonite.* Journal of Radioanalytical and Nuclear Chemistry, 2018. **316**(1): p. 301-312.

61. Blanco, S.P.D.M., F.B. Scheufele, A.N. Módenes, et al., *Kinetic, equilibrium and thermodynamic phenomenological modeling of reactive dye adsorption onto polymeric adsorbent.* Chemical Engineering Journal, 2017. **307**: p. 466-475.
62. Inoue, K., Y. Baba, K. Yoshizuka, et al., *Selectivity series in the adsorption of metal-ions on a resin prepared by crosslinking copper(II)-complexed chitosan.* Vol. 200. 1988. 1281-1284.
63. Acelas, N.Y., B.D. Martin, D. López, et al., *Selective removal of phosphate from wastewater using hydrated metal oxides dispersed within anionic exchange media.* Chemosphere, 2015. **119**: p. 1353-1360.
64. Selambakkannu, S., N.A.F. Othman, K.A. Bakar, et al., *Adsorption studies of packed bed column for the removal of dyes using amine functionalized radiation induced grafted fiber.* SN Applied Sciences, 2019. **1**(2): p. 175.
65. Asnani, C., R.B. Rao, and N. Mandre, *A Novel Process for Extraction of Uranium from Monazite of Red Sediment Using Activated Carbon of Waste Tyres Source.* Journal of The Institution of Engineers (India): Series D, 2019. **100**(1): p. 15-20.
66. Dąbrowski, A., *Adsorption—from theory to practice.* Advances in colloid and interface science, 2001. **93**(1-3): p. 135-224.
67. Xiao, B. and K. Thomas, *Adsorption of aqueous metal ions on oxygen and nitrogen functionalized nanoporous activated carbons.* Langmuir, 2005. **21**(9): p. 3892-3902.
68. Sanguthai, S. and J. Klamtet, *Preconcentration and Determination of Cadmium in Natural Water using Amberlite XAD-4/4-(2-Pyridylazo) Resorcinol Resin Prior to Flame Atomic Absorption Spectrometric Detection.* Naresuan University Journal: Science and Technology (NUJST), 2015. **23**(2): p. 8-20.
69. Hadjittofi, L. and I. Pashalidis, *Thorium removal from acidic aqueous solutions by activated biochar derived from cactus fibers.* Desalination and water treatment, 2016. **57**(57): p. 27864-27868.
70. Madrid, J.F., M. Barsbay, L. Abad, et al., *Grafting of N, N-dimethylaminoethyl methacrylate from PE/PP nonwoven fabric via radiation-induced RAFT polymerization and quaternization of the grafts.* Radiation Physics and Chemistry, 2016. **124**: p. 145-154.
71. Abd El-Magied, M.O., E.A. Elshehy, E.-S.A. Manaa, et al., *Kinetics and thermodynamics studies on the recovery of thorium ions using amino resins with magnetic properties.* Industrial & Engineering Chemistry Research, 2016. **55**(43): p. 11338-11345.
72. Selambakkannu, S., N.A.F. Othman, K.A. Bakar, et al., *A kinetic and mechanistic study of adsorptive removal of metal ions by imidazole-functionalized polymer graft banana fiber.* Radiation Physics and Chemistry, 2018. **153**: p. 58-69.
73. Khullar, R., V.K. Varshney, S. Naithani, et al., *Grafting of acrylonitrile onto cellulosic material derived from bamboo (Dendrocalamus strictus).* Express Polymer Letters, 2008. **2**(1): p. 12-18.
74. Khullar, R., V. Varshney, S. Naithani, et al., *Grafting of acrylonitrile onto cellulosic material derived from bamboo (Dendrocalamus strictus).* Express Polymer Letters, 2008. **2**(1): p. 12-18.
75. Princi, E., S. Vicini, E. Pedemonte, et al., *Synthesis and mechanical characterisation of cellulose based textiles grafted with acrylic monomers.* European Polymer Journal, 2006. **42**(1): p. 51-60.

76. Kontopoulou, M., *Advances in Chemically Modified and Functionalized Polymers.* Macromolecular Reaction Engineering, 2014. **8**(2): p. 67-68.
77. Wulff, G., W. Vesper, R. Grobe‐Einsler, et al., *Enzyme‐analogue built polymers, 4. On the synthesis of polymers containing chiral cavities and their use for the resolution of racemates.* Die Makromolekulare Chemie: Macromolecular Chemistry and Physics, 1977. **178**(10): p. 2799-2816.
78. Arshady, R. and K. Mosbach, *Synthesis of substrate‐selective polymers by host‐guest polymerization.* Die Makromolekulare Chemie: Macromolecular Chemistry and Physics, 1981. **182**(2): p. 687-692.
79. Jiang, Y. and D. Kim, *Synthesis and selective adsorption behavior of Pd (II)-imprinted porous polymer particles.* Chemical engineering journal, 2013. **232**: p. 503-509.
80. Liu, X., H. Chen, C. Wang, et al., *Synthesis of porous acrylonitrile/methyl acrylate copolymer beads by suspended emulsion polymerization and their adsorption properties after amidoximation.* Journal of hazardous materials, 2010. **175**(1-3): p. 1014-1021.
81. Zhao, G., X. Huang, Z. Tang, et al., *Polymer-based nanocomposites for heavy metal ions removal from aqueous solution: a review.* Polymer Chemistry, 2018. **9**(26): p. 3562-3582.
82. Bhattacharya, A. and B. Misra, *Grafting: a versatile means to modify polymers: techniques, factors and applications.* Progress in polymer science, 2004. **29**(8): p. 767-814.
83. Wojnárovits, L., C.M. Földváry, and E. Takács, *Radiation-induced grafting of cellulose for adsorption of hazardous water pollutants: A review.* Radiation Physics and Chemistry, 2010. **79**(8): p. 848-862.
84. Liu, H., D. Kong, W. Sun, et al., *Effect of anions on the polymerization and adsorption processes of Cu (II) ion-imprinted polymers.* Chemical Engineering Journal, 2016. **303**: p. 348-358.
85. Imprinting, S.f.M. *MIP Database*. 2019 [cited 2019 1 June 2019]; Available from: https://mipdatabase.com/all_items.php.
86. Ahmadi, S.J., O. Noori-Kalkhoran, and S. Shirvani-Arani, *Synthesis and characterization of new ion-imprinted polymer for separation and preconcentration of uranyl (UO22+) ions.* Journal of hazardous materials, 2010. **175**(1-3): p. 193-197.
87. Shakerian, F., K.-H. Kim, E. Kwon, et al., *Advanced polymeric materials: Synthesis and analytical application of ion imprinted polymers as selective sorbents for solid phase extraction of metal ions.* TrAC Trends in Analytical Chemistry, 2016. **83**: p. 55-69.
88. Ye, L., *Molecular imprinting: Principles and applications of micro-and nanostructure polymers*. 2013: CRC press.
89. Liu, Z., W. Wu, Y. Liu, et al., *Preparation of surface anion imprinted polymer by developing a La (III)-coordinated 3-methacryloxyethyl-propyl bi-functionalized graphene oxide for phosphate removal.* Journal of the Taiwan Institute of Chemical Engineers, 2018. **85**: p. 282-290.
90. Kuras, M.J. and E. Więckowska, *Synthesis and characterization of a new copper (II) ion-imprinted polymer.* Polymer Bulletin, 2015. **72**(12): p. 3227-3240.

91. Rahman, N., N. Sato, S. Yoshioka, et al., *Selective Cu (II) adsorption from aqueous solutions including Cu (II), Co (II), and Ni (II) by modified acrylic acid grafted PET film.* ISRN Polymer Science, 2013. **2013**.
92. Msaadi, R., G. Yilmaz, A. Allushi, et al., *Highly Selective Copper Ion Imprinted Clay/Polymer Nanocomposites Prepared by Visible Light Initiated Radical Photopolymerization.* Polymers, 2019. **11**(2): p. 286.
93. Adhikari, C.R., D. Parajuli, K. Inoue, et al., *Pre-concentration and separation of heavy metal ions by chemically modified waste paper gel.* Chemosphere, 2008. **72**(2): p. 182-188.
94. Zhang, W., M. Yun, Z. Yu, et al., *A novel Cu (II) ion-imprinted alginate–chitosan complex adsorbent for selective separation of Cu (II) from aqueous solution.* Polymer Bulletin, 2019. **76**(4): p. 1861-1876.
95. Suquila, F.A., L.L. de Oliveira, and C.R. Tarley, *Restricted access copper imprinted poly (allylthiourea): The role of hydroxyethyl methacrylate (HEMA) and bovine serum albumin (BSA) on the sorptive performance of imprinted polymer.* Chemical Engineering Journal, 2018. **350**: p. 714-728.
96. Lin, C., H. Wang, Y. Wang, et al., *Selective preconcentration of trace thorium from aqueous solutions with Th(IV)-imprinted polymers prepared by a surface-grafted technique.* International Journal of Environmental Analytical Chemistry, 2011. **91**(11): p. 1050-1061.
97. Xu, J., L. Zhou, Y. Jia, et al., *Adsorption of thorium (IV) ions from aqueous solution by magnetic chitosan resins modified with triethylene-tetramine.* Journal of Radioanalytical and Nuclear Chemistry, 2015. **303**(1): p. 347-356.
98. Liang, H., Q. Chen, J. Ma, et al., *Synthesis and characterization of a new ion-imprinted polymer for the selective separation of thorium (iv) ions at high acidity.* RSC Advances, 2017. **7**(56): p. 35394-35402.
99. Khalili, F.I., N.a.H. Salameh, and M.M. Shaybe, *Sorption of uranium (VI) and thorium (IV) by Jordanian bentonite.* Journal of Chemistry, 2012. **2013**.
100. Büyüktiryaki, S., R. Say, A. Ersöz, et al., *Selective preconcentration of thorium in the presence of UO22+, Ce3+ and La3+ using Th (IV)-imprinted polymer.* Talanta, 2005. **67**(3): p. 640-645.
101. He, F.F., H.Q. Wang, Y.Y. Wang, et al., *Magnetic Th(IV)-ion imprinted polymers with salophen schiff base for separation and recognition of Th(IV).* Journal of Radioanalytical and Nuclear Chemistry, 2013. **295**(1): p. 167-177.
102. Xiong, J., S. Hu, Y. Liu, et al., *Polypropylene modified with amidoxime/carboxyl groups in separating uranium (VI) from thorium (IV) in aqueous solutions.* ACS Sustainable Chemistry & Engineering, 2017. **5**(2): p. 1924-1930.
103. Bicim, T. and M. Yaman, *Sensitive determination of uranium in natural waters using UV-Vis spectrometry after preconcentration by ion-imprinted polymer-ternary complexes.* Journal of AOAC International, 2016. **99**(4): p. 1043-1048.
104. Anirudhan, T.S., J. Nima, and P.L. Divya, *Adsorption and separation behavior of uranium (VI) by 4-vinylpyridine-grafted-vinyltriethoxysilane-cellulose ion imprinted polymer.* Journal of Environmental Chemical Engineering, 2015. **3**(2): p. 1267-1276.
105. Mishima, K., X. Du, N. Miyamoto, et al., *Experimental and theoretical studies on the adsorption mechanisms of uranium (VI) ions on chitosan.* Journal of functional biomaterials, 2018. **9**(3): p. 49.

106. Zhang, L., S. Yang, J. Qian, et al., *Surface ion-imprinted polypropylene nonwoven fabric for potential uranium seawater extraction with high selectivity over vanadium.* Industrial & Engineering Chemistry Research, 2017. **56**(7): p. 1860-1867.
107. Cleland, M.R., L.A. Parks, and S. Cheng, *Applications for radiation processing of materials.* Nuclear Instruments and Methods in Physics Research Section B: Beam Interactions with Materials and Atoms, 2003. **208**(0): p. 66-73.
108. Clough, R.L., *High-energy radiation and polymers: A review of commercial processes and emerging applications.* Nuclear Instruments and Methods in Physics Research Section B: Beam Interactions with Materials and Atoms, 2001. **185**(1–4): p. 8-33.
109. Meister, J., *Polymer modification: principles, techniques, and applications*. Vol. 60. 2000: CRC Press.
110. Kerluke, D.R. and S. Cheng, *Radiation Processing of Polymers: The Current Status and Prospects for the Future.* ANTEC 2004 Plastics: Annual Technical Conference, Volume 3: Special Areas, 2004: p. p. 3738-3739.
111. Mansoori, G.A., T.F. George, L. Assoufid, et al., *Molecular Building Blocks for Nanotechnology: From Diamondoids to Nanoscale Materials and Applications*. 2007: Springer.
112. Drobny, J.G., *Modification of Polymers by Ionizing Radiation: A review*. ANTEC 2006 Plastics: Annual Technical Conference Proceedings, 2006: p. 2465-2469.
113. Chmielewski, A.G., M. Haji-Saeid, and S. Ahmed, *Progress in radiation processing of polymers.* Nuclear Instruments and Methods in Physics Research Section B: Beam Interactions with Materials and Atoms, 2005. **236**(1): p. 44-54.
114. Dole, M., *The radiation chemistry of macromolecules*. Vol. 1. 2012: Elsevier.
115. Bhardwaj, Y., M. Tamada, M. Nasef, et al., *HARMONIZED PROTOCOL for RADIATION-INDUCED GRAFTING*.
116. Rouquerol, J., F. Rouquerol, P. Llewellyn, et al., *Adsorption by powders and porous solids: principles, methodology and applications*. 2013: Academic press.
117. Freundlich, H., *Über die adsorption in lösungen.* Zeitschrift für physikalische Chemie, 1907. **57**(1): p. 385-470.
118. Langmuir, I., *The adsorption of gases on plane surfaces of glass, mica and platinum.* Journal of the American Chemical society, 1918. **40**(9): p. 1361-1403.
119. Brunauer, S. and P.H. Emmett, *The use of low temperature van der Waals adsorption isotherms in determining the surface areas of various adsorbents.* Journal of the American Chemical Society, 1937. **59**(12): p. 2682-2689.
120. Brunauer, S., P.H. Emmett, and E. Teller, *Adsorption of gases in multimolecular layers.* Journal of the American chemical society, 1938. **60**(2): p. 309-319.
121. Kreuzer, H.J. and Z.W. Gortel, *Physisorption kinetics*. Vol. 1. 2012: Springer Science & Business Media.
122. Ranganathan, S., *Selected Topics in Chemistry*. 2015: Lulu. com.
123. Kipling, J.J., *Adsorption from Solutions of Non-electrolytes*. 2017: Academic Press.
124. Igwe, J.C. and A.A. Abia, *Adsorption isotherm studies of Cd (II), Pb (II) and Zn (II) ions bioremediation from aqueous solution using unmodified and EDTA-modified maize cob.* Eclética Química, 2007. **32**(1): p. 33-42.

125. Brannon-Peppas, L. and R.S. Harland, *Absorbent polymer technology*. Vol. 8. 2012: Elsevier.
126. Ma, H., S. Yao, J. Li, et al., *A mild method of amine-type adsorbents syntheses with emulsion graft polymerization of glycidyl methacrylate on polyethylene non-woven fabric by pre-irradiation.* Radiation Physics and Chemistry, 2012. **81**(9): p. 1393-1397.
127. Hoshina, H., N. Seko, Y. Ueki, et al., *Synthesis of graft adsorbent with N-methyl-D-glucamine for boron adsorption.* 日本イオン交換学会誌, 2007. **18**(4): p. 236-239.
128. Reyna, J., M.C. García-López, N. Pérez-Rodríguez, et al., *Polystyrene degraded and functionalized with acrylamide for removal of Pb (II) metal ions.* Polymer Bulletin, 2018: p. 1-20.
129. Liu, C., R. Bai, and Q. San Ly, *Selective removal of copper and lead ions by diethylenetriamine-functionalized adsorbent: behaviors and mechanisms.* Water Research, 2008. **42**(6-7): p. 1511-1522.
130. Paredes, B., S. González, M. Rendueles, et al., *Influence of the amination conditions on the textural properties and chromatographic behaviour of amino-functionalized glycidyl methacrylate-based particulate supports.* Acta materialia, 2003. **51**(20): p. 6189-6198.
131. Liu, C. and R. Bai, *Extended study of DETA-functionalized PGMA adsorbent in the selective adsorption behaviors and mechanisms for heavy metal ions of Cu, Co, Ni, Zn, and Cd.* Journal of colloid and interface science, 2010. **350**(1): p. 282-289.
132. Goel, N., M. Rao, V. Kumar, et al., *Synthesis of antibacterial cotton fabric by radiation-induced grafting of [2-(Methacryloyloxy) ethyl] trimethylammonium chloride (MAETC) onto cotton.* Radiation Physics and Chemistry, 2009. **78**(6): p. 399-406.
133. Sekine, A., N. Seko, M. Tamada, et al., *Biodegradable metal adsorbent synthesized by graft polymerization onto nonwoven cotton fabric.* Radiation Physics and Chemistry, 2010. **79**(1): p. 16-21.
134. Goel, N., V. Kumar, S. Pahan, et al., *Development of adsorbent from Teflon waste by radiation induced grafting: Equilibrium and kinetic adsorption of dyes.* Journal of hazardous materials, 2011. **193**: p. 17-26.
135. Salih, S., *Fourier Transform: Materials Analysis*. 2012: BoD–Books on Demand.
136. Ravel, B. and M. Newville, *ATHENA, ARTEMIS, HEPHAESTUS: data analysis for X-ray absorption spectroscopy using IFEFFIT.* Journal of Synchrotron Radiation, 2005. **12**(4): p. 537-541.
137. Princi, E., S. Vicini, N. Proietti, et al., *Grafting polymerization on cellulose based textiles: a 13C solid state NMR characterization.* European Polymer Journal, 2005. **41**(6): p. 1196-1203.
138. Sehgal, T. and S. Rattan, *Graft-copolymerization of N-vinyl-2-pyrrolidone onto isotactic polypropylene film by gamma radiation using peroxidation method.* 2010.
139. Dilli, S., J. Garnett, E. Martin, et al. *The role of additives in the radiation induced copolymerization of monomers to cellulose*. in *Journal of Polymer Science Part C: Polymer Symposia*. 1972. Wiley Online Library.

140. Jimeno, A., S. Goyanes, A. Eceiza, et al., *Effects of amine molecular structure on carbon nanotubes functionalization.* Journal of nanoscience and nanotechnology, 2009. **9**(10): p. 6222-6227.
141. Kimmins, S.D., P. Wyman, and N.R. Cameron, *Amine-functionalization of glycidyl methacrylate-containing emulsion-templated porous polymers and immobilization of proteinase K for biocatalysis.* Polymer, 2014. **55**(1): p. 416-425.
142. Madrid, J.F., G.M. Nuesca, and L.V. Abad, *Amine functionalized radiation-induced grafted water hyacinth fibers for Pb 2+, Cu 2+ and Cr 3+ uptake.* Radiation Physics and Chemistry, 2014. **97**: p. 246-252.
143. Sarala* Selambakkannu, N.A.F.O., Siti Fatahiyah Mohamad, Khomsaton Abu Bakar, Hamdani Saidi, *Functionalization of Gma-Grafted Banana Fibers With Ethylenediamne For Metal Ion Adsorption.* Advances in Environmental Biology, 2015. **9**(13).
144. Petrovich, J., *FTIR and DSC of polymer films used for packaging: LLDPE, PP and PVDC.* SHAPE American High School, 2015.
145. Sharif, J., S.F. Mohamad, N.A.F. Othman, et al., *Graft copolymerization of glycidyl methacrylate onto delignified kenaf fibers through pre-irradiation technique.* Radiation Physics and Chemistry, 2013. **91**: p. 125-131.
146. Casarin, J., A.C.G. Junior, M.G. Segatelli, et al., *Insight into the performance of molecularly imprinted poly (methacrylic acid) and polyvinylimidazole for extraction of imazethapyr in aqueous medium.* Chemical Engineering Journal, 2018. **343**: p. 583-596.
147. Meylheuc, T., C. Methivier, M. Renault, et al., *Adsorption on stainless steel surfaces of biosurfactants produced by gram-negative and gram-positive bacteria: consequence on the bioadhesive behavior of Listeria monocytogenes.* Colloids and Surfaces B: Biointerfaces, 2006. **52**(2): p. 128-137.
148. Kamra, T., S. Chaudhary, C. Xu, et al., *Covalent immobilization of molecularly imprinted polymer nanoparticles on a gold surface using carbodiimide coupling for chemical sensing.* Journal of colloid and interface science, 2016. **461**: p. 1-8.
149. Borghi, E., P.L. Solari, M. Beltramini, et al., *Oxidized derivatives of octopus vulgaris and carcinus aestuarii hemocyanins at pH 7.5 and related models by X-ray absorption spectroscopy.* Biophysical journal, 2002. **82**(6): p. 3254-3268.
150. Yano, J., Y. Pushkar, P. Glatzel, et al., *High-resolution Mn EXAFS of the oxygen-evolving complex in photosystem II: structural implications for the Mn4Ca cluster.* Journal of the American Chemical Society, 2005. **127**(43): p. 14974-14975.
151. Gaur, A., B. Shrivastava, D. Gaur, et al., *EXAFS study of binuclear hydroxo-bridged copper (II) complexes.* Journal of coordination Chemistry, 2011. **64**(7): p. 1265-1275.
152. Gaur, A., B. Shrivastava, K. Srivastava, et al., *XAFS investigations of copper (II) complexes with tetradentate Schiff base ligands.* X‐Ray Spectrometry, 2012. **41**(6): p. 384-392.
153. Wang, F., Y. Pan, P. Cai, et al., *Single and binary adsorption of heavy metal ions from aqueous solutions using sugarcane cellulose-based adsorbent.* Bioresource technology, 2017. **241**: p. 482-490.
154. Bajpai, S.K. and A. Jain, *Removal of copper (II) from aqueous solution using spent tea leaves (STL) as a potential sorbent.* SA Journal of Radiology, 2010. **36**(3).

155. Erdem, Ö., Y. Saylan, M. Andaç, et al., *Molecularly imprinted polymers for removal of metal ions: an alternative treatment method.* Biomimetics, 2018. **3**(4): p. 38.
156. Ma, H., K. Morita, H. Hoshina, et al., *Synthesis of amine-type adsorbents with emulsion graft polymerization of 4-hydroxybutyl acrylate glycidylether.* Materials Sciences and Applications, 2011. **2**(07): p. 776.
157. Niu, Y., K. Li, D. Ying, et al., *Novel recyclable adsorbent for the removal of copper (II) and lead (II) from aqueous solution.* Bioresource technology, 2017. **229**: p. 63-68.
158. Park, S.-J. and M.-K. Seo, *Interface science and composites*. Vol. 18. 2011: Academic Press.
159. Bindu, M. and B. Mathew, *DESIGN OF COPPER ION SELECTIVE POLYMERS BY MOLECULAR IMPRINTING APPROACH.*
160. Kockler, K.B., F. Fleischhaker, and C. Barner-Kowollik, *Free Radical Propagation Rate Coefficients of N-Containing Methacrylates: Are We Family?* Macromolecules, 2016. **49**(22): p. 8572-8580.
161. Kong, Z., X. Wu, J. Wei, et al., *Preparation and characterization of hydrophilicity fibers based on 2-(dimethyamino) ethyl mathacrylate grafted polypropylene by UV-irradiation for removal of Cr (VI) and as (V).* Journal of Polymer Research, 2016. **23**(9): p. 199.
162. Saito, K., K. Fujiwara, and T. Sugo, *Revolution in the Form of Polymeric Adsorbents 2: Fibers, Films, and Particles*, in *Innovative Polymeric Adsorbents*. 2018, Springer. p. 109-143.
163. Nasser, I.I., C. Algieri, A. Garofalo, et al., *Hybrid imprinted membranes for selective recognition of quercetin.* Separation and Purification Technology, 2016. **163**: p. 331-340.
164. Ibrahim, M.M., C. Sipaut, and N.M. Yusof, *Purification of vanillin by a molecular imprinting polymer technique.* Separation and Purification Technology, 2009. **66**(3): p. 450-456.
165. Chen, L., X. Wang, W. Lu, et al., *Molecular imprinting: perspectives and applications.* Chemical Society Reviews, 2016. **45**(8): p. 2137-2211.
166. Nasef, M.M. and I.A. Sugiarmawan, *Radiation induced emulsion grafting of glycidyl methacrylate onto high density polyethylene: a kinetic study.* Malaysian Journal of Fundamental and Applied Sciences, 2010. **6**(2).
167. Taghizadeh, M.T. and M. Khosravy, *Kinetics and mechanism of graft copolymerization of vinyl monomers (acrylamide, acrylic acid, and methacrylate) onto starch by potassium dichromate as redox initiator.* Iranian Polymer Journal, 2003. **12**(6): p. 497-505.
168. Singha, A.S. and A.K. Rana, *Kinetics of Graft Copolymerization of Acrylic Acid Ontocannabis Indica Fibre.* 2011.
169. Sun, Y. and A.G. Chmielewski, *Applications of Ionizing Radiation in Materials Processing*. 2017: Institute of Nuclear Chemistry and Technology.
170. Burillo, G., J. Serrano-Gómez, and J. Bonifacio-Martínez, *Adsorption of chromium (VI) on radiation grafted N, N-dimethylaminoethylmethacrylate onto polypropylene, from aqueous solutions.* Journal of the Mexican Chemical Society, 2013. **57**(2): p. 80-84.

171. Li, J., W.D. He, S.c. Han, et al., *Synthesis and micellization of PSt‐PNIPAM‐PDMAEMA hetero‐arm star polymer with double thermo‐responsibility.* Journal of Polymer Science Part A: Polymer Chemistry, 2009. **47**(3): p. 786-796.
172. Ranogajec, F., *Kinetic and structural factors in graft polymerization of styrene on polyolefins.* Polimeri: časopis za plastiku i gumu, 2009. **29**(4): p. 217-227.
173. Kornacka, E.M., G. Przybytniak, and K. Mirkowski, *Selection of polymer matrices for radiation grafting.* Prof. Jacek Michalik, Ph. D., D. Sc. Wiktor Smułek, Ph. D., 2009: p. 38.
174. Rahmatpour, A., N. Goodarzi, and M. Moazzez, *A novel route for synthesis of cross-linked polystyrene copolymer beads with tunable porosity using guar and xanthan gums from bioresources as alternative synthetic suspension stabilizers.* Designed monomers and polymers, 2018. **21**(1): p. 116-129.
175. Shoravi, S., G. Olsson, B. Karlsson, et al., *On the Influence of crosslinker on template complexation in molecularly imprinted polymers: a computational study of prepolymerization mixture events with correlations to template-polymer recognition behavior and NMR spectroscopic studies.* International journal of molecular sciences, 2014. **15**(6): p. 10622-10634.
176. Sibrian-Vazquez, M. and D.A. Spivak, *Enhanced enantioselectivity of molecularly imprinted polymers formulated with novel cross-linking monomers.* Macromolecules, 2003. **36**(14): p. 5105-5113.
177. Haupt, K., *Molecular imprinting*. Vol. 325. 2012: Springer Science & Business Media.
178. Pereira, E., C. Caceres, F. Rivera, et al., *Preparation of molecularly imprinted polymers for diphenylamine removal from organic gunshot residues.* Journal of the Chilean Chemical Society, 2014. **59**(4): p. 2731-2736.
179. Sokker, H., A.A. Ghaffar, Y. Gad, et al., *Synthesis and characterization of hydrogels based on grafted chitosan for the controlled drug release.* Carbohydrate polymers, 2009. **75**(2): p. 222-229.
180. Walo, M., *Radiation-induced grafting*, in *Applications of ionizing radiation in materials processing*. 2017. p. 193-210.
181. Przybytniak, G., *Crosslinking of Polymers in Radiation Processing.* Applications of ionizing radiation in materials processing, 2017: p. 249-267.
182. Madrid, J.F., G.M. Nuesca, and L.V. Abad, *Gamma radiation-induced grafting of glycidyl methacrylate (GMA) onto water hyacinth fibers.* Radiation Physics and Chemistry, 2013. **85**: p. 182-188.
183. Kodama, Y., M. Barsbay, and O. Güven, *Poly (2-hydroxyethyl methacrylate)(PHEMA) grafted polyethylene/polypropylene (PE/PP) nonwoven fabric by γ-initiation: Synthesis, characterization and benefits of RAFT mediation.* Radiation Physics and Chemistry, 2014. **105**: p. 31-38.
184. Barsbay, M. and O. Güven, *RAFT mediated grafting of poly (acrylic acid)(PAA) from polyethylene/polypropylene (PE/PP) nonwoven fabric via preirradiation.* Polymer, 2013. **54**(18): p. 4838-4848.
185. Hayashi, N., J. Chen, and N. Seko, *Nitrogen-Containing Fabric Adsorbents Prepared by Radiation Grafting for Removal of Chromium from Wastewater.* Polymers, 2018. **10**(7): p. 744.
186. Othman, N.A.F., S. Selambakkannu, T.M. Ting, et al., *Integration of phosphoric acid onto radiation grafted poly (2, 3-epoxypropyl methacrylate)-PP/PE non-*

woven fabrics aimed copper adsorbent via response surface method. Journal of Polymer Research, 2019. **26**(12): p. 283.
187. Flora, S.J. and V. Pachauri, *Chelation in metal intoxication.* International journal of environmental research and public health, 2010. **7**(7): p. 2745-2788.
188. Flora, G., M. Mittal, and S.J. Flora, *Medical Countermeasures—Chelation Therapy*, in *Handbook of Arsenic Toxicology*. 2015, Elsevier. p. 589-626.
189. Alsharaeh, E., A. Othman, and M. Aldosari, *Microwave irradiation effect on the dispersion and thermal stability of RGO nanosheets within a polystyrene matrix.* Materials, 2014. **7**(7): p. 5212-5224.
190. Nurhayati, T. and I. Royani. *Synthesis and characterization of MAA-based molecularly-imprinted polymer (MIP) with D-glucose template*. in *Journal of Physics: Conference Series*. 2016. IOP Publishing.
191. Duan, G., Q. Zhong, L. Bi, et al., *The Poly (acrylonitrule-co-acrylic acid)-graft-β-cyclodextrin Hydrogel for Thorium (IV) Adsorption.* Polymers, 2017. **9**(6): p. 201.
192. Jin, C., J. Hu, J. Wang, et al., *An Amidoximated-UHMEPE Fiber for Selective and High Efficient Removal of Uranyl and Thorium from Acid Aqueous Solution.* 2017.
193. Mittal, A., R. Ahmad, and I. Hasan, *Poly (methyl methacrylate)-grafted alginate/Fe3O4 nanocomposite: synthesis and its application for the removal of heavy metal ions.* Desalination and Water Treatment, 2016. **57**(42): p. 19820-19833.
194. Soetaredjo, F.E., S. Ismadji, K. Foe, et al., *Recent advances in the application of polymer-based nanocomposites for removal of hazardous substances from water and wastewater*, in *New Polymer Nanocomposites for Environmental Remediation*. 2018, Elsevier. p. 499-540.
195. Chen, M., Z. Li, Y. Geng, et al., *Adsorption behavior of thorium on N, N, N′, N′-tetraoctyldiglycolamide (TODGA) impregnated graphene aerogel.* Talanta, 2018. **181**: p. 311-317.
196. Gado, M., *Sorption of Thorium Using Magnetic Graphene Oxide Polypyrrole Composite Synthesized from Water Hyacinth Roots.* Iran. J. Chem. Chem. Eng. Research Article Vol, 2018. **37**(3).
197. Anderson, M.J. and P.J. Whitcomb, *RSM simplified: optimizing processes using response surface methods for design of experiments*. 2016: Productivity press.
198. Kumar, A., B. Prasad, and I. Mishra, *Optimization of process parameters for acrylonitrile removal by a low-cost adsorbent using Box–Behnken design.* Journal of Hazardous Materials, 2008. **150**(1): p. 174-182.
199. Christodoulakis, K. and M. Vamvakaki. *pH‐Responsive Microgel Particles Comprising Solely Basic or Acidic Residues*. in *Macromolecular symposia*. 2010. Wiley Online Library.
200. Bütün, V., S. Armes, and N. Billingham, *Synthesis and aqueous solution properties of near-monodisperse tertiary amine methacrylate homopolymers and diblock copolymers.* Polymer, 2001. **42**(14): p. 5993-6008.
201. Ekberg, C., Y. Albinsson, M.J. Comarmond, et al., *Studies on the complexation behavior of thorium (IV). 1. Hydrolysis equilibria*. Journal of Solution Chemistry, 2000. **29**(1): p. 63-86.
202. Bhardwaj, Y., M. Tamada, Y.-C. Nho, et al., *Harmonized Protocol for Radiation-Induced Grafting*, in *Workshop on Harmonized Radiation Graft Protocol*. 2014.

203. Mondal, P., C. Majumder, and B. Mohanty, *Effects of adsorbent dose, its particle size and initial arsenic concentration on the removal of arsenic, iron and manganese from simulated ground water by Fe3+ impregnated activated carbon.* Journal of Hazardous Materials, 2008. **150**(3): p. 695-702.
204. Chen, X., *Modeling of experimental adsorption isotherm data.* Information, 2015. **6**(1): p. 14-22.
205. Ayawei, N., A.N. Ebelegi, and D. Wankasi, *Modelling and interpretation of adsorption isotherms.* Journal of Chemistry, 2017. **2017**.
206. Yaneva, Z.L., B.K. Koumanova, and N.V. Georgieva, *Linear and nonlinear regression methods for equilibrium modelling of p-nitrophenol biosorption by Rhizopus oryzae: Comparison of error analysis criteria.* Journal of Chemistry, 2012. **2013**.
207. Meroufel, B., O. Benali, M. Benyahia, et al., *Adsorptive removal of anionic dye from aqueous solutions by Algerian kaolin: Characteristics, isotherm, kinetic and thermodynamic studies.* J. Mater. Environ. Sci, 2013. **4**(3): p. 482-491.
208. Ogunmodede, O., A. Ojo, E. Adewole, et al., *Adsorptive removal of anionic dye from aqueous solutions by mixture of Kaolin and Bentonite clay: Characteristics, isotherm, kinetic and thermodynamic studies.* Iranica Journal of Energy & Environment, 2015. **6**(2): p. 147-153.
209. Ahmad, R. and R. Kumar, *Adsorption studies of hazardous malachite green onto treated ginger waste.* Journal of environmental management, 2010. **91**(4): p. 1032-1038.
210. Lima, E.C., A. Hosseini-Bandegharaei, J.C. Moreno-Piraján, et al., *A critical review of the estimation of the thermodynamic parameters on adsorption equilibria. Wrong use of equilibrium constant in the Van't Hoof equation for calculation of thermodynamic parameters of adsorption.* Journal of Molecular Liquids, 2019. **273**: p. 425-434.
211. Afroze, S., T.K. Sen, and H.M. Ang, *Adsorption removal of zinc (II) from aqueous phase by raw and base modified Eucalyptus sheathiana bark: Kinetics, mechanism and equilibrium study.* Process Safety and Environmental Protection, 2016. **102**: p. 336-352.
212. Chiou, M. and H. Li, *Adsorption behavior of reactive dye in aqueous solution on chemical cross-linked chitosan beads.* Chemosphere, 2003. **50**(8): p. 1095-1105.
213. Semerjian, L., *Equilibrium and kinetics of cadmium adsorption from aqueous solutions using untreated Pinus halepensis sawdust.* Journal of hazardous materials, 2010. **173**(1): p. 236-242.
214. Lagergren, S., *Kungliga svenska vetenskapsakademiens.* Handlingar, 1898. **24**(4): p. 1-39.
215. Ho, Y.-S. and G. McKay, *Pseudo-second order model for sorption processes.* Process biochemistry, 1999. **34**(5): p. 451-465.
216. Ho, Y. and G. McKay, *Kinetic model for lead (II) sorption on to peat.* Adsorption science & technology, 1998. **16**(4): p. 243-255.
217. Zhang, C., J. Su, H. Zhu, et al., *The removal of heavy metal ions from aqueous solutions by amine functionalized cellulose pretreated with microwave-H 2 O 2.* RSC Advances, 2017. **7**(54): p. 34182-34191.

218. Myers, R.H., D.C. Montgomery, and C. Anderson-Cook, *Process and product optimization using designed experiments.* Response surface methodology, 2002: p. 328-335.
219. Keshtkar, A.R. and M.A. Mousavian, *Application of response surface methodology for thorium (IV) removal using Amberlite IR-120 and IRA-400: Ion exchange equilibrium and kinetics.* Journal of Particle Science & Technology, 2017. **3**(2): p. 101-112.
220. Taleb, M.F.A., G.A. Mahmoud, S.M. Elsigeny, et al., *Adsorption and desorption of phosphate and nitrate ions using quaternary (polypropylene-gN, N-dimethylamino ethylmethacrylate) graft copolymer.* Journal of Hazardous Materials, 2008. **159**(2-3): p. 372-379.
221. Kavaklı, C., P.A. Kavaklı, B.D. Turan, et al., *Quaternized dimethylaminoethyl methacrylate strong base anion exchange fibers for As (V) adsorption.* Radiation Physics and Chemistry, 2014. **102**: p. 84-95.
222. Zhao, L., J. Sun, Y. Zhao, et al., *Removal of hazardous metal ions from wastewater by radiation synthesized silica-graft-dimethylaminoethyl methacrylate adsorbent.* Chemical engineering journal, 2011. **170**(1): p. 162-169.
223. Li, C., Y. Zhang, J. Peng, et al., *Adsorption of Cr (VI) using cellulose microsphere-based adsorbent prepared by radiation-induced grafting.* Radiation Physics and Chemistry, 2012. **81**(8): p. 967-970.
224. Bindu, M. and B. Mathew, *Design of Copper Ion Selective Polymers by Molecular Imprinting Approach.* International Journal of Latest Research in Science and Technology, 2015. **4**(2): p. 154-160.
225. Ting, T., M.M. Nasef, and K. Hashim, *Tuning N-methyl-D-glucamine density in a new radiation grafted poly (vinyl benzyl chloride)/nylon-6 fibrous boron-selective adsorbent using the response surface method.* RSC Advances, 2015. **5**(47): p. 37869-37880.
226. Xu, L., Y.-A. Huang, Q.-J. Zhu, et al., *Chitosan in molecularly-imprinted polymers: Current and future prospects.* International journal of molecular sciences, 2015. **16**(8): p. 18328-18347.
227. Thuéry, P., *Solid state structure of thorium (IV) complexes with common aminopolycarboxylate ligands.* Inorganic chemistry, 2011. **50**(5): p. 1898-1904.
228. Comba, P., *Metal ion selectivity and molecular modeling.* Coordination chemistry reviews, 1999. **185**: p. 81-98.
229. He, Q., X. Chang, Q. Wu, et al., *Synthesis and applications of surface-grafted Th(IV)-imprinted polymers for selective solid-phase extraction of thorium(IV).* Analytica Chimica Acta, 2007. **605**(2): p. 192-197.
230. Lin, C., H. Wang, Y. Wang, et al., *Selective solid-phase extraction of trace thorium(IV) using surface-grafted Th(IV)-imprinted polymers with pyrazole derivative.* Talanta, 2010. **81**(1-2): p. 30-36.
231. Cheng, Z., H. Wang, Y. Wang, et al., *Synthesis and characterization of an ion-imprinted polymer for selective solid phase extraction of thorium(IV).* Microchim Acta, 2011. **173**: p. 423-431.
232. Ji, X.Z., H.J. Liu, L.L. Wang, et al., *Study on adsorption of Th(IV) using surface modified dibenzoylmethane molecular imprinted polymer.* Journal of Radioanalytical and Nuclear Chemistry, 2013. **295**: p. 265-270.

233. He, F.F., H.Q. Wang, Y.Y. Wang, et al., *Magnetic Th(IV)-ion imprinted polymers with salophen schiff base for separation and recognition of Th(IV).* Journal of Radioanalytical and Nuclear Chemistry, 2013. **295**: p. 167-177.
234. Huang, D.-L., R.-Z. Wang, Y.-G. Liu, et al., *Application of molecularly imprinted polymers in wastewater treatment: a review*. Environmental Science and Pollution Research, 2015. **22**(2): p. 963-977.
235. Masoumi, F., P. Sarabadani, and A.R. Khorrami, *Synthesis, characterization and application of a new nano-structured samarium (III) ion-imprinted polymer*. Polymer Bulletin, 2019: p. 1-18.
236. Gomes, A., L. Costa, D. Brito, et al., *Development of a new ion-imprinted polymer (IIP) with Cd 2+ ions based on divinylbenzene copolymers containing amidoxime groups.* Polymer Bulletin, 2019: p. 1-13.
237. Kutner, W. and P.S. Sharma, *Molecularly imprinted polymers for analytical chemistry applications*. Vol. 28. 2018: Royal Society of Chemistry.
238. Muhammad, T., Z. Nur, E.V. Piletska, et al., *Rational design of molecularly imprinted polymer: the choice of cross-linker.* Analyst, 2012. **137**(11): p. 2623-2628.
239. Laatikainen, K., C. Branger, B. Coulomb, et al., *In situ complexation versus complex isolation in synthesis of ion imprinted polymers.* Reactive and Functional Polymers, 2018. **122**: p. 1-8.
240. Nasef, M.M., M. Tamada, N. Seko, et al., *Advances in the development of functional polymers using radiation induced emulsion polymerization.* Recent Res Dev Polym Sci, 2014. **12**: p. 107-128.
241. Seko, N., N.T.Y. Ninh, and M. Tamada, *Emulsion grafting of glycidyl methacrylate onto polyethylene fiber*. Radiation Physics and Chemistry, 2010. **79**(1): p. 22-26.
242. Mohamed, N.H., M. Tamada, Y. Ueki, et al., *Emulsion graft polymerization of 4-chloromethylstyrene on kenaf fiber by pre-irradiation method.* Radiation Physics and Chemistry, 2013. **82**: p. 63-68.
243. Eliseeva, V.I., S. Ivanchev, S. Kuchanov, et al., *Emulsion polymerization and its applications in industry*. 2012: Springer Science & Business Media.
244. McClements, D.J., *Food emulsions: principles, practices, and techniques*. 2015: CRC press.
245. Rañada, M.L., M. Akbulut, L. Abad, et al., *Molecularly imprinted poly (N-vinyl imidazole) based polymers grafted onto nonwoven fabrics for recognition/removal of phloretic acid.* Radiation Physics and Chemistry, 2014. **94**: p. 93-97.
246. Mafu, L.D., B.B. Mamba, and T.A. Msagati, *Synthesis and characterization of ion imprinted polymeric adsorbents for the selective recognition and removal of arsenic and selenium in wastewater samples.* Journal of Saudi Chemical Society, 2016. **20**(5): p. 594-605.
247. Fan, H.-T., X.-T. Sun, Z.-G. Zhang, et al., *Selective removal of lead (II) from aqueous solution by an ion-imprinted silica sorbent functionalized with chelating N-donor atoms.* Journal of Chemical & Engineering Data, 2014. **59**(6): p. 2106-2114.
248. Compton, R., C. Bamford, and C. Tipper, *Degradation of polymers*. Vol. 14. 1975: Elsevier.

249. Rosiak, J.M., *Gel/sol analysis of irradiated polymers.* Radiation Physics and Chemistry, 1998. **51**(1): p. 13-17.
250. Kaur, I., N. Sharma, and V. Kumari, *Modification of fiber properties through grafting of acrylonitrile to rayon by chemical and radiation methods.* Journal of advanced research, 2013. **4**(6): p. 547-557.
251. Tamada, M., *Radiation processing of polymers and its applications*, in *Radiation Applications*. 2018, Springer. p. 63-80.
252. Chang, J.H., H. Lee, S. Jang, et al., *Facile preparation of size-controlled mesoporous silica particles by metal-chelating surfactant micelle complexes.* Materials Letters, 2016. **173**: p. 50-54.
253. Flores-Rojas, G. and E. Bucio, *Radiation-grafting of ethylene glycol dimethacrylate (EGDMA) and glycidyl methacrylate (GMA) onto silicone rubber.* Radiation Physics and Chemistry, 2016. **127**: p. 21-26.
254. Chapiro, A., *Chemical modifications in irradiated polymers.* Nuclear Instruments and Methods in Physics Research Section B: Beam Interactions with Materials and Atoms, 1988. **32**(1-4): p. 111-114.
255. Chandler‐Temple, A., E. Wentrup‐Byrne, A.K. Whittaker, et al., *Graft copolymerization of methoxyacrylethyl phosphate onto expanded poly (tetrafluoroethylene) facial membranes.* Journal of applied polymer science, 2010. **117**(6): p. 3331-3339.
256. Tissot, C., *Radiation-grafted fabrics for the extraction of uranium from seawater*. 2014.
257. Wentrup-Byrne, E., S. Suzuki, J.J. Suwanasilp, et al., *Novel phosphate-grafted ePTFE copolymers for optimum in vitro mineralization.* Biomedical Materials, 2010. **5**(4): p. 045010.
258. Li, J. and A.R. Barron, *Fourier transform infrared spectroscopy of metal ligand complexes.* 2010.
259. Pan, N., L. Li, J. Ding, et al., *A Schiff base/quaternary ammonium salt bifunctional graphene oxide as an efficient adsorbent for removal of Th (IV)/U (VI).* Journal of colloid and interface science, 2017. **508**: p. 303-312.
260. Vasapollo, G., R.D. Sole, L. Mergola, et al., *Molecularly imprinted polymers: present and future prospective.* International journal of molecular sciences, 2011. **12**(9): p. 5908-5945.
261. Söylemez, M.A., Z. Ateş, and O. Güven, *Radiation induced synthesis of molecularly imprinted polymers.*
262. Lee, J.-Y., C.-H. Chen, S. Cheng, et al., *Adsorption of Pb (II) and Cu (II) metal ions on functionalized large-pore mesoporous silica.* International journal of environmental science and technology, 2016. **13**(1): p. 65-76.
263. Chi, Z., H. Huang, Y. Yin, et al., *SELECTIVE RECYCLE OF Cd (0) BASED ON pH/T SWITCH-ABLE CONTROLLED Cd (II) ADSORPTION ON ION-IMPRINTED POLYMER.* FEB-FRESENIUS ENVIRONMENTAL BULLETIN, 2019: p. 7449.
264. Shafizadeh, F., M. Taghizadeh, and S. Hassanpour, *Preparation of a novel magnetic Pd (II) ion-imprinted polymer for the fast and selective adsorption of palladium ions from aqueous solutions.* Environmental Science and Pollution Research, 2019: p. 1-16.